Self-assembled Lanthanide luminescent Cyclen Complexes, from material to biological application”

Bruno D’Agostino

February 2021

University of Dublin

Trinity College

Based on research carried out under the direction of
Prof. Thorfinnur Gunnlaugsson

A thesis submitted to the School of Chemistry,
University of Dublin, Trinity College for the degree of
Doctor of Philosophy

DWAYNE JOHNSON

"Blood, sweat and respect. First two you give. Last one you earn."

Declaration

I declare that this thesis has not been submitted as an exercise for a degree at this or any other university and it is entirely my own work, except where duly acknowledged. I agree to deposit this thesis in the University's open access institutional repository or allow the Library to do so on my behalf, subject to Irish Copyright Legislation and Trinity College Library conditions of use and acknowledgement.

_____

Bruno D'Agostino

Abstract

The Thesis is entitled "Self-assembled Lanthanide Luminescent Cyclen Complexes, from Material to Biological Application" covers the formation of different Ln(III) cyclen based complexes and self-assembly and their applications in several fields. This includes the use of such complexes in solution and on solid surfaces (as thin films) in the monitoring of enzymatic reactions in real-time. The work carried out in this PhD study is divided into five chapters.

The main focus of Chapter 1 is to give an introduction into the field of the luminescent sensing, with several examples of fluorescent sensors previously developed being featured and discussed. The unique photophysical properties that the lanthanide metal ions offer are then discussed, with several examples of lanthanide-based probes developed previously from the literature being featured, as well as those developed in the Gunnlaugsson group over the years are reviewed.

In Chapter 2 the design, synthesis and photophysical evaluation of a novel cyclen based ligand is discussed. This ligand was designed with the view of developing a series of Ln(III) complexes, possessing the amphiphilicity required to be deposited these onto a quartz slides. These systems (both Eu(III) and Tb(III) based) form a self-assembly monolayer (SAM) on the water-air interface, and were then used to form Langmuir Blodgett (LB) films. The ability of these Ln(III) complexes, which were coordinatively unsaturated, to recognise and bind at the metal ion centre, amino acids was investigated by observing the changes in the lanthanide centred emission. The systems were indeed show to be able to discriminate between several amino acids in solution. The key result demonstrating that the complexes were able to act as probes for phosphorylated amino acids. The same investigation was performed for the Ln(III) complexes deposited onto the quartz slide, confirming the ability of the LB-slides to act as probes.

In Chapter 3 a novel approach to monitor kinase assay activities is described. Using the Eu(III) complex developed in Chapter 2, an assay able to discriminate between ATP and ADP was developed. As was introduced in Chapter 2, the same experiment that showed this discrimination in solution, were also performed using SAM LB-films that had been deposited onto a quartz slide, forming, to the best of our

knowledge, the first examples of a LB based assay for monitoring kinetic activities in real-time using such lanthanide complexes as SAMs. As before, this recognition process was monitored by observing the changes in the photophysical properties of the lanthanide complexes.

Chapter 4 presents the wide field of applications of the Ln(III)-cyclen based complexes, by extending the application of such systems towards forming self-assemblies with other organic molecules in a host-guest manner. The main focus of the Chapter is to show the development of a self-assembled system in which a tripodal ligand based on the benzene-1,3,5-tricarboxamide (BTA) motif, functionalised with terpyridine ligands, binds to the Ln(III) ion involved in the complex with heptadentate cyclen ligand which contains a strongly hydrophobic tail. The resulting aggregates were studied in solution through spectroscopic means and their mophological features were studied by SEM after deposition onto silica substrates, to inspect the photophysical and supramolecular properties of the system.

Chapter 5 describes the synthesis, characterization and the potential of application of a new cyclen based ligand complexed with Tb(III) and Gd(III) ions, that could be applied in several research fields but the main focus is on the formation of Gd-**49** and its potential application as MRI contrast agent. The work in this chapter is quite preliminary and the complexes were studied in solution using luminescent spectroscopic means and by SEM after deposition on silica substrates. Studies in vitro was performed using a novel microscopic technique called “Two Photon Microscopy” in order to investigate the ability of the complex to interact with the cell wall and act as a probe. The future work from this chapter will focus on exploring the properties of the Gd-system in NMRD measurements, which unfortunately could not be done during this PhD studies.

Acknowledgments

DISCLAIMAR

Acknowledgements are deliberately written in Brunish

I would like to express my special thanks of gratitude to Prof Thorfinnur Gunnlaugsson for give me the possibility to work with him and for his support and encouragement, in a difficulty moment like this (is 2020, the corona virus year) you found the time for helping me, so many thanks. Oxana, there are no words to describe what you have done for me, I have a big debt for you, at least I own you a kidney or a lunge, your choice. To say "thanks at all the " group" It would be an understatement, so thank Bjorn, Jason, Amy, Dermot, Sandra, Anna, Eoin, Sam, Gearóid, Dawn, Sachi, Raju, Chris, Helen and Elena for all the help, thanks June for turning my brunish in English. Thanks Hannah and Isabel, my brother in arms (or maybe sister in arms????? I'm confused), we have been through a lot. A special thanks to Emanuele for all the time spent helping me, SAM images, correction, psychological support and as expert of cuneiform writing. Thanks to Adam, the Schrödinger Post Doc. Thanks to my future wife for still bear with me, for support me and for keeping me sane (more and less). Infine, grazie alla mia famiglia, grazie Mamma, grazie Papa, grazie Sorella, grazie Nonna, grazie Nonno, grazie Zia Lara e grazie Zio Gianfranco, grazie Agata e grazie Pietro, ma non voglio dirvi grazie per il supporto morale (o almeno non grazie solo per quello), ma grazie per avermi e par farmi ogni giorno, sentire una persona speciale.

All these years far from home have been really a great experience that make me grow as person. A different culture, I saw that the world is bigger than that I thought. There was bad moment and good moment, happiness a sadness, but even in the darkest time, there was always something to "lift me up" and this something is represented from all the people mentioned above, so again, THANK YOU.

List of Abbreviations

ATP	adenosine-5’-triphosphate
ADP	adenosine-5’-diphosphate
Boc-Osu	*N*-(*tert*-butoxycarbonyloxy)succinimide
BTA	benzene 1,3,5-tricarboxamide
btp	bis-triazolyl pyridine
DMSO	dimethyl sulfoxide
DNA	deoxyribonucleic acid
eq.	equivalents
Et_2O	diethyl ether
EtOAc	ethyl acetate
IR	infra-red
J	coupling constant (Hz)
m-	*meta-*
M	molar (mol dm^{-3})
m	multiplet
m/z	mass to charge ratio
MALDI	matrix-assisted laser desorption/ionisation
LB	Langmuir Blodgett
o-	*ortho-*
p-	*para-*
$PhCOO^-$	benzoate anion
ppm	parts per million
RT	room temperature
s	singlet
SEM	scanning electron microscopy
t	triplet
TBA	tetrabutylammonium
TEA	triethylamine

UV-vis	ultraviolet-visible
λ_{max}	wavelength of absorbance maximum (nm)
ν_{max}	frequency of molecular vibrations (cm^{-1})

Table of Contents

Chapter 1-

1.0 Introduction

Supramolecular chemistry is the chemistry of the intermolecular bond, covering the structures and functions of the entities formed by association of two or more chemical species.[1] The spatial organization of the molecules depends on many different, weak (electrostatic interactions, hydrogen bonding, π-π stacking interactions, van der Waals forces, and hydrophobic or solvophobic effects)[1] and strong (covalent and ionic) forces. The classical chemistry approach consists of breaking covalent bonds and creating new, different molecular structures. Supramolecular chemistry, by contrast uses weak (and/or dynamic) bonds in order to create structures, many of which was also formed by using reversible bond and ionic interaction. Supramolecular chemistry presents different advantages, one of the most important of which is the formation of supramolecular structures that can occur spontaneously, without using complicated organic synthesis. Pre-organization is the key property by which molecules achieve this; once a pre-organized system is subjected to the appropriate chemical conditions, the reaction reaches the thermodynamic or kinetic equilibrium spontaneously.[2] Such a process is termed "self-assembly". In nature, a combination of pre-organization and a variety of supramolecular interactions can lead to the formation of large complex and/or ordered biological structures with high precision. These processes dominate in systems such as folding of polypeptide chains into proteins and the folding of nucleic acids into their functional forms. Supramolecular chemistry has undergone exponential growth in the last 50 years, in line with the development of its key structures such as macrocyclic ligands[3], cryptands,[4] ethers,[5] catenanes[6], and calixarenes[7, 8]. Many researchers have studied self-assembly processes to understand the dynamics of the systems involved and it has been shown that one of the principle ways to exploit the pre-organization is to use the coordination properties of transition metal ions.[9, 10] Further research has shown that these properties can be extended to the lanthanide ions, which allows for the development of supramolecular lanthanide assemblies that can exhibit the unique luminescence and magnetic properties associated with these ions.[11-13] The focus of this Thesis is the development and evaluation of novel luminescent supramolecular cyclen based

architectures with a wide range of applications from biological analytes detection to the formation of novel luminescent gel arriving at the synthesis of new potential MRI contrast agents. In the first chapter the main topics discussed in this thesis will be introduced, starting from the basic information about the luminescence and application in the chemosensors area. The unique photophysical properties of the lanthanides will be explored and their applications in the probes area, quoting several examples from different groups, including Parker, Pope, Gunnlaugsson, *etc*. This chapter will feature a section on the deposition and the applications of the Langmuir-Blodgett films and their potential application in biology.

1.1 From the molecule to the supramolecular systems to the materials

As previously mentioned, supramolecular chemistry gives the framework for design of interactive system.[3] Because of this wide range of applications, it can be considered as a bridge between different areas such chemistry, biology *etc.* In 1987, the Nobel prize in Chemistry was awarded to Lehn, Pedersen and Cram for their discovery in developing new molecules such as cryptand,[14] cavitands [15] and crown ethers.[16] Starting from this, the interest in supramolecular chemistry has quickly increased among researchers, and we now understand how to build supramolecular structures, creating larger and complicated architectures like macromolecules such as the rotaxane,[17] MOFs (metallic organic frame works) and clusters.[18-21] The first concept of template synthesis was presented by Sauvage that using a template synesis made an interlocked molecule.[22-25] Going in most recent times, Gunnlaugsson and Leigh gave an important contribution in to the world of the interlocked systems and rotaxanes [26-30] and over the years this contribution became stronger, comprising the principles that leads to the intermolecular interactions and building of new supramolecular materials. One of the topics of the studies performed from the Gunnlaugsson group is the developing of tripodal system using the terpyridinic ligands based on the benzene-1,3,5-tricarboxamide (BTA). These systems proved to be able to undergo a self-assembly process themselves but also upon the addition of metal ions allowing to develop soft materials for different applications. It has been proven that the lanthanides metal ions can lead this self-assembly process, indeed ions such as Eu(III) and Tb(III) can induce self-assembly process forming gel with unique luminescence properties. These gels are formed through non-covalent bonds between the ligands and also metal-ligand interactions

since that induces the sol to gel transformation.[31-33] One of the main characteristic of the supramolecular gel is that it alters its phase or their photophysical properties are altered in response to an external stimulus (light, temperature, pH *etc*) and these properties can be employed for the development of stimuli responsive smart materials. One of the main advantages in the addition of the Ln(III) ions is the tuneable luminescence behaviour and stable photoexcited states and we have taken advantage of those in the development of this thesis.

1.2 Luminescence properties

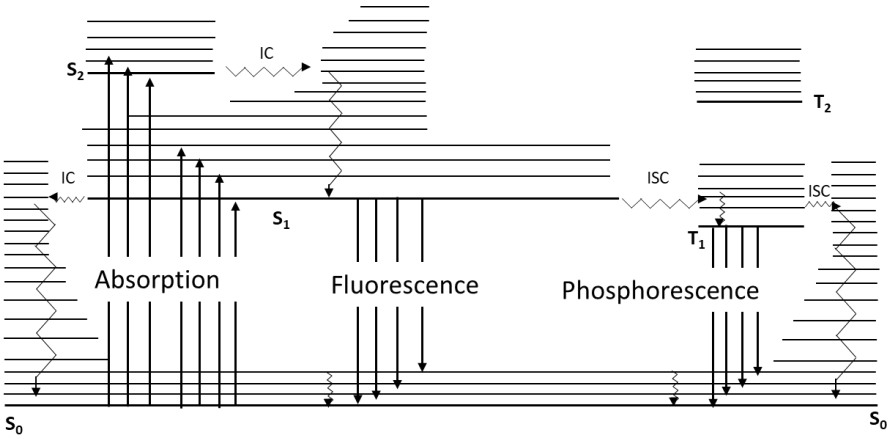

Figure 1.1*: Perrin- Jablonski diagram and illustration of the relative position of absorption, fluorescence and phosphorescence spectra.*[15]

The term luminescence describes all the processes of emission from a substance, generated by the decay of electrons from the excited states. The electrons can be excited by different ways: chemical reactions, biological processes, radioactivity and by the absorption of light. This last process is related to photoluminescence.[34] There are two main types of luminescence; fluorescence and phosphorescence. These processes differ in the nature of the electron spin undergoing the electronic energy transition. For fluorescence there is no associated change in electron spin, making it a spin-allowed transition which exhibits short-lived excited states. In phosphorescence, the electron changes spin, and thus it is formally a spin-forbidden transition. Spin orbital coupling (SOC) can nevertheless relax the spin selection rule, but forbidden nature of the process means phosphorescence exhibits longer lifetimes of the excited state. To better understand these two processes, we can refer to the Jablonski diagram[35] in **Figure 1.1** When the target molecule absorbs a photon of a particular energy, an electron jumps from the singlet ground state S_0 to a single excited state S_n. The permanence of the electron into the excited vibration state is

extremely short (the range is between10^{-7} to 10^{-15} seconds), undergoing rapid internal conversion (IC) processes down to the S_1 state (Kasha's rule). The electron can then relax back to the S_0 ground state by emitting a photon of light. This is called fluorescence. Another mechanism to release energy is the phosphorescence, we have again an S_0 ground state and the two excited states, S_1 and S_2 along with excited triplet states, T_n. As with fluorescence, the excitation happens through absorption of a photon, after which the excited state undergoes rapid internal conversions to the S_1 state. Between the singlet state and triplet states, a so-called intersystem crossing (ISC) can occur since the T_1 is a transition between isoenergetic vibrational levels belonging to electronic states of different multiplicity, the presence of the Ln(III) ion can allow this process due to the fact that it is an heavy atom, substantial amounts of spin-orbit coupling occur which make this otherwise forbidden process possible. This internal conversion is an electronic transition between two excited states. But contrary to internal conversion, in the ISC there is a spin reversal from singlet to triplet. In this process, the triplet states of the electrons have parallel spin which is noted as $(\uparrow\uparrow)$[35]. For example, exciting a molecule in the starting vibration level of the S_1, it can move it to the isoenergetic vibrational level of the T_n triplet state. The mechanism of vibrational relaxation brings it in to the lowest vibrational level T_1. In this case, ICT can compete with other de-excitation mechanism from S_1 (such as fluorescence and IC). Usually, the crossing between states of different multiplicity is forbidden, but spin orbit coupling can be large enough to allowed it. If the transition $S_0 \rightarrow S_1$ is of $n \rightarrow \pi^*$ type for instance, ISC is efficent.[35] However, the use of heavy atoms and of transition metal and lanthanides can greatly increase the ISC possibility.

1.3 Luminescent chemosensors

We can define a chemosensor as a structure being able to recognize a species, called guest, through supramolecular recognition using a receptor, this recognition has to produce a changing in the system that can be detected by means of physical parameters. In many cases the presence of the guest can "switch on" or "off" a physical property.[36] Luminescence is one of the most common methods for the detection of analytes as it has many advantages such as high sensitivity, high

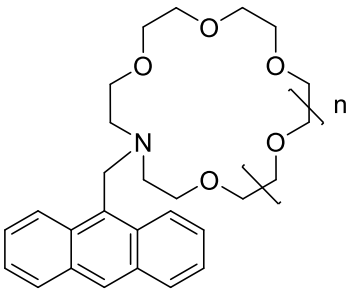

1

selectivity towards optical signatures and, most importantly, a fast response time. When we use a luminescent molecular sensor, a chromophore acts as a signal transducer that converts the input signal, by the receptor, into an optical "message", due to changes in the luminescence properties.[37] The mechanisms beyond this process are explained in section 1.2 because the ICT (internal charge transfer) states are observed in a push-pull π-system that consist of an electron donating and an electron withdrawing group. Many ICT chromophores are luminescent, and the ICT states can be energetically stabilized upon binding of the target analyte. One of the first example of a luminescent sensor dates from 1986 when de Silva *et al*[38] designed and developed a fluorescence sensor for Na(I) and K(I) ions (structure **1**). The selectivity is given from the type of crown ether used. To have a sensor able to bind selectively Na(I) n has to be 0, while if n=1 then the receptor will bind only K(I). When there is no metal bound the anthracene does not show fluorescence. The explanation for this is shown in **Figure 1.2**. In the absence of a metal, photoinduced electron transfer (PET) from the Ione pair of the nitrogen of the crown ether quenches the fluorescence emission. However, upon binding a metal ion, there is an increase in the oxidation potential of the receptor such that it becomes energetically unfavourable to participate in electron transfer (ET) to the anthracene excited state, meaning that the signal is no longer quenched, and an emission signal is observed. A more modern example of fluorescent sensor is the compound 2, developed for the detection of cobalt and nickel ions in water by Abebe *et al*.[39] In absence of the metal ions the fluorescence signal is really weak, but the addition of Co(II) or Ni(II) the ring opens allowing the metal binding causing a significant enhancement of the fluorescence signal.

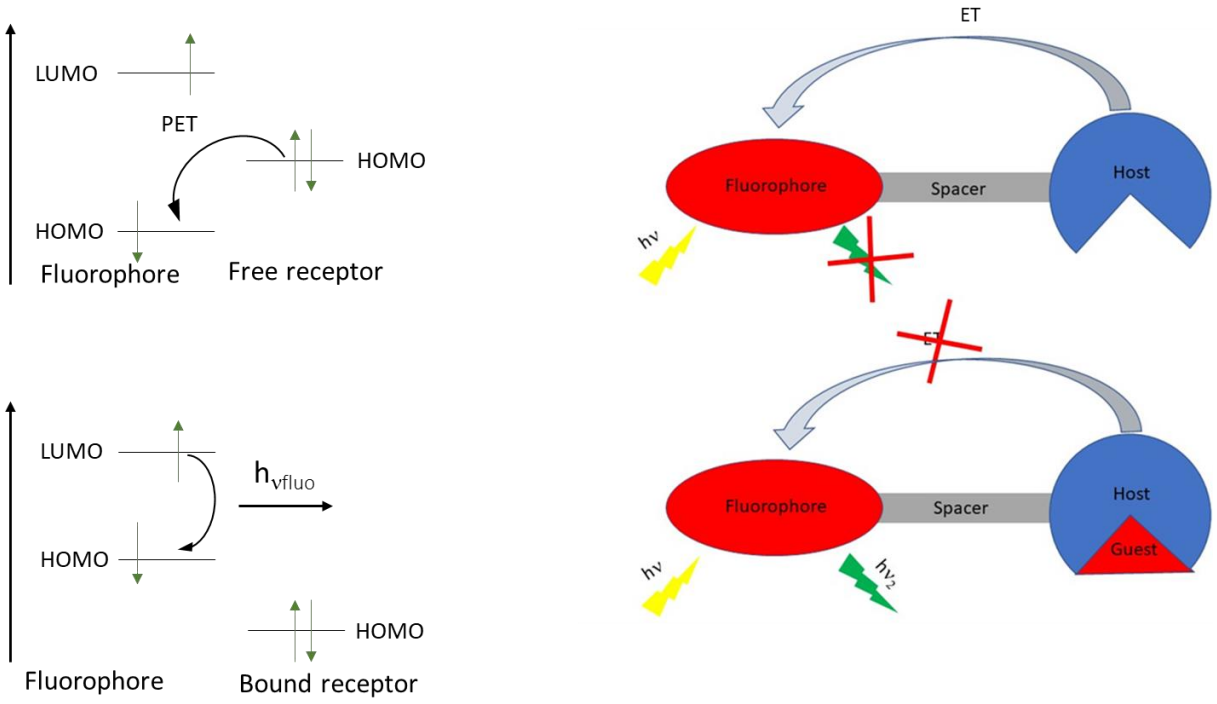

***Figure** 1.2: The PET signalling mechanism when the receptor is in free, electron transfer from the receptor's HOMO can occur, preventing fluorescence and when the receptor is bound to a guest, its oxidation potential increases and electron transfer from the receptor's HOMO becomes thermodynamically unfeasible, resulting in the "switching on" of the fluorescence due to removal of the quenching pathway, where HOMO – Highest Occupied Molecular Orbital; LUMO – Lowest Unoccupied Molecular Orbital.*[38]

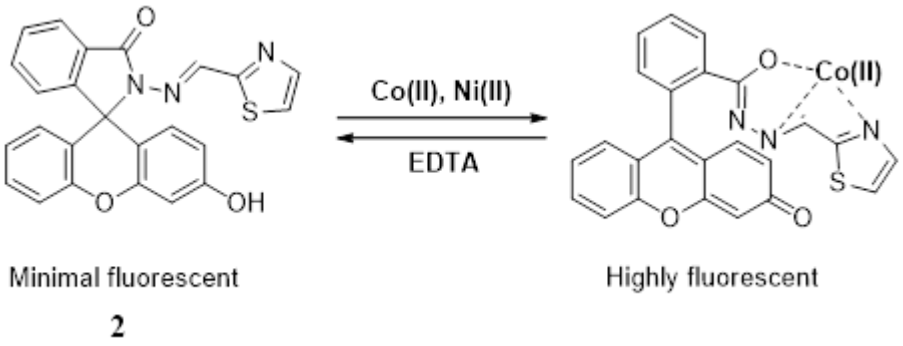

Another example of a chemosensor was published by Akkaya *et al*. This molecule has two BODIPY (boron-dipyrromethene) scaffolds bound together through a bipyridyl receptor and is able to sense phosphate ions.[40] When the compound is in organic solvent, the system shows a bright green fluorescence that can be quenched by addition of Zn(II) cations *via* PET, due to formation of the non-fluorescent BODIPY based-Zinc(II) complex (**Figure 1.3**). It is really interesting that it is not a displacement system since the phosphate does not displace the Zn(II) but it is able to neutralize (in part) the charge on the metal by electrostatic interactions

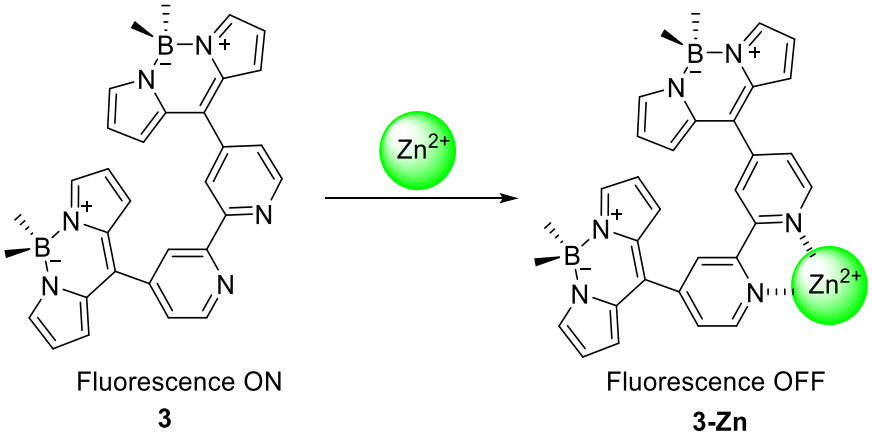

Figure 1.3 *BODIPY-based chemosensor and its fluorescence quenching process.*[40]

The last example, molecule **4** which is an ICT based ratiometric sensor for imaging cellular activity.[41] This sensor is the first mitochondrial molecular polarity probe that uses the ICT mechanism. This compound is called "BOB" and uses a donor-π-acceptor system wherein a coumarin donor group is conjugated with a benzothiazene acceptor group. The BOB emission band is predominating in the green spectra range with a weakly shoulder in the red region. The green emission band shows a high sensitivity to polarity changes, which allows for monitoring changes in polarity inside the mitochondria. ICD gives rise to polar excited state

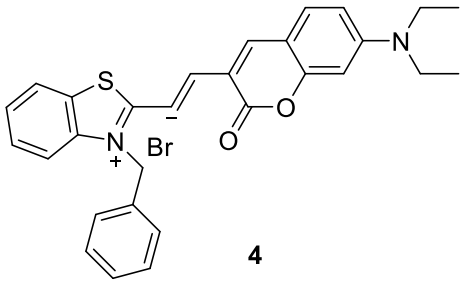

4

(with a big dipole moment) so the donor and acceptors part of the molecule can be stabilised by the solvent. So in organic non-polar solvent, the interaction is not strong, so the excited state gives rise to large emission, i.e.. high quantum yield. Here the HOMO-LUMO gap is big. But in polar and particularly in hydrogen bonding media the solvent can interact (via for instant hydrogen bonding) and stabilise the excited state. That lowers the HOMO-LUMO and the emission is shifted red. In the cells I am not sure, but obviously the environment is giving rise to the red emission, so its the HOMO-LUMO gap that is smaller there They successfully distinguished cancer cells from normal cells by detecting the mitochondrial polarity differences between the two.

1.4 The Lanthanides metals

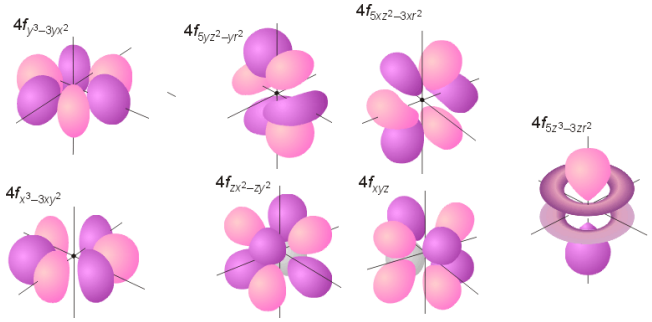

Figure 1.4: Lanthanides orbital configuration

Lanthanides are a family of metal ions that comprise 14 elements starting from cerium and arriving at lutetium and including lanthanum (with the addition of electrons into one of the seven 4f orbitals). Because of the low values of the three first ionization enthalpies of the lanthanides, in solution and in the solid state, they exist as complexes in the 3+-oxidation state. Other oxidation states (Ln^{4+} and Ln^{2+}) are uncommon but possible, with Ce existing mainly in it form Ce^{4+}, and Eu and Yb being metastable ions in the M^{2+} state in both polar and apolar solvents, and in the solid state.[42] The reason for this is due to the electronic configuration which stabilizes these states. Another characteristic of the lanthanides is an incomplete shell. The orbitals $5s^2$ and $5p^6$ shield the 4f orbitals that lie close to the nucleus. In terms of the HASB (hard and soft acid and base)[43] concept, lanthanides act as hard cations and so can form few complexes with hard ligands. They are not available to form new bond because the 4f electrons constitute the inner shells. The electronic structures of the lanthanides are described by the 4 quantum numbers n, L, S and J[44] and these give a description of the energy levels, represented by $^{2S+1}L_j$ (where 2S+1 represents the spin multiplicity of the state).[16] The interactions which separates the configuration into the L terms is the non-Coulombic repulsion between the electrons in the 4f orbitals, which results in a split of the terms by the spin and the orbital angular momenta. This is called spin-orbit coupling. In the case of any further splitting given by any small but significant field from the ligand, Ln^{3+}ions have the 4f orbitals fully shielded by the 5s and 5p orbitals. Ln(III) can be excited using electromagnetic transition[15] that causes a redistribution of the electrons into the 4f subshell. This process is formally Laporte forbidden (f-f transition) but nevertheless, there are different mechanisms that can make these transitions possible, such as vibronic coupling that causes a change in the geometry about the lanthanide ion. **Figure 1.5**[45] shows the energy gaps and the main luminescence transitions for the lanthanide aquo ions. Luminescent sensors based on Eu(III) and Tb(III) are the most

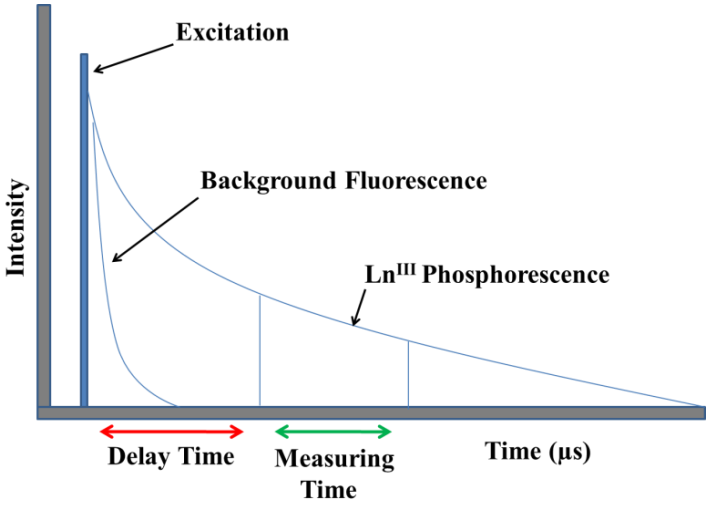

***Figure 1.6**: A time delay between excitation and Ln(III) phosphorescence detection allows background fluorescence to decay to negligible levels.*

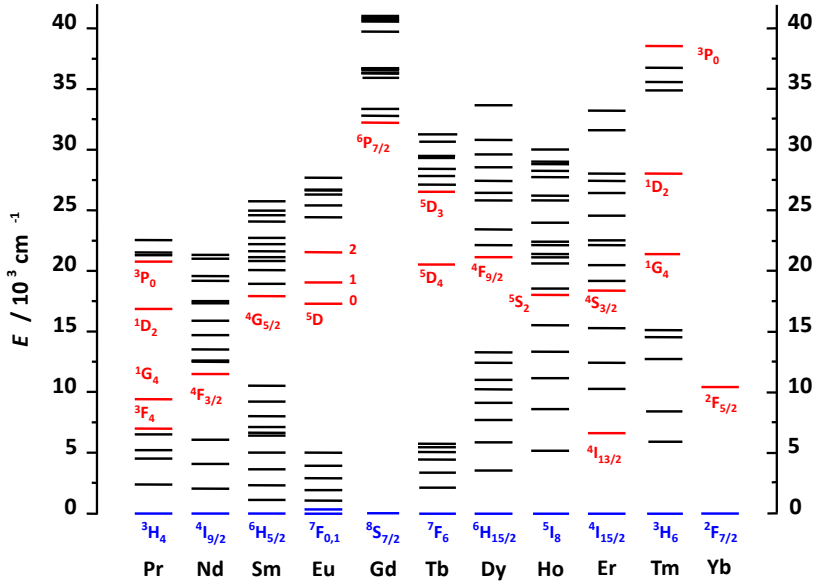

***Figure 1.5**: Partial energy diagram of the lanthanide aquo ions.*[27]

common because of the high luminescence intensity of its complexes with various organic ligands and their respective energy gaps ($\Delta E = 12300$ cm^{-1} for the $^5D_0 \rightarrow {}^7F_6$ for Eu(III) and $\Delta E = 14800$ cm^{-1} for the $^5D_4 \rightarrow {}^7F_6$ for Tb(III)), which correspond to the red emission for Eu(III) and green for Tb(III). The energy levels of the excited and ground states in Nd(III) ($^4F_{3/2} \rightarrow {}^4I_J$) and Yb(III) ($^3F_{5/2} \rightarrow {}^3F_{7/2}$) are however closer together giving less emissive species, and the emission generated in this case is in the near-infrared region of the electromagnetic spectrum.[45] One of the main advantages in the use of lanthanides is the long luminescence lifetimes, which are in the range of 10^{-2}-10^{-6} seconds (s) for Eu(III) and Tb(III) and microseconds (µs) for Sm(III) and Dy(III), while common organic dyes have luminescence lifetimes in the order of the nanosecond (ns).[11] Because of these luminescence properties,

lanthanides are also used to create biological probes for cellular imaging and for analyte detection in biological media.[46] In particular, the long lifetimes can be used to avoid the detection of short lived autofluorescence from fluorescent biomolecules; a technique known as Time Resolved Detection (TRD).[47] **Figure 1.6** shows the measuring (after the excitation) of the Ln(III) emission and displays how its long lived Ln(III)-centred luminescence after a particular time interval allows for elimination of background autofluorescence from biological organic fluorophores and light scattering, elucidating an intense signal with high resolution.[48] However, a major drawback in the use of Ln(III) ions as luminescent probes *in vivo* is that the *f-f* transitions are Laporte forbidden, and therefore they exhibit weak absorption with low extinction coefficients ($\varepsilon < 4\ M^{-1}\ cm^{-1}$),[11, 49] and hence also low quantum yield of Ln(III) luminescence, making them photophysically silent in acceptable concentration ranges. In order to overcome this problem, the so called "antenna effect" is exploited (**Figure 1.7** A).

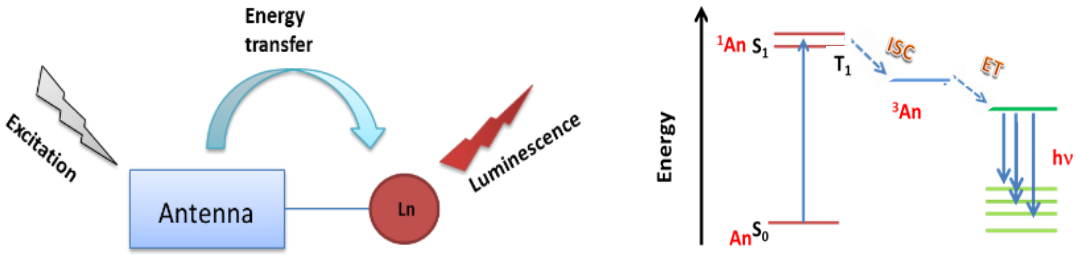

***Figure 1.7**: Energy transfer between the antenna and the lanthanide (A). Modified Jablonski diagram (B).*[12]

The antenna effect consists of using a chromophore as a sensitizer which absorbs a suitable wavelength of radiation that can undergo energy transfer to the lanthanide

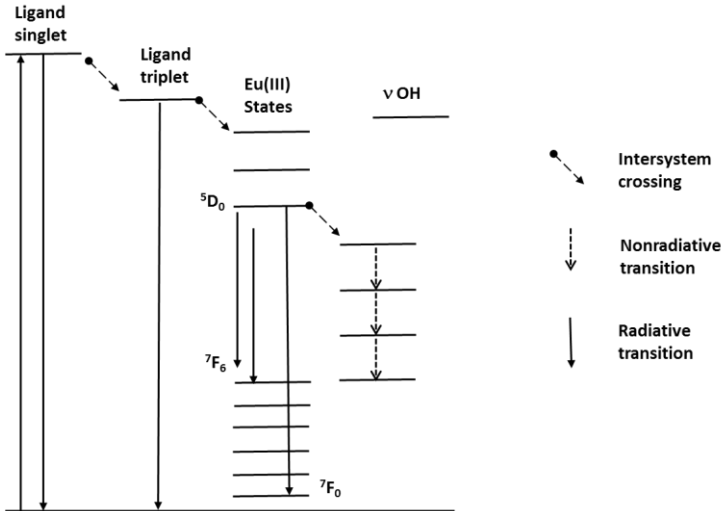

***Figure 1.8** Antenna effect along with Eu(III) luminescence and simultaneous quenching by the presence of O-H oscillators.*[12]

excited state (**Figure 1.7** B). The ground state antenna (An) absorbs excitation energy in the form of a photon of light (hυ), generating a singlet-excited state (^{1}An). This energy is then transferred to the triplet state of the antenna (^{3}An) *via* ISC (as said previously, fluorescence is usually extremely fast, and thus strong spin-orbital coupling (SOC) interaction is required enabling for the electron to flip its spin). Due to the presence of the Ln(III) ion, a heavy atom, substantial amounts of spin-orbit coupling occur which make this otherwise forbidden process possible. The excited state of the lanthanide, Ln(III)*, can now be efficiently populated from the antenna's triplet state through an intramolecular energy transfer (ET) process provided that the ^{3}An lies at least 1700 cm^{-1} higher in energy than the lanthanide excited state. This large energy gap prevents any significant back-energy transfer that would occur if the energy gap was smaller. The excited state of the Ln(III) is now able to relax to the ground state by emission of light, resulting in the characteristic lanthanide emission. The lanthanides Ln(III) such as Eu(III) and Tb(III) are the most frequently studied emissive Ln(III) ions and have their Ln(III)* states ($^5D_0$ and $^5D_4$) lying at 17200 cm^{-1} and 20500 cm^{-1}, respectively. Bipyridines, terpyridines, substituted phenyls, and naphthyl groups are preferred as chromophores as they possess excited states that lie above 1700 cm^{-1} of these values.[50, 51] Another issue that lanthanide luminescent complexes experience in aqueous solution is that another pathway is available for deactivation of the excited state of the lanthanide, in the form of vibrational energy quenching through O-H oscillators, particularly from water molecules. **Figure 1.8** shows the antenna effect along with Eu(III) luminescence and simultaneous quenching by the presence of O-H oscillators (only a selection of the radiative transitions is shown).[12] An empirical method to quantify the number of coordinated water molecules directly attached to the Ln(III) metal centre (q value) was developed by Horrocks *et al*. for a range of Eu(III) and Tb(III) complexes by measuring Ln(III)-centred emission decay in D_2O and H_2O. The O-D oscillators contribute only minimally to the deactivation process of the Ln(III) excited state and all other quenching processes are assumed the same in H_2O and D_2O.[11] The q value or the hydration states, (indicate the number of water molecules bound to the metal centre), is a parameter of the complexes that can be determined by the difference in the luminescent decay rates of the Ln(III) in H_2O and D_2O. This formula was modified by Parker *et al*. who took into account the deactivation by N-H oscillators in addition to O-H oscillators to give Equations 1 for Eu(III) and 2 for Tb(III), where

an additional correction factor of 0.075 ms^{-1} should be made for each carbonyl-bound amide NH oscillators with Eu(III):[17, 52]

Equation 1: $qEu(III) = 1.2[(1/\tau_{H2O})-1/\tau_{D2O})-0.25]$

Equation 2: $qTb(III) = 5[(1/\tau_{H2O})-1/\tau_{D2O})-0.06]$

There is a minimization of the energy transfer process thus the protection of the Ln (III) and prevention of surrounding solvent vibrating oscillators from entering the first coordination sphere and binding to the Ln(III). To achieve this, the designing of the ligand had to satisfy several conditions, the most important of which is that it has to fully occupy coordination environment of the Ln(III) ion and 'shield' them from the deactivation *via* processes of this nature.

1.5 Lanthanide macrocyclic complexes

The Ln(III) ions are toxic to biological systems, mostly due to their size, which means they can displace Ca(II) from the membrane of the cells.[53, 54] Until a few years ago there was no evidence of the presence of the lanthanides into the biological

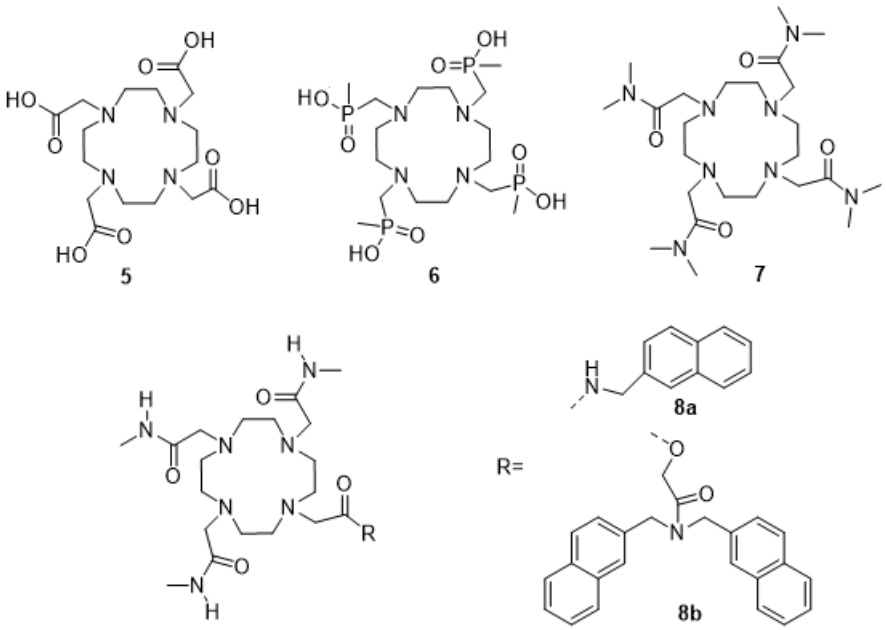

environments but in a recent study they were found it in some acidophilic microbe isolated from the mudpot of the Vesuvio (an Italian volcano).[55] The way to use Ln(III) for *in vivo* sensing is the encapsulation by thermodynamically and kinetically stable ligands which in turn form stable complexes.[18] This can be achieved by devising ligands that are suitable for encapsulation of the Ln(III) ions and can satisfy their high coordination requirements, hence shielding it from any solvent coordination that may cause quenching of the Ln(III) emission. A way to do so is by using macrocycles; these molecules have donor atoms arranged in fixed positions so that there is a preorganized cavity of a well-suited diameter for the binding of Ln(III) ions. Cyclen (1,4,7,10-tetraazacyclododecane) is one of the most used ligands for the complexation of the Ln(III) ions, the cavity perfectly fit the metal ions and one of the most useful features is the possibility to functionalise it with different pendant arms containing amine or carboxylate groups. The Ln (III) can coordinate four nitrogen's of the cyclen and four carboxylate's/nitrogen's of the pendant arms, satisfying the Ln(III) demanding coordination environment. This type of organized macrocyclic system allows the minimum amount of reorganization energy upon complexation, as the conformations of the free and bound ligands are relatively similar.[19, 45] The ligands **5**-**8** are all cyclen-based and were designed and synthetized to form stable Ln(III) complexes. These examples prove that a variety of pendant arm groups can be used in the functionalisation of the macrocyclic ring; the groups most frequently used to be carboxylates (**5**)[20], phosphinates (**6**)[21] and amides (**7**). [56] Ln(III) complexes of ligand **5**, 1,4,7,10-tetraazacyclododecane-1,4,7,10-tetraacetic acid (DOTA) have been studied since the 1980s and the very first Eu(III) crystal structure was solved first by Spirlet and collaborators.[22] The DOTA ligand is most commonly complexed with Gd(III) ions to form Dotarem, $[Gd(DOTA)H_2O]^-$ [53], a magnetic resonance imaging (MRI) contrast agent. Dotarem is ideal to be used *in vivo* as its high thermodynamic stability constant K_{GdL} ensures that dissociation of the Gd(III) metal ion from the ligand is not likely to occur.[23, 24] Parker *et al.*[25] investigated the ability of cyclen with appended amide arms (**5**) to bind to biologically relevant cations such Li(I), Mg(II) and Ca(II) and found that **5** selectively binds to Ca(II) due to its tendency to form octadentate complexes. The ligands **3**-**5** form stable complexes with Ln(III); however, they lack a sensitising chromophore which would allow for indirect excitation of the Ln(III) ion and this limits the luminescence studies unless an external chromophore is added to the

system. Ligands **8a** and **8b** were developed by Beeby *et al*.[57] The presence of aromatic chromophores in one of their pendant arms makes it possible to obtain Ln(III) centred luminescence. In the case of the Eu(III) complex with **8b**, it was observed that the naphthyl group acted as an antenna chromophore for Eu(III), but the quantum yields for the metal emission were low (0.12% in MeOH and 0.19% in MeCN).[58] Eu(III) emission from complex **8b** was expected to be much more intense than that of **8a**, as it emits strongly at 400 nm, overlapping with the Eu(III) absorption band at 397 nm. However, this was not the case and the fluorescence emission intensity were reduced. The authors proposed that the reason for the decrease in intensity was that the ET quenching pathway was too fast when compared to excimer formation and subsequent energy transfer to the metal. The strategy of incorporating aromatic systems into the pendant arms as signalling moieties to take advantage of luminescent Ln(III) has been reported numerous times.[59, 60] These ligands have been extensively studied as receptors for Ln(III) due to their ability to fulfil the high coordination requirement and entirely enclose the metal ion centre. The next section will go into detail on some examples of lanthanide luminescent based systems, emphasising the wide variety of applications they have to offer. Compound **9a** and **9b** were developed by Stephen J. Butler *et al* for the detection of fluoride in water.[61]

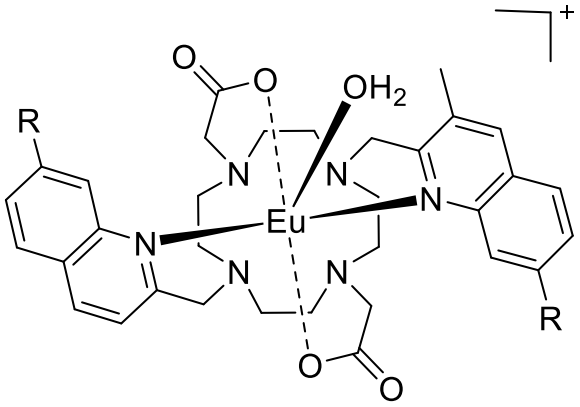

R

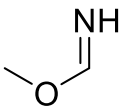

9a

H

9b

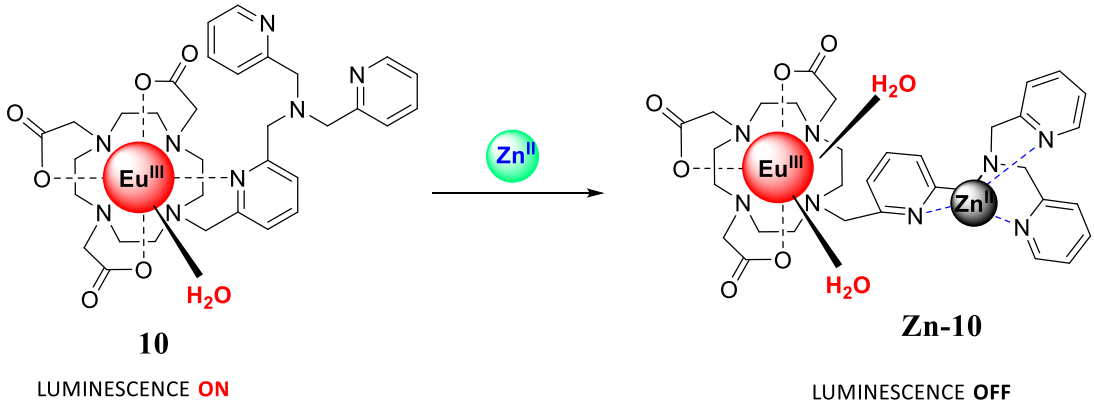

***Scheme 1**: Proposed mechanism for the quenching of the Eu(III) complex emission due to the binding of the Zn(II) ion.*[62]

The two-water soluble luminescent probes are able to bind and sense fluoride with a minimal interference from the other anions. The probes are based on a C_2-symmetric mono-cationic europium complex with bound two quinoline chromophores in trans position and with one molecular of water coordinated. Upon the binding of the fluoride the water is displaced resulting in an enhancement of the fluorescence signal. The pathway through which the antenna can sensitise the Ln(III) emission are reported in chapter 1.4 and through the next section, we will examine how those luminescent properties have been applied in the field of the Ln(III) based chemosensors for biological applications. Detection of metal ions such as Zn(II) has been growing an interest in the last few years because of the importance of this metal in many biological processes, such as human growth, and has been shown to be connected with degenerative conditions such as Alzheimer's disease. Different sensors have been developed, one of the most interesting of which was reported by Pope *et al*,[62] and it is a cyclen based Eu(III) complex (**10**). This is an ON/OFF luminescent system, where the presence of the Zn(II) ion can quench the emission of the Eu(III) centre (**Scheme 1**). Compound **10** consist of a functionalized cyclen Eu(III) complex incorporating a bis-picolyl unit that binds only Zn(II) ions over other biologically relevant metal ions, such as Mg(II) and Ca(II). All the luminescence studies were carried out in the HEPES buffer solution at pH 7.4 (140 mM NaCl, 4 mM KCl, 1.16 mM $MgCl_2$ and 2.3 mM $CaCl_2$). The pyridyl unit is serving as one of the arms of the cyclen unit and can act as an antenna and sensitise the metal centre emission. Once the Zn(II) is added the pyridyl unit is displaced from the Eu(III) in order to bind the metal ion. Without the coordination to the pyridyl unit, the Eu(III) has a free coordination site that can be occupied by a water

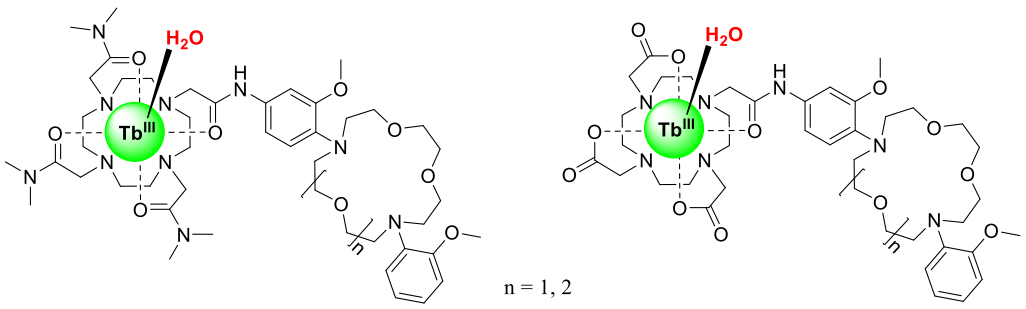

11 **12**

molecule and this results in a strong quenching of the luminescence. Furthermore, the emission band $J = 4$ undergoes significant changes, suggesting a major change in the coordination environment around the Eu(III) metal centre proving is ability to detect the Zn(II) in biological concentration (200-300 μM). Another example we given from the compounds **11** and **12,** developed by Gunnlaugsson *et al.*[62] and they showed that these complexes were able to recognize alkali metal ions such as Na(I) and K(I). These ions are involved in many cardiovascular diseases, stroke, and hypertension conditions. Both terbium complexes incorporating either a a diaza-15-crown-5 ether **11** for the recognition of the Na(I) and a diaza-18-crown-6 ether **12** for the selective recognition of the K(I) where developed.

A phenyl moiety links the crown ether to the cyclen framework to ensure an efficient sensitisation of the metal centre. Also, the aromatic crown ether works as an antenna and can sensitise the Tb(III), while the emission of the metal is modulated by the addition of the alkali metals. The pH effect on the emission was evaluated and has been demonstrated that in the range of pH of 4 to 9, there is a full "switch off" of the system luminescence, due to the protonation of the aniline and the deprotonation of the amide. Complexes **11** and **12** were titrated using a range of alkali and alkali earth cations in a buffered solution at pH 7.4 and it was found that only Na(I) and K(I) were able to switch on the luminescence, because they were able to fit the cavity of the crown ether, this binding affects lowering the HOMO-LUMO gap resulting in a change of the sensitisation of the Ln(III) centred emission, similarly as it was previously shown by de *Silva et al.*[38]

Two emissive lanthanide complexes have been developed from Andrew *et al*,.[64] to be used as luminescent probes for metal ions. They have incorporated an 8-aminoquinoline antenna for complex **13** and 1-amino-9,10-anthraquinone for the **14** into the cyclen framework, these antennae allow for long wavelength absorption and as such for the molecules luminescence in the near infrared region. Among the different lanthanides, Nd(III) and Yb(III) allow the sensitisation in this range. It was found that Nd(III) and Yb(III) complexes show a dual emission upon excitation of

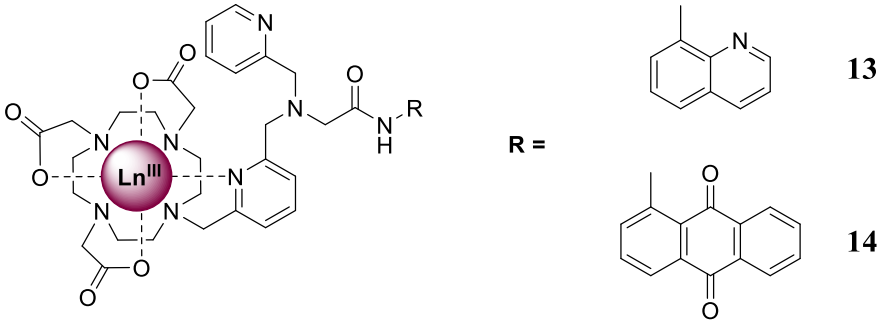

355 nm while the addition of d-block metal affects the emission of the complexes **13** and **14** formed using the Eu(III). Also, upon the addition of Cu(II) at pH 7.4 the Eu(III) centred emission had higher change quenching the pyridyl, anthraquinone, quinolone and Eu(III) emission bands. Upon the addition of Hg(II) the result was totally different, the Eu(III) centred emission had a slight enhancement in the anthraquinone and in the quinolone emission, but at the same time the band relative to the pyridine fluorescence decreased. The change in the relative ratio of the Eu(III) $^5D_0 \rightarrow {}^7F_J$ transitions is indicative of a change in the coordination environment of the Eu(III) metal centre.

Complex **15** was developed by Gunnlaugsson *et al*[65] and has no antenna moiety bound directly, but the analytes **16** and **18** work as external antennas, bound in a non-covalent fashion to the Tb(III) core. Tb-**15** is photophysically silent; however, upon the addition of one equivalent of the carboxylate external antennae, two molecules of water are displaced, forming a ternary complex. The Tb(III) luminescence can now switch on because of the efficient population of the excited states *via* indirect excitation from the antenna. The q value was evaluated and was found to decrease from two to zero, which indicate a displacement of the water molecules from the metal centre, substituted by the carboxylate groups of the antennae. Using compound **17** the binding process was followed by photophysical experiments and upon the addition of the ester derivatives, there was no

displacement of the water and consequently there was no modulation of the emission moving forward a displacement assay for the detection of *d*-metal ions that was developed by Gunnlaugsson *et al.*[26]

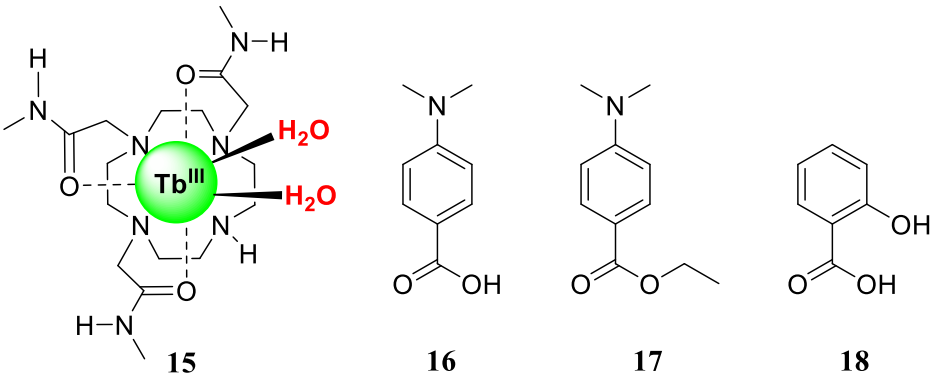

15 **16** **17** **18**

The Eu(III) complex **19** again does not have any antenna and two molecules of water are coordinated to the metal centre, so the luminescence is poor. In order to sensitise the metal centre an external antenna was added to the assay. BPS (4,7-diphenyl-1,10-phenanthroline-disulfonate) was chosen as it is known in the literature as a good Eu(III) sensitizer and for its selective colorimetric sensing of Fe(II).[27, 28]

At pH 7.4 the formation of the 1:1 complex was observed by monitoring the gradually increasing Eu(III) emission which reaches the maximum after the addition of 1 equivalent of BPS, then the photophysical properties of **19**-BPS complex were evaluated in the presence of different metal ions such as Ca, Cd, Co, Fe, Mg, Ni and Zn. Upon the addition of Fe(II) the emission of Eu(III) strongly decreased, reaching

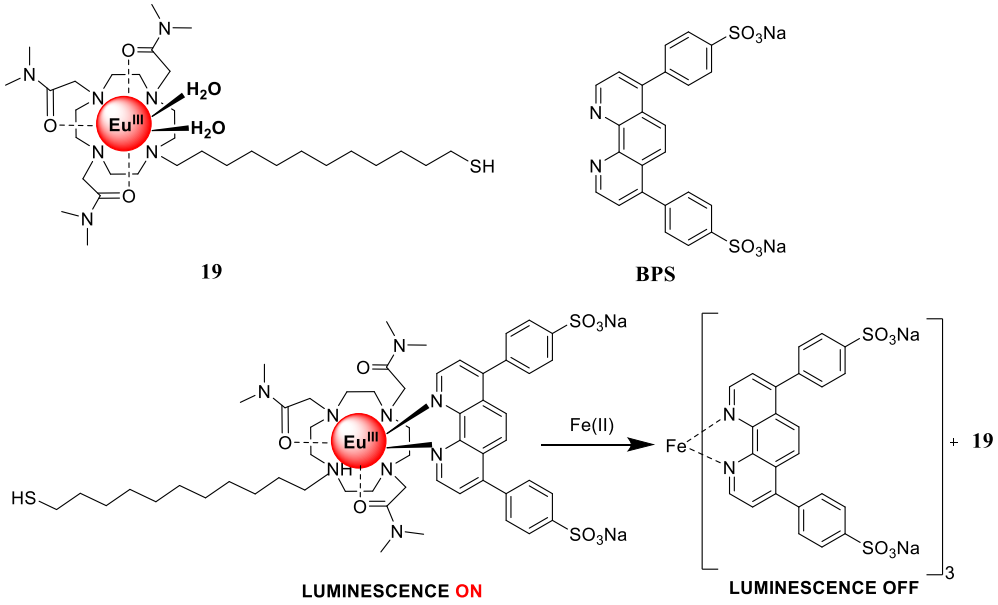

Scheme 1.1: *Proposed mechanism for the quenching of* ***19****-BPS complex due to the binding of the Fe(II) ions.*[26]

a plateau at *ca*. 0.33 equivalents, indicating the displacement of the BPS from **19** and the formation of a new complex BPS-Fe(II) in a 3:1 stoichiometry. The addition of similar cations such as Co(II), Cu(II) and Ni(II) caused a decrease in emission of the Eu(III) spectra comparable with the Fe(II) one, but only minor changes were observed in the absorption spectra. The complex thus proved to be able to sense Fe(II) in the presence of different anions such as carbonate, lactate, citrate and phosphate. The complex **19**-BPS has been shown to give both good selectivity and effective sensitivity for Fe(II) in competitive media and was the first example of a lanthanide luminescent displacement assay for biologically active *d*-metal cations.

1.7 Lanthanide complexes with cyclen ligands as biological probes

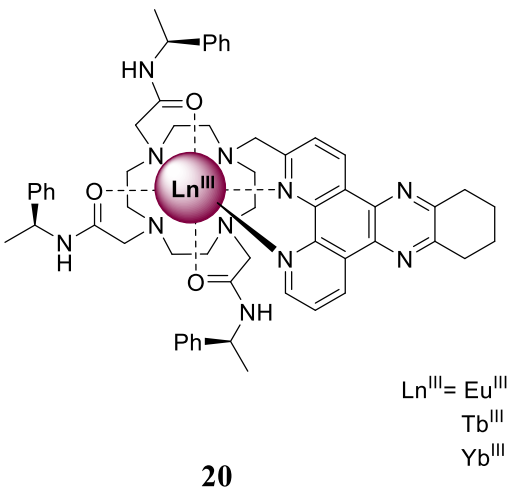

20

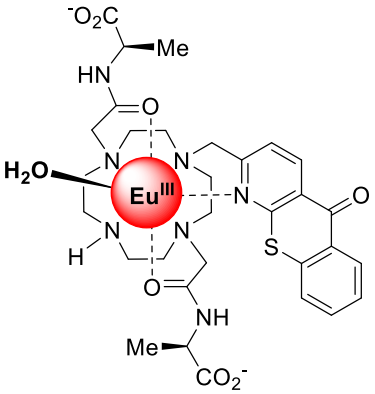

21

Over the last few decades, chemists and biologists have led a focused effort to design imaging and biological probes. Significant research efforts have focused on Ln(III) cyclen complexes that are highly emissive and can satisfy the conditions[29] for the use of metal based complexes in water, namely: high cell permeability, high thermodynamic and kinetic stability, high selectivity for the target substrate, water solubility, low toxicity and reversible biding with the substrate. Amongst various probes reported to date, complexes **20** and **21** are two elegant examples of cyclen-based biological probes, developed by Parker *et al*. Complex **20** was developed and investigated for its enantioselective ability to bind human serum albumin (HSA)[30, 66].

An NMR-base technique called STD (saturation transfer differences) was employed to investigate the ability of the complex to bind the HSA. STD spectroscopy allows for detection of transient binding of small molecule ligands to macromolecular

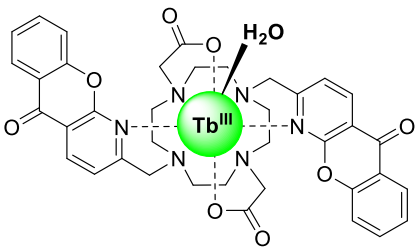

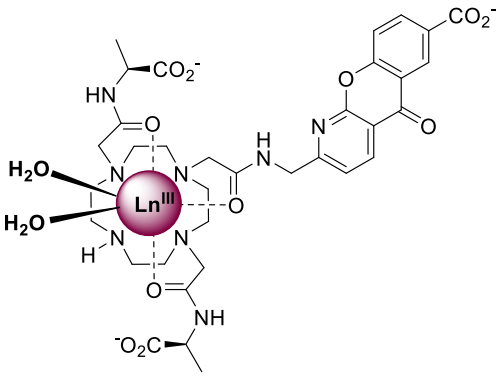

22 **23**

receptors. In this method the transfer difference relies on the possibility to selectively saturate protons of macromolecular receptor by irradiating the spectral region containing "wings" of broad resonances of the macromolecule which is also free of any smaller molecule signals. Due to effective spin diffusion saturation quickly propagates across the entire receptor. If the smaller molecule ligand binds the receptor, saturation will also spread onto the ligand. The result will be that intensity of the ligand signal will be attenuated. Subtraction of resulting spectrum from the reference spectrum without saturation yields the STD spectrum containing only signals of the binding ligands. The range of applicable dissociation constants is approximately 10^{-3}-10^{-8} M.[67] STD method can be used to determine which part of the ligand molecule (Ln(III) complex in this case) is responsible for binding since the most strongly interacting groups will show a stronger STD effect. For complex **20** the stereochemistry was investigated too, using the *SSS* and *RRR* isomers, and it was found that the *SSS* had higher affinity for HSA compared to the *RRR*-enantiomer. Another important marker to detect is the citrate present in the biological fluid. It has been proven that levels of citrate are significantly reduced in prostate cancer tissues, and so this feature can be used as a marker to diagnose prostate cancer.[68] With this in mind, a luminescence assay based on complex **21** was developed to detect citrate in biological media.[69, 70] The major antagonist in the detection of the citrate is lactate, so preliminary studies were focused on understanding the selectivity of the assay. The system proved to be able to discriminate between the citrate and lactate with a selectivity ratio of 89:1. The modulation of the emission of the Eu(III) is concentration dependent, with the concentrations used (0.08 and 0.45 mM) showing considerable changes in the ratio of the intensity of the various bands that are associated with the selective and

reversible binding of the citrate to the Eu(III) metal centre. The resulting complex is a 5-membered ring chelate of citrate molecules. From the different emission spectra, Parker and co-authors proved that it was possible to distinguish the **21**-citrate from the **21**-carbonate, -lactate and -phosphate ternary complexes. Relying on the enzyme citrate lyase, an enzymatic assay was developed. The luminescence analytical method had two clear advantages over enzymatic studies: firstly, it took less time (ten minutes) to complete than the enzymatic study, which took three hours in total; secondly, it required smaller sample quantities and fewer preparation steps. Parker and co-worker also developed compounds **22** and **23** that acts as sensor to monitor the changes in the bicarbonate level in the mitochondrial region of living cells.[71]It was proven that the incorporation of an amide linked azaxanthone moiety in an Eu(III) complex could promote the uptake and staining of the complex into the cells.[12]

The changes in the Ln(III) centred emission *in vitro* upon the additions of various biological analyte such as bicarbonate, Human Serum Albumin (HSA), citrate, lactate and phosphate were investigated. Upon the addition of the bicarbonate the largest changes were observed, indeed the ratio of the J = 1/J = 2 bands changes from 2:1 to >4:1 upon addition of the bicarbonate that causes the displacement of the water molecules. Upon the addition of HSA to **23** the result was not only a quenching of the Eu(III)-centred emission, but the resulting spectra changed its form, probably due to the quenching of the azaxanthone triplet state by a charge transfer process from the electron rich residues in the protein. For the studies *in vivo* different cells lines were used and all the co-localisation studies of **22** prove that the complex is incorporated from the cells in the mitochondrial region. Because the percentage of CO_2 in the incubator was altered and the Eu(III) centred emission increased with the increasing of the $\%CO_2$ the deduction was that this is given to the rise in the steady state bicarbonate concentration.

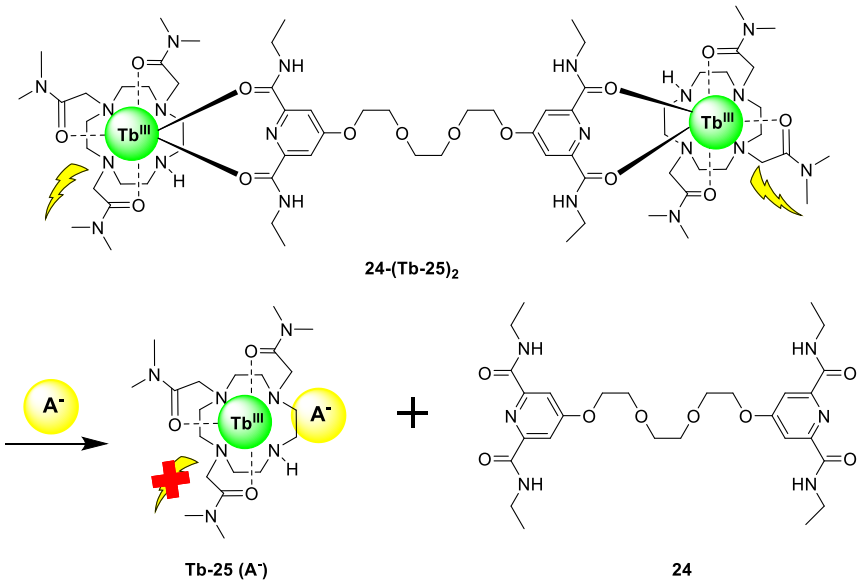

Scheme 1.2: *Schematic illustration of* ***24-(Tb-25)₂*** *(emission switched on) and the displacement assay upon addition of anion (emission switched off).*[72]

Gunnlaugsson and Caffrey developed a luminescent dimeric ternary lanthanide-cyclen complex **24-(Tb-25)₂** able to detect anions *via* displacement assay using spectrophotometric titrations in MeOH solution.[72] The stoichiometry of the complex was investigated and upon the addition of the 2 equivalents of **24** it was found that the most dominant species is the 1:1 complex. Upon the addition of four equivalents of **24** a mixture of both stochiometric species was found in solution. The 1:2 complex was investigated as probe for the detection of $H_2P_2O_7^{2-}$, $H_2PO_4^-$ and NO_3^- and the mechanism is shown in **Scheme 1.2**.

The ability of **24-(Tb-25)₂** to sense the anions was investigated using tetrabuytlammonium (TBA) salts of acetate, chloride, nitrate, phosphate and pyrophosphate. The addition of 1 equivalent of $H_2PO_4^-$ resulted in a quenching of the Tb(III) centred emission *ca* 90% and a full quenching after the addition of the second equivalent. This process of displacement was further investigated using a non-linear regression analysis that showed two stepwise equilibrium processes for displacing of **Tb-25** by the phosphate anion. It proved that the displacement of the two equivalents of the Tb(III) complex from **24-(Tb-25)₂** resulted in the formation of a new Tb(III) self-assembly in solution, consisting of the binding of two equivalents of **Tb-25** to a single anion. The addition of $CH_3CO_2^-$ and Cl^- cause only a minor quenching (*ca* 8% and *ca* 4 % after 4 equivalents of each anion). The higher quenching was found using the pyrophosphate, indeed upon the addition of only 0.5 equivalents the Tb(III) centred emission was quenched by *ca* 83% and the fully

quenched upon the addition of 0.8 equivalents. The last anion investigated was NO_3^- but the quenching that was found corresponded only to 60% after the addition of 4 equivalents of anions.

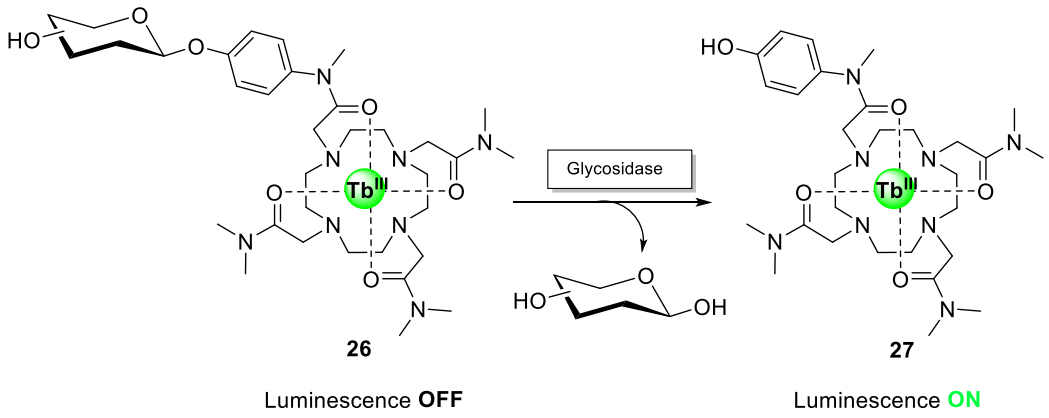

***Scheme 1.3**: Enzymatic hydrolysis and consequently switch on of the luminescence.*[61]

Gunnlaugsson and co-workers developed a synthetic chemical probe for the enzymatic detection of glycosidase enzyme activity in real time.[73] **Scheme 1.3** shows the mechanism through which the enzyme can modulate the emission of complex **26**.

Glycosylation is one of the most important and common posttranslational modifications of proteins. In fact, it is estimated that over 50% of all human proteins are glycosylated,[74] so it is easy to understand why the monitoring of this enzymatic activity is crucial. The system is a Tb(III) cyclen based complex **26** where the phenyl antenna is 1-4 substituted conjugate to a carbohydrate unit. Upon enzymatic hydrolysis of the glycosidic bond, the sugar would be cleaved off resulting in the release of the phenolic group. Is known from the literature that for ions such as Tb(III) this process could give rise to more efficient sensitisation of the Tb(III) excited state by the antenna, with concomitant modulation in the Tb(III) luminescence, which would be "switched on".[51] Based on this knowledge the complex was synthetized and its ability to recognize the enzymatic activities were investigated by exciting the phenyl chromophore to allow the indirect sensitisation of the Tb(III), giving rise to the characteristic line-like emission corresponding to the $^5D_4 \rightarrow {}^7F_J$ (J = 6–0) transitions. The system was excited at 273 nm in tris-buffer solution at pH 7.4. The experiment proved that there was no modulation of Ln(III)

luminescence at lower concentration ranges, although clear hydrolysis results were observed at higher concentrations.

An interesting advantage in the use of the lanthanides is that they are highly

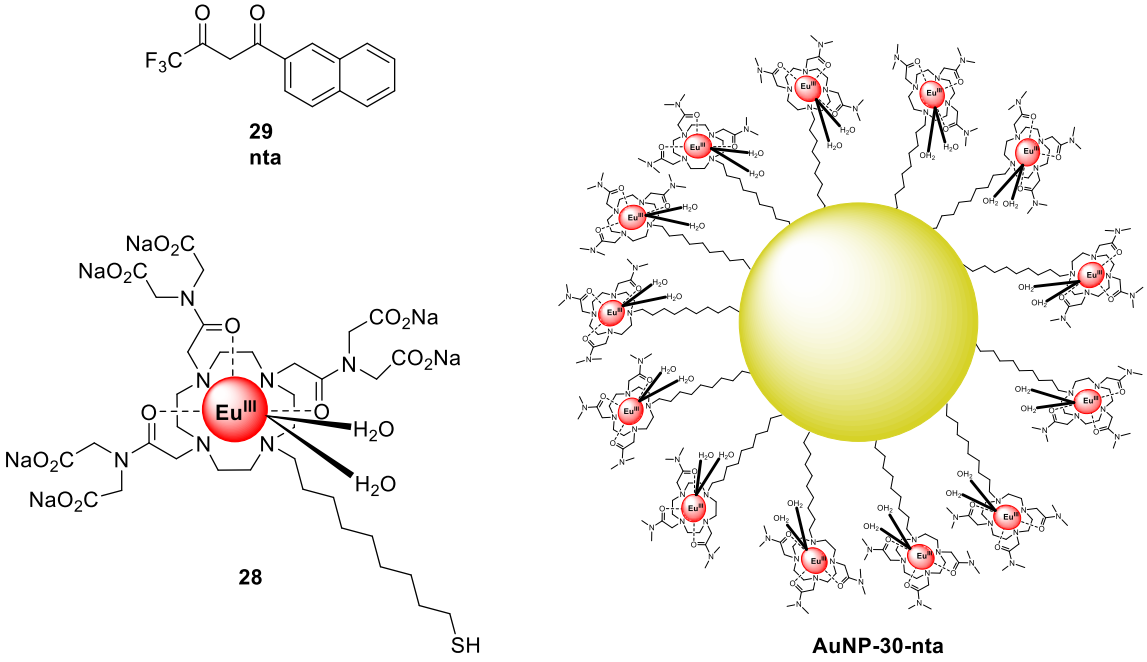

***Figure 1.9**: Structural design of the AuNPs imaging agent.*[75]

versatile, and they can frequently be used in combination with other chemical species. One of the most important examples is that of nanoparticle-lanthanide conjugates. For example, Gunnlaugsson and co-workers have undertaken the synthesis (using both Ln-complex and AuNPs conjugated) and photophysical study of luminescent nanoagents for use in imaging of damaged bone structures.[75] The Eu(III) cyclen based complexes were anchored to the surface of gold nanoparticles through covalent spacers and a S-Au bridge. The authors showed that a nanoagent bound to an exposed calcium site (*i.e.* due to a microcrack) could be imaged using a sensitizing antenna and two- photon microscopy, generating a 3D map of the damaged bone area by observing the long-wavelength lanthanide-centred emission.

Despite the promise of the nanoagents, the researchers observed several different issues, such as non-specific and weak binding.[76] Another drawback is that the development of contrast agents and the scanners utilized for imaging are not synchronized with each other, such that the MRI scanners lack of sensitivity and resolution often hinder the contrast agents from being detected. This was the reason why the nanoparticles were chosen, as they allow for the accumulation of high quantities of contrast agent in a small volume to give good signal and detection limit.

The synthesis passes through the tetra-substitution of the cyclen with various pendant arm groups (ligands possessing hard donor atoms) to give up to eight coordination sites.[45] The first 3 hydrogens were replaced with diethyl iminodiacetate pendant arms, each possessing the ability to coordinate the Eu(III) ion *via* its amide carbonyl oxygen atoms to yield a heptadentate coordination environment. Diethyl iminodiacetate proved to be able to bind the Ca(II) ions on the surface of the microdamaged regions of the bones.[76-78] The last hydrogen was functionalized with a C_{11} alkyl chain terminated with a thiol group that would act as a covalent spacer to minimize the quenching of the Eu(III) luminescence by the **AuNPs**.[79, 80] Complex **30** does not have an antenna incorporated in the main framework because this would allow chelating antennae to coordinate the Eu(III) ion through displacement water molecules and give rise to ternary supramolecular complexes, so an external antenna was chosen. Compound **30** (**nta**) was the perfect candidate due its ability to sensitise the Eu(III) centre and it would permit the use of the **TPE** (two photon emission microscopy) in the NIR region. **TPE** was crucial, because it provides a means of overcoming this drawback by utilizing low energy NIR excitation, which not only is less harmful but also allows for deeper penetration of biological tissues and gives rise to increased tissue transparency, a feature that is highly desirable for use *in vivo*.[81, 82] The system proved the importance of the introduction of **AuNPs**, allowing for significant reduction in the overall concentration of the active Eu(III) probe (**28**.Eu.nta) by a factor of 10 (1.0/0.1 mM). Adding an external antenna and utilizing **TPE** fluorescence microscopy to image this micro damaged bone structure eliminated the need for high-energy excitation (UV or blue-green visible light). Through compiling 3D maps (**Figure 1.11)** of the specimen, they were able to both

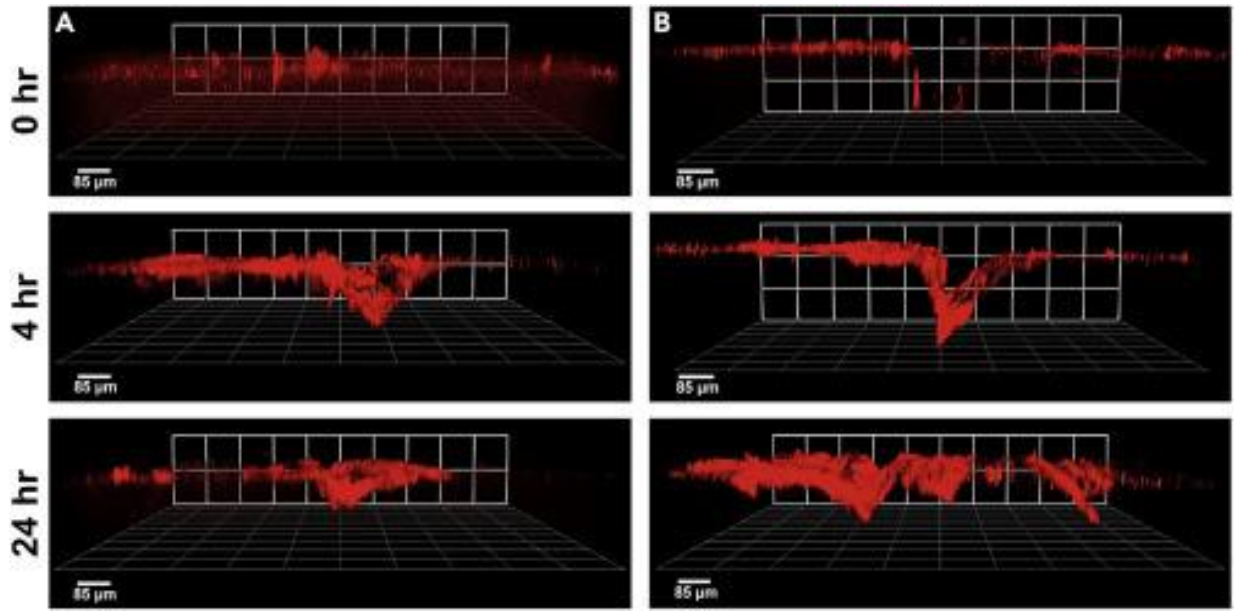

***Figure 1.10**: 2D TPE Microscopy of microdamaged Bovine Bone Structure.*[75]

visualize and interpret the nature of this damage. Such in-depth analysis of microcrack formation has not been previously achieved in this manner.

Gunnlaugsson and co-worker have developed also a material supported molecular logic gate that mimics (MGLMs) system based on the nanoparticle lanthanide conjugates.[83]

They presented the formation of 5 nm AuNPs that using a thiol linkage that have been conjugated with heptadentate cyclen based complexes of Eu(III) and Tb(III) for sensing applications using delayed lanthanide luminescence and as integrated logic gate mimics within competitive media. A molecular logic gate is a molecule

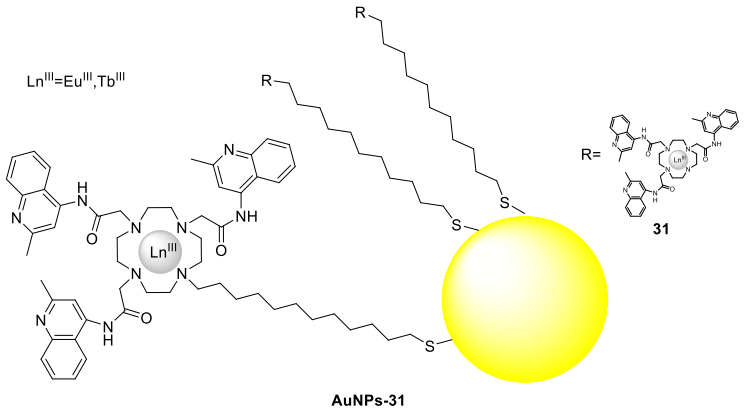

***Figure 1.11**: Structural design of the AuNPs functionalised with Ln(III) cyclen based complexes through thiol linkages.*[83]

that performs a logical operation based on one or more physical or chemical inputs

and a single output. The field has advanced from simple logic systems based on a single chemical or physical input to molecules capable of combinatorial and sequential operations such as arithmetic operations, moleculators and memory storage algorithms.[84] The photophysical properties of AuNPs-**31** were investigated and a structure consistent with complexes **[Eu-31]$^{3+}$** and **[Tb-31]$^{3+}$** in solution was observed, the absorption maximum at 318 nm (log=4.4) was found to be able to excited the Ln(III)-centred emission. An absorption band with a λ_{max}=540 nm was also observed, corresponding to the SPR of the AuNPs, which was red-shifted *ca.* 6 nm compared to the non-functionalised AuNPs; confirming the adsorption of the complexes to the surface, as eluded to above. The number of complexes bound to the each AuNPs was evaluated and was found that *ca.* 50 complexes bound each AuNPs.

The ability of these conjugates to work as probes were evaluated upon the addition of various chemical inputs as pH, pO_2 and ternary sensitive antennae. Upon the pH spectrophotometric titration a modulation of the Ln(III) centred with the changing of the pH was observed working as an ON/OFF system then the logical parameterisation of the **AuNPs-[Eu-31]$^{3+}$/[Tb-31]$^{3+}$** were evaluated and the photophysical properties of the mixed system showed similar properties compared to the Ln(III) complex alone. The changes in the Eu(III) emission and in the Tb(III) centred emission were evaluated upon changing the pH and for the input conditions the critical input concentrations were defined such that the extreme changes were achieved rapidly. Therefore, *Input 1* and *Input 2* were defined as sequential increases in the order of magnitude of [H^+] by 4 pH units; initial resting state set as [H^+] =1x10^{-11} M. The digitisation of the luminescence Output, as *Output 1* and *Output 2*, corresponding to changes in the 545 nm and 592 nm transitions, from Tb(III) and Eu(III), respectively, was achieved by placing suitable OFF/"0" to ON/"1" thresholds MLGM, the changes were considered as [H^+] aliquots. Two separate Inputs channels, Input1 and Input2, could therefore be described of the same chemical species, that is, H^+. The output thresholds, expressed in terms of I/I0, corresponded to I/I0 = 2and 0.5 for emission at 545 nm (Tb(III), $^5D_4 \rightarrow {}^7F_5$)and at 615 nm (Eu(III), $^5D_0 \rightarrow {}^7F_2$) creating a two channel system corresponded to logic function of NAND and XOR (**Figure 1.12** A). The same investigation was performed using an external antenna, DMAB for the Tb(III) complex and nta for the

Eu(III) one and the complexes were bound to the AuNPs. The system was operated at extreme input conditions (*i.e.* stoichiometric excesses), for Input1 and Input 2 these were defined to be ON/"1"only when [nta] or [DMAB] = 120 [AuNP], respectively.

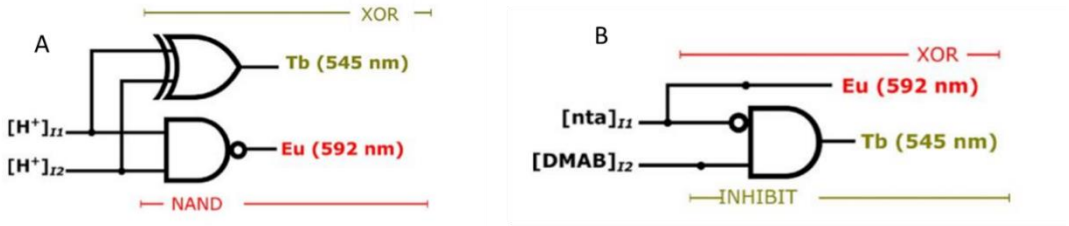

***Figure 1.12**: (A) Logic circuit describing the behaviour of AuNP-**[Eu-31]**$^{3+}$ +/**[Tb-31]**$^{3+}$ + with [H+]inputs ; (B) Logic circuit describing the behaviour of AuNP-**[Eu-31]**$^{3+}$+/**[Tb-31]**$^{3+}$+ with [DMAB]and [nta]inputs.*[83]

The emission spectra in the antenna-Ln(III) complex showed a different band ratiometry and relative intensities (this is the results of more efficient population of the **Eu($^5D_0$)** than **Tb($^5D_4$)** states by the ternary antennae). Since the emission from Tb(III) was partially quenched (by *ca.* 5% in excess DMAB after the maximum emission), the Tb(III) output threshold was assigned as I/I0=4.5. For Eu(III) emission, the output threshold of I/I0=180 was applied following the same criteria described for the first part of the experiment, then the luminescence spectra were recorded using the four possible combinations of input 1 (nta) and input 2 (DMAB) shown in Table 1

Table 1: Truth table representation of [H$^+$] parameterised MLGM from AuNP-**[Eu-31]**$^{3+}$+/**[Tb-31]**$^{3+}$ and the corresponding mimicked logic functions.

Input 1 (DMAB)	Input 2 (nta)	Output 1 (λ_{em}545nm)	Output 2 (λ_{em}592nm)
0	0	0	0
1	0	1	0
0	1	0	1
1	1	0	1

Since the Eu(III) emission was only ON/"1"in the presence of nta, the output corresponded a YES function within a two input system and can be characterised as TRANSFER[nta].

The Tb(III) output reported ON/"1"only in the case where DMAB was present alone, corresponding to INHIBIT[nta], the system is schematised in **Figure 1.12** B. The versatility and easy modification of these ligands open the possibility to apply them in a wider or different field and it is possible to create chiral luminescent sensing, bioimaging, logic gates, LED. Despite the main advantages of these systems, often they required water solubility, bio-conjugation or deposition onto the solid substrate. This last field got a large interest from those researchers that work in the lanthanide area. Indeed Ln(III) system are excellent candidates for the deposition not only because through the functionalization of the ligand it is possible to anchor it onto the solid support, but they usually maintain the same luminescence properties. The outcome allows for the construction of two logic circuits: the XOR–NAND half-subtractor, with [H^+] inputs, and the TRANSFER–INHIBIT circuit which relied on the nature of the ternary complex formation. The XOR–NAND circuit was shown to be reversible and reusable, while unfortunately, the TRANSFER–INHBIT circuit could not return from the (1,1) state. Because of this one of the main aims of this work is to develop novel lanthanide complexes lanthanides based to form highly organised Langmuir monolayers at an air-water interface deposited onto a solid substrate. Langmuir-Blodgett (LB) is crucial to the main chapter of this thesis, for this reason the following section is focused onto the LB film theory, apparatus and application.

1.8 Langmuir Blodgett films

Irving Langmuir was the first to report studies about the formation of thin films at air water interface using non polar molecules, the ideas behind was that the a part of the oil molecules was attracted from the water while the other "prefer" to stay with the other oil molecules than to water.[85] Later he started a collaboration with Katherine Blodgett and they extended the application depositing these films onto a

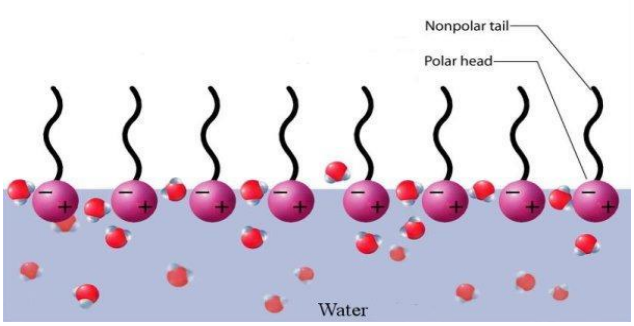

Figure 1.13 *Surfactant molecules arranged on an air–water interface.*

solid substrate.[86-88] Langmuir and Blodgett have established the criteria to form and deposit a monolayer at an air-water interface, to form that, the molecule have to possess an hydrophilic head group able to interact with the water and an hydrophobic part to avoid the solubilization in water.[89] Hence, the Langmuir-Blodgett technique[90] involves the self-assembly of amphiphilic molecules into an ordered mono-layer (Langmuir film) at an interface (usually air/water) and subsequent transfer (*via* vertical deposition) of the self-assembled mono-layer onto a solid substrate (Langmuir-Blodgett film). For the monolayer formation the amphiphilic compound is initially dissolved in a water immiscible solution for the work described in this thesis was used chloroform and was spread onto the water surface using a micro-syringe, at this stage the molecules resulted in a state of disorder onto the water surface as shown in **Figure 1.13.** The apparatus used is called Langmuir–Blodgett trough.

The density of surfactant molecules as well as the surface pressure increases upon reducing the surface area ('compression' of the 'gas'). Further compression of the surfactant molecules on the surface shows behaviour similar to phase transitions. The 'gas' gets compressed into 'liquid' and ultimately into a perfectly closed packed array of the surfactant molecules on the surface corresponding to a 'solid' stat (**Figure 1.13**) When coupled with the unique photophysical properties of the Ln(III) ions the LB technique allows for the development of new generation sensors that allow for sensing on surface rather than the traditional solution-based approach, thus allowing the development of functional sensing devices.[91] **Figure 1.14** (A-D) shows the trough set-up and a side-on view of the interface. At first an amphiphile is spread onto the sub-phase on a Langmuir trough resulting in a 2D 'gaseous' arrangement of amphiphiles

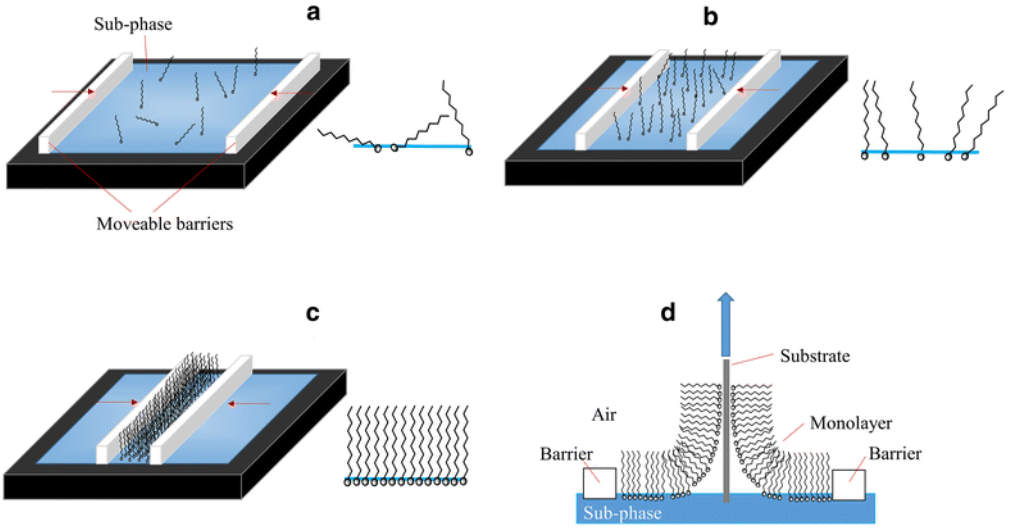

Figure 1.14: *Schematic representation of the steps involved in formation of Langmuir-Blodgett films.*[73]

(no interactions between the molecules). Then the barriers are compressed to reduce the surface area of the interface and molecules begin to interact forming a 2D 'liquid expanded' phase. In order to evaluate the monolayer stability, the film is holden in the LC phase for a period of time and the surface pressure is monitored. Te be considered stable will hold its surface pressure over the time, unstable films instead will collapse, displaying a decrease in the surface pressure. Upon further compression, the amphiphiles are self-assembled into a monolayer forming a 2D 'compressed liquid' phase and when a monolayer has formed it can be transferred onto solid support *via* vertical deposition.

If the substrates are hydrophilic the slide is lowered and submerged through the subphase before the amphiphile is spread onto the surface. Removal of the slide by means of an upward stroke results in monolayer attachment to the slide via hydrophilic interactions between the polar headgroups and slide. Hydrophobic coated slides remain above the subphase/monolayer interface before the material is deposited onto the water surface. A downward stroke of the slide causes attachment of the hydrophobic chains to the slide upon submersion.[89] Three different packing patterns are possible depending from the process of slide emersion (upstroke) and immersion. The three architectures are shown in **Figure 1.15.**

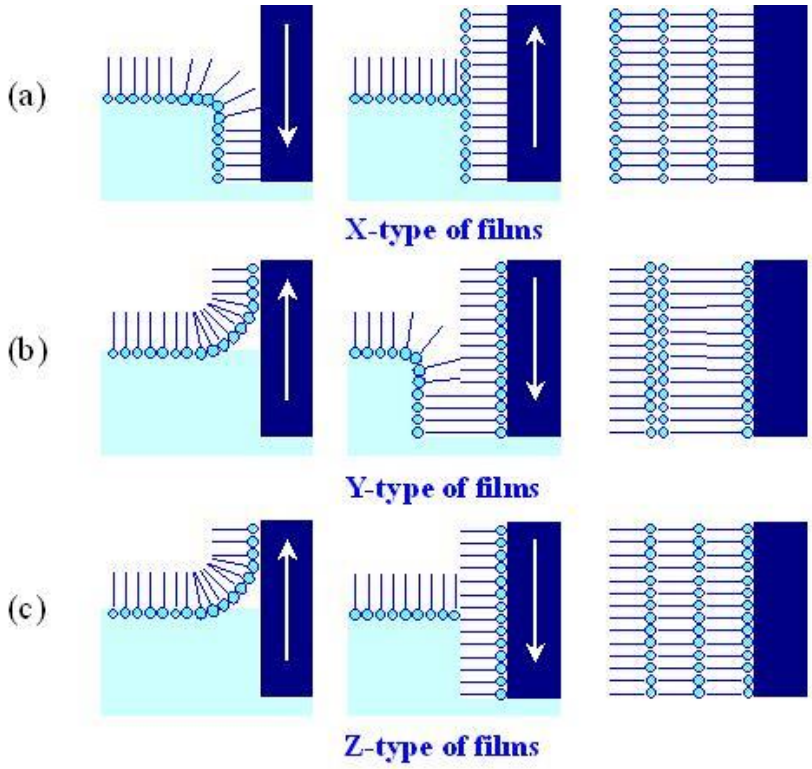

***Figure 1.15**: (a) Y-type, (b) X-Type and (c) Z-type deposition on a solid substrate.*

To evaluate the quality of the film transfer a parameter called transfer ratio (τ) is calculated using the following equation

$$Equation\ x\text{:}\ \tau = \frac{Al - W\ interface}{As}$$

This is defined as the ratio between the decrease in monolayer area during a deposition stroke, Al, and the area of the substrate, As. For ideal transfer the τ is equal to 1. Using the LB technique it is possible to obtain the deposition of well-ordered and highly structured ultrathin immobilised layers, to perform a layer by layer coating of monofilm forming multi-layered films with different function or properties.[89] The unique photophysical properties of the Ln(III) series has led to significant research efforts being directed towards their application as sensors (how has been explained in the previous section).

1.8.1 Luminescent Langmuir-Blodgett films

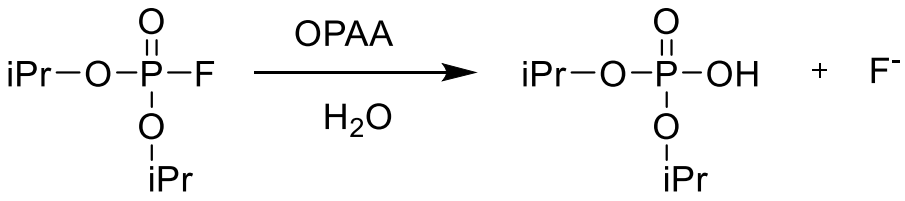

***Scheme1.4**: Schematic representation OPAA enzyme activity.*[79]

The luminescent film for chemo-/bio-sensing should exhibit high selectivity and sensitivity. The molecular scale of the LB technique has been proposed for the preparation of biosensors using bioactive molecules (*e.g.* antibodies and enzymes). An enzyme-based sensor not only provides high selectivity, but also works in an environmentally friendly way as enzymes can be adequately immobilized in an organized ultra-thin monolayer while their biological activities are retained. An example is the FITC-labeled enzyme organophosphorus acid anhydrolase (OPAA) that was prepared for the detection of diisopropylfluorophosphate (DFP).[92] OPAA is an enzyme that been shown to be particularly effective in detoxifying organophosphorus-containing compounds, such as deadly nerve gases used in chemical warfare. A scheme of a reaction occurring in the presence of OPAA is shown in **Scheme 1.4** OPAA rearranges during the enzymic hydrolysis of DFP, leading to self-quenching of FITC fluorescence in the FITC-OPAA film. Semiconducting quantum dots (QDs) are another example of luminescent materials used in LB films for biosensing.[92]

As shown in **Figure 1.16**, a thin film of OPO–ODA–ZnS–CdSe and TOPO–TDPA–ZnS–CdSe QDs was constructed *via* the LB technique and further modified using an amphiphilic polymer, poly(maleic anhydride-alt-1-tetradecene) (PMA), through self-assembly. Then avidin was immobilized on the PMA-coated QD film *via* electrostatic

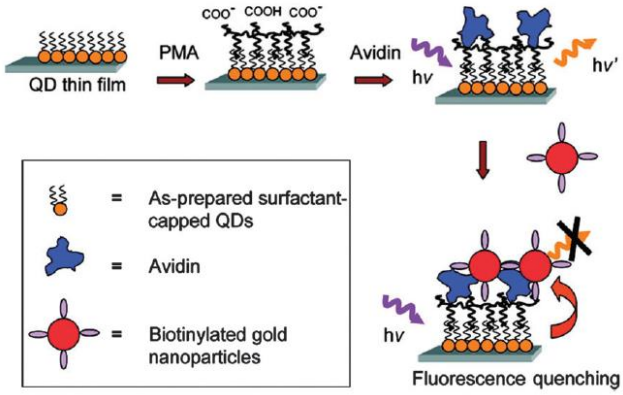

***Figure 1.16:** LB film of OPO–ODA–ZnS–CdSe and TOPO–TDPA–ZnS–CdSe.*[79]

interactions. When immersed in a biotinylated gold solution, the avidin-coated QD film attracts the biotinylated gold nanoparticles by specific interaction between avidin and biotin. The fluorescence emission of the films was quenched due to FRET between the QDs and gold nanoparticles. This is possible because the two conditions necessary to have the FRET (fluorescence resonance energy transfer) occurred at the same time. FRET is phisyical process where the energy is transferred nonradiatively from an excited molecular fluorophore (the donor) to another fluorophore (the acceptor) by means of intermolecular long-range dipole–dipole coupling. The first condition is the overlap of emission spectral features of the donor with the absorption features of the acceptor and the second is the <10 nm distance between the donor and acceptor,[93] because QDs act as donor and the gold nanoparticles act as acceptor, they form an ideal FRET couple.[93]

Thin film materials containing rare earth complexes are of particular interest due to the unique optical and magnetic properties of lanthanides. In the last decade, many luminescent lanthanide complexes have been deposited as ordered ultrathin films using the Langmuir–Blodgett method. Most of the research groups that work with the Ln-based LB luminescent films use different ligands such as calixarenes,[94] β-diketonates,[95-99] polyoxametalates (POMs),[100, 101] and also heterocyclic pyridine ligands.[102] Hemicyanine of Eu(III) complex have been used as LB film not only for the energy transfers luminescence, but also because it exhibit a good second harmonic generation properties.[103] Saja *et al* developed a bisphthalocyanines compounds with electrochromic and electrochemical behaviour for gas sensing purpose.[104, 105] Complex **32** was developed by Qian *et al* and because of the counter anion shows a high level of amphiphilicity that should facilities the formation of the LB-monolayer.[95] Despite the formation of the stable monolayer confirmed by a surface pressure-area isotherm, the

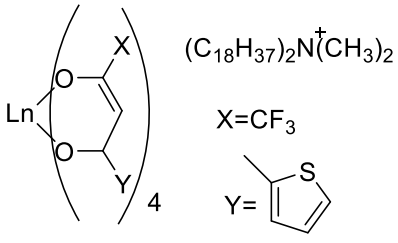

32: Ln= Eu(III)

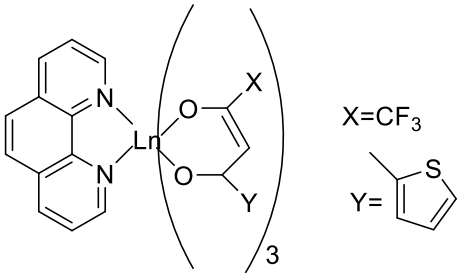

33: Ln= Eu(III)
34: Ln= Sm(III)

deposition of **32** onto solid substrate was found difficult, pushing the researchers to

investigate the LB monolayer forming abilities in a mixture of **32** with arachidic acid (AA) and octadecane (OD). A really high collapse pressure was observed when the mixture of **32-OD,** increasing the molar fraction the OD a rise of the collapse values was found, probably because in presence of the OD there is a closer packing of the molecules. Mixed monolayer of **32**: **AA** 1:16 and greater were deposited onto a quartz slide by vertical dipping while mixed monolayers of **32** and **OD** 1:4 were deposited by a horizontal lifting. Absorption and emission spectra of **32** in the mixed monolayer assemblies (50 layers) with **OD** and **AA** in comparison to organic solutions of **32** show the difference in symmetry in going from the solution to the solid state. The $^5D_0 \rightarrow {}^7F_2$ transition split into two peaks and the emission of the higher energy excited $^5D_1$ state was observed and usually weakly observed symmetry forbidden transition $^5D_o \rightarrow {}^7F_0$ was enhanced when the complex was deposited into the LB film.[95] The non-amphiphilic complexes **33** and **34** were developed by Zhang *et al*. and they found a method to assemble these complexes at the air water interface in which an appropriate

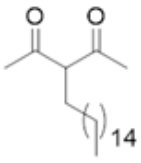

35

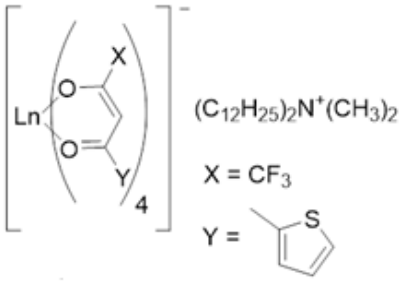

36

composite subphase is chosen.[97] The process consists in the saturation of the aqueous solution using TTA, 1-10-phenantroline (phen) and **33**, it was found that the dissociation of **33** was inhibited by the components, because of this they chose to add a lipophilic compound (AA) and to the deposit the mixture of **33**/**AA** and **34**/**AA** onto the composite subphase surface homogeneously dispersed, and stable monolayers were formed and successfully transferred onto the glass substrates. Luminescent studies were performed and a linear dependence of the absorbance on the number of layers was also obtained indicating that the films have vertical uniformity. The LB films maintained the Ln(III)-centred emission *via* energy transfer from the coordinating chromophores emission intensity.[97] Gomes *et al.* combined the methods of introducing a long aliphatic chain into the parent ligand structure for spreading ability and assembly of the amphiphilic ligands into Langmuir films using a Eu(III) 0.1 mmol L^{-1} solution subphase to fabricate a luminescent films based on Eu(III).[99] Ligand **35** was complexed

with Eu(III) and the monolayer were then transferred onto quartz slides yielding Z-type architecture with three layers of Eu-**35**n·xH_2O.

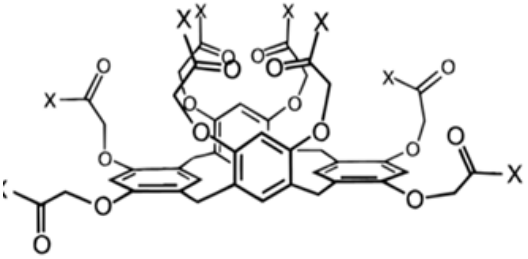

37: X = OMe
38: X = NEt_2

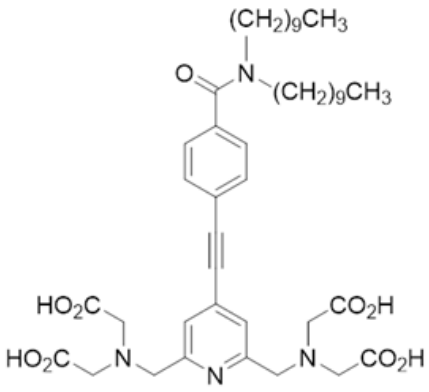

39

Complex **36** was developed from Adati *et al.* and its design is based on the complex **33** where an amphiphilic group was added as counter anion in order to eliminate the need of co-spreading surfactant.[106] Instead, Eu-**36** coordinate four TTA β-diketonates bearing a negative charge which is neutralised by the amphiphilic cation. A stable LB monolayer of **36** was obtained and the investigation proved that it was deposited in a Y-type architecture. Upon an excitation at 307 nm intense Eu(III)-centred emission was observed, proving that the luminescence properties were maintained upon the deposition onto the solid substrate.[106] As previously mentioned, calixarenes have been employed for the fabrication of LB films. The first calixarene-based systems are compound **37** and **38,** indeed Dutton *et al.*[94, 102] reported that those system exhibit an energy transfer luminescence when they are incorporated onto the solid support. Solutions of each compound were spread onto either solution of water or $TbCl_3$ (c= 2 x 10^{-4} M) and the stability of the monolayer were monitored for 8 hr. The obtained film was very stable and it was then transferred onto the solid substrate, the transfer ratio was evaluated, and it was found close to 1, indicating a good transfer. The luminescent properties were recorded and shown a good signal relative to the Tb(III)-centred emission, comparable to the Tb(III)-centred emission of the corresponding solution. Lemmetyinen *et al.* carried out a study relative to the mechanism of the energy transfer of **39** to Ln(III) (the lanthanides employed were Eu(III), Gd(III) and Tb(III)) in LB films.[102] The Langmuir monolayer was formed using a $LnCl_3$ subphase and the film was than deposited onto the quartz slide (transfer ratio close the unity). The luminescence studies showed a slight red shift in the absorption spectra of **39** upon the

complexation with the Ln(III), but there was no difference between the complex in solution and the complex deposited on the solid substrate. Upon an excitation at 300 nm the Eu(III) and Tb(III) luminescence was exhibited, proving that the energy transfer *via* sensitisation of the coordinating ligand **39** to the Ln(III) occurs within each film.[102]

Another example is given from the ligands **40** and **41** which can form Ln(III)-directed self-assembled "half-helicate" systems.[107] This system was developed within

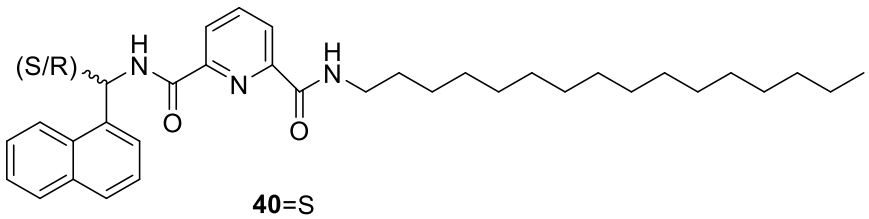

40=S
41=R

Gunnlaugsson group. It has been shown that the stoiochiometry of the systems were 1:3 metal to ligand ratios using Eu(III) as metal, the complexation could be monitored *in situ* using spectroscopic techniques. Circularly Polarised Luminescence (CPL) was employed to show the chiral Ln(III)-centred luminescence from the self-assembled structures. Molecular modelling calculations (MM2) were also implemented in order to gain insight into the stereochemistry of these mononuclear systems. The results from these calculations indicated that these structures all had the three naphthalene antennae residing on the same side, directed towards the inside of a "half-helicate", with the methyl groups outside the coordination sphere of the Ln(III) ion, giving rise to the most stable complex arrangement.[107]

With the development of a hierarchical organization it is possible to achieve the target properties of a material with a minimum of constituents and less energetic effort possible. In the last 30 years, a significant number of studies have focused on the development of layer by layer self-assembly formation in order to make thin films to apply in different areas of research such as in the deposition of polyelectrolytes and charged virus,[108] as well as deposition of proteins[109, 110] and DNA.[111, 112] The Langmuir-Blodgett (LB) technique is widely used for biological application purpose, for example, it is used to prepare models mimicking biological membranes.[113] The preparation of biosensor thin films is one of the most active research fields where their application is demostrated.[114-116]

In the next chapter we will discuss the intends to build on and enhance previously started research, within the Gunnlaugsson group into the formation of Ln(III)-LB monolayer and multilayer sensors for biological applications. This includes the modification of the previous reaction protocols, in order to improve the yield, performing photophysical studies on the Ln(III)-cyclen (1,4,7,10-tetraazacyclododecane) complexes to elucidate structural and behavioural information which will aid in understanding the potential of the use of Ln(III) complex to recognize phosphorylate amino-acids, this because the phosphorylation of tyrosine to phosphotyrosine (pTyr) is a critical process within cellular regulation; its exact role is not fully understood and furthermore, pTyr only accounts for < 1% of the phosphorylated amino acids in the body.
In summary, the biosensor employed was designed by focusing on the following criteria:

- The ability of the Ln(III) complex to overcome the short lifetimes that characterize the fluorescence of the biological background;
- Efficient sensitization of the Ln(III) emission;
- Selective sensing of tyrosine and *O*-phospho-L-tyrosine.
- The ability of Ln(III) complex to form LB mono and multilayers.

The ability of the complexes to selectively discriminate between a set of α-amino-acids was also investigated in different solvents and the effect of the different buffers on the recognition process at physiological pH has been addressed. The design of the Ln(III)-cyclen complex was based on creating an amphiphilic molecule by modifying the cyclen framework with three long hydrophobic alkyl chains in order to form a system with a hydrophilic "head" ensured by the Ln(III) positively charged metal complexed within the cyclen to form a monolayer on the air-water interface and to deposit it on a quartz slide to form a luminescent LB film capable of sensing different amino-acids with a particular interest on the phosphorylated ones.

As previously mentioned, one of the major drawbacks in using the luminescent properties of the Ln(III) ions is their low extinction coefficients that result in inefficient direct luminescence excitation.[117] In order to overcome this issue, an external antenna will be employed here in order to populate the excited states of the Ln(III) ion by transferring the energy its triplet state giving rise to sensitised

lanthanide luminescence these antennas were also tested in some of the example discussed in Chapter 1.[11, 58]

The first part of this chapter focuses on the synthesis and characterization of ligand, complexes and their ability to discriminate different α–amino-acids in different solvents. The second part of this thesis discusses the formation and the characterization of the LB films and their ability to sense the amino-acids in competitive media.

Chapter 2

2.1 Design of novel LB sensor of amino-acids and synthesis of the ligand 49

Ligand **49** was developed starting from the necessity to create a system with an ability to discriminate between different amino-acids and being able to form a monolayer that could be transferred onto the quartz slide. Starting from the previous work of Laura Truman within the Gunnlaugsson group, we chosen to develop a system with three alky chains where the amphiphilicity of the cyclen framework was strongly altered. In order to allow for adequate sensitisation of the Eu(III) and the Tb(III)metal centre due to the large energy gap between the excited state of Eu(III) and the excited state of the phenyl ring an external antenna is necessary if Eu(III) emission is to be achieved. However, the Tb(III) metal centre of the Tb(III) complex may be sufficiently sensitised by the aromatic phenyl ring and the use of an external

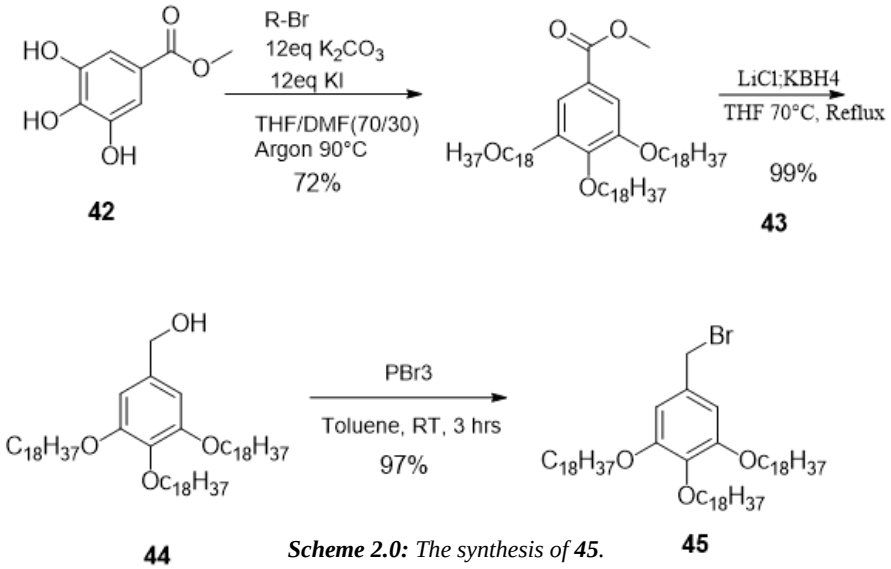

Scheme 2.0: *The synthesis of **45**.*

antenna may be required. The cyclen framework was modified through monoalkylation reaction where one of the amines was substituted (**46**) with a methyl gallate derivate (**42**) where the three hydroxy groups were coupled with three long octadecane chains ($C_{18}H_{37}$) through reaction with 1-bromooctadecane (**45**, **Scheme 2**). The remaining amino groups were alkylated with dimethyl acetamide arms by reacting with three equivalents of 2-chloro-*N*,*N*-dimethylacetamide to yield the ligand **48** (**Scheme 2.1**). The only chromophore present in the ligand is the phenyl ring which would not act as a sensitizer for the Eu(III)-centred emission in Eu-**49** (due to the large gap between the excited state of the europium ion and the triplet excited state of the phenyl ring).[118] Therefore in this case an external antenna is required in order to switch on the Eu(III) centred emission. For **Tb-49** complex the phenyl ring would be a suitable antenna for sensitisation of the Tb(III) excited state, but an external sensitizer may be used here as well in order to achieve higher emission intensities.

In this work the synthesis of ligand **49** was achieved *via* two different synthetic routes (**Scheme 2.1**), with 5-(bromomethyl)-1,2,3-tris(octadecyloxy)benzene **45** as intermediate (**Scheme 2**). Compound **45**, containing three hydrophobic octadecane (C_{18}) chains, was synthesised in three steps from methyl gallate **42**. The tris(octadecyloxy) derivative **43** was formed through a Finkelstein reaction and was crystallised from the resultant brown oil with heptane as a white solid in 77% yield. The ^{1}H NMR spectrum (400 MHz, $CDCl_3$) shows the multiplet at 1.24 ppm, which is characteristic of the 84 H (from the long alkyl chains). The ester **43** was reduced

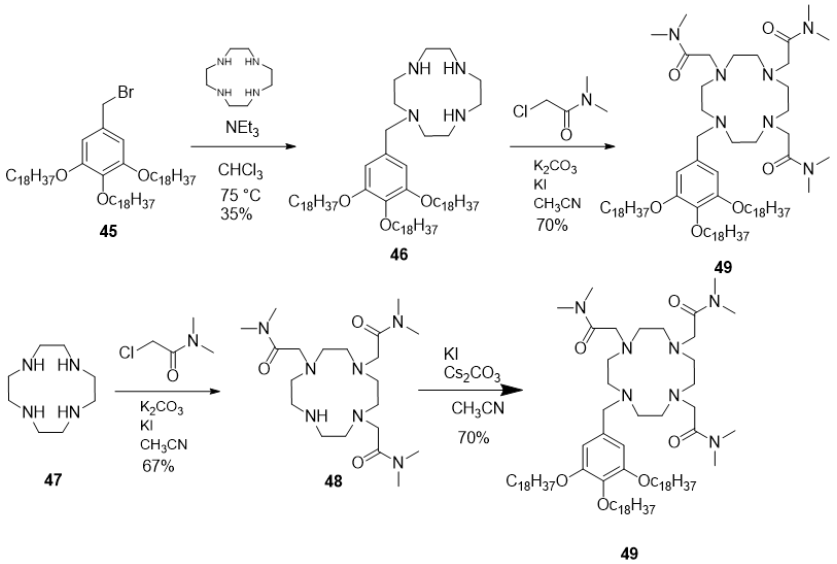

Scheme 2.1: *Two synthetic pathways (A and B) towards the synthesis of ligand **49**.*

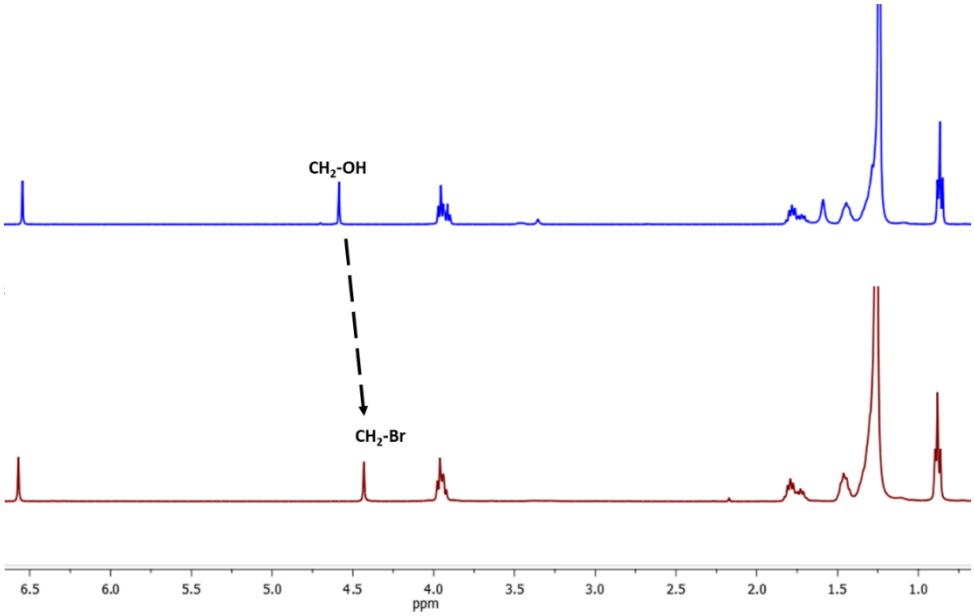

Figure 2.1: *^{1}H-NMR (400 MHz, $CDCl_3$) of **44** (blue) and **45** (red).*

to the methyl alcohol by refluxing in the presence of LiCl and KBH_4 in dry THF for 24 hours producing **44** in 90% yield. The ^{1}H NMR (400 MHz, $CDCl_3$) spectrum of **44** confirmed that reduction had indeed occurred as the singlet at 3.91 ppm of the ester methyl protons of the starting material **43** disappeared.

The IR spectra also produced evidence of the disappearing of the carbonyl stretch as appear of a band of OH stretch. The bromination of **44** was achieved by dissolving the starting material in dry toluene and adding PBr_3 drop-wise at 0 °C, and then stirring the reaction mixture at room temperature for 3 hours. The brominated product **45** was generated in 92% yield. The formation of **45** was verified by mass spectrometry, elemental analysis and ^{1}H NMR (400 MHz, $CDCl_3$) spectroscopy showing the slight upfield shift of the benzyl CH_2 proton from 4.63 ppm to 4.46 ppm (**Figure 2.1**). IR spectra confirmed the results of ^{1}H NMR analysis as the OH

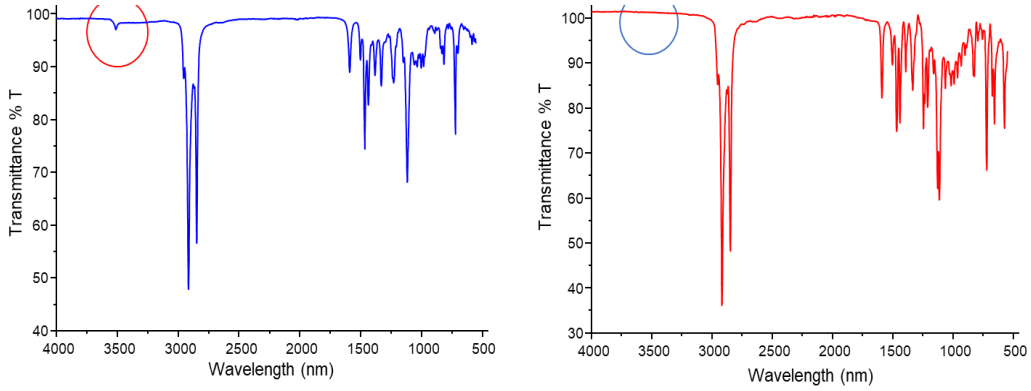

Figure 2.2: *IR Spectra of **44** (blue) and **45** (red).*

vibration observed at 3650 cm^{-1} for **44** (**Figure 2.2**, blue) is not present in the IR spectra of the **46** (**Figure 2.2**, red), which proves that the OH was fully replaced by the brominated product

Two different approaches were followed in order to obtain the target ligand **49**, the first (**Scheme 2.1 A**) consists of the monoalkylation of the cyclen macrocycle (producing intermediate **46**), followed by the alkylation of three remaining amines with 2-chloro-*N*,*N*-dimethylacetamide. In the second approach (**Scheme 2.1 B**) the target molecule was synthesised by obtaining the trisubstituted cyclen **47** that was then reacted with **45** to yield the ligand **4**. The first approach was developed by Gunnlaugsson *et al* as the monoalkylation method of cyclen does not involve the use of protecting group chemistry or any additional purification enabling the high yield of the reaction.[59] This synthesis utilised 1 equivalent of **45**, 4 equivalents of cyclen and 1.2 equivalent of triethylamine. The reaction was refluxed for 24 h in $CHCl_3$ and the resulting solution was washed with HCl 0.1 M in order to remove the triethylamine in excess and after with water to remove the unreacted cyclen. Upon extraction with DCM the organic layer was collected, and the solvent was removed under vacuum to obtain **46** as a brown oil in 50 % yield. The conversion of **46** to ligand **48** involved the trialkylation of the mono-substituted cyclen with 2-chloro-*N*,*N*-dimethylacetamide, using K_2CO_3.The reaction was left under reflux for 72 h in CH_3CN. The purification of the product was achieved using alumina column chromatography with a gradient elution 100 → 80:20 CH_2Cl_2:CH_3OH and the product was obtained as a brown oil in 49% yield. The formation of the ligand was monitored by mass spectrometry where the signal at *m/z* 1684.2732 was observed corresponding to $[M + Na]^+$. ^1H NMR (400 MHz, $CDCl_3$) of the ligand **49** is shown

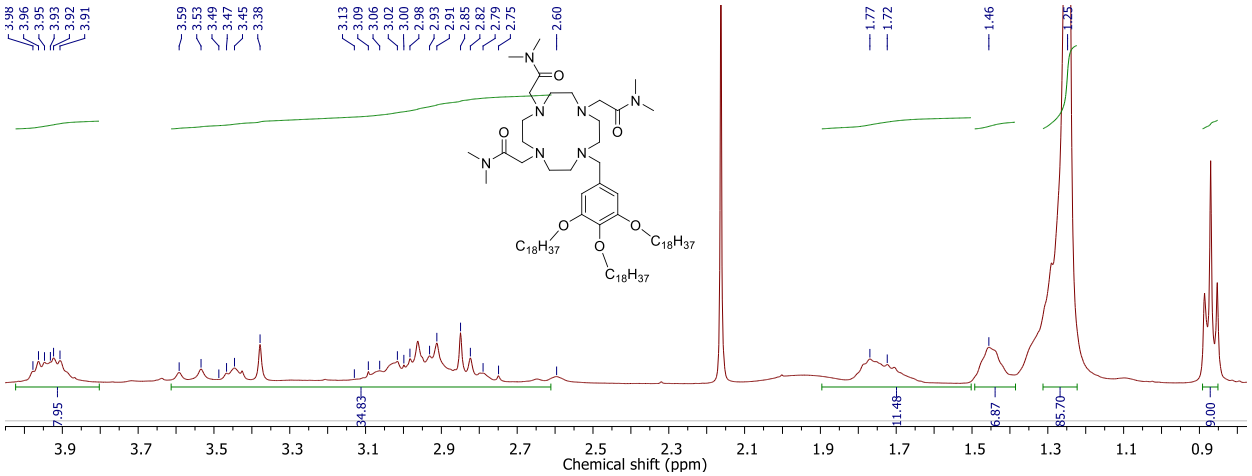

***Figure 2.3**: ^1H NMR spectrum (400 MHz, $CDCl_3$) of ligand **49**.*

in **Figure 2.3**. The 9 CH_3 protons terminating the alkyl chains resonate as a triplet at 0.90 ppm while the cyclen 16 CH_2 protons are located as the multiplet between 3.06 ppm and 2.91 ppm. For this reason, the second approach was chosen. In the second approach, compound **49** was obtained by *N*-alkylation of three cyclen N–H groups using 2-chloro-*N*,*N*-dimethylacetamide. The product was purified by alumina column chromatography with the gradient elution from CH_2Cl_2 to 95:5% CH_3OH:CH_2Cl_2 to yield the product **47** as a yellow oil 64%yield. On the next step the compound **48** was mixed with compound **45** in CH_3CN in presence of Cs_2CO_3 base and the resulting solution was refluxed under argon for 24 hours. The product **49** was purified by alumina column chromatography, gradient elution from 100% CH_2Cl_2 to 95:5 % CH_2Cl_2: CH_3OH to yield the product as yellow solid in 72% yield. While the second approach requires two different purification steps, by column chromatography, to achieve the final product, then in this work, the conversion of **45** to **46** in the first approach proved troublesome, strongly limiting the yield, and negatively influencing the overall conversion of the starting materials to the final ligand **49**.

2.2 Synthesis of the complexes Eu-49 and Tb-49

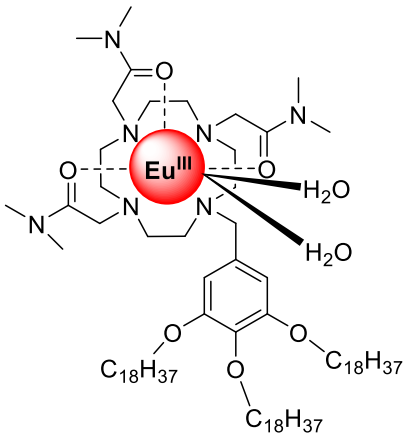

Eu-49

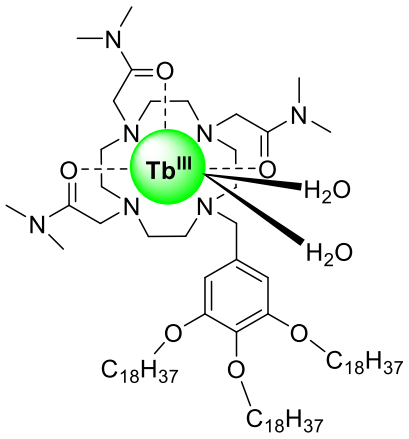

Tb-49

49	**Eu-49**	**Tb-49**
1667	1643	1643

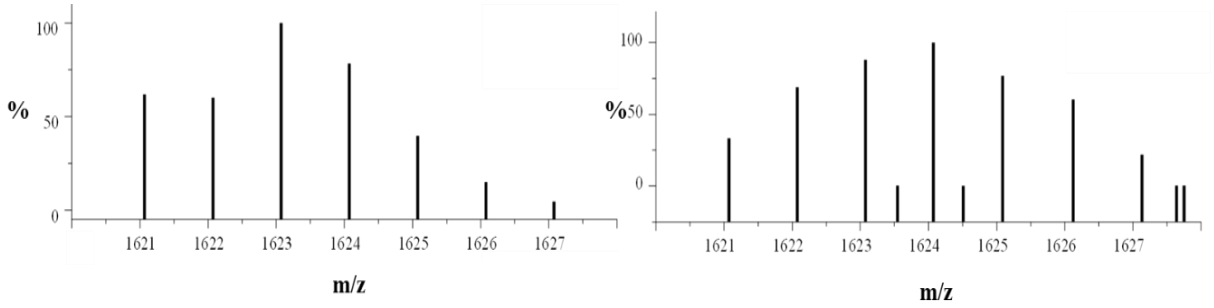

Figure2.4:*(left) Theoretically calculated isotopic distribution diagram for [**Eu·49** + $CF_3SO_3]^{2+}$ and (right) experimentally observed MALDI mass-spectrum for **Eu-49**.*

After the synthesis and the characterization of ligand **49**, the next step was the complexation with Eu(III) and Tb(III). To obtain these complexes, ligand **49** was reacted with 1.1 equivalent of corresponding Ln $(CF_3SO_3)_3$ (Ln = Eu(III), Tb(III)) in 5 ml of MeOH under a microwave irradiation for 60 minutes at 100 °C. The resulting solution was triturated in diethyl ether and the obtained precipitate was successfully isolated by centrifugation. The characterization of the complexes was achieved by ^{1}H NMR, IR spectroscopy, mass spectrometry and elemental analysis. Due to the paramagnetic nature of the lanthanide ions, the ^{1}H NMR presented a broad signal significantly shifted and broadened compared to the original ligand (appendix x). IR spectroscopy was crucial to verify the complexation of the lanthanides in the cyclen framework as the carbonyl bond of the ligands was shifted (as shown in **Table 2.0**) by approximately 30 cm^{-1} after the complexation with these metal ions.

Using MALDI-ToF mass spectrometry analysis a peak at 1624.0772 *m/z*, corresponding to a [Eu-**49** + $CF_3SO_3]^{2+}$ was found. **Figure 2.4** shows the theoretically calculated (left) and experimentally observed (right) spectra. Showing that the observed result displayed the expected isotopic patterns distribution. The same MALDI-ToF analysis was performed an Tb-**49** and the peak at *m/z* = 1629.0778 corresponding to a [Tb-**49** + $CF_3SO_3]^{2+}$ species in solution was found with the appropriate distribution pattern related to the Tb(III) as is shown in **Figure 2.5**. Having formed these two complexes, the next step was to investigate their photophysical properties in solution starting with Eu-**49**.

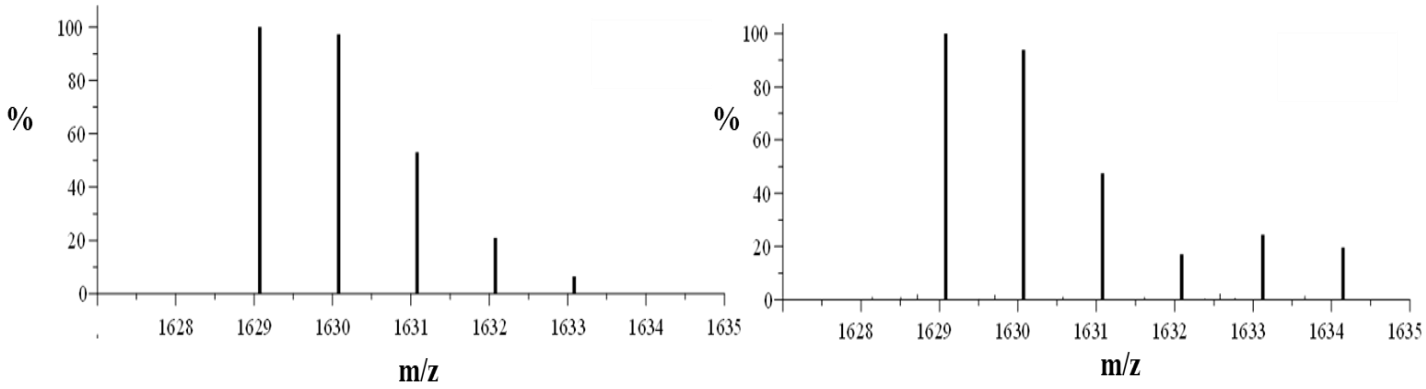

Figure 2.5: *(left) Theoretically calculated isotopic distribution diagram for [**Tb-49** + $CF_3SO_3]^{2+}$ species and (right) the experimentally observed spectrum for **Tb-49**.*

2.3 Luminescent properties of Eu-49

As both Tb-**49** and Eu-**49** are coordinatively unsatured complexes (with 7 coordination for the ligand and a "poor" antenna, that for their analysis it was necessary use another antenna to populate their excited state that for ternary complexes) For Eu-**49** compound **50** (**nta**) was chosen as ancillary ligand and an antenna because it has been shown to be able to increase significantly the Eu(III) emission,[119] as was discussed in the first chapter. With the purpose to determine the hydration states (*q*) of the complex Eu-**49**, lifetime studies were also carried out. The above hypothesis, that two water molecules bind to the Eu(III) centre in order to fulfil its coordination sphere, was confirmed by measuring the luminescence lifetime of the complex in both H_2O (τ_{H2O}) and D_2O (τ_{D2O}) by direct excitation of the Eu(III) centre at 394 nm, utilising the Horrocks *et al* derived equation (see Section 1.3).[17, 58] The luminescence lifetimes of Eu-49 were determined by recording the decay of the Eu(III) luminescence with respect to time and in both cases they were fitted to a mono-exponential fit.

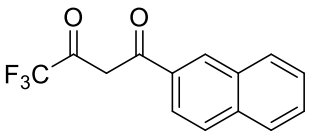

4,4,4-trifluoro-1-(naphthalen-2-yl)butane-1,3-dione
50

The lifetimes of complex Eu-**49** were measured in H_2O and D_2O, in the presence and absence of one equivalent of the ligand **nta**. The *q* values are shown below in

Table 2.1. It was determined that there were two metal bound water molecules for the complex Eu-**49** alone and that the addition of **nta** displaced both water molecules, yielding a *q* value of 0 (**Figure 2.6)**. The results shown are an average between three different measurements.

Table 2.1: *Luminescence life times of Eu-**49** in the presence and in the absence of 1 equivalent of **nta**, and the corresponding q values λ_{ex} = 395 nm.*

Sample	τ_{H2O} (ms)	τ_{D2O} (ms)	k_{H2O} (ms^{-1})	k_{D2O} (ms^{-1})	*q* (±0.5)
Eu-**49**	0.39 ± 0.01	1.02 ± 0.01	2.59	0.97	1.6
Eu-**49** + **1eq nta**	0.81 ± 0.01	1.23 ± 0.01	1.23	0.81	0.1

2.3.2 Evaluating the change in the luminescent properties of Eu-49 and nta

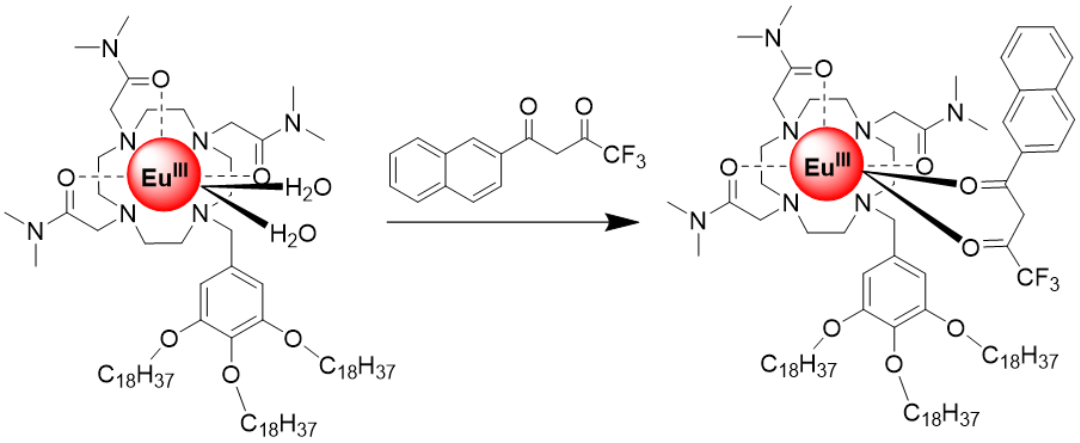

Figure 2.6: *Coordination of **nta** to the Eu(III)centre forming Eu-**49**-**nta**.*

Solution-state binding studies next then were carried out at a concentration of 1×10^{-6} M in MeOH. MeOH was used as a solvent in preference to either water or $CHCl_3$ as the solubility of Eu-**49** was too low in water to obtain satisfying results for the preliminary studies. The UV-visible absorption, fluorescence, phosphorescence, and

excitation spectra along with lifetimes of Eu-**49** were all recorded in the presence and absence of one equivalent of the external antennae **nta** (**Figure 2.7**).

Without the external antenna, the only significant absorption band was located at ca. 280 nm and can be attributed to the π-π* transition of the phenyl ring of the ligand. The addition of **nta** to a solution of Eu-**49** resulted in a UV-visible absorption with bands centred at 250 nm, 280 nm and 330 nm, characteristic of the **nta** antenna. The mechanism of action of **nta** is shown in **Figure 2.6**. Both carbonyl moieties of the β-diketone coordinate to the Eu(III) centre, displacing the two water molecules. Upon excitation the energy is absorbed by **nta** antenna and the Eu(III) metal centre

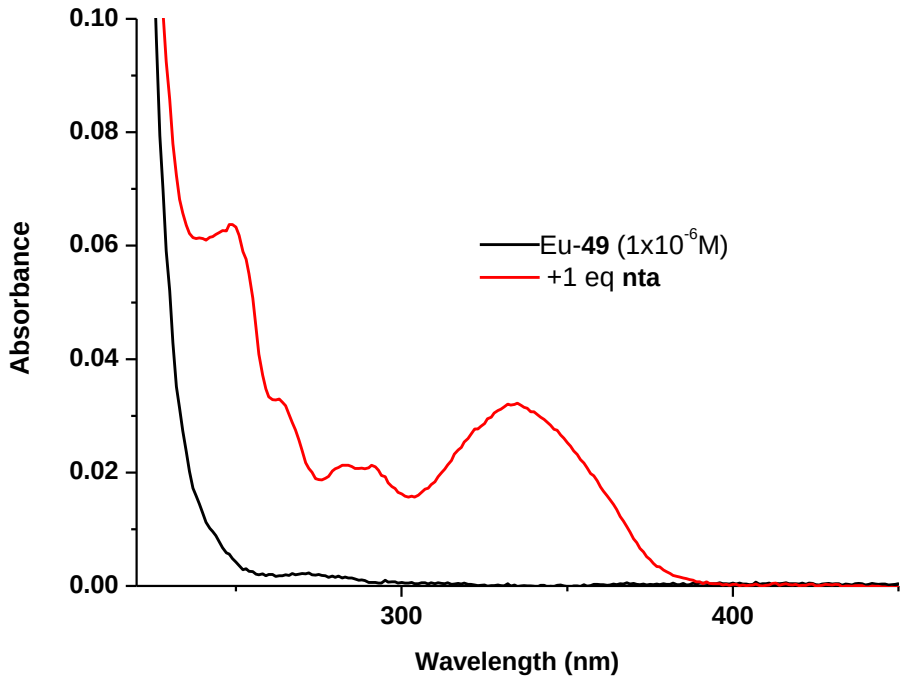

Figure 2.7: *The UV-vis absorption spectra of* ***Eu-49*** *in the absence (-) and presence (-) of one equivalent of the antenna* ***nta*** *in MeOH solution (1× 10^{-6} M).*

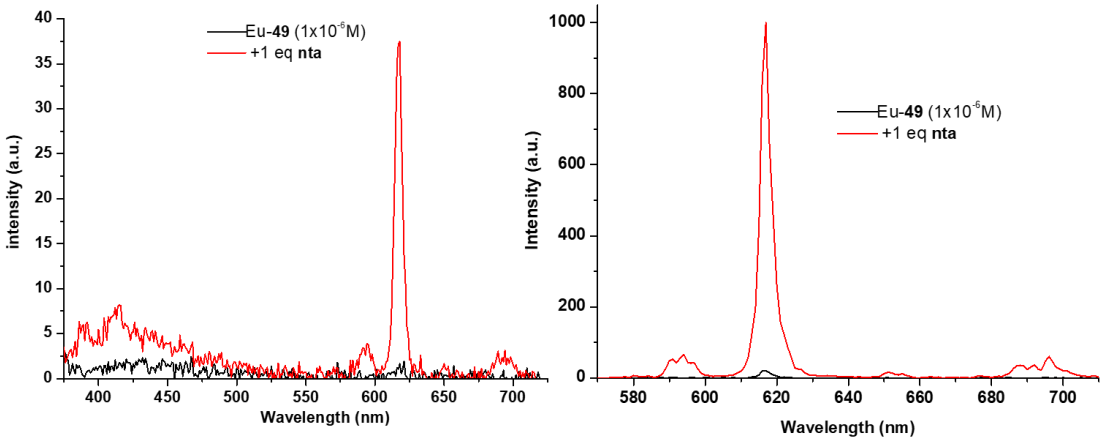

Figure 2.8: *(left) The fluorescence and (right) phosphorescence spectra of* ***Eu-49*** *in the absence (-) and presence (-) of one equivalent of the antenna* ***nta*** *in MeOH solution (λ_{ex} = 330 nm, 1 x 10^{-6} M).*

is excited *via* energy transfer (*via* antenna). In **Figure 2.8** the luminescence spectra of the complexes Eu-**49** and are shown.

As can be seen from Figure 2.8, in the absence of **nta** the Eu(III) emission was very weak and almost indistinguishable from the baseline (λ_{ex}= 330 nm). However, upon the addition of **nta**, and excite of same wavelength the sensitisation of the Eu(III)-metal centre of Eu-**49** occurred. This was verified by recording the phosphorescence spectrum of both Eu-**49** and Eu-**49-nta** (**Figure 2.8** B). here, coordination of the antenna to the Eu(III) centre resulted in displacement of the water molecules

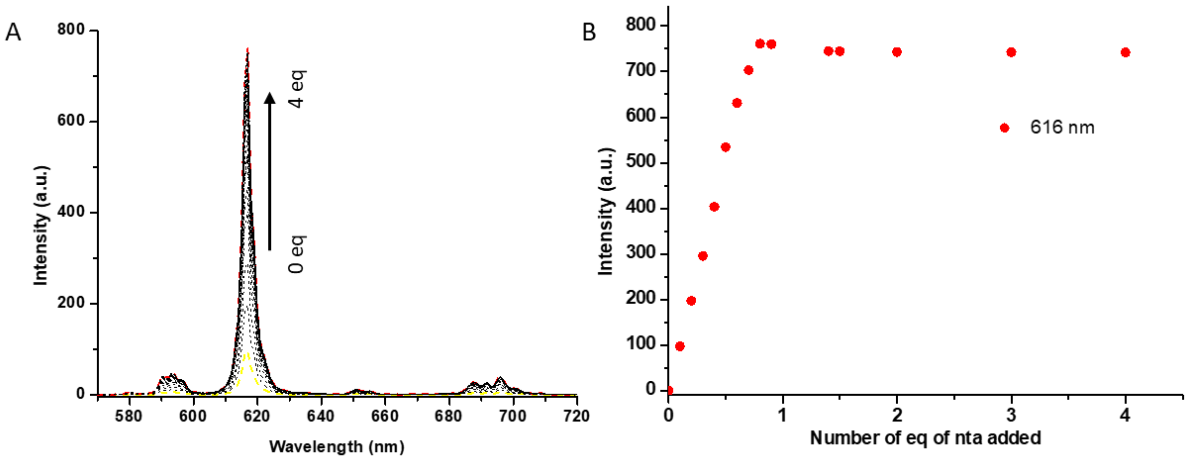

Figure 2.9*: (A) Change in the* ***Eu-49*** *complex emission spectrum (1 × 10^{-6}M) in MeOH (λ_{ex} = 330 nm) upon the addition of 0 to 4 equivalents of f* ***nta****. () **Eu-49** complex luminescence at 616 (red), nm as a function of number of equivalents of* ***nta*** *added.*

coordinated (as seen by changes in the spectra above) to the Eu(III) centre, resulting in a considerable increase in the Eu(III)-centred emission. The enhancement could be seen both in the fluorescence as well as in the delate phosphorence mode of the spectrometer as is evident in **Figure 2.8** Having demonstrated the large enhancement in the Eu-centred emission using **nta**, the stoichiometry between the

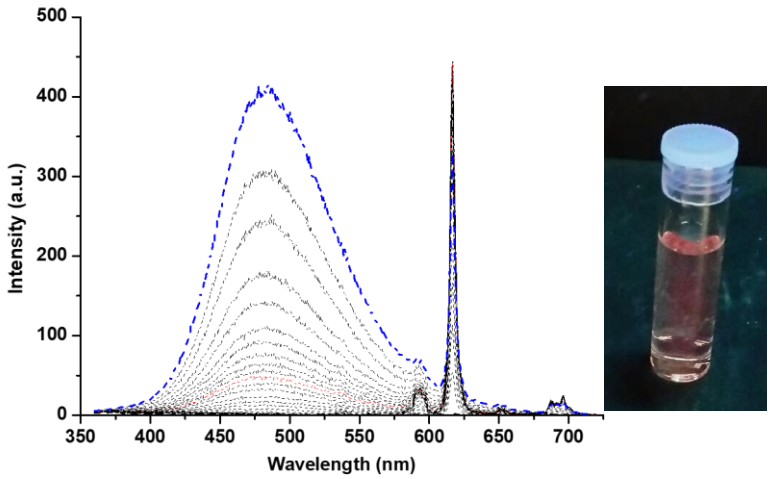

Figure 2.10: *Luminescence spectra of* **Eu-49** *(1×10^{-6} M) in MeOH in presence of different equivalents of* ***nta****, (Inset) The photograph showing luminescence of the* ***Eu-49-nta*** *in MeOH at λ_{ex} = 330 nm. The emission is not visible with the naked eye.*

two was next investigate by carry out the titration way. **Figure 2.9** shows the phosphorescence spectra obtained during the titration of Eu-**49** with **nta**. The Eu(III)centred emission ($^5D_0 \rightarrow {}^7F_J$, J = 0–4) initially increases with the amount of **nta** added, reaching a maximum when the stoichiometric ratio between Eu-**49** and **nta** was 1:1 with no changes their effects. The fact that the Δ2 band is so intense shows that the antenna is bound directly to the Eu(III) ion. The 1:1 complex the most luminescent species in solution due to the effective binding of the **nta** antenna with both carbonyl groups to the metal, and the concomitant enhancement of the Eu(III) centred emission. Upon the addition of further equivalents of the antenna, there was a slight quenching in the Eu(III) signal, probably due to inner filter effect due to the increasing of the amount of 1:1 species in solution or possible partial dissociation of Eu-**49**-**nta** in the solution.

Having demonstrated the large enhancement in the Eu-centred emission using **nta** the stoichiometry between the two was next investigate by carry out the titration way. Simultaneously upon recording the phosphorescence spectra the fluorescence spectra were also recorded and upon the addition of the **nta** antenna and exciting into the 330 nm band of Eu-**49**-**nta** the fluorescence spectrum a maximum centred at 470 nm was observed (**Figure 2.10**). The titration proves that the interaction between the antenna and the metal centre can be interpreted without the additional complication posed by the overlap of the signals. When the stoichiometric ratio between Eu-**49** and **nta** is 1:1 the intensity reaches a maximum, after which it again decreases. The emission intensity of the $^5D_0 \rightarrow {}^7F_J$ transitions located at 593 (ΔJ =

1), 616 ($\Delta J = 2$), 651 ($\Delta J = 3$) and 690 nm ($\Delta J = 4$) was plotted against the number of equivalents (**Figure 2.10A).**

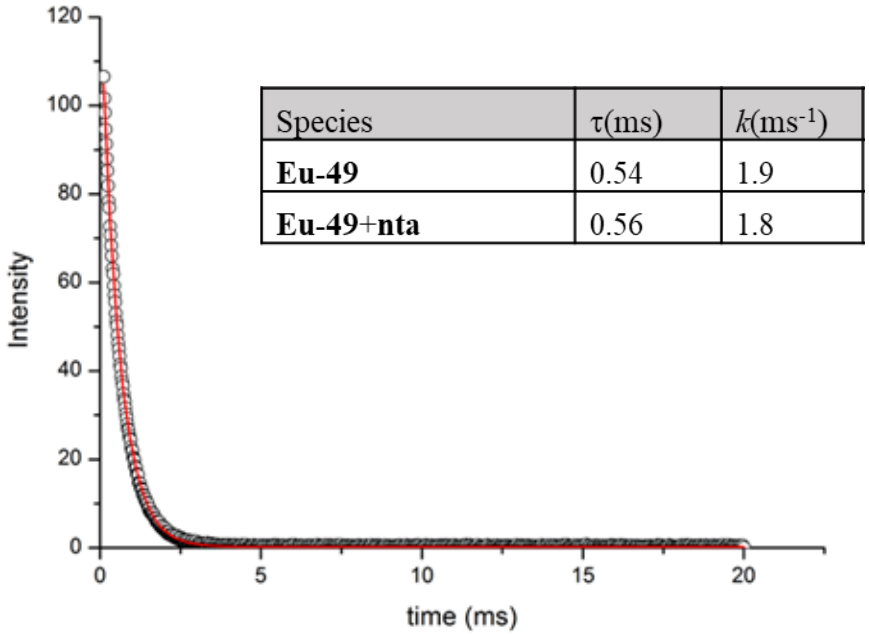

Species	τ(ms)	k(ms^{-1})
Eu-49	0.54	1.9
Eu-49+nta	0.56	1.8

Figure 2.11: *The luminescence decay of the complex* ***Eu-49*** *and its fit to a monoexponential decay in MeOH.* (λ_{ex} = 330 nm).

Excited state lifetime studies were also carried out an Eu-**49** in MeOH solution in the absence and presence of the external antennae **nta**. The values of $\tau = 0.54 \pm$ ms and $\tau = 0.56 \pm$ ms (**Figure 2.11**), were obtained for Eu-**49** in the absence and

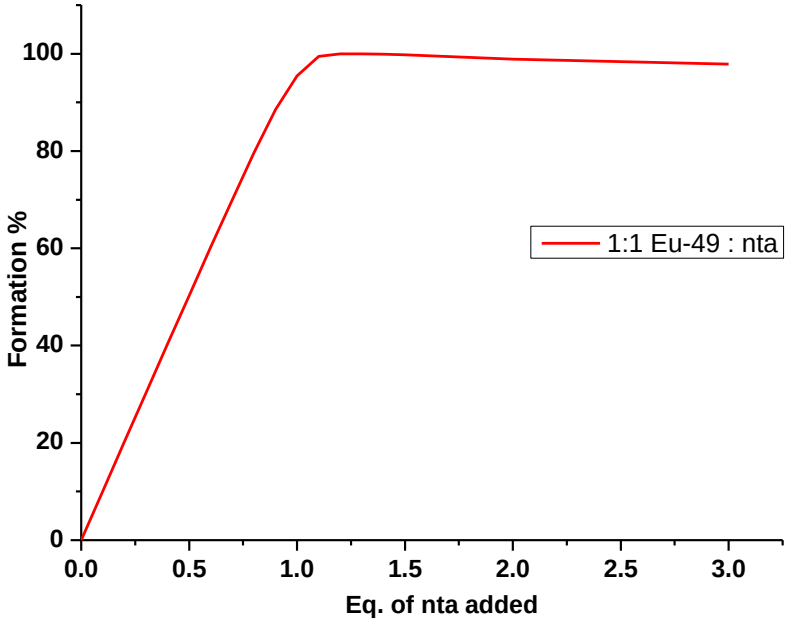

Figure 2.12: *Speciation distribution diagram obtained from non-linear regression analysis of the phosphorescence titration data of* ***Eu-49*** *with* ***nta*** *in MeOH.*

presence of one equivalent of **nta**, respectively, upon fitting the luminescence to monoexponential decay, the lifetime values were very similar. The binding constant of Eu-**49**-**nta** was calculated using a React Lab global analysis software by fitting the experimental titration data recorded in phosphorescence mode and was found to be $\log K_1 = 7.5 \pm 0.5$, A binding constant is a particular case of general equilibrium constants, which measures the bonding affinity between two or more molecules at equilibrium, this value indicates a relatively strong binding between the antenna and the complex. The speciation-distribution diagram has been generated for this set of data and it is represented on **Figure 2.12**. Upon the addition of **nta** the formation of 1:1 complex was observed to reach the maximum of 99% upon the addition of 1 equivalent of the antenna. All the experiments were performed at least 3 times, in order to demonstrate that all the experiments are reproducible.

Having successfully completed the luminescent investigation of the Eu-**49** the photophysical properties of Tb-**49** were next investigated. The same protocol applied for Eu-**49** were used and all the experiments were performed at least 3 times, in order to ensure their reproducibility.

2.4 Photophysical properties of Tb-49

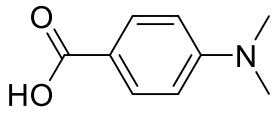

DMAB

The same photophysical studies as presented above were also performed for Tb-**49.** The phenyl ring incorporated into the ligand is able to partially sensitise the Tb(III)-centred emission but to have an efficient sensitisation an external antenna was chosen, a commercial product, compound **32** dimethylaminobenzoic acid (**DMAB**). **Figure 2.13** shows the UV-vis absorption of Tb-**49** in the absence (black) and in the presence (green) of 1 equivalent of **DMAB** antenna. Similarly, to the absorbance of Eu-**49**, the only significant absorption in the absence of any antenna is located between 230 nm a Eu and 250 nm (π-π^* transition of the phenyl ring). The addition of 1 eq of **DMAB** antenna resulted in the appearance of a band centred at *ca*. 300 nm, representative of the DMAB antenna moiety. As in the case of the Eu(III) ternary complex, excitation into the main absorption band of the antenna of Tb-**49** at λ_{ex} = 306 nm, gave rise to the emission spectrum of Tb-**49 (Figure 2.14**, left) in MeOH. Contrary to what happened in the Eu-**49**, a weak Tb(III) emission signal was present in the Tb-**49** even without the external antenna, as the phenyl ring can

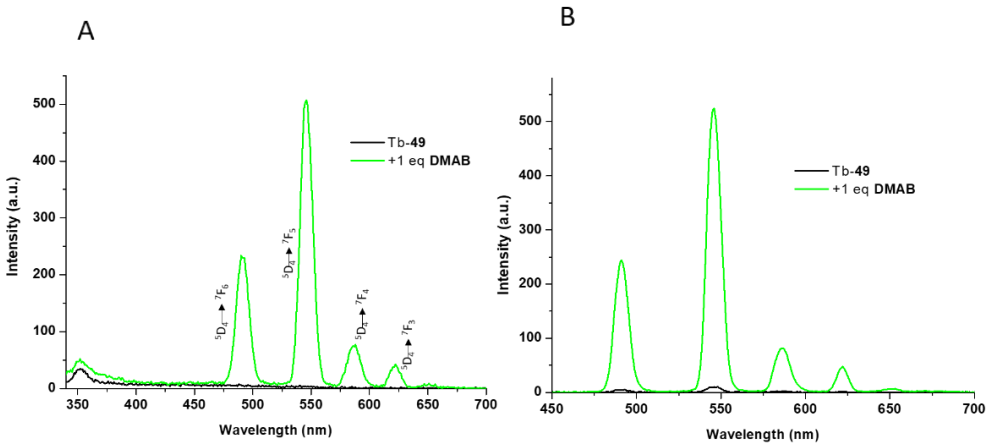

Figure 2.14: *(A) The fluorescence and (B) phosphorescence spectra of* ***Tb-49*** *in the absence (-) and presence (-) of one equivalent of the antenna* ***DMAB*** *in MeOH solution (1 x 10^{-6} M) at λ_{ex} = 300 nm.*

partially sensitise the metal centre. However as can be seen in **Figure 2.14**, right **B**, intensity was minor compared to the ternary complex.

Table 2.2*: Luminescence lifetimes of* ***Tb-49*** *in the presence of and in the absence of 1 equivalent of* ***DMAB****, and the corresponding q values.*

Sample	τ_{H2O} (ms)	τ_{D2O} (ms)	k_{H2O} (ms^{-1})	k_{D2O} (ms^{-1})	*q (±0.5)*
Tb-49	0.96	1.431	1.04	0.96	2.2
Tb-49+1 eq DMAB	0.88	1.49	1.13	0.67	0.10

Recording the spectra in phosphorescence mode a weak Tb(III) metal centred emission was observed for Tb-**49** in absence of the external antenna (λ_{ex} = 300 nm). However, upon the addition of the **DMAB** antenna a strong enhancement in the Tb(III) metal centred emission was observed which appears as the sensitisation from both of the phenyl ring of the ligand **49** and **DMAB** occurs (**Figure 2.15**, B). The lifetimes of Tb-**49** were also measured in H_2O and D_2O in the presence and absence of one equivalent of **DMAB** antenna and consequently, the *q* values were obtained, shown below in Table 2.2.

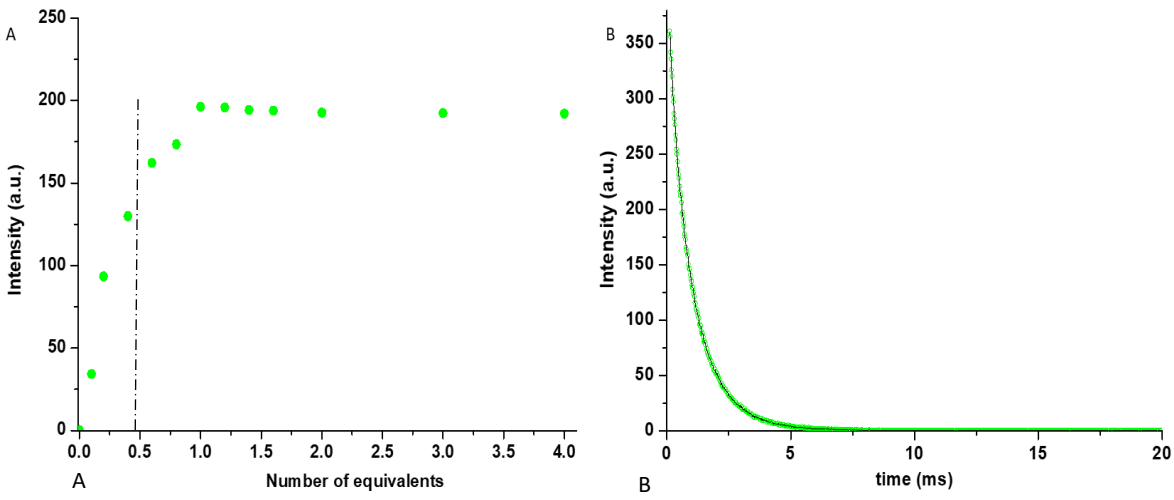

***Figure 2.15**: (A) The changes in the Tb(III)-centred emission of **Tb-49** complex (1 x 10^{-6}M) in MeOH at 545 nm as a function of number of equivalents of **DMAB** added, (B) Luminescence decay of the complex **Tb-49** and its fit to a monoexponential decay and recorded in MeOH.*

Having determined that the Tb-ternary complex was strongly emissive compared to the free complex, were next carried out the titration where the Tb(III) that It was determined that two water molecules bound the metal centre of Tb-**49** alone, while the addition of the antenna displaced these water molecules, yielding a *q* value of 0. **Figure 2.15**, left, shows that upon the addition of the **DMAB** antenna the Tb(III)-centred emission ($^5D_0 \rightarrow {}^7F_J$, J = 0–4) initially increases, reaching a maximum when the stoichiometric ratio between Tb-**49** and **DMAB** is 1:1 and the plateau is formed. The 1:1 complex is the most luminescent species in solution due to the effective binding of the antenna to the metal complex, and the concomitant enhancement of the Tb(III)-centred emission. Upon the addition of further equivalents of the antenna, no other species seems to be formed in which there is less efficient energy transfer from the ligand to the metal centre. The binding constant between Tb-**49** and **DMAB** has been calculated using React Lab global analysis software[120] by analysing the data obtained from the phosphorescence titration of the Tb(III) complex with the **DMAB** antenna, and was found to be $\log K_{1:1} = 5.0 \pm 0.5$ for Tb-**49**-**DMAB**, indicating relatively strong binding between the antenna and the complex but weaker compared to binding between **Eu**-**49** and **nta**.

After the synthesis and the characterization of both complexes and their ternary antenna complexes. and having established the photophysical properties of Eu-**49** and Tb-**49**, the ability of the complexes to form LB monolayers on a water subphase and to form LB films was investigated.

2.5 Formation of the Langmuir Monolayer of Eu-49 and Tb-49

The ability of both complexes to form Langmuir monolayers at an air-water interface was next investigated. The experiment process was carried out in collaboration with three different groups in three different stages starting at the University of Southampton, in collaboration with the group of Professor Jonathan Kitchen, after at the University of Bern, with Prof. Martin Albrecht and finishing at the University of Catania, in collaboration with the group of Professor Giovanni

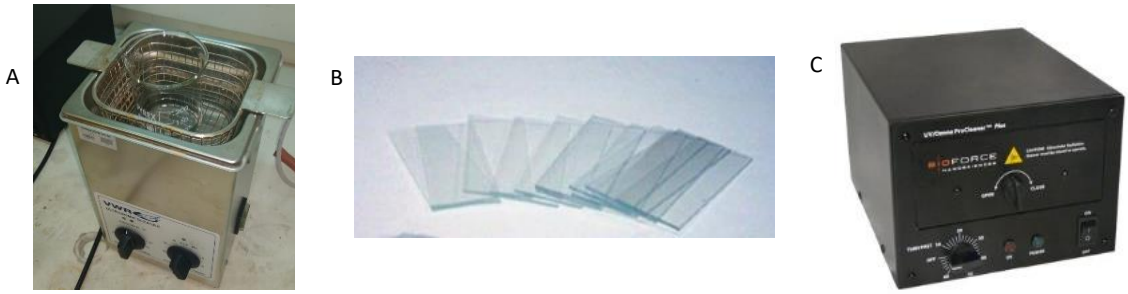

***Figure 2.16**: (A) Beaker with solvent placed inside the sonicator, (B) quartz slides, (C) UV-ozone extinguisher.*

Marletta. Before performing the deposition, the quartz slides (**Figure 2.16 B**) have been thoroughly cleaned, they were first sonicated with chloroform, methanol and water (**Figure 2.16 A**) and finally they were placed in a UV-Ozone generator (**Figure 2.16 C**) in order to remove the radical species in the surface. The deposition was performed using a Langmuir-Blodgett through (**Figure 2.17**, **A**), an apparatus made of a pool filled with water and two mobile barriers. A Wilhelmy plate (**Figure 2.17 B**), that is a thin plate used to measure equilibrium surface or interfacial tension in the air-liquid interface and an immersion/emersion system was used to determinate the LB film formation. The entire apparatus is placed in a glass box to isolate from external atmosphere and pollution present in the air.

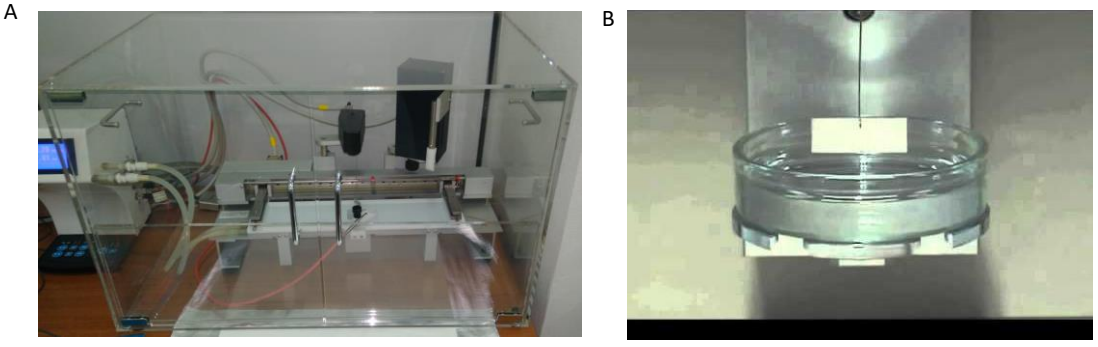

***Figure 2.17:** (A)The photograph of Langmuir-Blodgett through; (B) The photograph of a Wilhelmy plate and Petri dish.*

Once that the cleaning process was completed, a monolayer formation was

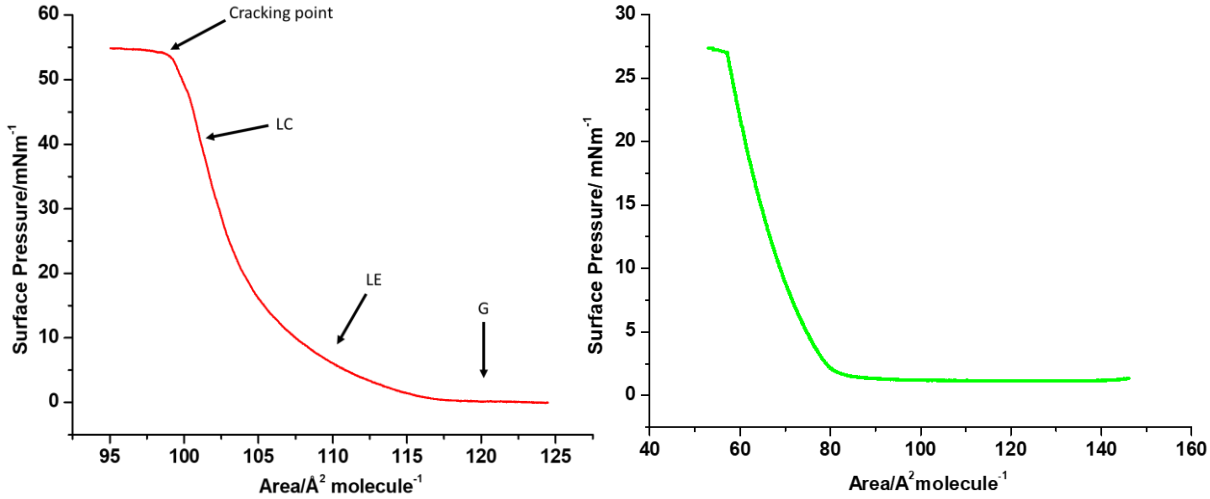

***Figure 2.18**: Surface pressure-area isotherm of (left) Eu-**49** and (right) Tb-**49**indicating phase transitions and a cracking point.*

investigated by spreading 20 µL of a solution of Eu-**49** in $CHCl_3$ (2.5×10^{-4} M) onto the surface of the water subphase at room temperature (22°C). The solvent was allowed to evaporate over a period of *ca.* 20 minutes before the barriers were closed at a rate of 6 mm min^{-1} while the surface pressure of the decreasing area was continuously monitored.

The graph in **Figure 2.18** shows the steps relative to the formation of the film on the water surface. While the barriers are closed a gas-like phase (G) is initially observed and it is maintained at areas greater than 115 $Å^2$ for Eu-**49** and 85 for Tb-**49** , while the compression is going on, there is the formation of the LE states (Liquid Expanded state), which existed over only short surface area of 115-107 $Å^2$ for the Eu-complex and only for a short surface between 70 and 85 $Å^2$ for Tb-complex. After that the surface pressure value drastically increase until the condensed liquid state (LC) arrive at the cracking point that resulted slighty higher for Eu-**49** (around 100 $Å^2$) compared to the Tb-complex, that crack around 60 $Å^2$. As previously mentioned, all the experiments were carried out by myself in different countries and over a period of time, and all the results were comparable, proving the reproducibility of the systems.

2.6 Stability of the Langmuir Monolayer

Before depositing the monolayer onto the quartz slide, the stability of the monolayers was investigated. Once the barriers of the Langmuir-Blodgett trough reached the position of LC phase, they were held at that position in order to monitor the alteration in the surface pressure for a period of 110 minutes. The results for **Eu-**

49 and **Tb-49** are shown in **Figure 2.19**. The monolayers were stable for a relatively long time (over 1 hour), this indicated that both Langmuir monolayers were relatively stable at the air/water interface.

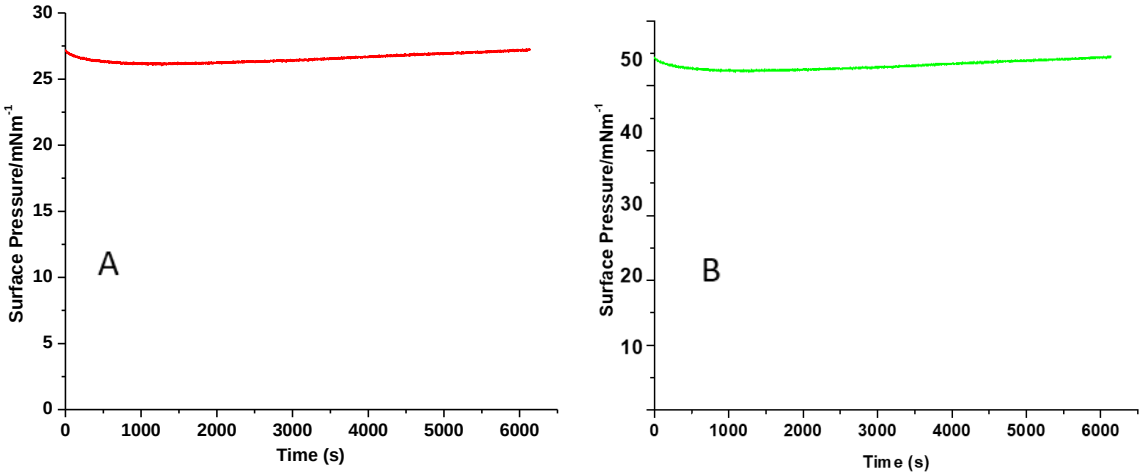

Figure 2.19: *Stability plots for (A)* ***Eu-49*** *and (B)* ***Tb-49.***

Having performed this experiment we proved the successful Langmuir monolayer formation of both lanthanide complexes. Therefore we next decided to apply the Langmuir-Blodgett technique to immobilise the complexes onto a solid support and examine the photophysical properties of the LB films using absorption and steady-state spectroscopy.

2.7 Deposition of Langmuir-Blodgett mono and bilayers onto the quartz slides

For the dipping process a quartz slide as solid support has been employed. The isotherm measurements proved that the deposition would happen through interactions of hydrophilic nature between the polar head groups of the amphiphilic chains of the complex and the hydrophilic surface of the quartz slide. Because of this LB depositions of **Eu-49** and **Tb-49** were carried out by the vertical dipping method, the quartz slide was lowered and submerged to a depth of 5 mm below the water subphase surface. Having submerged the quartz slide, 20 µL of a solution of Eu-**49** or Tb·**49** in $CHCl_3$ (2×10^{-4} M) was spread onto the water surface. The solvent

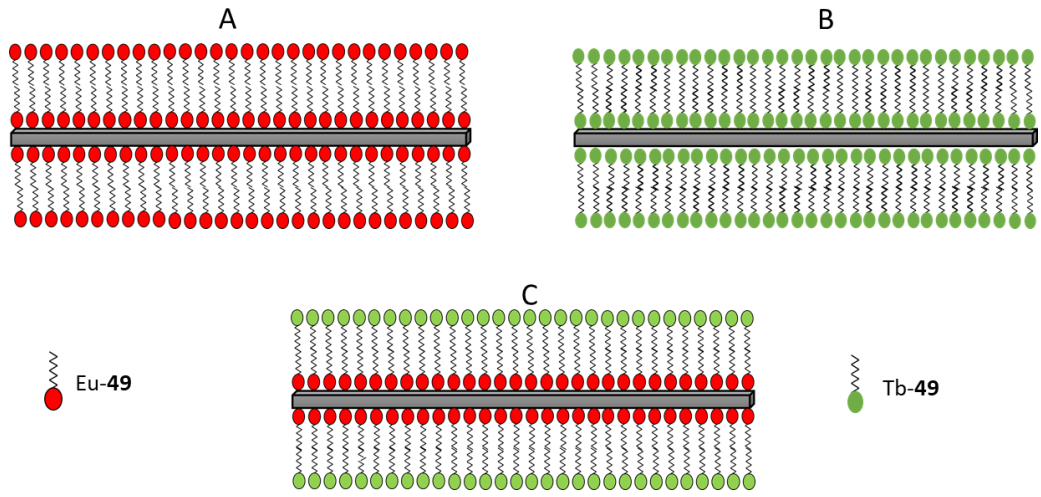

Figure 2.20: *Deposition of the complexes onto the quartz solid substrate.*

was allowed to evaporate for 20 minutes and the barriers were slowly closed and eventually locked, holding the surface pressure of 27 mN/m allowing the monolayer to equilibrate for 10 min. At this pressure the amphiphile was organised into its LE phase and allowed to stabilise for 20 minutes before emersion of the slide occurred by an upward stroke, resulting in successful monolayer transfer. For bilayer deposition, initial immersion of the clean slide resulted in no film transfer. Emersion, however, gave full monolayer transfer, and a subsequent final immersion step gave a transfer ratio of 0.8 for the second layer. This allows us to infer that the hydrophilic Eu-containing moieties adhere to the glass on the upstroke, leaving the surface decorated with hydrophobic alkyl chains onto which the second layer is deposited in a Y-type regime (Y-type deposition film possess head-to-head and tail-to-tail configuration). The dipping speed was maintained at 3 mm/min and three different bilayers were formed (**Figure 2.20**) through incorporation and additional immersion step, followed by aspiration of the surface. At least 20 minutes drying time was allowed following each deposition. To measure the efficiency of the transfer from the water surface onto the quartz slide, the transfer ratios were recorded and are reported in Table 2.3. All the deposition were performed at least 3 times.

Table 2.3: *Transfer ratio values for different deposition experiments*.

LB film	**Eu-49**	**Tb-49**	**Eu-49/Tb-49**
Monolayer	1.20	1.18	-
Bilayer	1.03 (emersion)	0.94 (emersion)	1.02 (emersion)

	0.80 (immersion)	1.00 (immersion)	1.02 (immersion)

All the deposition performed in the different groups resulted in a transfer ratio >1 for the monolayer and ~1 for the bilayer proving the reproducibility within LB monolayers formation for this system. The transfer ratio values indicating a high-quality transfer of the monolayers and of the bilayer onto the quartz slide was observed as the system seems to have high order and uniformity. From these results it was clear that the molecules had the correct hydrophobicity, indeed the ration between it and the large polar head group was sufficient for the formation of Langmuir monolayers. Having successfully performed the deposition of the monolayers, the next step was to investigate the emission properties of these.

2.8 "Switching On" the Eu(III) and Tb(III) emission from Langmuir-Blodgett films of Eu-49 and Tb-49

Since the LB monolayers of Eu-**49** and Tb-**49** were successfully deposited, their photophysical properties were next investigated. The spectra were recorded with plane of the slide oriented perpendicular to the incident measuring beam using a support. Unfortunately, the UV-Vis absorption signal was too low and too noisy to be recorded accurately, confirming the previous studies carried out from the

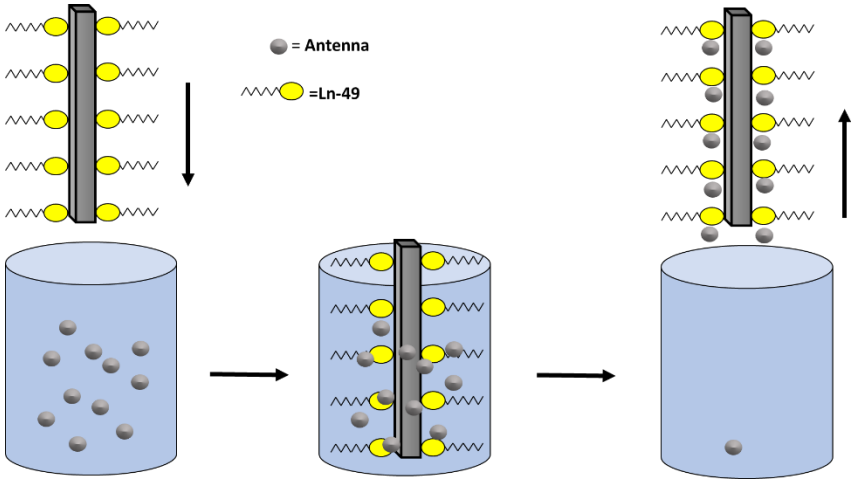

Figure 2.21: *Schematic representation of the dipping process.*

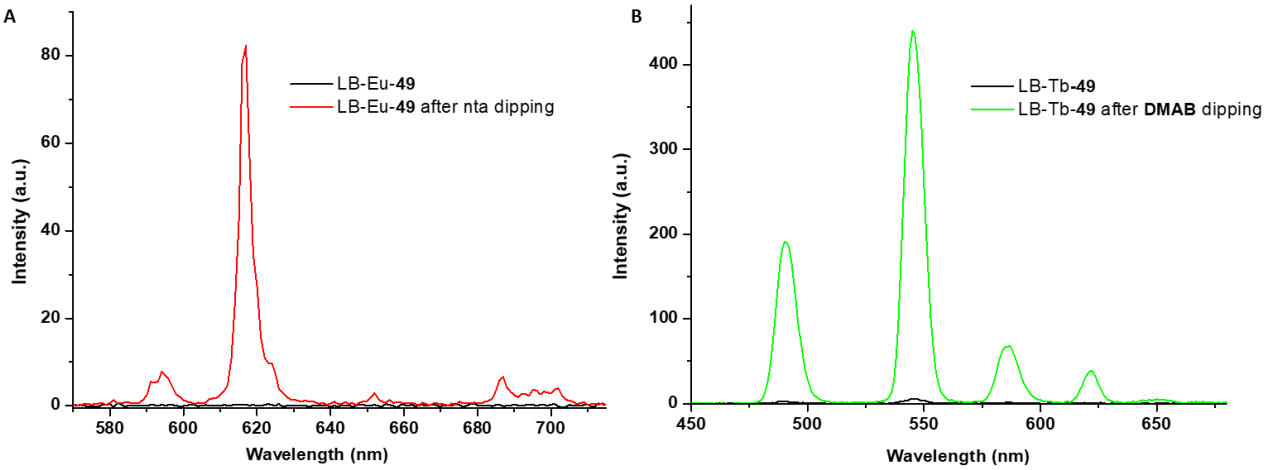

Figure 2.22: *(A) Eu(III)-centred emission from the monolayer LB-**Eu-49** before (black) and after (red) the dipping into an aqueous solution of **nta** 1 x 10^{-4}M, λ_{ex} = 330 nm and (B) (A Tb(III)-centred emission from the monolayer LB-**Tb-49** before (black) and after (green) the dipping into an aqueous solution of **DMAB** 1x10^{-4}M, λ_{ex} = 306 nm.*

Gunnlaugsson group. The luminesce emission recorded in phosphorescence mode was however for both complexes not detectable but became visible upon titration with the antenna and forming ternary complex as a result. The slides were immersed in an aqueous solution of the respective antenna (**nta** or **DMAB**, 1×10^{-4} M) for one minute as shown in **Figure 2.21** after which a red emission for Eu-**49-nta** and a green emission for Tb-**49-DMAB** was visible under the UV lamp and the characteristic emission spectra were observed (**Figure 2.22**).

These results demonstrate that it was possible to "switch on" the emission of both complexes by simply dipping the slides of Eu-**49** and Tb-**49** monolayers in an aqueous solution of the corresponding antenna such as **nta** and **DMAB**. Even if the amphiphilic molecules are oriented with the head on the slide, the antenna is still able to access and bind the Ln(III) metal centre and allow an efficient sensitisation of the Ln(III) metal centre as is displaced in **Figure 2.21** schematically.

There is the possibility that the antenna might not be directly coordinated to the metal centre and be rather adsorbed or associated with Ln-**49** through surface adhesion interactions, however the $\Delta J=2$ band is too intense. Nevertheless the energy transfer from the antennas **nta** or **DMAB** can still occur *via* electrostatic multipolar (Förster) mechanism that may extend through long distances (up to 1000 pm) and its specific dependence on the distance *d* separating the donor D from acceptor A is d^{-6}.[121] The next part of the study was focused to probe the limit of detection (LOD) of **nta** by the LB-Eu-**49** and of the **DMAB** for LB-Tb-**49**. The

effect of the slide immersion time in the solution of the antenna and its concentration were investigated too.

2.9 Investigation of LOD for Langmuir-Blodgett films of Eu-49 and Tb-49

The first film to be investigated was the LB-Eu-**49** and the minimum concentration of **nta** necessary to "switch on" the Eu(III) emission was evaluated by dipping the slide into the six aqueous solutions of **nta** with concentration ranging from 1 x 10^{-8} to 1 x 10^{-3} M for 60 seconds. All the experiments were repeated using different slide in order to guarantee the reproducibility of the experiments.

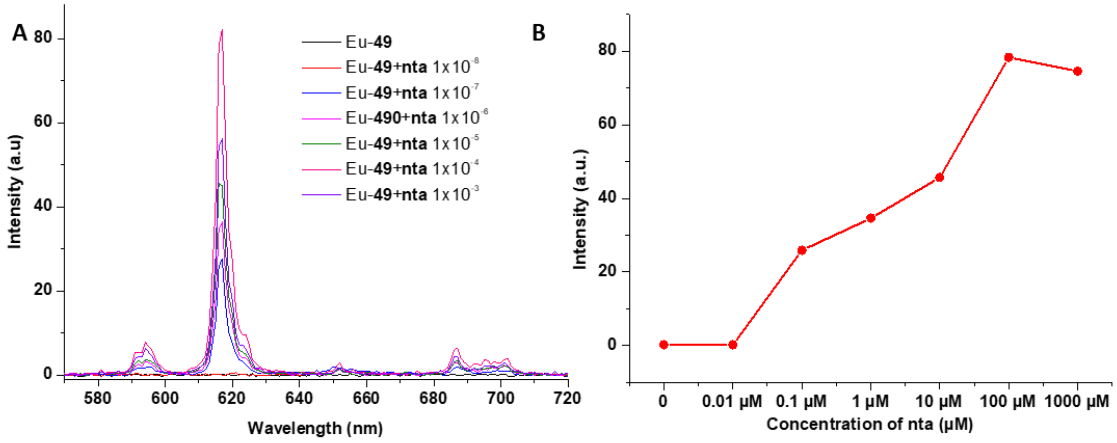

Figure 2.23: *LOD studies of LB-**Eu-49** monolayers upon dipping into **nta** aqueous solution at different concentrations from 1 x 10^{-8} M to 1 x 10^{-3} M (λ_{ex} = 330 nm) showing (left) Eu(III)-centred emission spectra and (right) increase of emission at 616 nm vs concentration. –*

As shown in **Figure 2.23**, then the 1 x 10^{-8} M solution of **nta** was not able to switch on the Eu(III) centre emission, and it was determined that the minimum concentration required to activate the system is 1 x 10^{-7} M. Increasing the concentration of the **nta** solution from 1 x 10^{-7} M to 1 x 10^{-6} M resulted in further enhancements while when going from the concentration of 1 x 10^{-6} M to 1 x 10^{-5} M a minor increase in the Eu(III)-centred emission was observed. However, when the concentration of 1 x 10^{-4} M was used the emission reached its highest value. Further increase of the concentration of **nta** to 1 x 10^{-3} M lead to a slight quenching as the Eu(III) binding centres in this case should be fully saturated.

The LOD of **DMAB** by LB-Tb-**49** was also investigated in order to determine the minimum concentration of **DMAB** necessary to "switch on" the Tb(III)-centred emission. The results reported in **Figure 2.24** show that initial LB-Tb-**49** monolayer possess a weak Tb(III)-centred emission as in this case the phenyl ring is able to

sensitise Tb(III) centred emission. The LOD for **DMAB** by the LB-Tb-**49** monolayer was evaluated and it was found it higher than LOD of **nta** using LB-Eu-**49** monolayer. As shown in **Figure 2.24**, the lowest concentration of **DMAB** being able to "switch on" the emission of LB-Tb-**49** monolayer was 1 x 10^{-8} M. Increasing the concentration of the **DMAB** solution from 1 x 10^{-7} M to 1 x 10^{-4} M results in further Tb(III)-centred emission enhancements. Moving to higher concentrations, such as 1 x 10^{-3} M, leads to a weak luminescence quenching (**Figure 2.24** B**)**.

As the immersion time is an important variable to consider, it was also next investigated. **Figure 2.25** A shows the results of kinetic studies where the same sample of LB-Eu-**49** monolayer was dipped six times for respectively 5, 10, 20, 30 and 60 seconds in an aqueous solution of **nta** 1 x 10^{-4} M. The results show the highest enhancement when the slide is dipped for 30 seconds where the luminescence intensity saturation occurs, after this there was only a slight increase

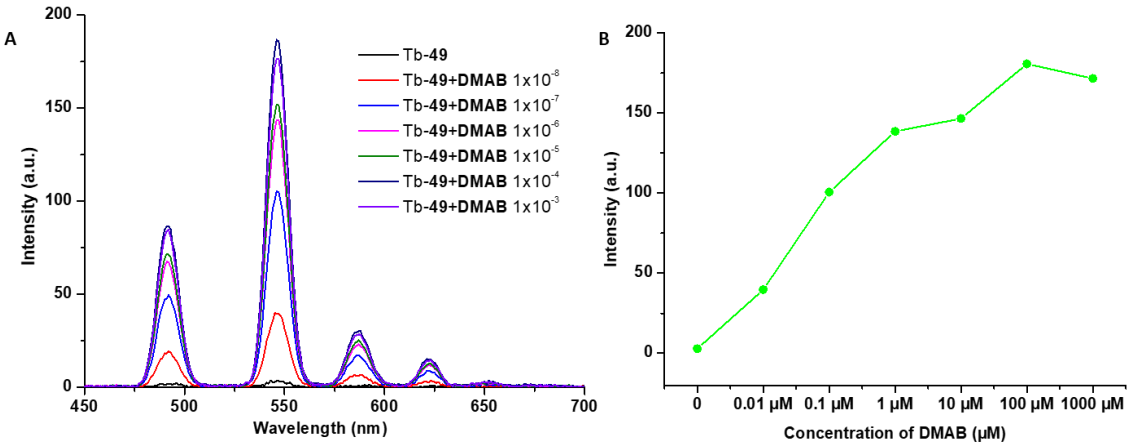

Figure 2.24: *LOD studies of LB-**Tb-49** upon dipping into **DMAB** aqueous solution at different concentration from 1 x 10^{-8} M to 1 x 10^{-3} M (λ_{ex} = 306 nm) where () shows the changes in Tb(III)-centred emission spectra and (B) increase of the emission at 545 nm vs concentration recorded in phosphorescence mode.*

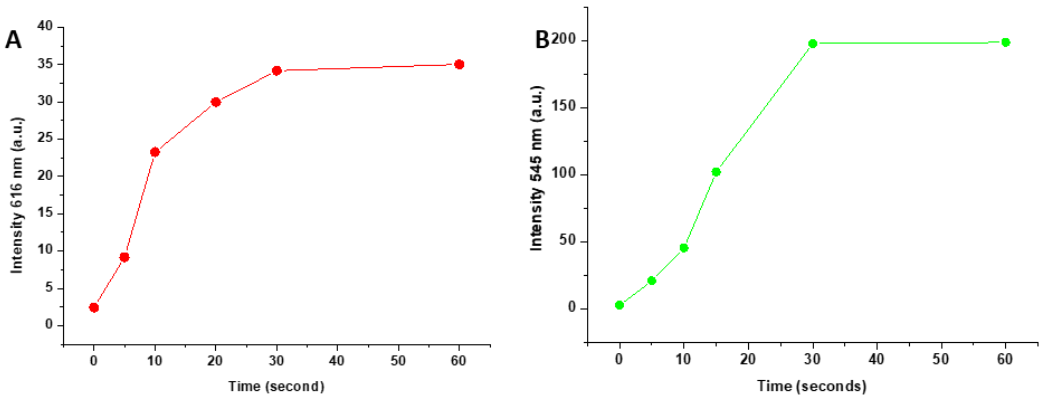

Figure 2.25: *Kinetic studies where (A) LB-**Eu·49** was immersed into an aqueous solution of **nta** at 1 x 10^{-4}M for different times (0-60 sec), λ_{ex} 330 nm and (B) LB-**Tb·49** was immersed into an aqueous solution of **DMAB** at 1 x 10^{-4} M for different times (0-60 sec), λ_{ex} 306 nm*

when the slide was dipped for 60 seconds. This shows that in 30 seconds all the Eu(III)-centres Eu-**49** molecules within LB monolayer coordinate the antenna molecules.

The same investigation was performed for LB-Tb-**49** where the monolayer was immersed into the aqueous solution of **DMAB** at the concentration of 1 x 10^{-4} M for various time in the range of 0-60 seconds. The Tb(III)-centred emission was then recorded, and the results are represented on **Figure 2.25**, B. The maximum luminescence enhancement was observed after dipping time of 30 seconds which gave the highest enhancement after which a plateau was observed most likely because all the molecules of Tb-**4**9 were saturated with the **DMAB** antenna.

Once the LOD of **nta** and **DMAB** in aqueous solution by the LB monolayers of Eu-**49** and Tb-**49** was determined, the next step was to investigate the stability of the LB monolayers under a constant flow of water.

2.10 Flow test for Eu-49 and Tb-49 Langmuir-Blodgett monolayers

In order to understand the stability of LB-Eu-**49** and LB-Tb-**49** on the quartz slide within aqueous medium, a flow test was carried out. In this experiment the quartz slides coated with the LB monolayers were clamped within a beaker into which a slow flow of water would pass through. **Figure 2.27** shows the schematic representation of the experiment setup of the flow system and the obtained luminescence response results. The slide LB-**Eu-49-nta** was tested over various period of time (from 0 to 60 minutes) after being immersed under the water flow of 75 mL / minute. The slide showed a significant decrease in the emission intensity at 616 nm upon the excitation at 330 nm. After 5 minutes under the water flow, the emission intensity decreased by 75 % and after 1h the observed quenching was over 97 %. After one hour under the water flow this quartz slide was dipped into a **nta** solution (c = 1 x 10^{-4} M) but upon an excitation at 330 nm, no Eu(III)-centered

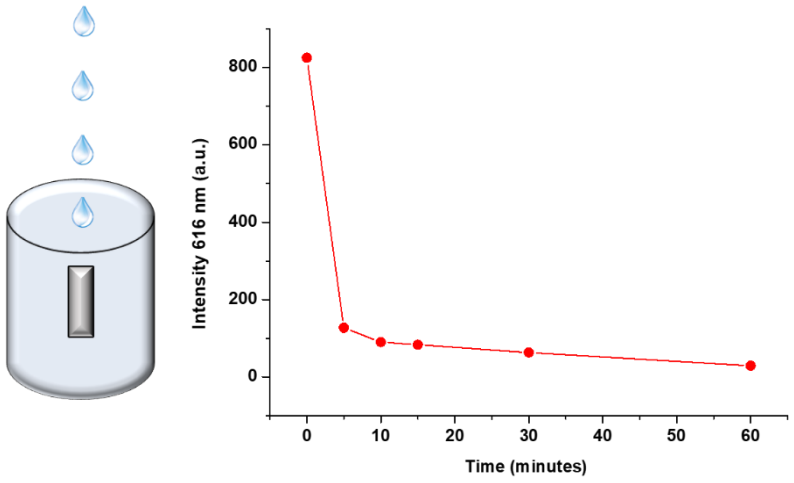

Figure 2.26: *Representation of flow cell setup with quartz slide inside the beaker under constant water flow (left). The changes in the LB-**Eu-49** emission at 616 nm for 60 minutes (λ_{ex} = 330 nm) under the water flow.*

emission was found. Therefore, it is possible to deduct that the quenching is not due to a displacement of the antenna from an external analyte but that the water flow "washed out" the monolayer from the quartz slide.

The same experiment was performed for the LB-Tb-**49** monolayer and **Figure 2.28** represents the change of Tb(III)-centred emission at 545 nm after LB-Tb-**49** was put under the water flow for various period of time (0 – 60 minutes). The slide with the LB-Tb-**49** was tested in range of time between 5 and 60 minutes, the same as the LB-Eu-**49**, under a water flow with the rate of 75mL / minute. After 5 minutes the emission drastically decreased (emission at 545 nm upon the excitation at 306 nm) by 95% and after 60 minutes it was undetectable. As for the LB-Eu-**49**, after the flow test the quartz slide was dipped again into a solution of **DMAB** and the emission was measured, but no Tb(III) centred emission was found, the molayer was

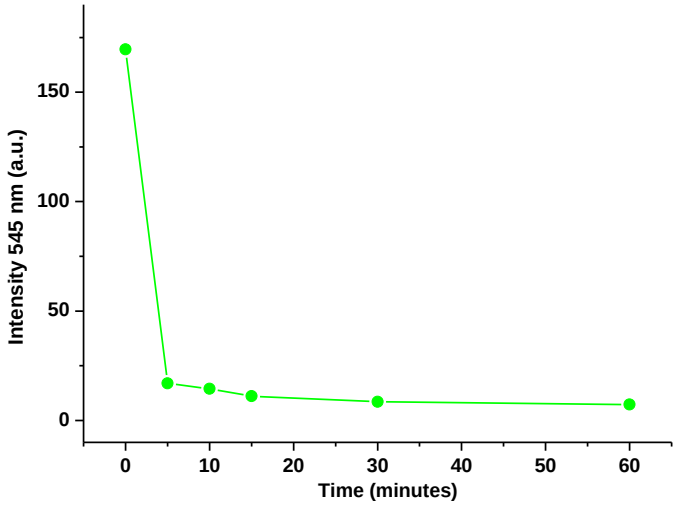

Figure 2.27: *The changes in the Tb(III)-centred emission of LB-**Tb-49** over a period of 60 minutes under the water flow (λ_{ex} = 306 nm).*

most likely removed from the quartz slide by the water flow. This experiment was not performed only to test the mechanic stability of the monolayer on the quartz slide but was also because the tap water containing various impurities (as metal ions and salts) that are analytes and that might displace the antenna and modulate the Ln(III)-centered emission. From these studies it is possible to conclude that the LB-Eu-**49** and the LB-Tb-**49** have approximately the same durability in highly competitive media.

2.11 Bilayer Deposition

The formation of bilayers on a solid support is also a crucial experiment to perform in order to obtain an enhanced emission signal which is very important in the fabrication of signaling devices.[122] The deposition of the bilayer onto the quartz slide offers the possibility to obtain hierarchical arrangements of the molecules.

Therefore, the ability of both Eu-**49** and Tb-**49** to form bilayers on the surface of quartz slides was examined.

2.11.1 Bilayer deposition of Eu-49

As reported in section 2.7, a bilayer of Eu-**49** was successfully deposited onto the quartz slide. The cleaning process of the quartz slide was the same as described in the section 2.7. The volume of 20 μL (c = 1mg/ml) of Eu-**49** solution in chloroform was spread onto the water surface. The solvent was allowed to evaporate for 10 minutes and barriers were closed until the required pressure. Initial immersion of the clean slide resulted in no film transfer. Emersion, however, gave full monolayer transfer, and a subsequent final immersion step gave a transfer ratio of 0.8 for the second layer. This allows us to infer that the hydrophilic Eu-containing moieties adhere to the glass on the upstroke, leaving the surface decorated with hydrophobic alkyl chains onto which the second layer is deposited in a Y-type regime whereby the molecules are stacked onto the quartz slide in a head to head/tail to tail pattern. When this bilayer was dipped into a **nta** 1 x 10^{-4} M aqueous solution the organization of the system became the one that is is deoicted on the **Figure 2.28**.

The slide with the bilayer was dipped into the **nta** solution for different time intervals and the results are reported in **Figure 2.29 A** were very similar to the monolayer one. After the slide was immersed for 5 seconds in an aqueous solution of **nta** 1 x 10^{-4} M its Eu(III)-centred emission increased almost 4 times, after 30 seconds the signal was almost at the maximum value, that was achieved after 60 seconds. Going beyond the 60 seconds did not give any further increase in the Eu(III)-centred emission. The investigation was perfomed using the same

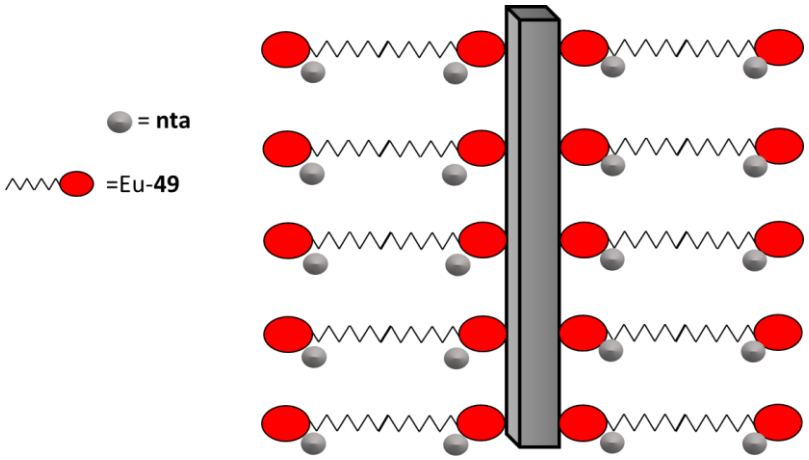

Figure 2.28: *Schematic representation of the **nta** antenna binding to the Eu(III) centres of LB-**Eu-49**.*

parameters used for the monoloyer, so that it is possible to compare the data and it was discovered that the Eu(III) emission in bilayer is significantly more intense than the one found for the monolayer (**Figure 2.29** B). For the bilayer it was possible to observe a weak emission before the slide was dipped into the **nta** solution. After dipping the sample for one minute the emission of the bilayer was four times higher than the monolayer one. This indicates higher number of **Eu-49** molecules on the surface of the quartz slide in the case of the bilayer compared to the monolayer slide.

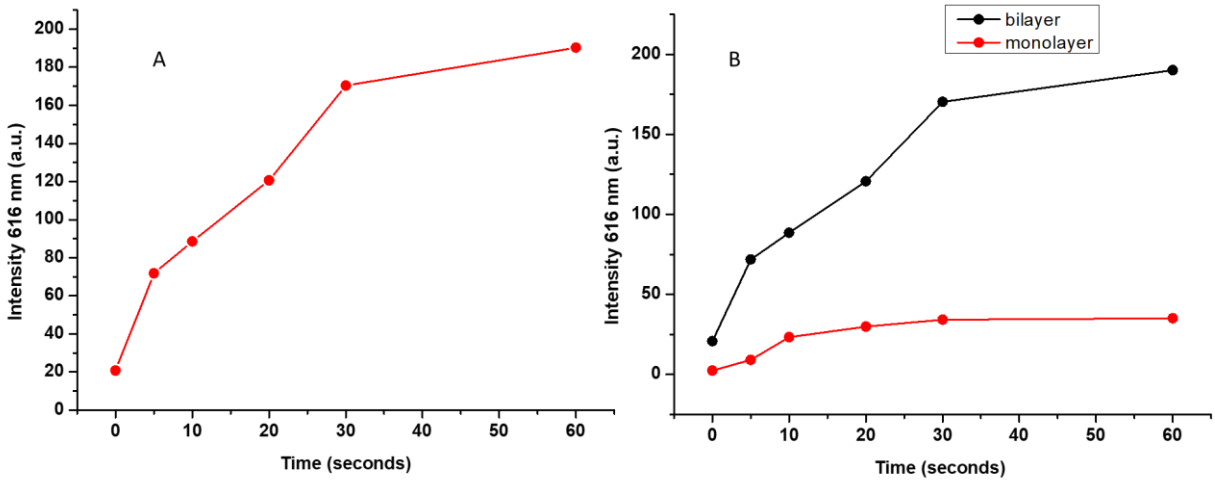

Figure 2.29: *(A) The changes of the Eu(III)-centred emission of LB-**Eu-49** bilayer upon dipping the slide into the **nta** 1 x 10^{-4} M aqueous solution (λ_{ex} = 330 nm) for different amount of time (0 – 60 seconds); (B) the comparison of the Eu(III)-centred emission intensity between the LB-**Eu-49** monolayer (red) and bilayer (black) using the same instrumental parameters.*

2.11.2 Bilayer deposition of Tb-49

As reported previously, the bilayer of Tb-**49** was successfully transferred onto the quartz slide. The procedure was the same for the Eu-**49** and even in this case, the first immersion did not give any transfer, instead the emersion resulted in an excellent transfer ratio (1) and, like in the case of Eu-**49** the second layer is deposited in a Y type regime. The bilayer was dipped in a solution of **DMAB** 1 x 10^{-4} M to "switch on" the luminescence of the system. The instrument has been set up using the same parameters for monolayers in order to compare the emission intensities. As reported in **Figure 2.30**, the emission intensity at 545 nm upon excitation at 306 nm is significantly stronger in the case of the double layer (4 time more) compared to the monolayer. Moreover, the highest emission intensity was achieved by dipping the quartz slide into the **DMAB** aqueous solution (1 x 10^{-4} M) for 15 seconds. However when keeping the slide in the solution for longer there was no significant increase in Tb(III)-centred luminescence intensity.

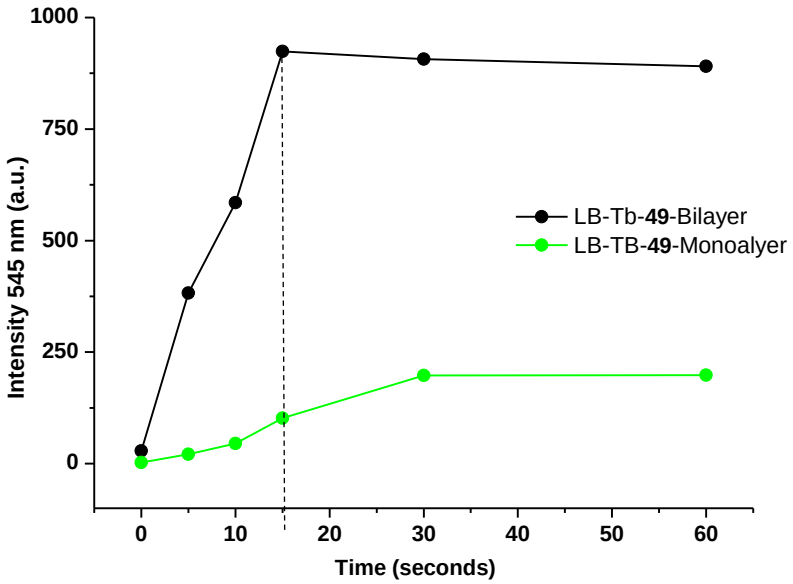

Figure 2.30: *The comparison of the Tb(III)-centred emission intensity of the LB-**Tb-49** monolayer (green) and the bilayer (black) when dipped in aqueous solution of **DMAB** 1 x 10^{-4}M (λ_{ex} = 306 nm).*

Because the 2 layers (on each side) are being present on the surface of the quartz slide, then theoretically the overall emission of the sample should be two times more intense than the one for the monolayer **SAM**. However, it was not the case and, indeed, the Tb(III)-centred emission was higher than the expected, probably the hydrophibic effect playing an important role here because it provides the hydrophobic enviroment that affect the emission,[123] mimicking shielding when the emission is not quenched by the solvent.

To conclude, here it has been demonstrated that the multilayer fabrication was limited to a maximum of three layers of Y-type deposition for both the Eu-**49** and the Tb-**49** (monolayers) on the quartz substrate. Both of the complexes proved to be able to form double layers with a good transfer ratio and both of the bilayers gave rise to more intense the Ln(III)-centred emission compared to the monolayer centred emissions, respectively employed the same multilayering process, we next set out to achieve dual Ln(III) emission using Eu(III) and Tb(III) complexes from the a single quartz slide. All the experiments were perfomed at least three times and were fully reproducible.

2.11.3 Dual Eu-49/Tb-49 Langmuir-Blodgett bilayers

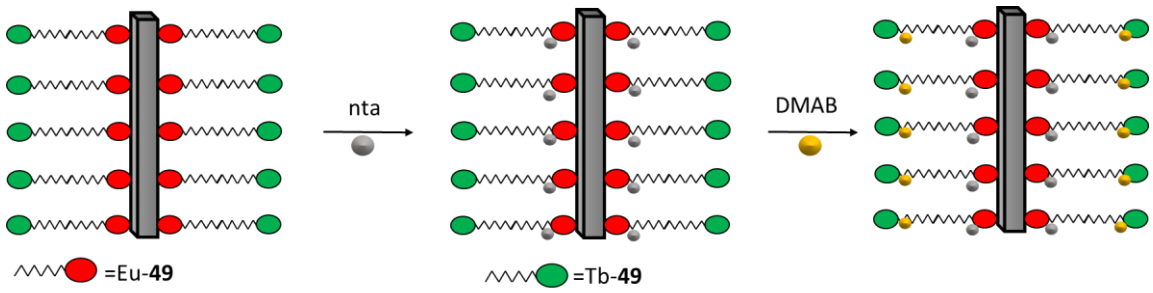

Figure 2.31: *Illustration of the dual LB-bilayer system after the dipping into a solution of* ***nta*** *1x10^{-4}M and* ***DMAB*** *1 x 10^{-4}M.*

With the purpose to achieve dual Eu(III) and Tb(III)-centred emission from a single quartz slide, the bilayer deposition was required. Employing the same multilayering process, we next set out to form Eu(III) and Tb(III) mixes quartz slides. The main advantage of the dual emission from one LB slide is its ability to monitor the Ln(III) emission over a wider range of wavelengths and the possibility to form multi ternary complexes on different antennas and enable a response from a single sample for two different analytes (**Figure 2.31**).

To achieve this, the quartz slide of the LB-Eu-**49**, monolayer formed in section 2.5 was coated with a second monolayer of Tb-**49 by** using the same protocol as described in section 2.11.1, where the quartz slide with the monolayer of Eu-**49** was dipped into the water subphase of the Langmuir-Blodgett through to generate the second layer of Eu-**49 -49** on its surface.

The slide was then slowly removed from the water by an upward stroke while monitoring the transfer of the monolayer after the Tb-**49** was formed. The transfer ratio after each deposition was close to 1, indicating a good quality of film formation. The Ln(III) emission spectra of the Eu-**49**/Tb-**49** LB was recorded before

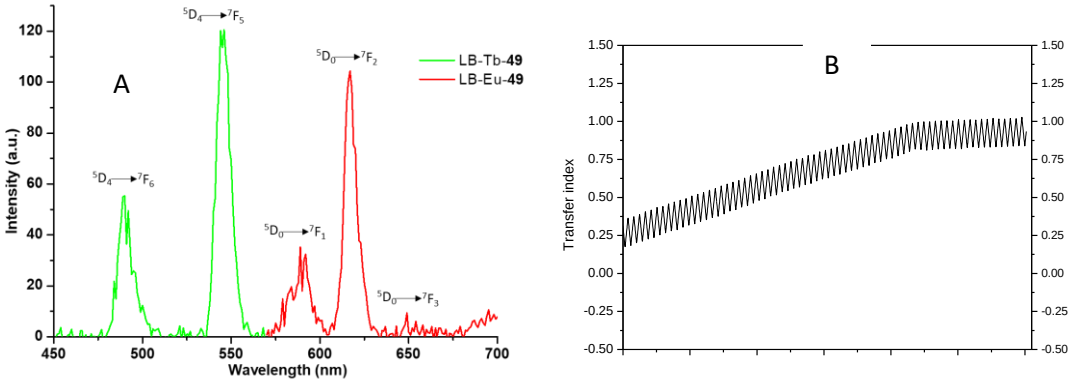

Figure 2.32*: (A): Luminescence spectra of LB-**Tb-49 -Eu-49** showing the characteristic Tb(III) $^5D_4 \rightarrow ^7F_J$ (J = 6, 5) and Eu(III) $^5D_0 \rightarrow ^7F_J$ (J = 1–3) transitions (λ_{ex} = 300 nm). (B): Transfer index transfer graph of **Tb-49 -Eu-49** bilayer.*

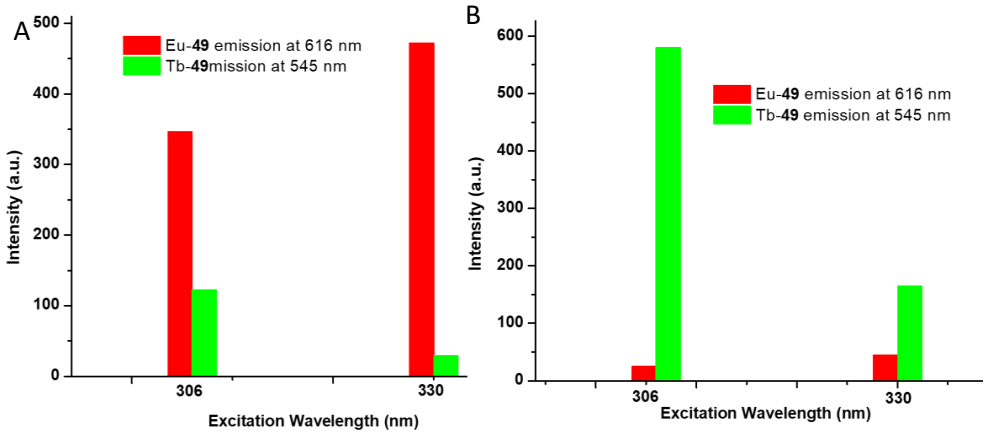

***Figure 2.33**: Eu(III)- or Tb(III)-centred emission at 545(λ_{ex} = 306 nm) nm and 616 nm (λ_{ex} = 330 nm) of LB-**Eu-49**/**Tb-49** bilayer after dipping into (A) the aqueous solution of **nta** 1 x 10^{-4} M and the following dipping of the same layer (B) into the aqueous solution of **DMAB** 1 x 10^{-4} M.*

dipping into the antenna solution and its luminescence spectrum is shown on **Figure 2.32**.

The characteristic emissions at 545 nm for LB-Tb-**49** and 616 nm for LB-Eu-**49** without the addition of an external antenna was detected. For the LB-Tb(III) complex it was expected, as previously mentioned, that the phenyl ring of the ligand would be able to sensitise the Tb(III) metal centre. For the LB-Eu(III) a bright emission like that one shown in **Figure 2.32** it usually not expected without the use of an external antenna. It is possibile that this is due to the fact that the energy level of the Tb(III) is higher compared to Eu(III) one,[47] allowing the energy transfer from Tb(III) to Eu(III) levels and in turn leading to the brighter signal from the LB-Eu-**49** in this case. The response of the bilayer sample towards the presence of antenna

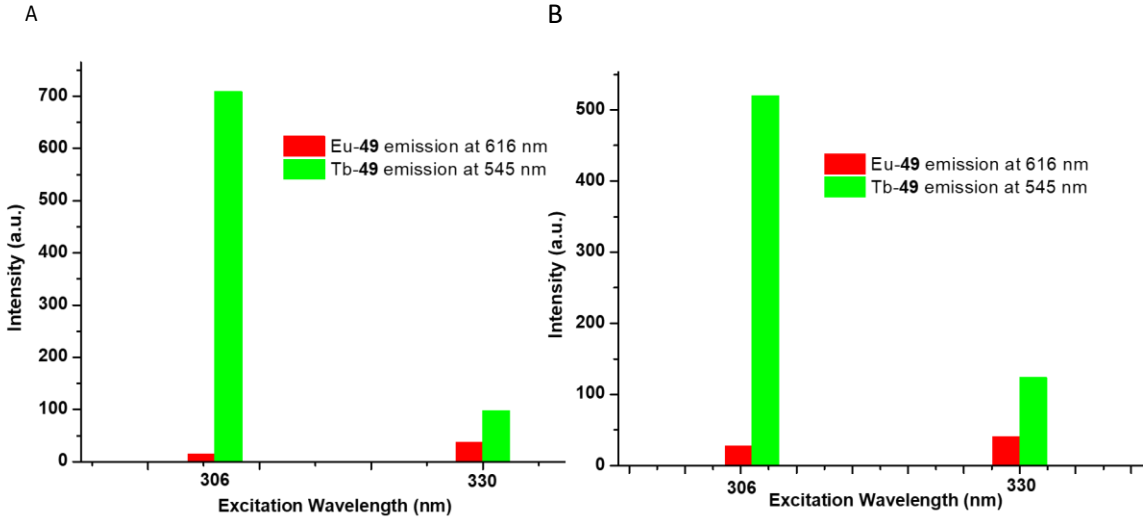

***Figure 2.34**: Eu(III)- or Tb(III)-centred emission of LB-**Eu-49**/**Tb-49** bilayer at 616 nm and 545 nm after dipping into (A) the **DMAB** aqueous solution 1 x 10^{-4} M and the following dipping of the same layer into (B) aqueous solution of **nta** 1 x 10^{-4} M.*

was then studied where one slide was first dipped into a **nta** solution (1 x 10^{-4} M), and after it was dipped into a **DMAB** solution at the same concentration. For the second slide the opposite process was performed, where the slide was first dipped into the **DMAB** solution and after into the **nta** solution. The emission was then recorded after each dipping. All the emissions for this experiment were recorded exciting at 306 and 330 nm (corresponding to the max absorption of **DMAB** and **nta**) (**Figure 2.33**).

The dipping into the **nta** solution "switching on" the Eu(III) emission as shown in **Figure 2.34**, left, where upon excitation of both the 306 nm and λ_{ex}=330 nm suggesting the binding of **nta** and its efficent sensitisation of Eu(III) centre. Upon the second dipping into the **DMAB** solution the emission of the Tb(III) was also enanced. As expected it became stronger than that seen for the Eu(III)-centred one, because of this, it was necessary to change the setup, decreasing the voltage, the results of which are shown in **Figure 2.33**, right. Exciting into the **DMAB** antenna, the Tb(III)-centred emission was 25 times higher than the Eu(III) emission.

The "opposite" experiment was performed as well, were a new quartz slide with the same deposition of bilayers was first dipped into the **DMAB** solution (**Figure 2.34**, left). As expected the Tb(III) emission was switched, on the other hand the Eu(III) emission is barely measurable upon the second dipping into the **nta** solution, even upon exciting at 330 nm,. **Figure 2.31** where it can be seen that B the emission of the Eu(III) centre did not increase significantly upon formation of the ternary complex on the surface. This indicate that since the Eu-**49** layer is deposited as the first layer, the antenna struggled to bind the Eu(III) centre, instead of the Tb-**49** one form the second outer layer, therefore **DMAB** antenna can easily reach and bind to the Tb(III) and sensitize its emission.

2.12 Comparison of the emission of Tb-49 and Eu-49 in solution and deposited onto the Langmuir-Blodgett films

In order to complete the photophysical evaluation of the LB-Eu-**49** and LB-Tb-**49**, the Ln(III)-centered emission of the compound deposited onto the solid substrate was compared with the emission of the complexes in solution.

As previously mentioned, in the absence of the **nta** antenna, the Eu(III) levels are not efficiently populated to give a detectable signal, however upon the addition of the antenna the Eu(III)-centered emission was significantly enhanced and it was possible to record the same trend when the complex was deposited onto the solid substrate. As can be seen in **Figure 2.35** the obtained signal was lower compared to the same compound in solution. This could be explained by the fact that the solution studies were performed in MeOH and using a concentration of Eu-**49** being 1 x 10^{-5} M and adding 1 equivalent of the antenna. For the studies on the solid substrate, despite the dipping of the quartz slide into the **nta** solution with the concentration of 1 x 10^{-4} M, it is possible that not all the "antenna molecules" were able to reach the Eu(III) metal center, to generate the ternary complex and sensitize it. It is also possible that the Eu(III) emission is quenched to some degree by collision with solvent molecules in MeOH more significant quenching of the Eu(III)-centered emission for LB monolayer could be the result of the surface quenching or the reabsorption of the Eu(III)-centered emission by closely packed molecules within monolayer.

In the **Figure 2.35** the same comparison is shown for the the Tb-**49** metal complex and it is clear that the observed trend is the same as observed for the Eu-**49** complexes, but the Tb(III)-centred emission intensity of the LB-Tb-**49** monolayer is only slightly lower in comparison to the same Tb-**49** in MeOH solution. The explanation for the observed difference is probably the same as discussed for Eu-**49**

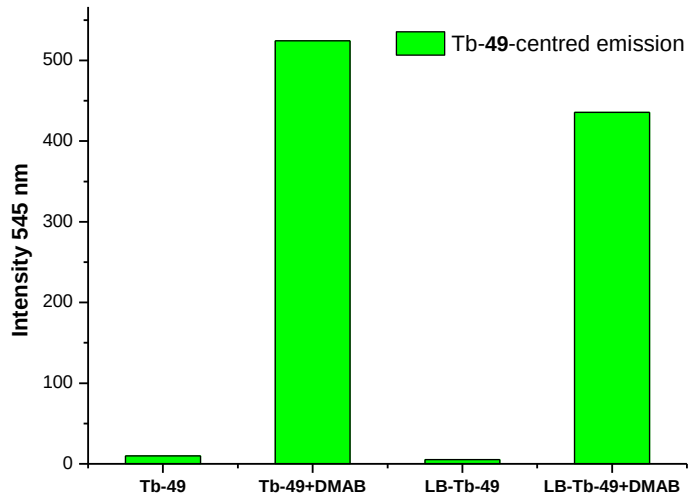

***Figure 2.35**: Comparison of Tb(III)-centred emission at 545 nm for **Tb-49** in the solution of MeOH at 1 x 10^{-5} M and upon addition of 1 equivalent of **DMAB** with the same system deposited onto the surface of the quartz slide LB-**Tb-49** and upon its dipping into the aqueous solution of **DMAB** 1 x 10^{-4} M.*

previously, as the Tb(III)-centred emission can be sensitised from the phenyl ring that is present within the framework of ligand **49**. This can have an enhancement effect on the Tb(III)-centred emission and thus the system does not require that all the Tb(III) centres are coordinated with **DMAB** antenna.

In summary, we have demonstrated the possibility to achieve dual Ln(III) emission from a multilayered LB film deposited on a quartz slide, with the intensity of the Eu(III) and Tb(III) emission dependant on the excitation wavelength and whether the layer lies on the top or bottom of the slide.

2.13 Measuring of the thickness of Langmuir-Blodgett monolayers using ellipsometry

Ellipsometry is a nondestructive technique for investigating the dielectric properties (refractive index or dielectric properties) of thin films. It is an optical technique that measure the change of the polarization upon reflection on transmission and uses a model to fit the data. This technique measures the change in the polarization of radiation that interacts with the structure of interest. This change is quantified by the amplitude ratio, Ψ, and the phase difference, Δ. Because the signal depends on the thickness as well as the material properties, ellipsometry can be a universal tool for contact free determination of thickness and optical constants of thin films, including LB-films.[124, 125]

Figure 2.36 shows the schematic setup of the ellipsometry experiment. Electromagnetic radiation comes from a light source and it is polarized by a polarizer. After reflection the light pass from a second polarizer that has been called analyzer, from there it passes into the detector.

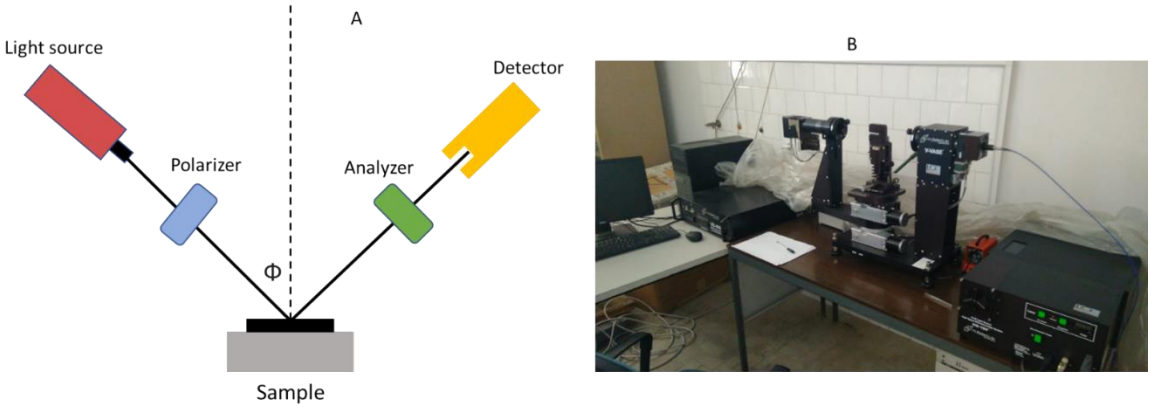

***Figure 2.36**: Schematic representation of (A) the Ellipsometry experimental setup and (B) the photograph of spectroscopic ellipsometer setup*

Ellipsometry measure the complex reflectance ratio of the system that has been described by two components: amplitude **Ψ** and phase difference Δ. The polarization state of the incident light can approximately be decomposed into two components: 1) s component oscilalting perdendicular to the plane of incidence and parallel to the surface of the sample and 2) p component parallelto the plane of incidence. The amplitude of s and p components, after reflection and normalising to their initial values, are named rp and rs. The angle of incidence coincides with Brewster angle of the sample (an angle of incidence at which light with a particular polarization is perfectly transmitted through a transparent dialectric surface, with no reflection). When unpolarized light is incident at this angle, the light that is reflected from the surface is therefore perfectly polarized.[126] The data analysis for the ellipsometry is indirect and model analysis must be performed, those models can be physically based on energy transitions or simply free parameters used to fit the data.

2.13.1 Ellipsometry of LB-Tb-49 and LB-Eu-49 monolayers

As showed above, ellipsometry was used to determine the thickness of the LB monolayers. The experiments were performed at the University of Catania, under the supervision of Professor Giuseppe Marletta. All the samples were analysed at room temperature (25°C) in air at two angles of incidence (65° and 75°) and the reported thickness values are the avarage of four different measurements of each sample. For the Eu(III) complex the variation of the amplitude **Ψ** and phase difference Δ are reported in **Figure 2.37** (left and right). The thickness of the LB-**Eu-49** was found to be 3.14±0.02 nm.

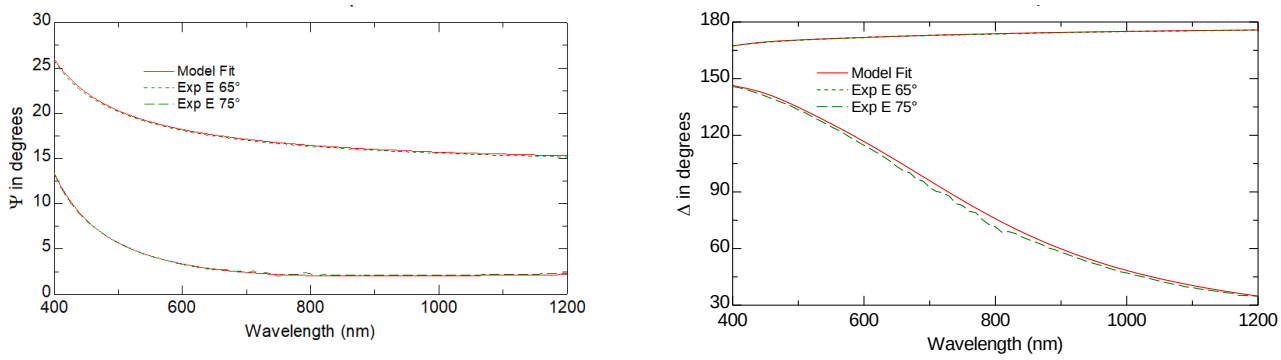

Figure 2.37: *(left) Variation of the amplitude and (right) of the phase as function of wavelength for LB-**Eu-49.***

The same experiment was performed for LB-Tb-**49**, the variation of the amplitude **Ψ** and phase difference Δ are reported in Figure **2.38** and the data fitting show a thickness of 2.72±0.02 nm for the monolayer of LB-Tb-**49**.

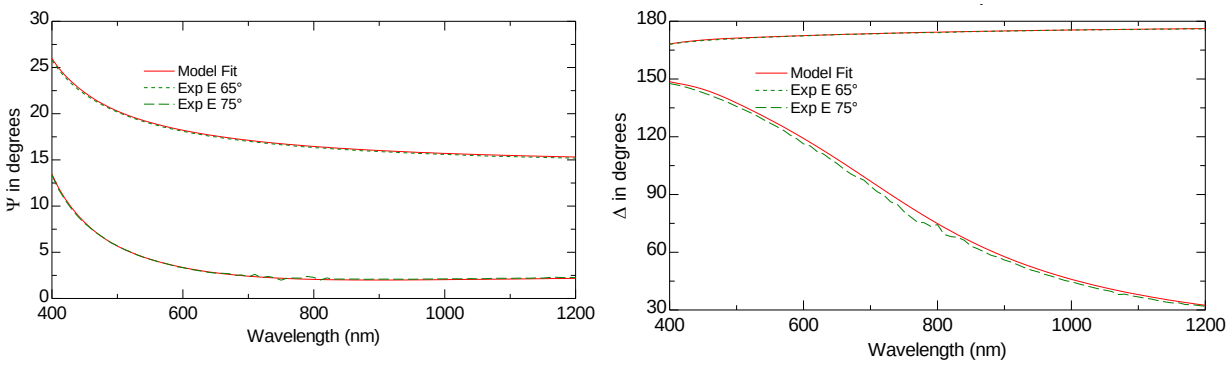

Figure 2.38: *Variation of (left) the amplitude and (right) the phase as function of wavelength for LB-**Tb-49.***

The thickness of the films corresponds to the size of Tb-**49** and Eu-**49** molecules which was approximated from ChemiBio 3D software therefore confriming monolayer nature of the samples. Unfortunately we were not able to find the appropriate model for the fitting of the data where two refractive surfaces are deposited onto one another so the measurement of the Ln(III)-**49** complexes dipped in the solution of respective antenna was not possible.

In summary the ellipsometry experiment gave a further confirmation of the deposition of Tb-**49** and Eu-**49** on the quartz slide.

The ability of Eu-**49** and Tb-**49** to act as a sensor for phosphorylate amino acids by the modulation of the Ln(III) emission from the slide was next investigated.

The thickness of the bilayer films could not be measured because we were not able to find the correct mathematical model

2.14 Sensing of amino-acids using Eu-49 and Tb-49

The phosphorylated amino acids are essential in the body as they serve as building blocks for many important neurotransmitters, such as epinephrine, norepinephrine, and dopamine.[127] Our main focus was in the amino-acid tyrosine (**Tyr**) and in the corresponding phosporylated form phospho-tyrosine (**pTyr**).

The tyrosine has a crucial role in the human body not only because it is the starting block for the synthesis of many neurotransmitters such as epinephrine and dopamine,[128] but also because the phosphorylation of the tyrosine to phosphotyrosine within protein is a crucial step within cellular regulation and even if its exact role is not fully understood it has been proven that an increment of the phosphorylation processes is related to many of diseases, including cancer.[129] Therefore, the development of specific sensors for this amino-acids is crucial and this was one of the main objective of this thesis. As mentioned in the Chapter 1, the idea behind this project is to create a displacement system (**Figure 2.39)** where the Ln(III) centre is sensitised from an external antenna but the target molecule is able to replace the antenna, quenching the signal.

The α-amino-acids chosen for the investigation here were tyrosine (**Tyr**), tyrosine methyl ester (**Me-Tyr**), phosphotyrosine (**pTyr**), tryptophan (**Trp**), phenylalanine (**Phe**) and histidine (**His**). Tyrosine methyl ester was added to the investigation list in order to understand the binding mode between the amino-acid and the Ln(III) metal centre.

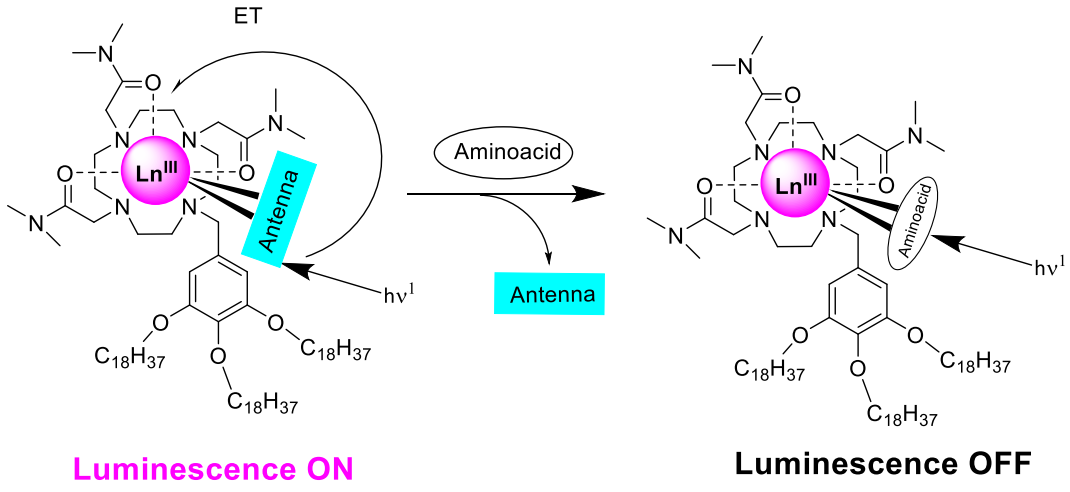

***Figure 2.39**: Schematic representation of the displacement assay.*

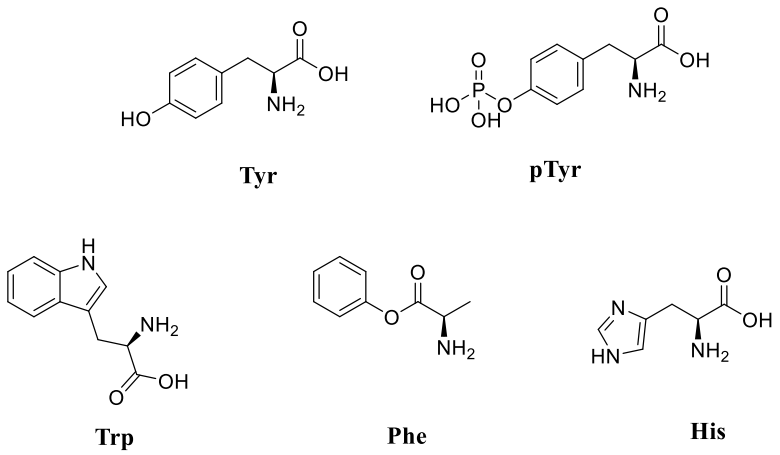

Solution studies were initially carried out to determine the effect of various amino acids on the luminescence properties of Eu-**49-nta** and Tb-**49-DMAB**. It was envisaged that the amino acids would displace the antenna (either **nta** or **DMAB**) from the Ln(III) metal centre, hence modulating the lanthanide (Eu(III) or Tb(III)) emission.

2.14.1 Sensing of aminoacids in methanol with Eu-49 and Tb-49

As it was previosly shown Eu-**49** form 1:1 complex with **nta** upon addition of 1 equivalent of **nta** in order to switch on the luminescence and form the Eu-**49** complex in solution. Increasing concentration of α-amino-acids were added in a range between 1 x 10^{-6} M to 5 x 10^{-5} M, corresponding to 1-50 equivalents added.The results as show in **Figure 2.40** shown the ability of the Eu-**49** complex to discriminate among the different amino acids and it was possible to distinguish between the **pTyr** and the **Tyr**. As can be seen in **Figure 2.40**, the signal reflecting the quenching upon interaction with **pTyr** is the highest, *c.a.* 75%, as opposed to

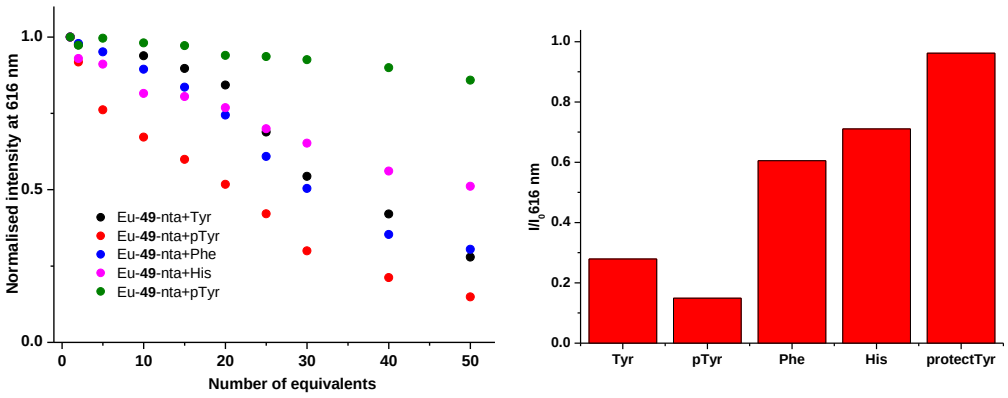

***Figure 2.40**: Normalised Eu(III) emission at 616 nm (λ_{ex} = 330 nm) of **Eu·49nta** (c = 1 × 10^{-6} M) in MeOH upon the addition of 50 equivalents of various amino acids,*

the quenching by **protectTyr** which was only at the value of *c.a.* 10%. This can be explained by the presence of the protective group with BOC in **protectTyr** that does not allow the coordination of the carboxylic group to the Ln(III) metal center. The same investigation was performed using Tb-**49-DMAB** and the results are shown in **Figure 2.41**. The amino acids were added to the solution of Tb-**49-DMAB** (1×10^{-6} M in MeOH) in a range between 0.1 and 1 equivalent and in all the cases Tb(III)-centered emission was almost fully quenched. This can be explained by the lower binding constant value for Tb-**49-DMAB** compared to Eu-**49-nta** (as mentioned in the sections 2.3 and 2.4).

Based on the results of these solution studies, it can be concluded that Tb-**49** was unable to discriminate among different amino-acids in MeOH solution as the association constant between the Tb(III) complex and the antenna is not strong enough to ensure a controlled displacement of the antenna. Therefore here the amino-acids are able to replace the antenna and quench the Tb(III) emission at a very low concentration (~ 5×10^{-7} M).

2.14.2 The effect of aqueous buffer medium on sensing properties of Eu-49 and Tb-49

In order to understand if Eu-**49** and Tb-**49** sensing properties are solvent dependent and if the compound could be used in the biological environment other solvent media such as aqueous buffer solutions were next investigated. The first buffer that has been studied was the HEPES (4-(2-hydroxyethyl)-1-piperazineethanesulfonic acid). HEPES is often used in cell culture to maintain the

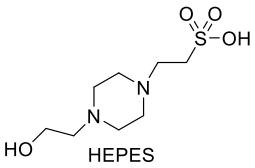

HEPES

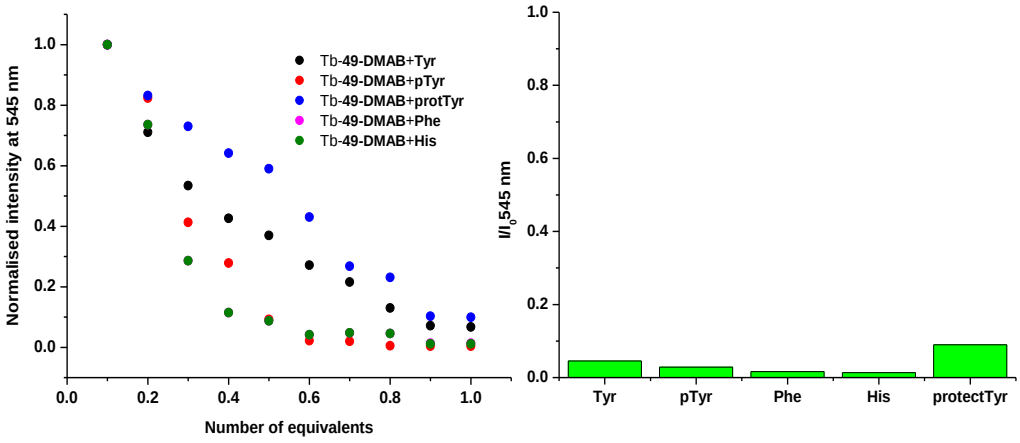

***Figure 2.41**: Normalised Tb(III) emission at 545 nm (λ_{ex} = 306 nm) of **Tb-49-DMAB** ($c = 1 \times 10^{-6}$ M) in MeOH upon the addition of 1 equivalent of amino acid.*

physiological pH. Eu-**49** is only partially soluble in aqueous medium, but it was enough to prepare a solution of the concentration 1 x 10^{-6} M to which 1 equivalent of **nta** antenna was added. The same titration as in Section 2.15 was performed and the results are shown in **Figure 2.43**.

The addition of up to 50 equivalents of **Phe** and **protect Tyr** resulted in less than *ca.* 3% modulation in the Eu(III)-centered emission while the quenching due to the presence of **His** was *ca.* 40%. The major quenching observed here was due to the presence of **Tyr** and **pTyr**, respectively of 90% and 99%.

Comparing the results with the experiments performed in MeOH, we can conclude that in HEPES buffer has a strong effect onto the sensing ability of Eu-**49-nta**. Indeed despite the solubility of the complex in aqueous media is not optimal, it can be used in aqueous buffer.

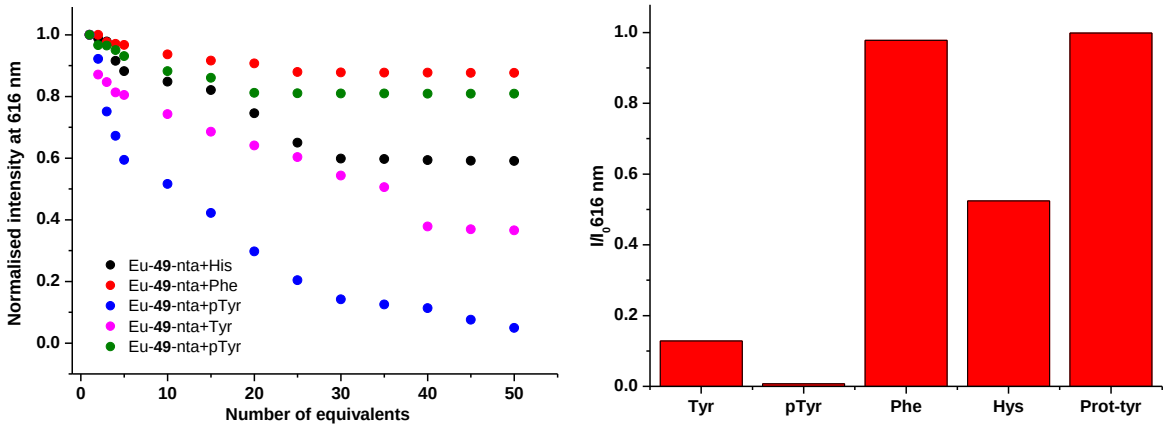

Figure 2.42: *Normalised Eu(III)-centred emission at 616 nm (λ_{ex} = 330 nm) of* ***Eu-49-nta*** *(c = 1 × 10^{-6} M) in HEPES pH 7.2 upon the addition of 50 equivalents of different amino acids.*

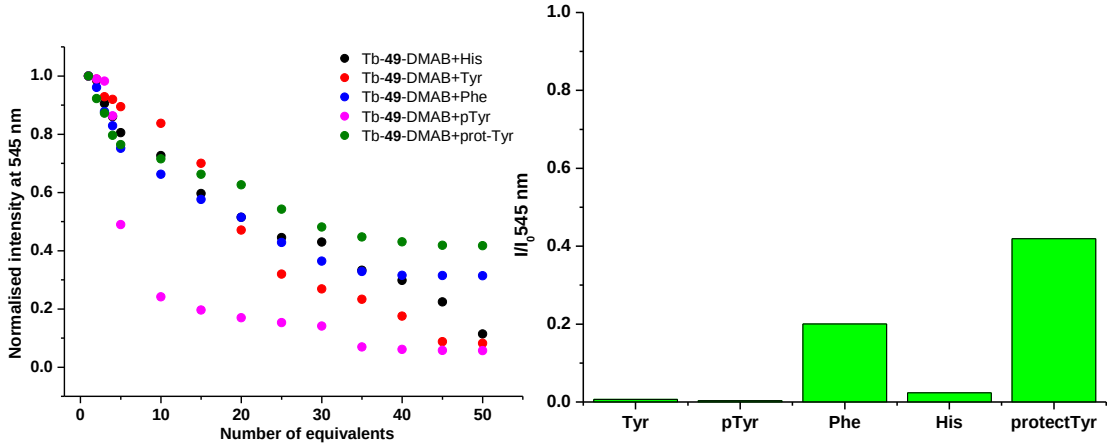

Figure 2.43: *Normalised Tb(III)-centred emission at 545 nm (λ_{ex} = 306 nm) of* ***Tb-49-DMAB*** *(c = 1 × 10^{-6} M) in HEPES pH 7.2 upon the addition of 50 equivalents of different amino acids*

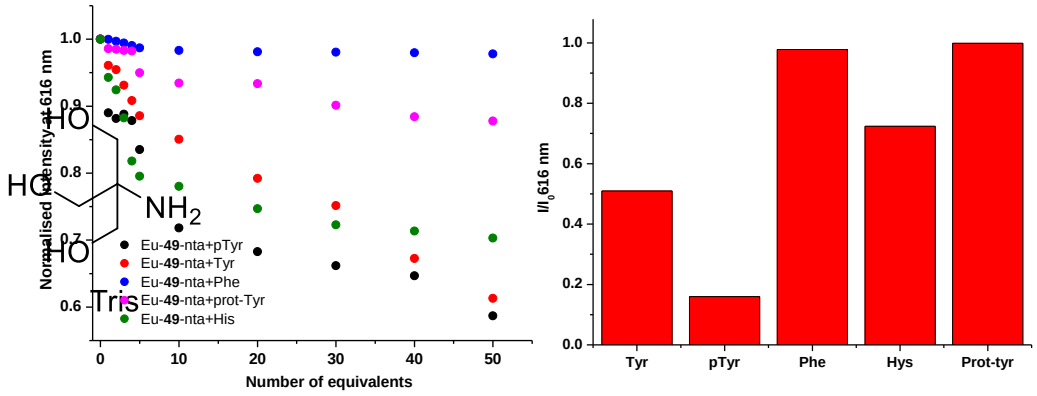

***Figure 2.44**: Normalised Eu(III)-centred emission at 616 nm (λ_{ex} = 330 nm) of **Eu-49-nta** (c = 1 × 10^{-6} M) in Tris buffer pH 7.2 upon the addition of 50 equivalents of different amino acid*

For **Tb-49-DMAB** the titration in HEPES buffer (**Figure 2.43**) shows slightly different results compared to the experiment performed in methanol (**Figure 2.41**). The experiment was repeated using the same conditions described in section 2.15 except for the amount of the α-amino-acids equivalent added, indeed in aqueous HEPES buffered medium the displacement of the **DMAB** antenna was less efficent, so two equivalents of the amino-acids were required to quench the Tb(III) emission because as previously mentioned, the binding constant for **Tb-49-DMAB** is lower than the binding constant found for **Eu-49-nta**. **Phe** and **Prot-Tyr** represent the exception, because the phenyl ring of the **Phe** is able to partially sensitise the Tb(III) metal centre when it replaces the **DMAB** antenna and therefore a partial emission is still observed. As the carboxylic group in **Tyr** is protected compared to **Tyr**, it is not able to bind only the metal centre and therefore can not displace **DMAB** antenna molecules. Hence, only negligible Tb(III)-centred luminescence decay was observed within experimental error of the luminescence measurement.

In order to understand further the contibution of the solvent medium such as buffer onto the discrimination process of the selected amino-acids a second buffer was investigated such as tris(hydroxymethyl)aminomethane. This is another common buffer used in biochemistry and biology to investigate solutions of nucleic acids. Due to the pKa of the conjugated acid being 8.0, the buffer range is between 7.1 and 9.1. All the titration were performed at least 3 times in Tris buffer and NaCl at pH 7.2 1mM.

The titration was performed in the same conditions as for the previous experiment in HEPES buffer and is illustrated in **Figure 2.44** and **Figure 2.45**. The overall quenching of Eu(III)- and Tb(III)-centered emission upon addition of aminoacids was found to be similar to the results previously observed in HEPES buffered

solution with the exception of **pTyr** and the **Tyr** showing less significant quenching compared to the one found previouly in HEPES buffer. Upon the addition of 2 equivalents of the amino-acids to the solution of **Tb-49-DMAB** (c = $1x10^{-6}$ M) in Tris buffer (**Figure 2.45**) the same trend observed for the HEPES buffer was observed with the only difference in the behaviour for **pTyr** that shows a bigger quenching in the Tris buffer.

As reported by Faulkner *et al.*[130] the binding constant for the lanthanide cyclen assemblies with external ligands can vary depending on the buffer medium used. this is probably due to the stronger binding constant between the antenna and the lanthanide metal center, 50 equivalents of **pTyr** resulted in sufficient for the displacement of all the **DMAB** molecules, this could explain the different behavior.

Based on the results obtained from the solution studies, studies were next carried out to investigate the ability of a LB monolayers of Eu-**49-nta** and Tb-**49-DMAB** to sense and distinguish between **Tyr** and **pTyr**.

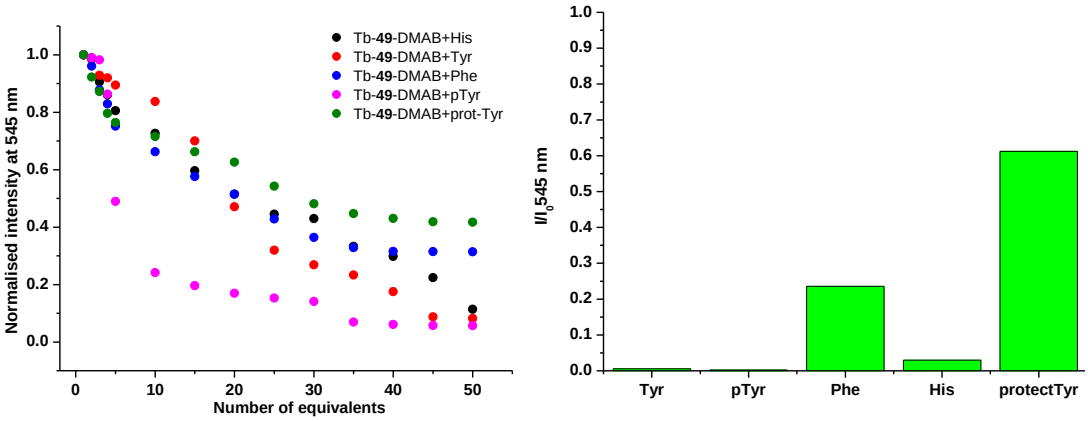

***Figure 2.45**: Normalised Tb(III)-centred emission at 545 nm (λ_{ex} = 306 nm) of **Tb-49-DMAB** (c = 1 × 10^{-6} M) in Tris buffer pH 7.2 upon the addition of 50 equivalents of different amino acid.*

2.14.3 Langmuir-Blodgett monolayer as amino-acid sensor

After investigating the sensing ability of both Ln-sensors in both aqueous media and MeOH we then investigated the luminescent sensing of their respective LB monolayers towards the same amino-acids (**Figure 2.47**). The investigation was performed in HEPES and Tris buffered aqueous media as it was not possible to investigate the LB-films sensing activity in MeOH due to the possibility of the monolayer being washed out from the quartz surface in this case.

The first film investigated was the LB-Eu-**49** LB-system. As described in the Section 2.8 the luminescence of the monolayer LB-Eu-**49** was "switched on" upon dipping into an aqueous **nta** solution at c = 1 x 10^{-4} M for one minute. The sensing ability of the slides was tested too by dipping the resulting LB-Eu-**49-nta** into a

solution of the alpha-amino-acid **Tyr**, **pTyr** respectively in aqueous HEPES buffered solution with c = 1 x 10^{-5} M and recording the emsission before and after the displacement of the antenna. The results are shown in **Figure 2.46** A. Immersing the slide into the solution containing 50 equivalents of amino-acids, totally quenched the Eu(III)-centred emission for both amino-acids. In the case of LB-Eu-49-nta the solution was analyzed after the slides dipping and no emission of the Eu(III) was found, proving the "switch off" of the emission is due to the **Tyr**/**pTyr** binding (and the resulting displacement of the relative antennae) and it is not due the film being washed off from the quartz slide. The results compared well with the solution studies in the same solvent medium (**Figure 2.42**), suggesting that the behavior of the compound deposited onto the solid substrate is different, Indeed both of the amino-acids were able to full quench the Eu(III)-centered emission, while in the solution studies, the addition of **Tyr**, only partially quenched the lanthanide emission. One of the possible explanations for thes difference, is the sensing in solution and on the solid surface is that within the monolayer LB-Eu-**49-nta** are oriented with the head towards the quartz slide and therefore the access to the Eu(III) metal centre is limited, so only a few molecules of **nta** are able to bound the metal centre and sensitise its emission. As displayced antenna to displace, **pTyr** and **Tyr** are both equally able to displace it and quench the signal. Also the mode of the **nta** binding might be different in the case of the monolayer resulting in easier displacement of the antenna from the monolayer.

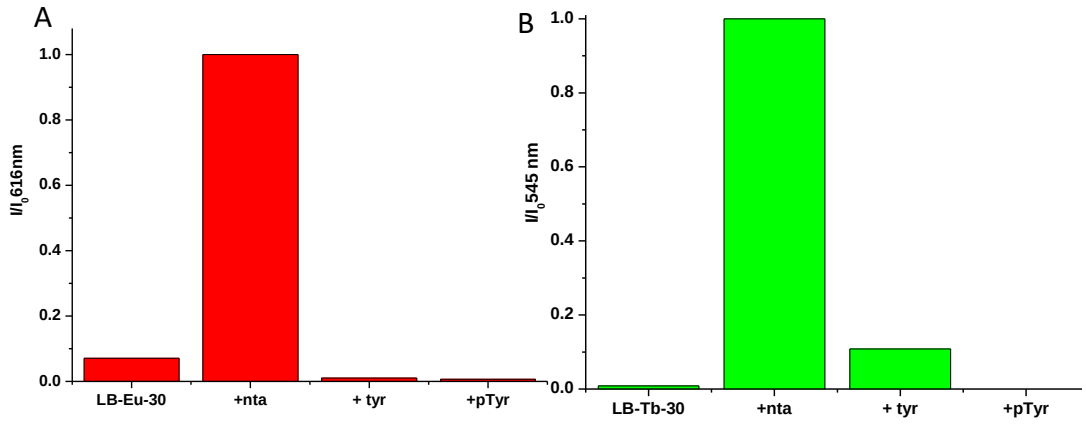

***Figure 2.46**: (A) Normalised Eu(III)-centred emission at 616 nm (λ_{ex} = 330 nm) of LB-**Eu-49** after the dipping into an aqueous solution containing of **nta** (c = 1 x 10^{-} M) with the following immersion into the aqueous HEPES buffered pH 7.2 solution containing 50 equivalents of selected amino-acids. (B) Normalised Tb(III)-centred emission at 545 nm (λ_{ex} = 306 nm) of LB-Tb-**·49** upon the dipping in an aqueous solution containing of **DMAB** (c = 1 x 10^{-4} M) with the following immersion into the aqueous HEPES buffered pH 7.2 solution containing 50 equivalents of selected amino-acids*

The next film studied was the LB-**Tb-49** monolayer. First, the luminescence of this monolayer was "switched on" by dipping the slide into a solution of **DMAB** 1 x 10^{-4} M in HEPES buffer. As for the LB-Eu-**49**, the ability of the LB-**Tb-49** to discriminate between **pTyr** and **Tyr** was investigated. The slide LB-**Tb-49-DMAB** was then dipped in a solution of amino-acid in HEPES buffered aqueous medium (c = 1 x 10^{-5} M) and as for the previous film, the results obtained were different to these obtained from the solution studies. In HEPES aqueous buffered medium **Tb-49** complex was unable to discriminate among between the**Tyr** and **pTyr** (**Figure 2.44**), but deposited onto a quartz slide, it does (**Figure 2.47** B). Upon dipping into **Tyr** solution, a quenching of the Tb(III) emission of *ca.* 10% was estimated, whereas the same concentration of **pTyr** gave a full quenching in the Tb-emission. Even in this case, the emission of the solution after the dipping was evalutaed and no emission was found, meaning that the quenching was due to the displacement of the **DMAB** antenna and not from the washing out of the monolayer from the slide. A possible explanation to this discrepancy between the studies in solution and in the complex deposited onto the quartz slide could be that because the binding between **DMAB** and Tb-**49** is less strong compared to Eu-**49** and the **nta**, even if the organization of the film is the same. The Tb-**49** have a weaker binding constant with the antenna, so even if it is difficult for the amino-acid to reach the Tb(III) metal centre, it is enough for displacement it and **pTyr**, as the phosphate group is able to displace more **DMAB** molecules and there is the possibility the binding mode of the antenna on the film might be different to the one in solution.

2.15 Conclusions

In this chapter, I have described the development of two lanthanide based luminescent complexes with the purpose to deposit them onto a quartz slide in the attempt to form mono and bilayers of these. A full characterization of the ligand and complexes has been shown and the photophysical evaluations of the complexes in solution and on the LB films was carried out.

Solution studies prove the ability of these antennae to "switch on" the lanthanide-centred emission for both systems using different antennae.

Having established that these complexes were attached on the quartz slide *via* Y-type deposition with a transfer ratio of *ca* 1, the ability of LB monolayer to retain on the surface of the quartz slide was evaluated under a constant flow of water (75 mL / minute) and their emissions were measured every 5 minutes for 1 hour. For both of the films, after 5 minutes of retaining the monolayers under the water flow the Ln-centred emission was quenched by *ca.* 70 % and was barely measurable after 1 hour.

After the evaluation of the stability for LB monolayers, their bilayers were successfully obtained with a transfer ratio *ca.* 0.9 for both of the layers using a double dipping technique

The last films deposited where the dual Eu(III)/Tb(III) bilayers. This was achieved using Eu-**49** and Tb-**49**. In order to "switch on" both the Eu(III)- and the Tb(III)-centred emission different dipping experiments were performed.

Using a nondestructive technique called ellipsometry it was possible to estimate the thickness of these monolayers and it was found that the monolayer thicknes was 3.14±0.02 nm for LB-**Eu-49** and 2.72±0.02 nm. for LB-Tb-**49**.

The ability of both of the Ln(III) complexes to distinguish between different α-amino-acids in solution (in different solvents) and of their monolayers deposited onto the quartz substrate was investigated and the complex proved to be able to discriminate among several aminoacids in different solution.

The same experiments were performed using the respective LB monolayers and the results disagreed with the solution studies. Indeed here the LB-Eu-**49** monolayer was unable to discriminate between **Tyr** and **pTyr**, as its dipping into the aqueous solution of amino-acids with c = 1 x 10^{-4} M resulted in the same quenching effect.

One of the possible explanations for the different results between the solution studies and the solid state ones, is that within the LB-Eu-**49**-**nta** monolayers the Eu-**49** molecules are oriented with the polar Eu(III)-containing head towards the quartz slide leading to the Eu(III) metal centres being not fully accessible to the **nta** antenna, and thus a partial displacement by **nta** is possible. Therefore not all the complexes on the surface are being active in the displacement process when titrating with **pTyr** and **Tyr**. The displacement process could also be affected by solvation effects in aqueous medium and also by surface effects that would not be present in the case of sensing in solution.

For LB-**Tb**-49-**DMAB** the sensing results also disagree with the solution studies. However, the monolayers in this case were able to discriminate between **pTyr** and **Tyr**, when dipping in aqueous solution of each amino-acid ($c = 1 \times 10^{-4}$ M) the Tb(III)-centred emission being quenched by 90% for the **Tyr** and *ca.* 100% for the **pTyr**. Even in this case the explanation can be related to the organization of the film and binding constant, as it was previously said Tb-**49** have a weaker binding constant with its antenna, so even if it is difficult for the amino-acid to access the metal centre, it was enough to fully displace **DMAB** antenna from Tb(III) centres on the surface of the monolayer using **pTyr** thanks to the presence of the phosphate group

Future work involed in the study in a better comprension of the formation of the double layer, including the possible application of the dual layer as ratiometric sensor

The next chapter was focused on the developing of a novel assay to monitor the enzimatic phosphorilation of a Protein kinase, using the lantahnide complexe developed in this chapter.

Chapter 3

3.0 Introduction

Enzymes are the catalyst of the biological world, almost all the metabolic processes in cell required an enzyme catalysis[14] and is estimated that they are involved in over 5000 processes.[131] Enzymes are usually globular proteins that can work alone or act in a larger complex and every enzyme activity depends on the sequence of the amino-acids present in the structure.[132] In order to work, enzyme must bind a specific substrate before catalysing any reaction. The monitoring of enzymatic activities plays a crucial role in the biomedical research because the failure of these processes has been correlated to several diseases including stroke,[133] cancer[134] and even into neurodegenerative states such as Alzheimer.[135] A thorough understanding of these processes is the first step into the developing of new inhibitors or enzyme activators.[136]

Among the different substrates, the nucleoside polyphosphate anions (NPPs) such the **ATP** (adenosine triphosphate) and **ADP** (adenosine diphosphate) are really important substrates for pharmaceutically relevant enzymes.[137] An important family of enzymes is the kinase, macromolecules that catalyses the transfer of phosphate group from a phosphate donor molecule to a specific substrate. This process is called phosphorylation. When the donor is the substrate the process is called dephosphorylation. In some cases these two processes can occur consecutively one after the other, for example in the glycolysis they occur 4 times.[138]

Mutation or defects in these regulatory mechanisms are the first step for the oncogenesis for multiple tumours.[139-141] For all these reasons the research in this area has grown in recent years. The first step to create new kinase inhibitors is to understand the mechanism of kinase activity and its selectivity. Currently the assays produced commercially require the use of antibodies to detect the phosphorylated substrate which can be fluorescent and the major problem of both is that they are expensive. A few lanthanide based probes were developed in the past years[142] to monitor phosphorylation process in solution, one of the most interesting example is given from the work of Butler and co-worker, where a lanthanides complex assay was employed to monitor enzyme reaction for detecting peptide modification by phosphorylation and de-phosphorylation.[143] However, in this work we have

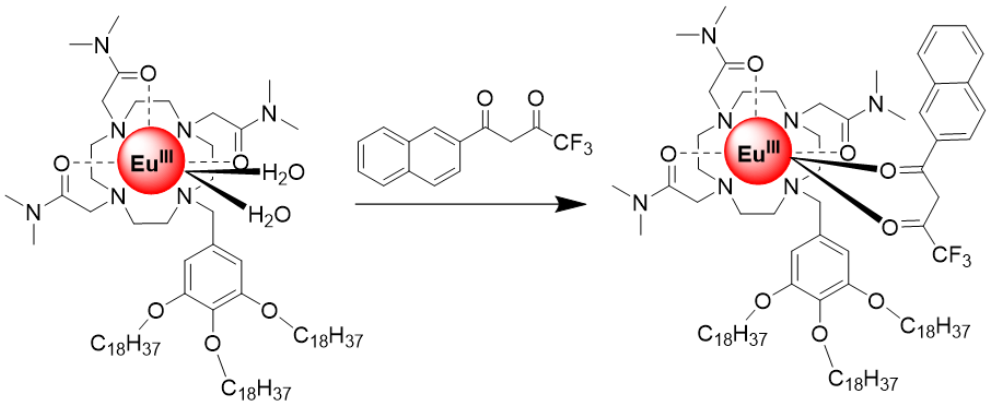

Scheme 3.0: *Coordination of* ***nta*** *to the Eu(III) centre forming* ***Eu-49-nta****.*

developed a probe based on a displacement system where the Eu(III) cyclen complex is initially non-luminescent, and the emission is "switched on" by the coordination of an external antenna (**Scheme 3.0**), this system is able to bind reversibly to **ATP** and **ADP** providing a different quenching of the signal. The limitation of concentration, given from the low solubility of the complex in water has been exceeded depositing the Eu(III) complex in solid substrate, creating an LB monolayer.

The main advantages of molecular deposition using the LB method are related to the possibility of forming ultrathin films, being a precise technique for packing and stacking molecules; as well as it is able to fabricate biomimetic membrane materials. As a result, films fabricated with the LB technique has shown a high potential for improving the performance of sensors since they offer a wide selection of materials in a close-packed structure (as shown in **Scheme 3.1**). Taking this into consideration, it was decided to design an appropriate experiment in order to develop a lanthanide-based system, able to recognize the enzymatic conversion of

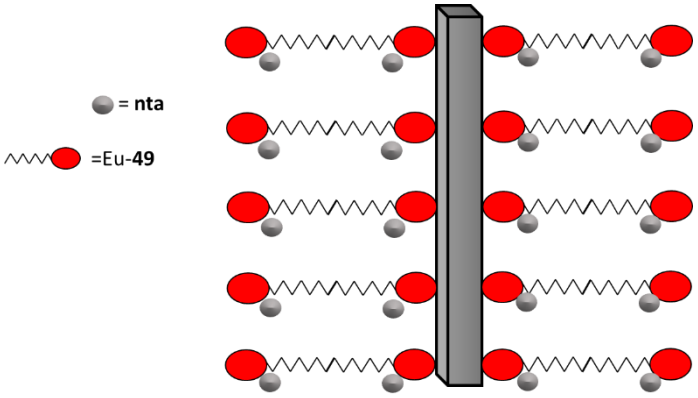

Scheme 3.1: *Schematic representation of the* ***nta*** *antenna binding to the Eu(III) centres of LB-****Eu-49.***

the **ATP** in **ADP**. In the next section, the reason why all the single components of the assay are chosen is reported.

3.1 Design of the experiment

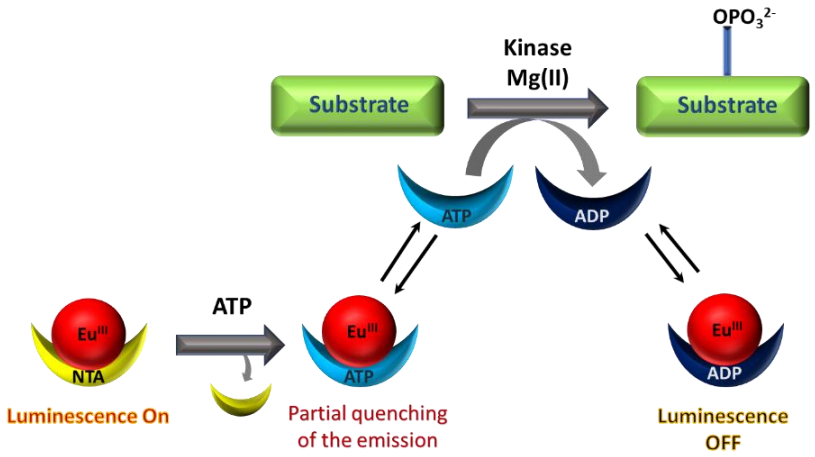

Figure 3.0: *Schematic illustration of the Eu(III) cyclen complex assay use for monitoring the kinase activity.*

As previously stated the assay is based on a displacement system where the emission of Eu-49-**ATP** complex is different from the emission of Eu-**49**-**ADP** complex. **Figure 3** show an illustration of the lanthanide-based assay which is composed from the lanthanide complex (Eu-**49**) where the luminescence is "switched on" by the coordination with the **nta** antenna (as explained in the first chapter). The **ATP** and from a kinase enzymatic. To work the enzyme, a substrate is required where the phosphate group from the **ATP** can be transferred. The **ATP** to be coordinated from the enzyme require the presence of the Mg(II), so $MgCl_2$ is added.

The use of Eu(III) complex has many advantages, as when the complex is luminescent its spectrum has the typical line-like Eu(III) emission, lifetime of its emission is long, allowing the use of time-resolved detection to eliminate the autofluorescence arising from protein substrates[144] and it can reversibly bind the **ATP** and **ADP**. A (PKA) (**Figure 3.1)**, which is a catalytic subunit from bovine heart and has been used to catalyse the transfer from a terminal phosphate of **ATP** to threonine or serine residues in several protein substrates. **ATP** is comprised of an adenine ring, a ribose sugar, and three phosphate groups. **ATP** is often used for energy transfer in the cell. **ATP** synthase produces **ATP** from **ADP**.

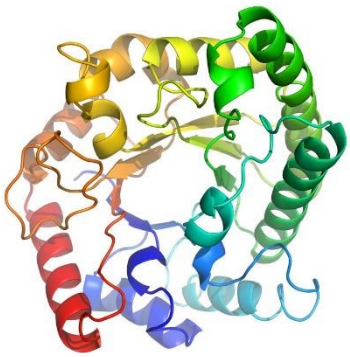

Figure 3.1: *Schematic structure of the subunit of the protein kinase A (PKA).*

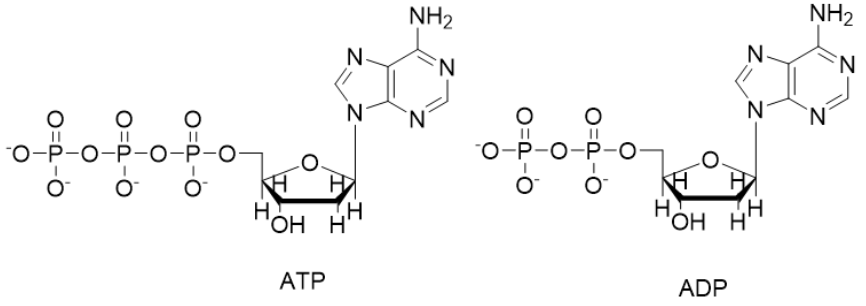

Figure 3.2: *Structures of* ***ATP*** *and* ***ADP****.*

ATP has many uses; it is also found in nucleic acids in the processes of DNA replication and transcription. In a neutral solution, **ATP** has negatively charged groups that allow it to chelate metals. Removing or adding one phosphate group interconverts **ATP** to **ADP** (**Figure 3.2**). Breaking one phosphoanhydride bond

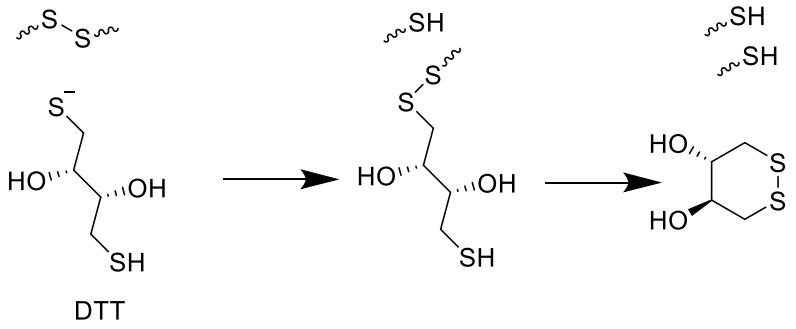

Figure 3.3: *Reduction of a generic disulfide bond by DTT.*

releases 7.3 kcal/mol of energy.[145] **ATP** is the primary energy transporter for most energy-requiring reactions that occur in the cell. The continual synthesis of **ATP** and the immediate usage of it results in **ATP** having a very fast turnover rate. This means that **ADP** is synthesized into **ATP** very quickly and *vice versa*. In a kinase assay the presence of a reducing agent is crucial because almost all the cytosolic proteins lack disulphide bonds because in the cytosol there is a constant reducing environment due to presence of reducing agents (such as glutathione). To simulate this environment in solution, DTT (dithiothreitol), also called Cleland's reagent[146] was added. This helps to keep the cysteine (and methionine) residues from oxidizing, which might reduce enzyme activity. After the oxidation, DTT forms a 6 membered ring with a disulfide bond passing through a two steps thiol-disulfide reaction (**Figure 3.3**). In addition to this $MgCl_2$ also has a crucial role in the enzymatic process. Mg(II) is one of the most abundant metal ions in the living cells

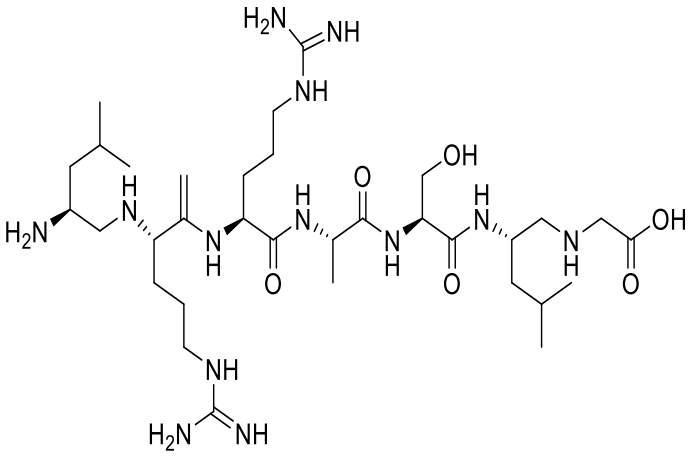

Figure 3.5: *Molecular structure of the Kemptide.*

and a lot of enzymes are Mg(II) dependent and are involved in almost all the reactions that requires a release of energy from the **ATP**,[147, 148] where positively charged magnesium ions help to stabilize the **ATP**, moreover, it changes the "shape" of the molecule (**Figure 3.4)** and it allows to be allocated in enzyme cavities.[149] The last component of the assay is the substrate, for this experiment, Kemptide has been chosen, Kemptide is a phosphate acceptor peptide that acts as a synthetic substrate for PKA. It is one of the most common phosphate acceptors used in the kinase assay's, but several studies have proven the high affinity of the PKA with this substrate.[150] The amino-acids sequence (Leu-Arg-Arg-Ala-Ser-Leu-Gly) of Kemptide is shown in **Figure 3.5**.

Having established what are the components to be used and why, the ability of Eu-**49** to act as sensor for **ATP** and **ADP** by the modulation of the Eu(III)-centred emission was next investigated in order to determine whether Eu-**49** could distinguish between **ATP** and **ADP** (**Figure 3.0**).

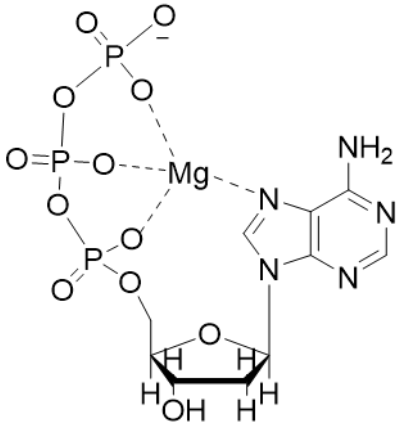

Figure 3.4: *Modified structure of **ATP** upon the addition of the Mg(II).*

3.2 Detection of the phosphorylated nucleotides ATP and ADP in Buffer solution

Solution studies to investigate the ability of **ATP** and **ADP** to displace the **nta** antenna and quench the Eu(III)-centred luminescence signal of Eu-**49**-**nta** was

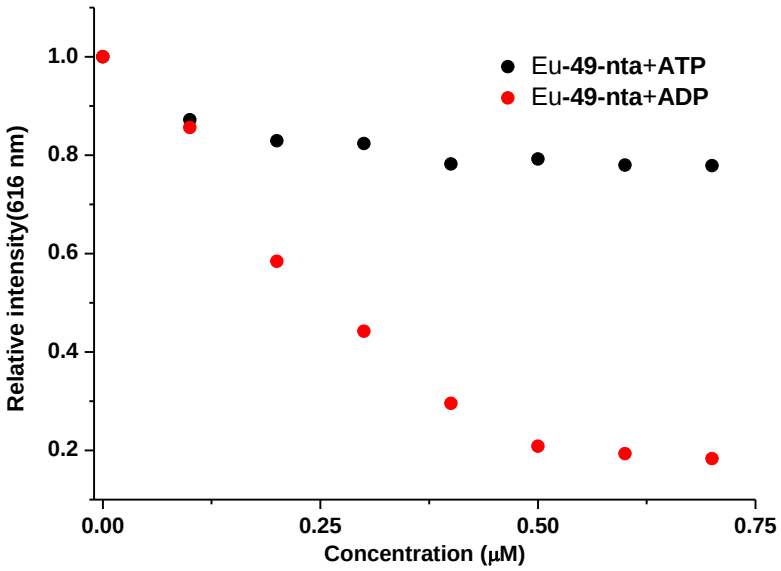

Figure 3.6: *Changes in the Eu(III)-centred emission at 616 nm (λ_{ex} = 330 nm) of* ***Eu-49-nta*** *(c = 8 x 10^{-3} M) in HEPES buffer pH 7.2 upon the addition of several equivalents of* ***ATP*** *or* ***ADP.***

carried out. To a solution of Eu-**49** at c =

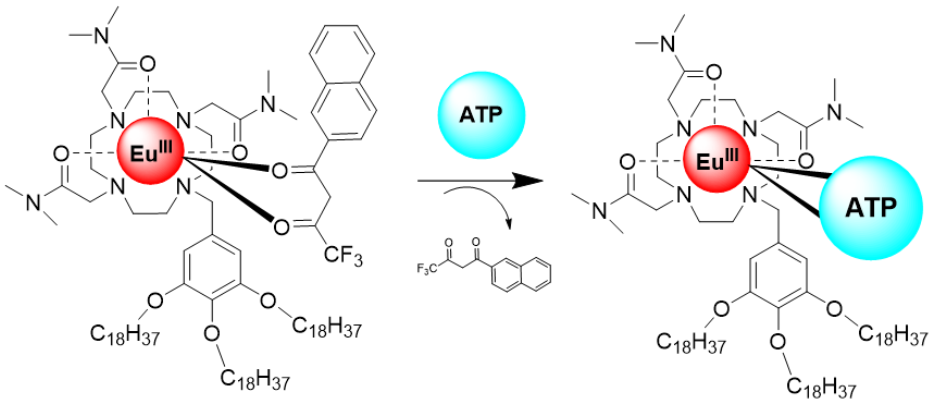

Scheme 3.2: *Schematic illustration of the displacement system.*

8 x 10^{-3} M in HEPES buffer at pH 7 1 equivalent of **nta** antenna was added. This resulted in intense Eu(III)-centred emission upon excitation at λ_{ex} = 330 nm. The formation of Eu-**49**-**nta** complex was also previously proven in Chapter 2.

Then, to this solution of Eu-**49-nta** increasing concentration of **ATP** and **ADP** were added (0 to 7 x 10^{-4} M) and all the experiments were repeated at least 3 times. The results of these titration are shown in **Figure 3.6 A** where the changes in the Eu(III)-centred emission upon interaction of Eu-**49-nta** complex with **ATP** and **ADP** allows to discriminate between these two. Addition of **ADP** results in a higher quenching of the $\Delta J = 2$ signal, probably due to a full displacement of the **nta** antenna from the metal centre. Since that **ATP** and **ADP** (**Figure 3.0**) can be coordinated by the Eu(III) centre, there is a possibility that they are able to enhance the Eu(III)-centred emission through the displacement of two water molecules from the Eu(III) centre, distorting the final results. Hence the titrations of the Eu-**49** with the both of them in absence of the antenna have been performed (**Figure 3.7**). To a solution of Eu-**49** at c = 8 x 10^{-3} M in HEPES buffer, increasing concentrations of **ATP** and **ADP** were added. The results shown in **Figure 3.7** proved that even increasing the concentration of the phosphorylated nucleotides no increase of Eu(III) centred emission was observed (λ_{ex} = 395 nm, corresponding to the max absorption of both of **ATP** and **ADP** and the band corresponding to the direct excitation of Eu(III)-centred emission) proving that in absence of the antenna, there is no changes in the

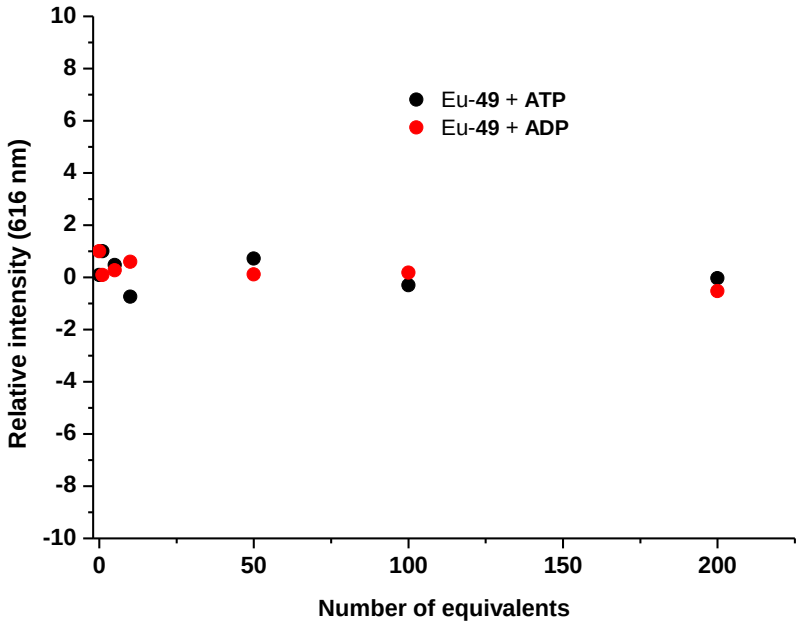

Figure 3.7: *Changes in the Eu(III) centred emission at 616 nm (c = 8 x 10^{-3} M, λ_{ex} = 330 nm) of Eu-**49** in HEPES buffer pH 7.2 upon the addition of several equivalents of **ATP** and **ADP**.*

emission of the Eu(III) metal centre upon the interaction with **ATP** and **ADP**.

As previously said, the kinase converts **ATP** to **ADP** transferring a phosphate group to a substrate. It is possible to simulate this reaction by varying the molar ratio

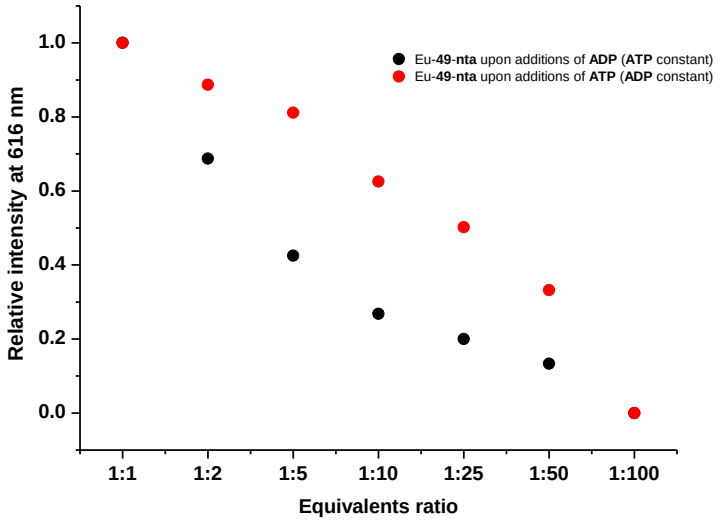

Figure 3.8**: Changes in the Eu(III)-centred emission of **Eu-49-nta** (c = 8 x 10^{-3}M) at 616 nm (λ_{ex} = 330 nm) in HEPES buffer pH 7.2 upon the addition of 0→100 equivalents of **ATP** (**ADP** constant, c = 8 x 10^{-3} M) and **ADP

between **ATP** and **ADP** keeping constant the total concentration of **ADP** and **ATP**. Two solutions of Eu-**49** in HEPES buffer plus 1 equivalent of **nta** antenna were prepared, the luminescence, initially silent, switched on after the addition of the antenna. With these solutions, two different experiments have been performed.

In the first experiment, to the solution of Eu-**49-nta** 1 equivalent of **ATP** was added and the luminescence was measured, after 100 equivalents of **ADP** were added and the quenching of the emission was evaluated (after each addition). The same

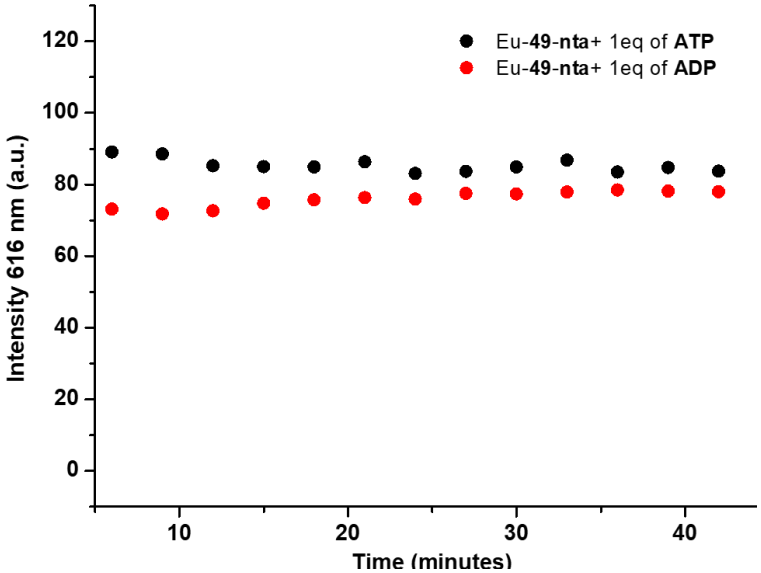

***Figure 3.9:** Change in the Eu(III)-centred emission of Eu-**49-nta** at 616 nm (c = 8x10^{-3} M) (λ_{ex} = 330 nm) in HEPES buffer pH 7.2 upon the addition of 1 equivalent of **ATP** (black) or **ADP** (red) monitored versus the time.*

experiment keeping the **ADP** constant and adding 1 to 100 equivalents of **ATP** was carried out and the results are reported in **Figure 3.8**.

The Eu-**49-nta** proved to be able to distinguish between solutions having different ratio between **ATP** and **ADP** even in a mixture of both, indeed the **ADP** quenches Eu(III) centred emission $\Delta J=2$ more compared to the **ATP**.

Kinetic studies of the modulation of emission upon the addition of both phosphorylated nucleotides to Eu-**49**-**nta** were also performed. Two solutions of Eu-**49**-**nta** in HEPES buffer were prepared, then the kinetic effect upon the addition of 1 equivalent of phosphorylated nucleotides was evaluated by monitoring the changes in the Eu(III) centred emission $\Delta J = 2$ versus time and the results are reported in **Figure 3.9**. The first point in the graph represents the emission intensity of Eu-**49**-**nta** upon excitation at 330 nm. Upon the addition of 1 equivalent of **ATP**, no significant changes were recorded, the signal remains more or less the same over a period of 45 minutes. As it was already shown in **Figure 3.6**, **ADP** quenches the Eu(III)-centred emission more compared to the same for **ATP**. Indeed, upon the addition of 1 equivalent of **ADP** to the solution of Eu-**49**-**nta** the initial quenching occurs within the first 5 minutes of the measurement, but no significant change in the Eu-centred emission was reported for the following 40 minutes.

Based on the result from these studies, and taking into consideration that the experiments were repeated at least 3 times, we can deduct that Eu-**49**-**nta** proved to be able to distinguish between **ATP** and **ADP**, consequently in the next investigation, focus was on study of the interaction among the Eu-**49-nta** complex and the components of the assay.

3.3 Control experiments

As already mentioned, the purpose of this project was to develop an assay able to monitor the enzymatic activity of a PKA using the assay described on previous pages. In an advanced system like this and to ensure to establish that the kinase output signal that we are monitoring is only due to the conversion of the **ATP** to **ADP**, and not due to other interaction from the background the interaction between

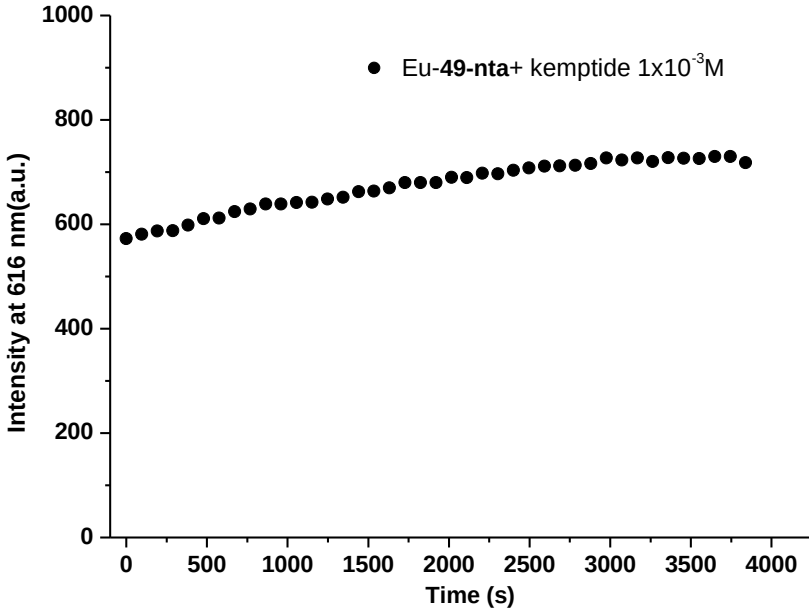

Figure 3.10: *Change in the Eu(III)-centred emission of* ***Eu-49-nta*** *at 616 nm (c = 8 x 10^{-3} M) (λ_{ex} = 330 nm) in HEPES buffer pH 7.2 upon the addition of kemptide (c = 1 x 10^{-3} M) versus the time (0→4000 seconds).*

the **Eu-49-nta** and all the other components necessary for the enzymatic reaction to occur was evaluated. All the control experiments have been performed at the same concentration as were used in the proposed assay.

In **Figure 3.10** the first control experiment is illustrated, where the intensity of the Eu(III) centred emission of the Eu-**49-nta** complex was monitored upon interaction with Kemptide, which act as the substrate, where the kinase transfers the phosphate group. The possible interference would be formed the terminal carboxyl group of the glycine which could coordinated the Eu(III) metal centre, displace the **nta** antenna and as such can affect the emission which would result in false positive

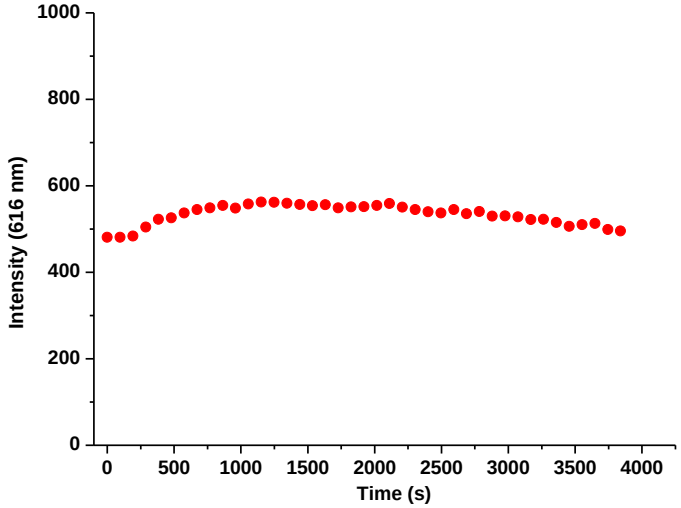

Figure 3.11*: Change in the Eu(III)-centred emission of Eu-****49-nta*** *at 616 nm (c = 8 x 10^{-3} M) (λ_{ex} = 330 nm) in HEPES buffer pH 7.2 upon the addition of $MgCl_2$ (c = 1 x 10^{-3} M) versus the time (0→4000 seconds*

results. Therefore, in the first control experiment to a solution of Eu-**49-nta** (c = 8 x 10^{-3} M) in HEPES buffer, the Kemptide (that has been rehydrated with milli-q water to reach the concentration of 1 x 10^{-3} M) was added, and the luminescence monitored from the Eu(III) centred emission at 616 nm over 4000 seconds (66 minutes). As can be seen from **Figure 3.10**, then only a slight, but not significant enhancement (*c.a.* 5 %) in the enzyme the signal was recorded. This would involve that the substrate is not binding in any significant way to the Eu-centre. The second control experiment that was performed involved adding $MgCl_2$ (c = 1 x 10^{-3} M) to a solution of the complex 8 x 10^{-3} M and the results reported in **Figure 3.11** show that there was no significant change in the emission due to the addition of the magnesium salt. Next the interaction of the DTT with the Eu-**49-nta** was evaluated the results as shown in **Figure 3.12**. As previously mentioned DTT is crucial for the working of the enzyme due to its reducing properties. As can be seen from **Figure 3.12** a slow quenching was observed upon the addition of 1 equivalent of DTT. As shown in **Figure 3.3**, the oxidated form of the DTT is a six membered ring with an internal disulfiide bond and 2 hydroxyl groups that probably slowly displace a part of the **nta** antenna from the Eu(III) metal centre and resulting in a quenching of the emission.

The last control has been evaluated upon adding the PKAc enzyme alone to the complex. Into an aqueous solution in HEPES buffer of Eu-**49-nta**, PKAC c= 3 x 10^{-5} M was added and the changes of the Eu(III) centred emission at 616 nm were

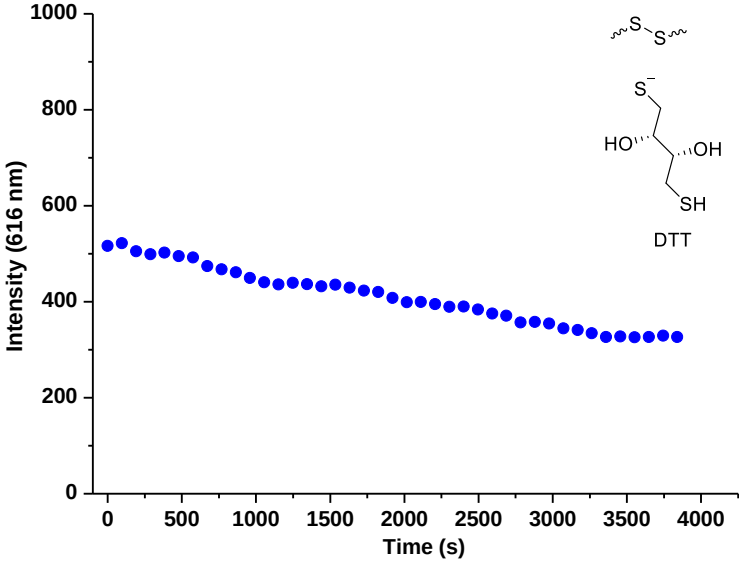

Figure 3.12: *Change in the Eu(III)-centred emission of* ***Eu-49-nta*** *at 616 nm (c = 8 x 10^{-3} M) (λ_{ex} = 330 nm) in HEPES buffer pH 7.2 upon the addition of DTT (c = 2.5 x 10^{-3} M) versus the time (0→4000 seconds).*

monitored. This part of the experiment is crucial to make sure that the change in signal from the assay is given from the conversion of the **ATP** in **ADP**, indeed we need to prove that the enzyme does not affect the luminescent properties of the Eu(III) complex.

The results shown in **Figure 3.13** proved that there is no interaction between the enzyme alone and **Eu-49-nta** complex, the signal remains stable over the time this means that the enzyme is not able to displace the antenna and quench the emission of the Eu(III) metal centre. As all the other experiments, we repeated the test at least 3 times in order to guarantee that there is no relevant interaction with the components of the assay and the luminescence properties of **Eu-49**.

Having determined the effect of the single components of the assay on the **Eu-49-nta** complex we decided to monitor the enzymatic transferring of the phosphate

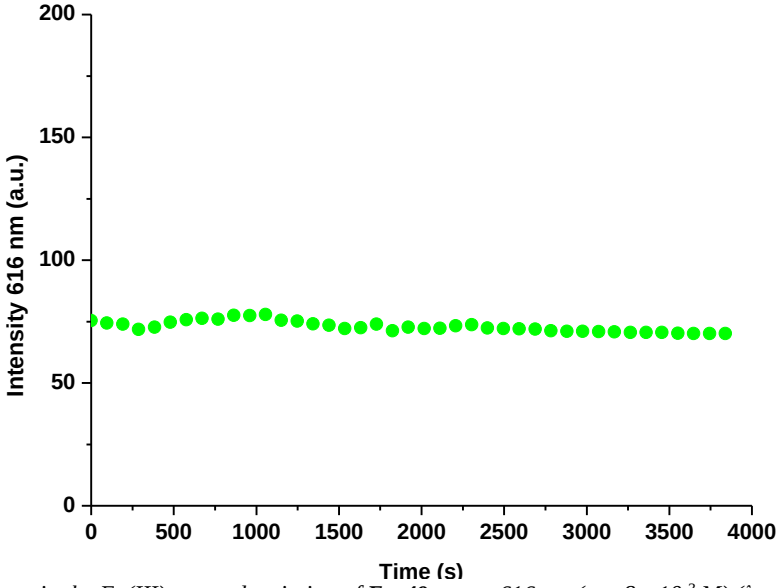

***Figure 3.13**: Change in the Eu(III)-centred emission of **Eu-49-nta** at 616 nm (c = 8 x 10^{-3} M) (λ_{ex} = 330 nm) in HEPES buffer pH 7.2 upon the addition of PKAC (c = 3 x 10^{-5} M) versus the time (0→4000 seconds).*

group from the **ATP** to the **ADP**.

3.4 Enzymatic reaction transferring ATP to ADP using Ln-complex kinase assay

In order to prove the ability of the Eu-**49** complex to monitor the kinase activities, experiments with different concentration of PKAc were performed. All the tests were performed in HEPES buffer pH 7.2 in a final volume of 300 μL in a range of 3 days from the reconstitution of the enzyme, the activity of the enzyme is time and

temperature dependent (as shown in Table 1), hence, it was important that the fresh samples were used through all these investigation

Table 2: *Solution activities study of PKAc.*

Solvent	Protein concertation	Temperature	Activities change after 8 days
Water	50 µg/ml	-15 °C	40% loss when thawed
Water	50 µg/ml	+4 °C	15% loss
Water+DTT	50 µg/ml	-15 °C	98% loss when thawed
Water+DTT	50 µg/ml	+4 °C	15% loss

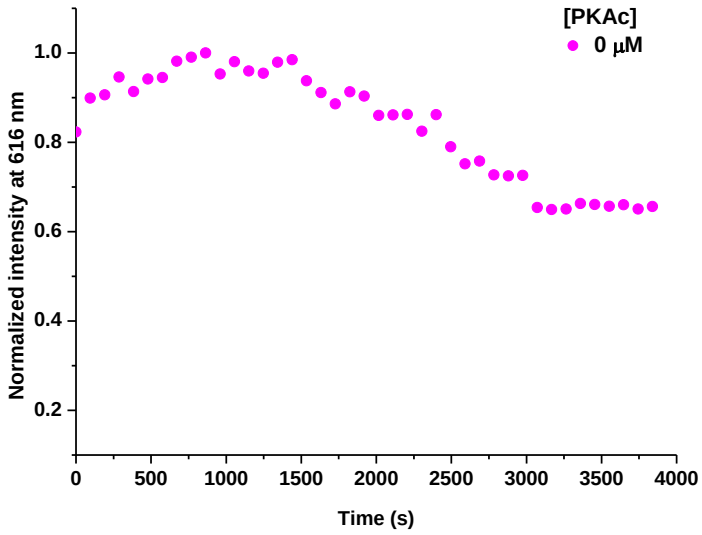

Figure 3.14: *Change in the Eu(III)-centred emission of* ***Eu-49-nta*** *(c = 8x10^{-3} M) at 616 nm (λ_{ex} = 330 nm) in HEPES buffer pH 7.2 upon the addition of kemptide (c = 1 x 10^{-3} M), DTT (c = 2.5 x 10^{-3} M), $MgCl_2$ (c = 3 x 10^{-3} M) and* ***ATP*** *(c = 1 x 10^{-3} M) simultaneously.*

The first experiment was performed by monitoring the changes in the Eu(III)-centred emission of the **Eu-49-nta** upon the addition of all the assay components with the exception of the enzyme, in this way it is possible to create a "baseline" of the modulation of the emission in absence of the enzyme (so without conversion of **ATP** to **ADP**).

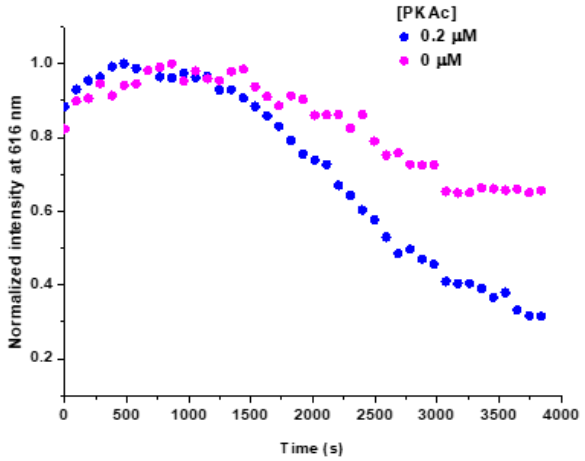

Figure 3.15: *Change in the Eu(III)-centred emission of* ***Eu-49-nta*** *(c = 8 x 10^{-3} M) at 616 nm (λ_{ex} = 330 nm) in HEPES buffer pH 7.2 upon the addition of kemptide (c = 1 x 10^{-3} M), DTT (c = 2.5 x 10^{-3} M), $MgCl_2$ (c = 3x10^{-3} M) and* ***ATP*** *(c = 1 x 10^{-3} M) and PKAc (c = 0.2 x 10^{-3} M) added simultaneously.*

The results reported in **Figure 3.14** shows a slight increase in ΔJ = 2 of the signals of 10 % in the first 1000 seconds and a small quenching of 20% after 1500 seconds. This could be the results of some partial displacement of the antenna given from the steric effects of the enzyme. This signal was used as a baseline in order to ensure that the signal that was monitored is due to the enzymatic conversion of **ATP** to **ADP** and not from other factors.

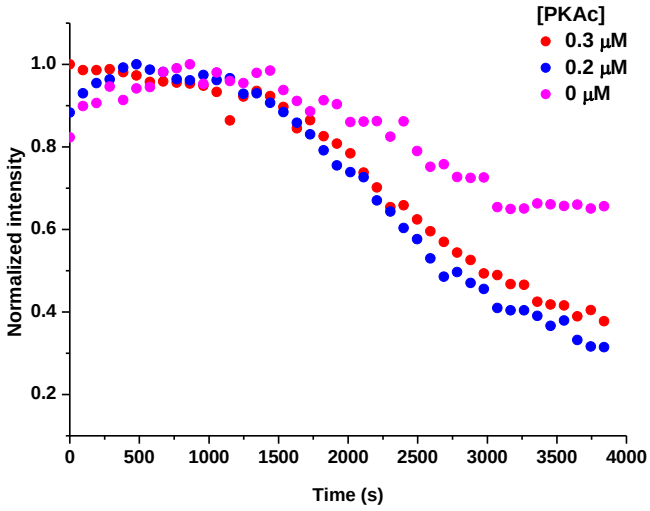

Figure 3.16*: Change in the Eu(III)-centred emission of* ***Eu-49-nta*** *(c = 8 x 10^{-3} M) at 616 nm (λ_{ex} = 330 nm) in HEPES buffer pH 7.2 upon the addition of kemptide (c = 1 x 10^{-3} M), DTT (c = 2.5 x 10^{-3} M), $MgCl_2$ (c = 3 x 10^{-3} M) and* ***ATP*** *(c = 1 x 10^{-3} M) and PKAc (c = 0.3 x 10^{-3} M) added simultaneously.*

From the preliminary investigation, it was seen then that maximum enzyme concentration achieved in HEPES buffer is 0.4 µM so we decided to start our investigation with the concentration of PKAc being 0.2 µM. The kinase was added last to a solution containing all the other components and the spectra were recorded every 100 seconds for a total of 4000 seconds. As shown in **Figure 3.15** the results

are slightly different from that one shown in **Figure 3.14.** The Eu(III)-centred emission is more quenched in the presence of the enzyme, however, the trend is similar to that seen in its absence. Indeed, the enzyme alone gives a quenching of *ca*.7%, in the presence of the (PKAc (0.2 x 10^{-3} M) while the ΔJ = 2 signal is quenched by 37%. The conversion of **ATP** to **ADP** is a fast process while as the emission ΔJ = 2 started to be quenched after 1500 seconds, so it is unlikely that it is due to the conversion of the **ATP** to **ADP** and it is probably more likely due to the kinetic effect resulting from the addition of all the compounds in the assay. Then the amount of enzyme was increased; hence the second investigation has been performed using a concentration 0.3 μM of PKAc following the same procedure as above. The results are shown in **Figure 3.16** and demonstrate to be very similar to that one obtained using the lower concentration of the enzyme. Hence, it is likely that, the concentration of the enzyme was not high enough to convert a detectable quantity of **ADP**.

With these results in the hand we further increased the concentration of the enzyme. Using a concentration of 0.4 μM of PKAc, the assay proved to be able to detect the enzymatic conversion as shown in **Figure 3.17** as it was demonstrated from the reduction in the ΔJ = 2 band. While performing the experiment in the same way as all the previous ones, here the results show a faster reaching the of the signal quenching in up to 1000 seconds. As the phosphorylation of the substrate is happening, the concentration of **ADP** is increasing while the **ATP** is decreasing, resulting in more significant quenching of the Eu(III)-centred emission. All the experiments were performed three times always giving the same result, so it can be

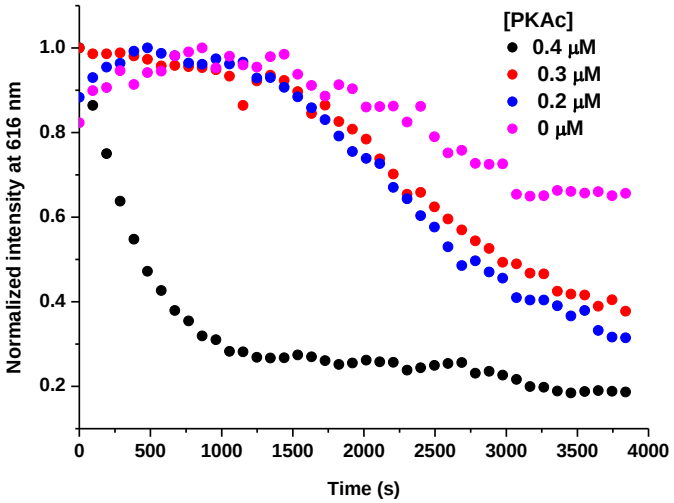

***Figure 3.17**: Change in the Eu(III)-centred emission of **Eu-49-nta** ($c = 8 \times 10^{-3}$ M) at 616 nm (λ_{ex} = 330 nm) in HEPES buffer pH 7.2 upon the addition of kemptide ($c = 1 \times 10^{-3}$ M), DTT ($c = 2.5 \times 10^{-3}$ M), $MgCl_2$ ($c = 3 \times 10^{-3}$ M) and **ATP** ($c = 1 \times 10^{-3}$ M) and PKAc ($c = 0.4 \times 10^{-3}$ M) added simultaneously.*

concluded that the minimum concentration to convert enough **ATP** to **ADP** using 0.4 μM of the enzyme. Unfortunately, we have not been able to perform experiments at higher concentration because the solubility of **Eu-49** in aqueous media is not high enough, so the addition of more than 0.4μM enzyme, resulted in a precipitation the Eu(III) complex. Based on the results from these solution studies, preliminary studies were carried out on the deposition of a LB film of **Eu-49-nta** with the appropriate sizes to act as sensor to monitor the kinase activities.

3.5 Monolayer of Eu-49 to monitor the kinase activities

The application of Langmuir Blodgett monolayers for biological purpose was discussed in detail in the first and the second chapters of the thesis. While the use of lanthanide complexes has been investigated in such assay in the past and various research work was done during the past few years but there are no studies published where the use of LB-lanthanides monolayers have been developed to monitor the kinase activities. The main advantage of using the LB-monolayer system for this purpose is that it is possible to overcome the problem of the solubility of the Eu(III)

Figure 3.18: *LB-**Eu-49** monolayer deposited into a 1x2 cm quartz slide.*

complexes as the enzymatic reaction will occur on the surface of the monolayer. This also allows for repeated use of such systems for sensing purpose. As indicated above, then working in aqueous medium is troublesome as higher concentration of the enzyme result in the Eu-**49**-**nta** complex to possibly aggregate and precipitate, which could be also due to the interaction with enzyme.

The deposition of the LB-Eu-**49** has been performed as described in Chapter 2, the only difference was in the size of the quartz slides. Here we employed a small

volume that was necessary to use for a smaller slide to deposit the **Eu-49** (1 x 2 cm, **Figure 3.18**) and here the transfer ratio was 0.8, which indicates that the film was successfully incorporated onto the quartz slide. After the deposition of the film onto the quartz slid, the next step was to investigate the ability of the LB-Eu-**49** to discriminate between **ATP** and **ADP** and act as sensor for monitoring the enzymatic activities.

3.6 Monitoring of the enzymatic conversion of ATP and ADP using LB-monolayer of Eu-49

The obtained quartz substrate with the monolayer was first dipped into a solution of **nta** ($c = 1 \times 10^{-4}$ M) for 1 minute in order to "switch on" the luminescence of LB-Eu-**49**. The changes in the $\Delta J = 2$ are shown in **Figure 3.19**. In the following step this emissive monolayer was dipped in a solution of the respective phosphorylated nucleotide ($c = 1 \times 10^{-3}$ M) in HEPES buffer at pH 7.2 and the emission of the Eu(III) centre was monitored. The results shown in **Figure 3.19** prove that the LB-Eu-**49-nta** monolayer is able to discriminate between **ATP** and **ADP** on the quartz slide substrate. To prove that the quenching is due to the displacing of the **nta** antenna and not from the washing of the film from the substrate, we investigated the solution

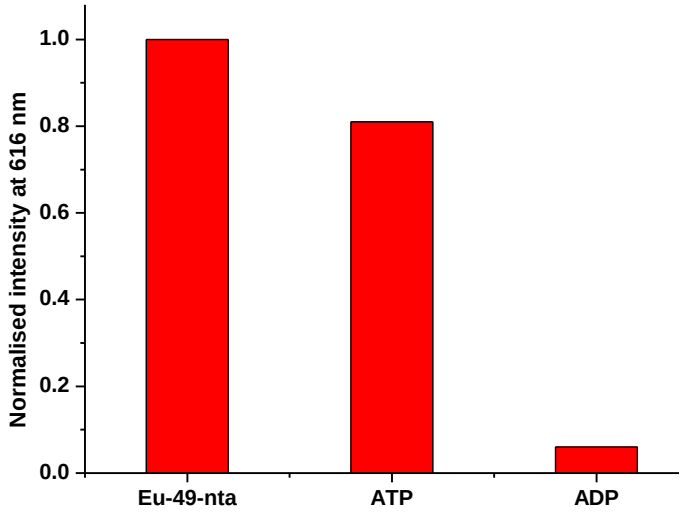

Figure 3.19: *Normalised Eu(III)-centred emission of LB-**Eu-49-nta** at 616 nm (λ_{ex} = 330 nm) HEPES buffer pH 7.2 upon the dipping in a 1 x 10^{-3} M solution of **ATP** and **ADP** in HEPES buffer.*

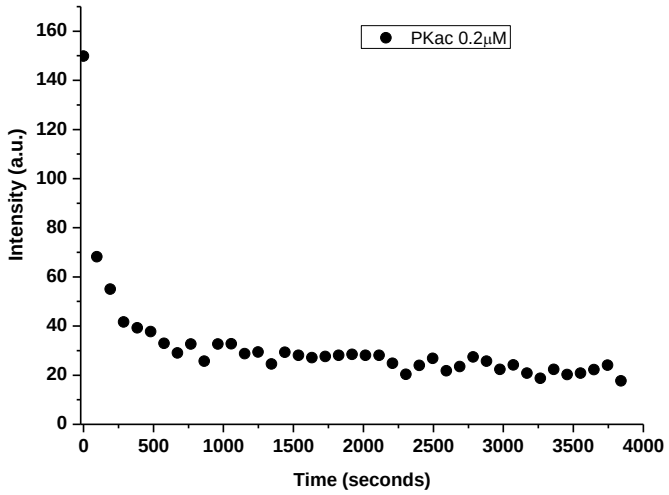

Figure 3.20: *Change in the Eu(III)-centred emission of LB-**Eu-49-nta** monolayer at 616 nm (λ_{ex} = 330 nm) upon the dipping in a solution of Kemptide (c = 1 x 10^{-3} M), DTT (c = 2.5 x 10^{-3} M), $MgCl_2$ (c = 3 x 10^{-3} M) and **ATP** (c = 1 x 10^{-3} M) and PKAc (c = 0.2 x 10^{-3} M) in HEPES buffer pH 7.2.*

where the quartz slide was dipped (without the LB-**Eu-49**) and no Eu-emission could be recorded from the solution. The assay was assembled, in the same condition as described previously for the homogenous solution studies and two different concentrations of the enzyme were investigated, 0.2 and 0.4 μM, respectively. The results from the 0.2 μM concentration of the enzyme are shown in **Figure 3.20.** In

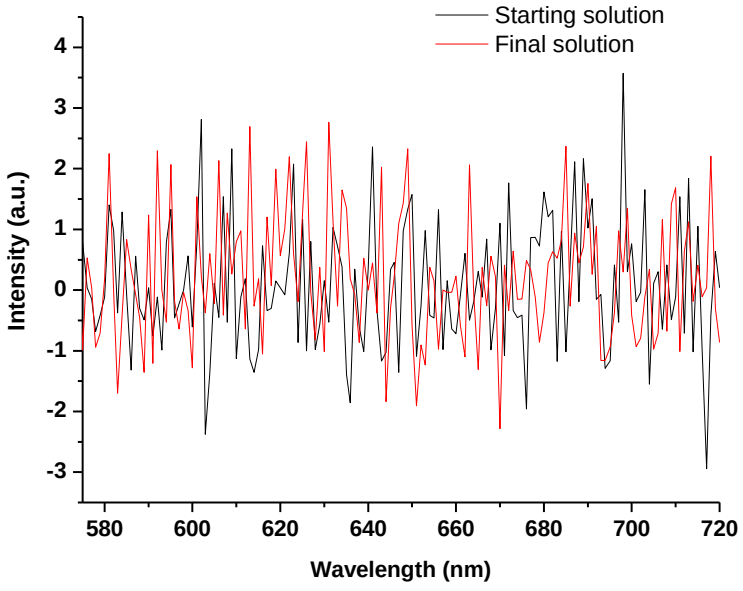

Figure 3.21: *Eu(III)-centred emission at 616 nm (λ_{ex} = 330 nm) of a solution containing kemptide (c = 1 x 10^{-3} M), DTT (c = 2.5 x 10^{-3} M), $MgCl_2$ (c = 3 x 10^{-3} M) and **ATP** (c = 1 x 10^{-3} M) and PKAc (c = 0.2 x 10^{-3} M) before (black) and after (red) the dipping of the LB-**Eu-49** monolayer in HEPES buffer pH 7.2.*

order to exclude the possibility that the observed quenching is due to the removal of the monolayer from the quartz slide we recorded the emission spectrum of the solution before and after the enzymatic reaction was performed. As can be seen in

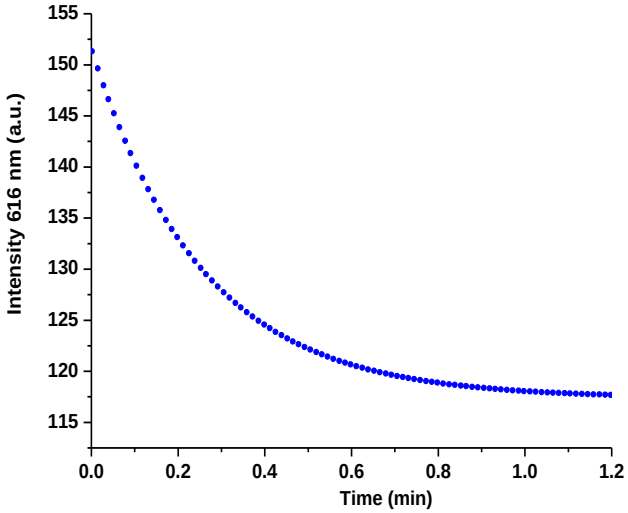

Figure 3.22: *Change in the Eu(III)-centred emission of LB-**Eu-49-nta** at 616 nm (λ_{ex} = 330 nm) upon dipping in a solution of kemptide (c = 1 x 10^{-3} M), DTT (c = 2.5 x 10^{-3} M), $MgCl_2$ (c = 3 x 10^{-3} M) and **ATP** (c = 1 x 10^{-3} M) and PKAc (c = 0.3 x 10^{-3} M) in HEPES buffer pH 7.2.*

Figure 3.21 no evidence of Eu-emission from the solution was seen. This proves that the quenching shown in **Figure 3.20** is due to the enzymatic conversion of the **ATP** to **ADP**. The enzymatic conversion is a quick process, as shown in **Figure 3.20**, the quenching of the signal happening within in the first 300 seconds. To better understand this process, the experiment in the same conditions was repeated changing the settings of the instrument, where instead of collecting one spectrum every 96 seconds, the spectrometer has been set to collect the emission at 616 nm every second and result is shown in **Figure 3.22**. In the first minute the signal is fully quenched, and the LB-Eu-**49** prove to be able to monitor this conversion in real time and shows a higher sensitivity compared to the same assay used in the solution. The same experiment was repeated using a higher concentration of the PKAc

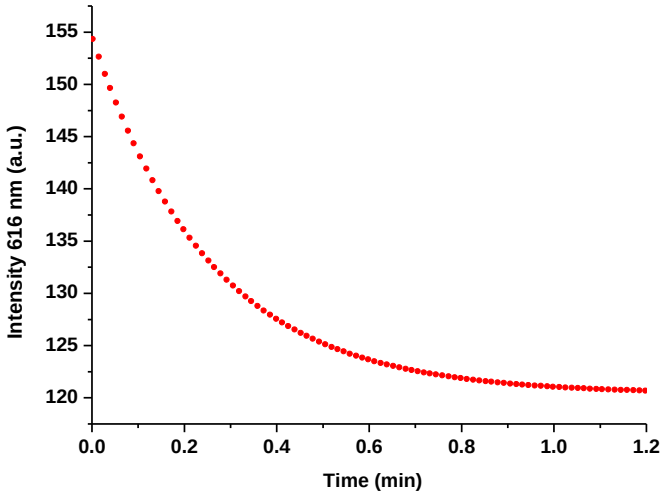

Figure 3.23: *Change in the Eu(III)-centred emission of LB-**Eu-49-nta** at 616 nm (λ_{ex} = 330 nm) upon dipping in a solution of kemptide (c = 1 x 10^{-3} M), DTT (c = 2.5 x 10^{-3} M), $MgCl_2$ (c = 3 x 10^{-3} M), **ATP** (c = 1 x 10^{-3} M) and PKAc (c = 0.2 x 10^{-3} M) in HEPES buffer pH 7.2.*

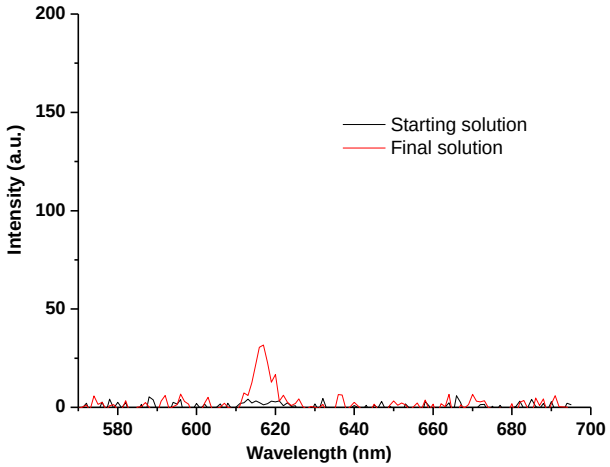

Figure 3.24: *Eu(III)-centred emission at 616 nm (λ_{ex}= 330 nm) a solution containing Kemptide (c = 1 x 10^{-3} M), DTT (c = 2.5 x 10^{-3} M), $MgCl_2$ (c = 3 x 10^{-3} M) and* ***ATP*** *(c = 1 x 10^{-3} M) and PKAc (c = Figure 3.24: Eu(III)-centred emission at 616 nm (λex= 330 nm) a solution containing Kemptide (c = 1 x 10-3 M), DTT (c = 2.5 x 10-3 M),*

(0.4μM) without changing the concentrations of the other components of the assay. The result is shown in **Figure 3.23**.

Again, here to exclude the possibility that the observed quenching is due to delamination of the Eu-**49** monolayer from the quartz slide, the emission of the solution upon excitation at 330 nm, has been evaluated before and after the quartz slide with LB-Eu-**49-nta** was removed from the solution, the results are shown in **Figure 3.24**. As usually, the same experiment was repeated 3 times.

In contrast to what happened for the lower concentration of the PKAc, it is possible to measure a weak emission in the Eu-centred emission in the solution after the experiment. However, this is minimal emission in comparison to what was seen

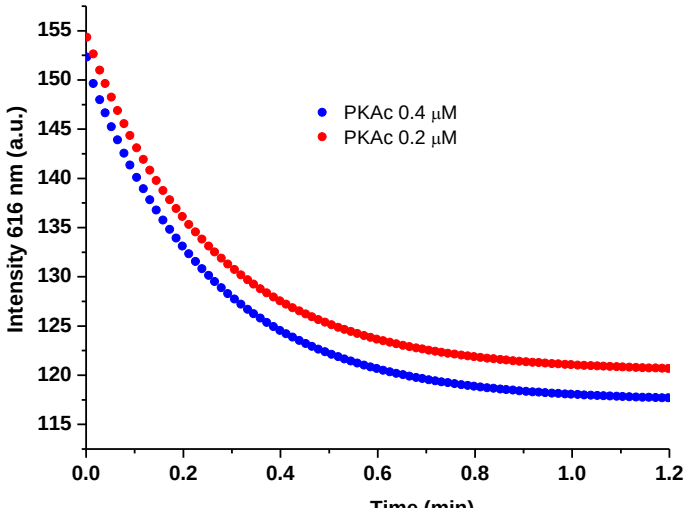

Figure 3.25: *Comparison of the change in the Eu(III)-centred emission at 616 nm (λ_{ex} = 330 nm) of LB-Eu-****30-nta*** *upon the dipping in a solution of Kemptide (c =1 x 10^{-3} M), DTT (c = 2.5 x 10^{-3} M), $MgCl_2$ (c = 3 x 10^{-3} M) and* ***ATP*** *(c = 1 x 10^{-3} M) and PKAc (c = 0.2 x 10^{-3} M, red) and (c = 0.4 x 10^{-3} M blue).*

from the film itself. One of the possible explanations to this is that increasing the concentration of the enzyme changes the polarity of the solution enough to solubilize part of the Eu(III) complex but this need be further investigated and despite this, the emission of the solution is really weak so the quenching of the LB-Eu-**49** during the experiment is most probably due to the conversion of the **ATP** to **ADP**. To better understand the difference between the two experiments with different concentration of PKAc, the comparison of the two graphs is shown in **Figure 3.25**. The two results are comparable, the higher concentration seems to quench more (77%) compared lower concentration (70%), but this can be due to the solubilization of the films into the solution. An issue was found in trying to increase the concentration of the enzyme (0.5μM), the solution became cloudy and it was not possible to perform the experiment.

3.7 Conclusions

In this chapter we have reported the first LB-Eu(III) luminesce assay for monitoring the enzymatic conversion of the **ATP** to **ADP** performed by a Protein Kinase A, an enzyme that is part of a wide family of enzymes involved in many biological processes such as regulation of the glycogen, sugar and lipid metabolism and even in the cancerogenic processes. The ability of the Eu(III) complex to discriminate between the two phosphorylated nucleotides in aqueous media was investigated proving that Eu-**49-nta** proved to be able to discriminate between **ATP** and **ADP**, as the emission of the Eu(III) metal centre resulted in more significant quenching in the presence of **ADP**.

Once having proven the ability of the Eu-**49** of monitoring the enzymatic activities we deposited the Eu(III) complex in a LB monolayer to develop the first LB-Eu(III) monolayer able to monitor the enzymatic activities.

The quartz slide used as support was smaller than the one described in the Chapter 2, in this way it can fit in the small cuvette used for the experiment. The Eu-**49** complex was successfully incorporated into the quartz slide with a transfer ratio of 0.8. The assay was then assembled in the same conditions of that one in solution studies but instead of adding the **Eu-49**, the quartz slide with its LB monolayer was dipped in the solution. The results showed a faster quenching using a concentration

of 0.2 μM, and with the first 200 seconds a full quenching of the Eu-centred emission was observed. The results show a full quenching of the signal within the first minute. The results obtained here correspond to the literature where it was found that the enzymatic conversion of the **ATP** to **ADP** is a fast process. Increasing the concentration of the PKAc to 0.4 μM did not affect the quenching rate. It was not possible to perform the same enzymatic assay experiment using a concentration of PKAc at c = 0.6 μM because the solution was able to remove the major part of the complex from the quartz slide and make it precipitate in the cuvette.

The future works will consist in the use of different ligand to improve the accuracy of the assay to monitor the phosphorylation process.

The next Chapter is focused on the formation of self-assembly to construct hierarchical materials[151-153]. As mentioned in Chapter 1, the use of lanthanide ions has become an important strategy for the development of luminescent self-assembly structures, and indeed lanthanide ions can be used to 'direct' the synthesis of various supramolecular assemblies.[29, 48, 154] However, one of the most difficult tasks in this area is to use the self-assembly process for the development of hierarchical lanthanide-based materials, this process is relatively rare.[155-158]

Chapter 4.0

Introduction

The Gunnlaugsson group is known for developing novel luminescent Ln(III) probes. In Chapter 1 it was explained that one of the keys to achieve supramolecular structures is the self-assembly process. One of the most important works in the research group is the achieving of Ln(III) based soft materials that can be used in several fields such cosmetics, food processing, coating, lubrification, protein crystallization *etc*[159, 160] where metal directed synthesis is one of the most central points for the formation of these assemblies.

This has allowed them to be used across a range of different fields, from sensing applications[11, 26, 161] to theoretical structural studies.[162] In particular, it has been recently reported that these systems are able to participate in the self-assembly of complex structures involving tripodal ligands in conjunction to with cyclen. In a recent paper, Gunnlaugsson and co-workers reported the use of a heptadentate cyclen complex of Eu(III) and Tb(III), in which the coordination would be completed by the carboxylic moiety of the tripodal ligand, which would also act as a photosensitizer for the lanthanide ions. In this chapter we will show our work in the developing a self-assembled system in which a tripodal ligand based on the terpyridinic ligands based on the benzene-1,3,5-tricarboxamide (BTA) motif binds the Ln(III) ion involved in a complex with heptadentate cyclen ligand which contains a strongly hydrophobic tail. One of the most interesting features that these frameworks present is the ability to form supramolecular 3-D structures able to retain large amounts of solvents, therefore forming supramolecular gels. The reticulation necessary in order to form these systems is achieved thanks to the use of Ln(III) ions, which act as cross-linking points and turn the one-dimensional aggregates into the intertwined fibrous systems necessary for retention of the solvent. The resulting aggregates were studied in solution through spectroscopic means and by SEM after deposition on silica substrates, to inspect the photophysical and supramolecular properties of the systems. The synthesis of the Tb(III) complex Tb-**49** is reported in Chapter 2.

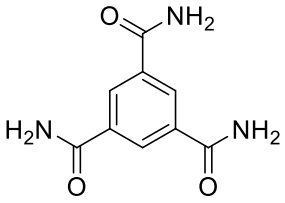

1,3,5-tricarboxamide
(**BTA**)

4.1 Synthesis of the tripodal ligand

The synthesis of the tripodal ligand here reported has been performed by Emanuele Cappello, a PhD student from the Gunnluaggson group. While the details are given in his thesis, a short discussion of the synthesis is presented here. The syntheses of the ligands were based on similar BTA-based architecture already present in the literature, using a multi-step approach. The first step for the synthesis of the tripodal system was to obtain the benzoic acid derivative of the 1,3,5-benzene, which was accomplished by dissolving 1,3,5-benzene tricarbonyl chloride (**50**) in DCM at 0 °C, then 4-aminobenzoate (**51**) was added to the solution and stirred at room temperature for 72 hours under inert conditions. The resulting precipitate was isolated and dried, then washed with boiling MeOH to remove unreacted starting material present in

the sample, before being filtered and dried once again, resulting in the formation of **52** with *ca.* 55% yield. The ^{1}H-NMR spectrum (400 MHz, DMSO-d6) confirms the success of the reaction, with the appearance of the methyl ester protons signal at 3.85 ppm, the aromatic protons resonances at 8.00 ppm for the spacer and at 8.76 ppm for the core, with the characteristic aromatic protons for the amide at 10.91 ppm. This amide signal presents a peculiarity: N-H protons are defined as "mobile" protons, for their ability to "exchange" with the solvent, analogously to acid protons; this normally leads to broad signals in ^{1}H-NMR spectra. In the case of **52** the signal at 10.91 ppm is unusually sharp. To verify that the assignment was correct, a spectrum in DMSO-d6 was taken before and after the addition of D_2O. In the following step, the ester was hydrolysed to obtain the equivalent tri-carboxylic acid. This was achieved by suspending **52** in a MeOH/THF mixture (75:25) and treating the solution with 1M NaOH for 6 hours at reflux (60 °C). The reaction mixture was then left to cool and subsequently neutralised with aqueous HCl (36% v/v). This results in the formation of a suspension, which was filtered and then washed with water and THF to recover the tri-carboxylic acid. The formation of **53** was confirmed by the ^{1}H-NMR spectrum (**Figure 4.0**), which showed the absence of the signal of the ester protons at 3.85 ppm and the presence of a broad signal at 12.79 ppm, indicating the presence of a mobile proton (-OH). The product was obtained with a 90% yield

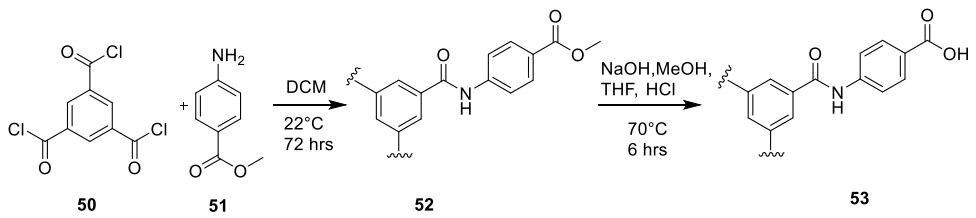

***Scheme 4.0**: Synthesis of the tripodal carboxylic acid **53**.*

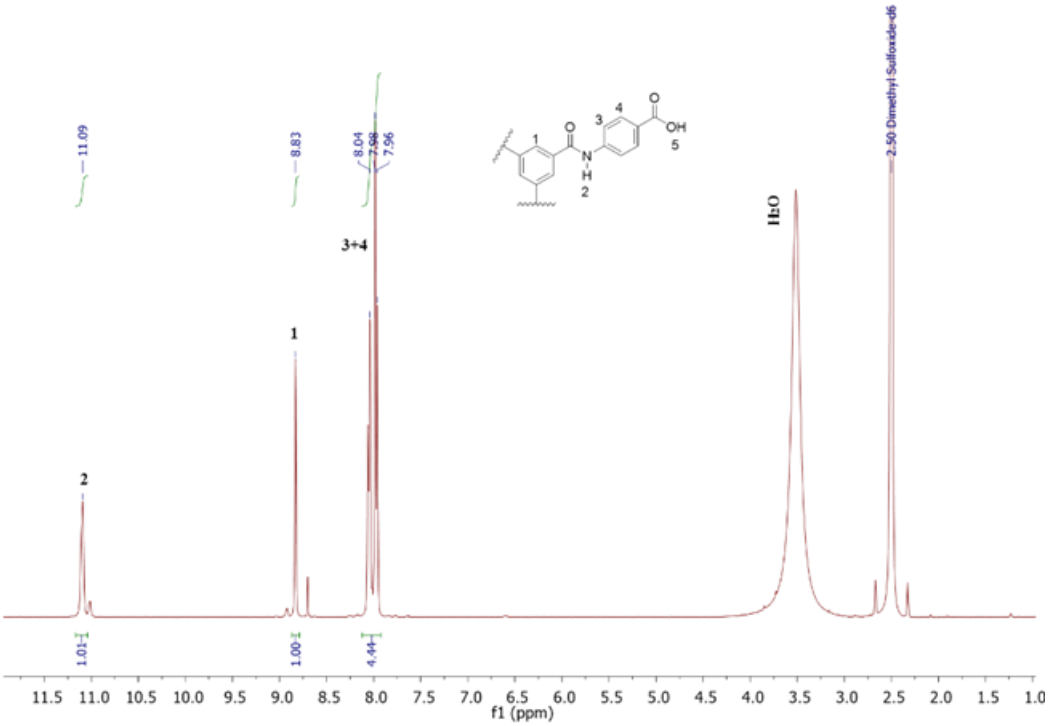

***Figure 4.0**: [1]H-NMR (400 MHz, DMSO-d_6) spectrum of **53**.*

As shown in **Scheme 4.1,** the carboxylic acid **53** reacted with the protected amino-acid tert-butyl-ester hydrochloride salt (L-Ala) dispersing **53** in anhydrous DCM and cooled to 0 °C. The solution containing the amino-acid and the hydroxybenzotriazole (HOBt) was slowly added. One equivalent of triethylamine (NEt_3) was necessary to fully dissolve the HCl salt of the amino acid. A solution of *N*-(3-dimethylaminopropyl)-*N´* -ethylcarbodiimide hydrochloride (EDCI·HCl) and NEt_3 were added after 15 minutes and the mixture was stirred at room temperature.

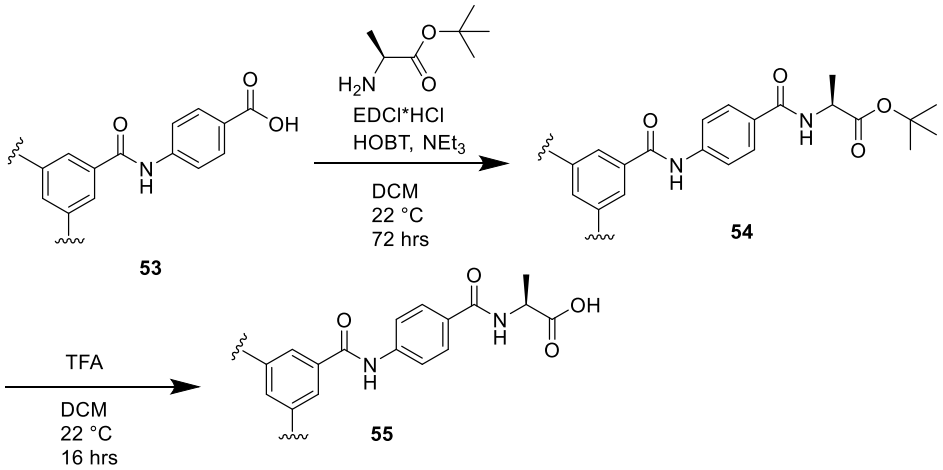

***Scheme 4.1**: Synthesis of the tripodal ligand **55**.*

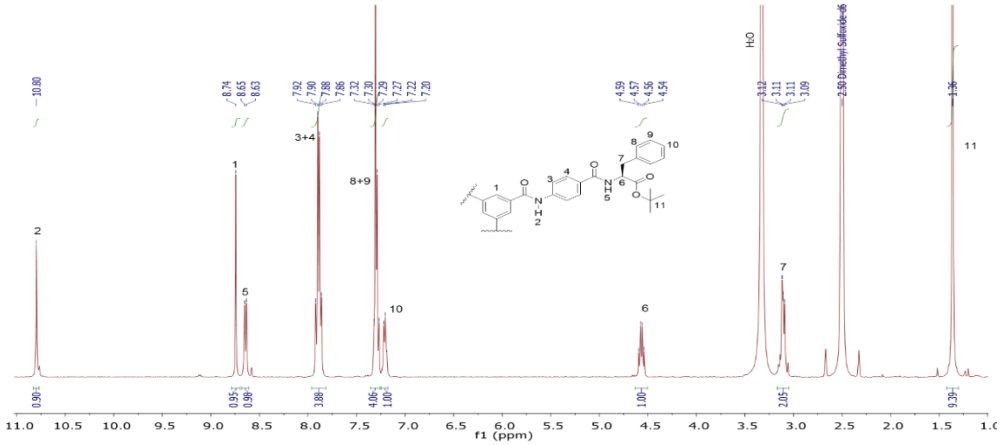

***Figure 4.1**: [1]H-NMR (400 MHz, DMSO-d_6) spectrum of **54**.*

After 72 hours under argon the reaction mixture was quenched and worked up in order to remove the unreacted reagents. Solid by-products of the reaction were removed by gravity filtration and concentrated *in vacuo*. The resulting solid mixture was then re-dissolved in DCM and then washed with saturated aqueous $NaHCO_3$ solution, water and finally with a saturated NaCl solution. The organic layer was then dried over $MgSO_4$, which was then removed by filtration. The product appears as a yellow oil but adding diethyl ether it precipitates as white solid (yield 40%). The [1]H-NMR shown in **Figure 4.1** confirms that the product **54** has been obtained, indeed the signal at 4.35 ppm (the proton in alpha position respect of the carbon of the amino-acid) the doublet at 1.38 ppm (protons for the first carbon of the side chain) and the proton of the tert-butyl protection at 1.42 ppm.

4.2 Sensitisation of the Tb(III) luminescence

The next step was the investigation of the photophysical properties and the stoichiometry of the product obtained upon titrating of Tb(III) complex (**Tb-49**) with the **55.**

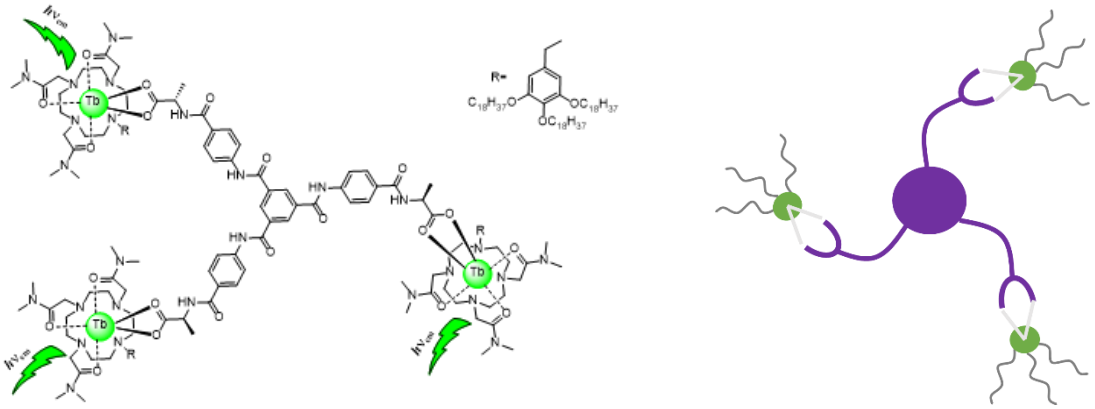

Tb-**49**-**55**

Scheme 4.2: *Schematic representation of the supramolecular complex Tb-**49**-**55**.*

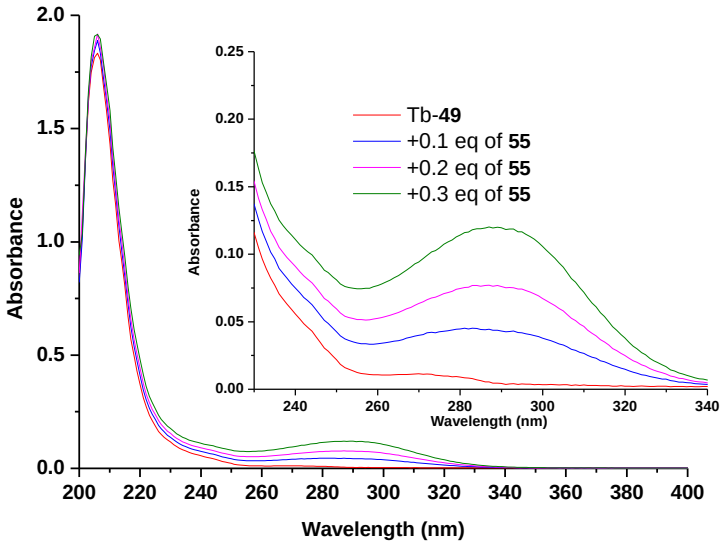

Figure 4.2*: UV-Vis absorption spectra of Tb-**49** (c = 1 x 10^{-5} M) upon the addition of 0.3 equivalents of **55** in MeOH.*

The self-assembly between Tb-**49** and the tripodal ligand would result in the formation of a system with stoichiometry 3:1 (Tb-**49**:**55**). To investigate the formation of the expected Tb-**49**-**55** the luminescence properties of the system have been studied. To a solution of Tb-**49** at c = 1 x 10^{-5} M in MeOH 0.1, 0.2 and 0.3 equivalents of **55** were added. The aim was to use the tripodal ligand as "antenna" (like the **DMAB** used in Chapter 2) to sensitise the Tb(III) metal centre. As

mentioned in Chapter 2, the phenyl ring present in Tb-**49** can only partially sensitise the metal centre, to have a remarkable emission it needs an external antenna. In **Figure 4.2** the UV-visible absorption of Tb-49 is shown relative to the addition of 0.3 equivalents of **55**.

The maximum of absorption of the tripodal ligand is located at 288 nm and it is growing after each addition as expected. Exciting at 288 nm, the delayed Tb(III) emission was recorded (**Figure 4.3**).

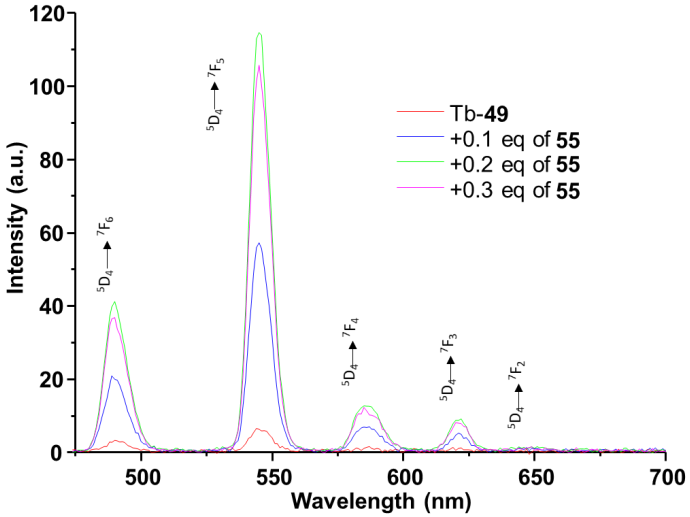

Figure 4.3: *The enhancement of Tb(III)-centred emission for Tb-**49** ($c = 1 \times 10^{-5}$ M in MeOH, λ_{ex} = 288 nm) upon the addition of antenna 0 to 0.3 equivalents of **55**.*

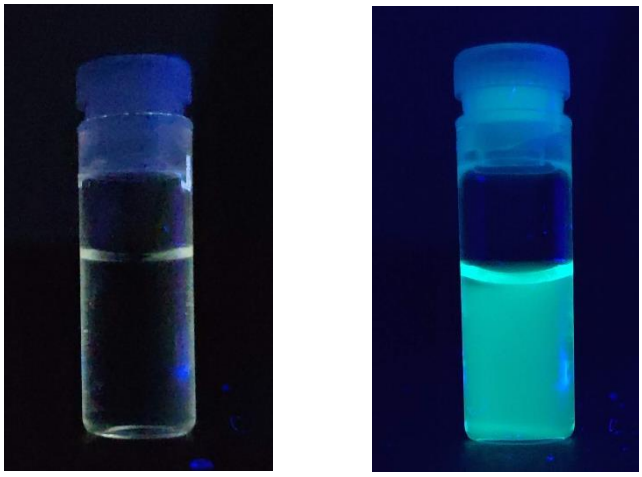

Figure 4.4: *(A) Solution of Tb-**49** and (B) Tb-**49** with 0.3 equivalents of **55** (MeOH, $c = 1 \times 10^{-5}$ M, λ_{ex} = 288 nm) under the*

Upon the addition of **55,** the Tb(III)-centred emission ($^5D_0 \rightarrow {}^7F_J$, J= 0–4) initially increases, reaching a maximum when the stoichiometric ratio between **Tb-49** and **DMAB** is 1:3. The 1:3 ratio gives the brightest emission because of full coordination of the three binding sites of the tripodal system. Each spectrum was recorded waiting 10 minutes between each addition and no kinetic effect was found. Observing the solutions of Tb-**49** and Tb-**49**-**55** under UV light at 330 nm it is clear that there are significantly differences. **Figure 4.4 A** shows the Tb-**49** solution before starting the titration, while **Figure 4.4** B after the addition of 0.3 equivalents of the tripodal ligand where bright green emission can be clearly detected.

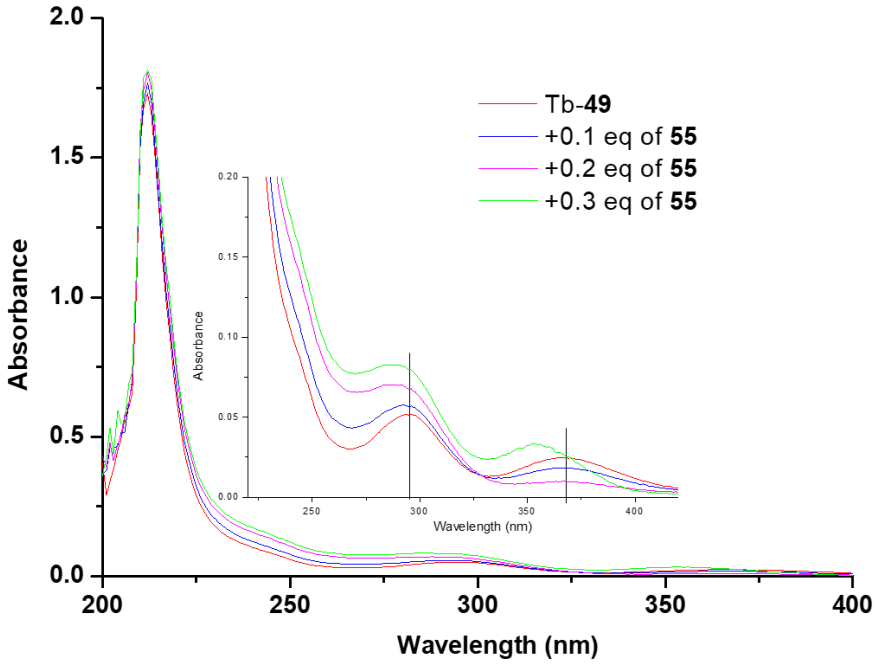

***Figure 4.5**: UV-Vis absorption spectra of Tb-**49** (c = 1 x 10^{-5} M) upon the addition of 0.3 equivalents of **55** in THF.*

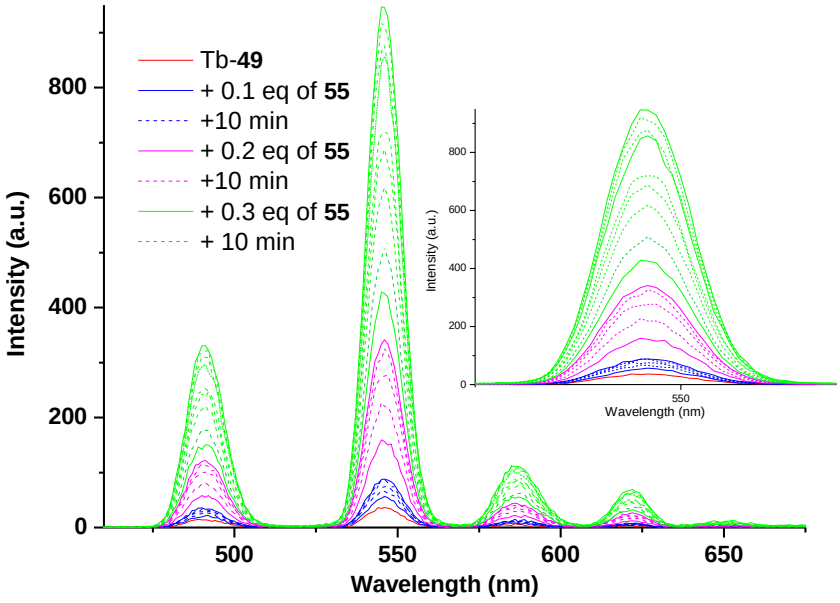

***Figure 4.6**: Change in the Tb(III)-centred emission of Tb-**49** (c = 1x10^{-5} M in THF, λ_{ex}= 288 nm) upon the addition of antenna 0 to 0. 3 equivalents of **55**.*

The same titration was performed in THF in order to investigate the effect of the solvent on the self-assembly process. To a solution of Tb-**49** (c = 1 x 10^{-5} M) 0.1, 0.2 and 0.3 equivalents of **55** in THF were added. The UV-Vis spectra are reported in **Figure 4.5**.

In contrast to what was seen in **Figure 4.2** the UV-vis spectra show two bands initially located at 296 and 371 nm. Upon the addition of ligand **55,** the two bands blue shift. After the addition of 0.3 equivalents of the tripodal ligand the band initially located at 296 nm moved to 288 nm, while the band initially located at 371 nm was shift of to 356 nm. Both bands also show a hyperchromic shift probably due to strong communication between the chromophores. The shift is probably due to the formation of a 1:1, 1:2 and 1:3 complexes that adsorb at different wavelength. The corresponding phosphorescence spectra are reported in **Figure 4.6**.

The luminescence spectra were measured using the same parameters applied for the methanol studies and the spectra were again recorded every 10 minutes to evaluate the kinetic effect. It is clear from **Figure 4.6** that the kinetic effect in THF is much more pronounced than in MeOH. The first emission recorded for Tb-**49** alone was first recorded, as previously mentioned the phenyl ring of the ligand is able to partially sensitise the Tb(III) metal centre and this is the reason why a weak signal relative to transition ($^5D_4 \rightarrow {}^7F_J$; J= 6–2) is observed. Upon the addition of 0.1 equivalent of compound **55** a slight increase in the Tb-centred emission was

observed (blue). The same solution was tested every 10 minutes and the increase of the signal intensity was constant for 30 minutes, reaching a plateau 40 minutes after addition. Once the signal was stable another addition was performed, adding 0.1 equivalents of **55** (having 0.2 total equivalents in solution) and the luminescence was recorded again every 10 minutes (pink) as before in this case the plateau was achieved after 40 minutes. After that the last equivalent has been added, reaching a total of 0.3 equivalents of **55** in solution and the plateau was achieved after 60 minutes. Performing the experiment using the same parameters applied for the studies in MeOH at the same concentration, the luminescence was much brighter in THF (almost 90% higher). One of the possible explanations is that the compound **55** has poor solubility in THF, to stay in solution it binds stronger the Tb-**49**, establishing a stronger communication. Further proof of complexation was obtained fitting the changes in the phosphorescence emission of the Tb(III) using nonlinear regression analysis.[163] Using this software, it was possible to monitor the formation of the three species. The stoichiometry and the respective binding constant is shown in **Table 4.0.**

Table 4.0: *Association binding constant of the different species obtained from the luminescence titration in MeOH..*

Stoichiometry	logβ	Error
1:3	21.997	± 0.071
1:2	14.625	± 0.052
1:1	7.102	±.0.032

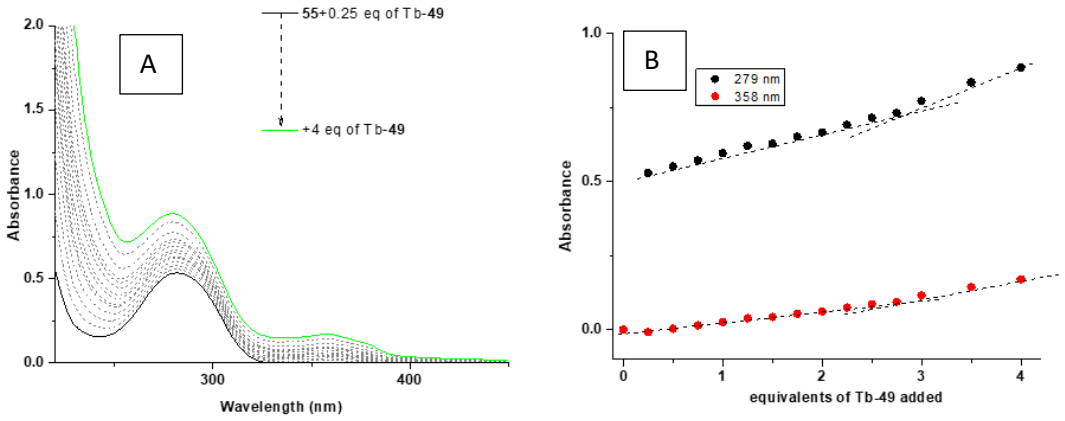

Figure 4.7: *(A) Changes in the absorption spectra of* ***55*** *(c = 1 x 10^{-5} M) upon titrating with Tb-**49** (0 to 4 equivalents) in MeOH. (B) Binding isotherms recorded at 279 and 358 nm.*

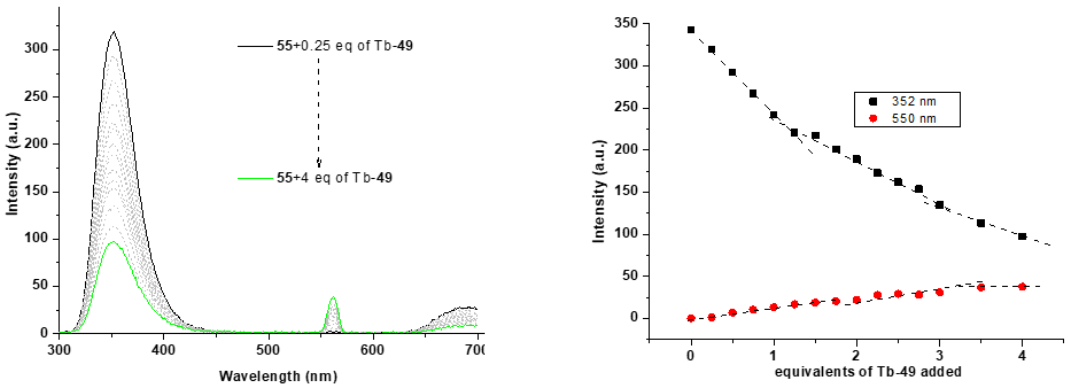

Figure 4.8: *(A)Fluorescence spectra of* ***55*** *(c = 1 x 10^{-5}M in MeOH, λ_{ex} = 288 nm) upon titrating with Tb-****49*** *(0 to 4 equivalents) in MeOH. (B) binding isotherms recorded at 352 and 550 nm*

A different titration was performed next. To a solution of **55** in MeOH (c = 1 x 10^{-5} M) several equivalents of Tb-**49** (0 to 4) were added. The UV-vis- spectra (**Figure 4.7**) shows 2 bands located at 279 and 358 nm. Fitting this data to a 2:1 or 1:1 binding model was not possible, only the 3:1 binding model allowed the experimental data to be fitted successfully. The explanation for this is shown in **Figure 4.7** B. Plotting the binding isotherms and drawing the tangents was possible to observe the change in the pendency only after adding 3 equivalents of Tb-**49**. The data recorded in fluorescence mode are shown in **Figure 4.8**, here the band relative to the fluorescence of **55** appears at 352 nm and the signal shows a constant quenching after every addition of Tb-**49**, concomitantly the band relative to the Tb(III) emission complex increases at the same time, demonstrating the successfully population of the Tb-excited state. In contrast to the UV-vis absorption data, in this case it was possible to find the correct model for the 3:1 and the 2:1 complex but not the 1:1 complex formation. This is shown in **Figure 4.8** B where the binding isotherm relative to the Tb(III)-centred emission (red) has 2 changing in the pendency, the first one upon the addition of 2 equivalents of Tb-**49** and the second in correspondence to the addition of 3 equivalents.

The data recorded in the phosphorescence mode are reported in **Figure 4.9** and it shows an enhancement in all the Tb-centred emission bands signal upon each addition of Tb-**49**. This sensing process so-called "switching" of the Tb luminescence and achieving the maximum emission enhancement when the stoichiometric ration between **55** and Tb-**49** is 1:3, confirming the data shown in **Scheme 4.2**. **Figure 4.9** B show the binding isotherms obtained during the titrations (all the titrations were performed 3 times in order to guarantee the reproducibility). Drawing the tangent relative to the emission of the Tb(III) metal centre at 545 nm, it is possible to distinguish three inflection points corresponding to the 1:1, 1:2 and 1:3 complexes. Fitting these data using reactlab[163] it was possible to determine the three species in solution, and the resulting speciation distribution diagram was

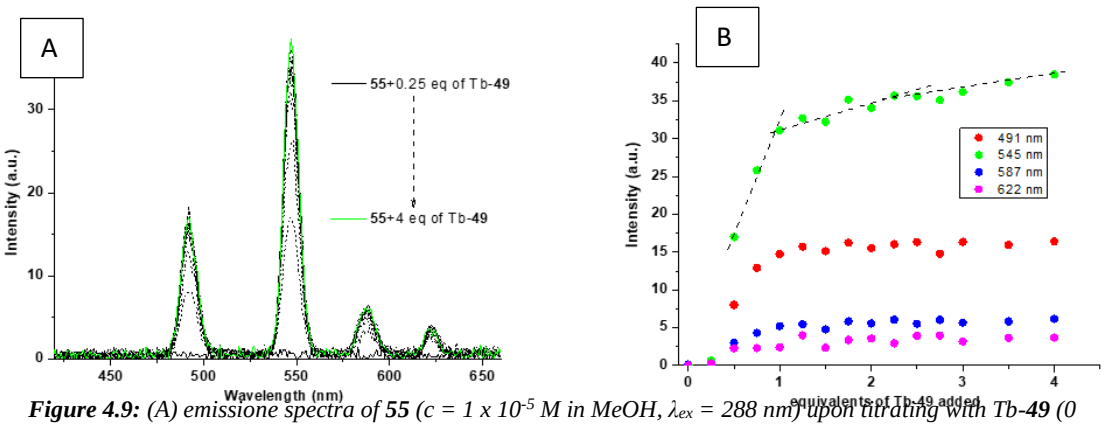

Figure 4.9: *(A) emissione spectra of* ***55*** *(c = 1 x 10^{-5} M in MeOH, λ_{ex} = 288 nm) upon titrating with Tb-****49*** *(0 to 4 equivalents) in MeOH. (B) Binding isotherms recorded at 491, 545,587 and 622 nm.*

shown in **Figure 4.9**. Upon the addition of Tb-**49** the formation of 1:1 complex was observed to reach the maximum of 18 % at one equivalent of Tb-**49**. Simultaneously

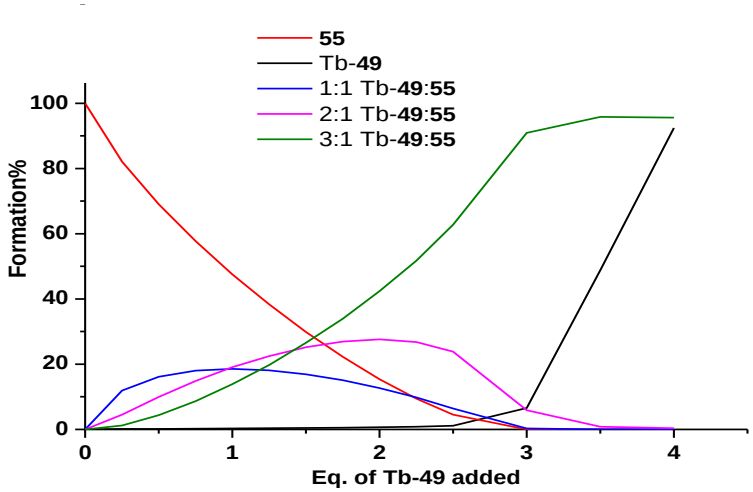

Figure 4.10: *Speciation distribution diagram obtained from the fitting of the phosphorescence titration of* ***55*** *with Tb-****49*** *in MeOH.*

the 1:2 complex began to form and reached the maximum of 28% at 2 equivalents. The formation of the 1:3 complex also started simultaneously with the 1:1 and 1:2 species and reaches the maximum of 95% after the addition of 3.5 equivalents of Tb-**49**. Further additions of Tb(III) complex resulted in an increase of the signal relative to free Tb-**49** in solution. The results are confirmed by the binding constant shown in Table **4.0**. Indeed, the constant of to the 1:3 complex is higher compared to the 1:2 and the 1:1. From the luminescence investigation, the distribution diagram and the binding constants obtained, we were able to confirm the formation of a highly stable self-assembled 1:3 complex.

Once that the photophysical studies proved the formation of complex Tb-**49**-**55** (3:1 complex), we next focused our investigation on the study of the morphology. In order to investigate the self-assembly properties of the ternary complex its micro/nano scale properties were investigated using SEM microscopy.

4.3 Morphological studies

The morphology of **55**, Tb-**49** and Tb-**49**-**55** was investigated by Scanning Electron Microscopy (SEM) in different solvents. Each sample was prepared by spreading 20 μL of solution with c = 1 x 10^{-6} M and c = 1 x 10^{-5} M onto a silica wafer, which was then dried in air for 24 hours and then *in vacuo* for 2 hours prior to imaging. The images were taken from Emanuele Cappello, the PhD student mentioned above that synthesized compound **55.**

4.3.1 Scanning Electron Microscopy studies

Tb-**49** complex was initially imaged alone (**Figure 4.11**) after spreading 20 μL of its solution (c = 1 x 10^{-5} M) in MeOH on to the silica wafer. The sample was then subjected to the coating process. Coating of samples is required in the field of electron microscopy to enable or improve the imaging of samples. Creating a conductive layer of metal on the sample inhibits charging, reduces thermal damage, and improves the secondary electron signal required for topographic examination in the SEM. In this case sputter coating was performed, where an ultra-thin coating of electrically conducting metal (gold in this case) was applied onto the surface of Tb-**49** (non-conducting material). The images do not show any particular structure, the processes result in a self-aggregation of the Tb(III) complex. The same imaging process was performed for Tb-**49** (c = 1 x 10^{-5} M) prepared in THF. The results

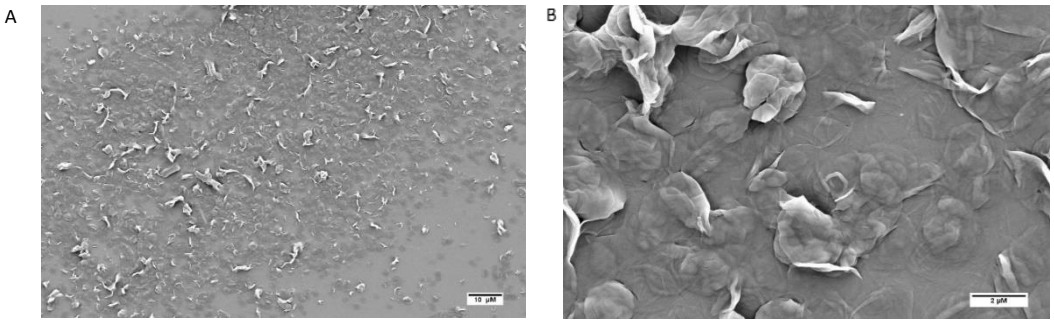

Figure 4.11: *SEM images of Tb-**49** when its 20 µL of solution in MeOH with c = 1 x 10^{-5}M was deposited onto the silica wafer; scale bar (A) 10 µm and (B) 2 µm.*

sho

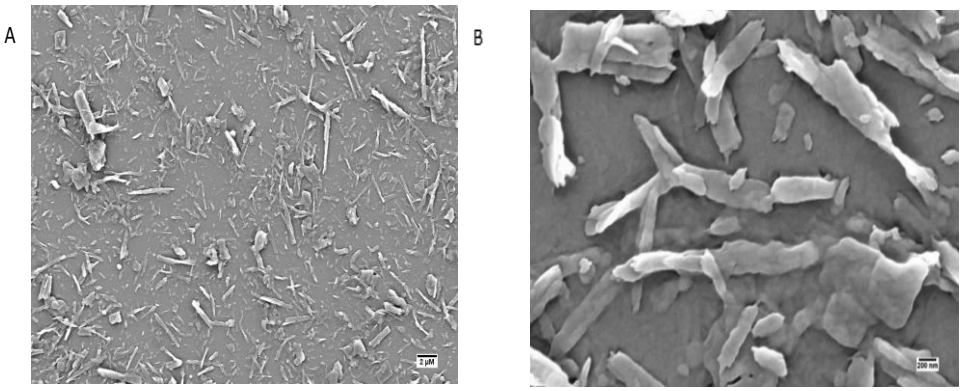

Figure 4.12: *SEM images of Tb-**49** when its 20 µL of solution in THF with c = 1 x 10^{-5}M was deposited onto the silica wafer; scale bar (A) 10 µm and (B) 2 µm.*

structures, resulting from the start of Tb-**49** crystallization.

Compound **55** was imaged too but only in methanol, indeed **55** alone was not fully soluble in THF. The results are shown in **Figure 4.13** and it is possible to observe a beautiful "snowflake" like structures, where the sample aggregates in a relatively big crystal (*c.a* 445 nm each crystal)

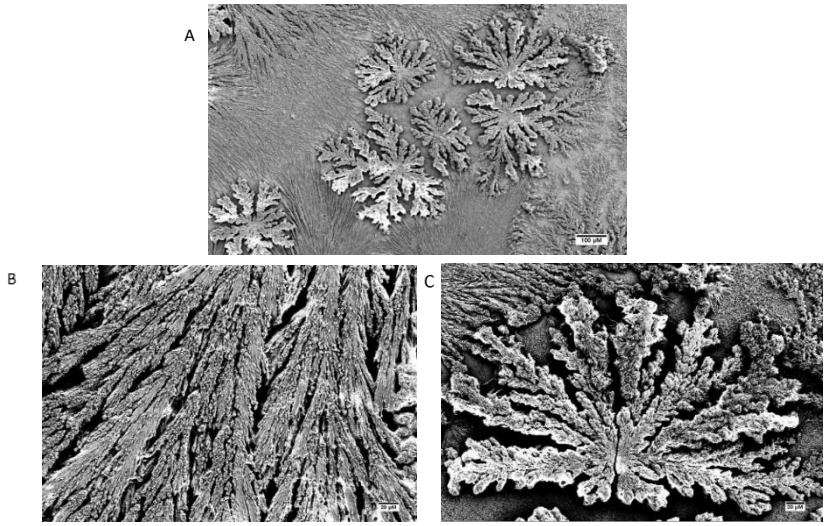

Figure 4.13: *SEM images of* ***55*** *when 20 µL of its solution in MeOH with c = 1 x 10^{-5} M was deposited onto the silica wafer: scale bar (A) 10 µm (B and C) 20 µm.*

The 1:3 complex **55**-Tb-**49** was formed by adding three equivalents of Tb-**49** into a solution containing **55** at c = 1 x 10^{-5} M. The self-assembled formation was firstly investigated in methanol and then in THF. The first solvent was chosen because both compounds are soluble in this media, in THF instead, **55** is not fully soluble alone, but is solubilized upon the addition of Tb-**49**. All the experiments were performed imaging the dried compound deposited onto the silica surface from the solution of methanol and THF without and after microwave irradiation in order to use the hard conditions generated from the apparatus to "force" the two compounds to form a supramolecular aggregate. The **Figure 4.14** shows the SEM images relative to the **55**-Tb-**49** complex mixture in a ratio of 1:3 and prepared in MeOH upon mixing the components without microwave irradiation.

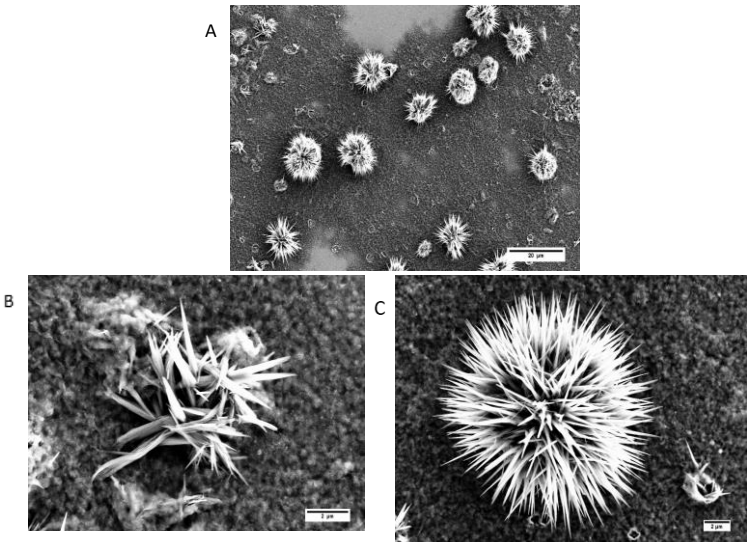

Figure 4.14: *SEM images of* ***55****-Tb-****49*** *when 20 µL of its solution in MeOH with c = 1 x 10^{-5} M was deposited onto the silica wafer; scale bar (A) (B) 20 µm and (C) 2 µm.*

The SEM images of the dropcasted films demonstrated the formation of a "soft material" with the molecules aggregated in a form of "coils" with a diameter of *c.a* 17 mm. The structure is not yet the result of a self-assembly of the two compounds but seems to be a starting of the process. Most probably the kinetic effect is the driving force to lead those process, so the same images were taken after that the solution was placed in the microwave initiator for 1 hr at 100 °C. The results are shown in **Figure 4.15**. Compared to the previous image shown in **Figure 4.14** the result shows a very different morphology. The coils present before the irradiation are totally disappeared, the new structures having diameter of 34 μm look like the product of a self-assembly process. From the studies performed before and after the using of the microwave initiator it is possible to distinguish the importance of the kinetic and the thermodynamic contribution. Before irradiation the kinetic product is a fluffy material that is not self-assembled yet, but the thermodynamic product given from irradiation is a larger block of solids. Since the solvent is a crucial

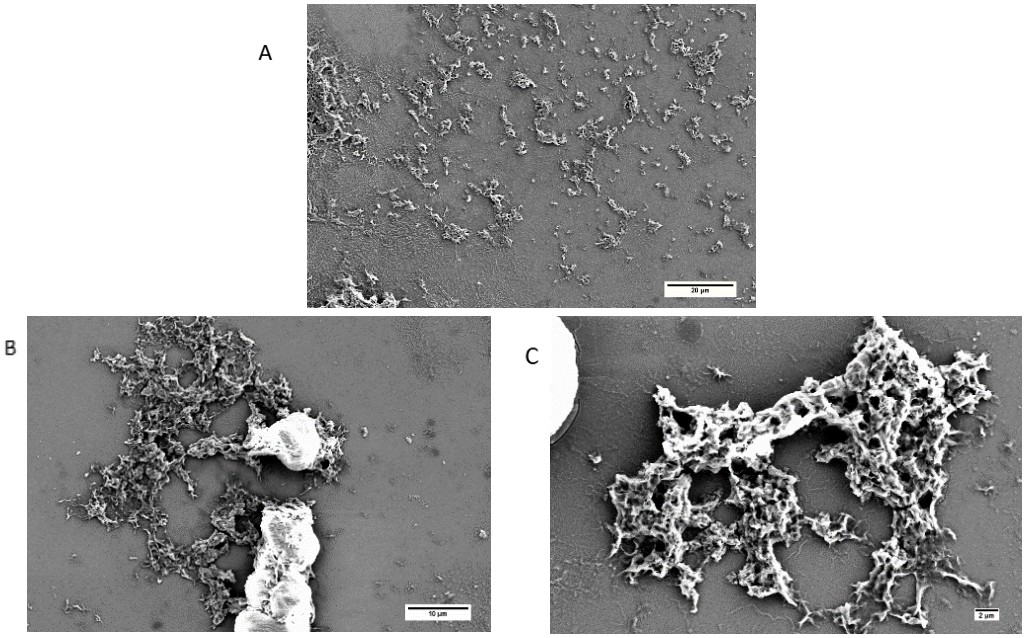

Figure 4.15: *SEM images of* ***55****-Tb-****49*** *when 20 μL of its solution in MeOH with c = 1 x* 10^{-5} *M was deposited onto the silica wafer after 1hr in the microwave initiator at 100 °C. Scale bar (A) 20 μm (B) 10 μm and (C) 2 μm.*

parameter for the formation of the structures, the same experiments were performed in THF. The particularity of this solvent is that compound **55** is not fully soluble, but upon the interaction with **Tb-49**, it goes fully in solution. From the luminescence studies it is possible to foresee that binding between Tb-**49** and **55** is stronger resulting in a higher luminescence signal.

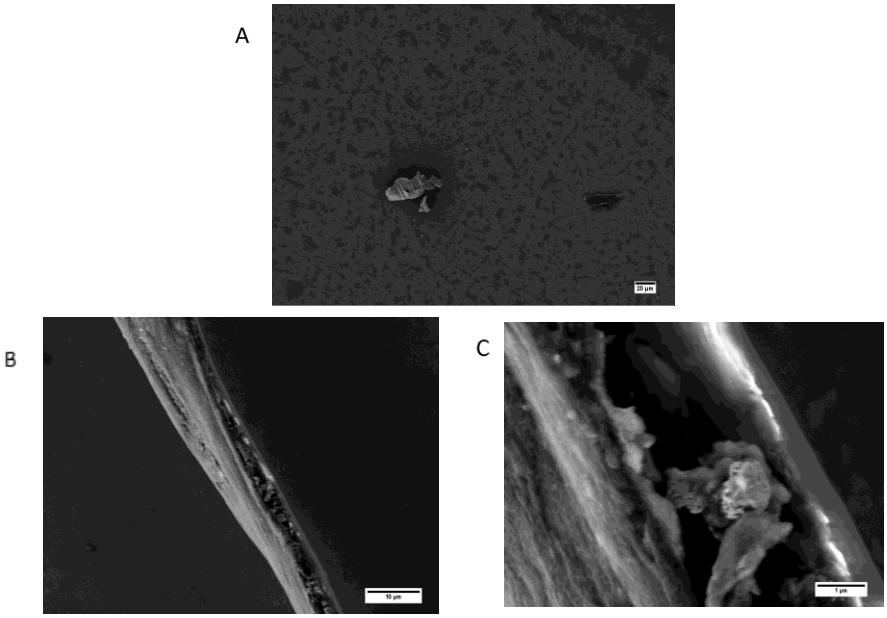

Figure 4.16: *SEM images of* ***55****-Tb-****49*** *when 20 µL of its solution in THF with c = 1 x 10^{-5}M was deposited onto the silica wafer from THF. Scale bar (A) 20 µm (B) 10 µm and (C) 1 µm.*

The SEM images of the dropcasted samples from THF (c = 1 x 10^{-5} M) have been taken and are reported in **Figure 4.16**. In this case the self-assembly of **55**-Tb-**49** was prepared by mixing **55** and Tb-**49** in THF with the ratio of 1:3 and without applying microwave irradiation to the solution. The images taken in THF presented a different structure compared to the images taken in MeOH. The image at high magnification (**Figure 4.16 B**) shows a structure comparable with an entangled network of fibres that can potentially trap the solvent inside. The structures have a

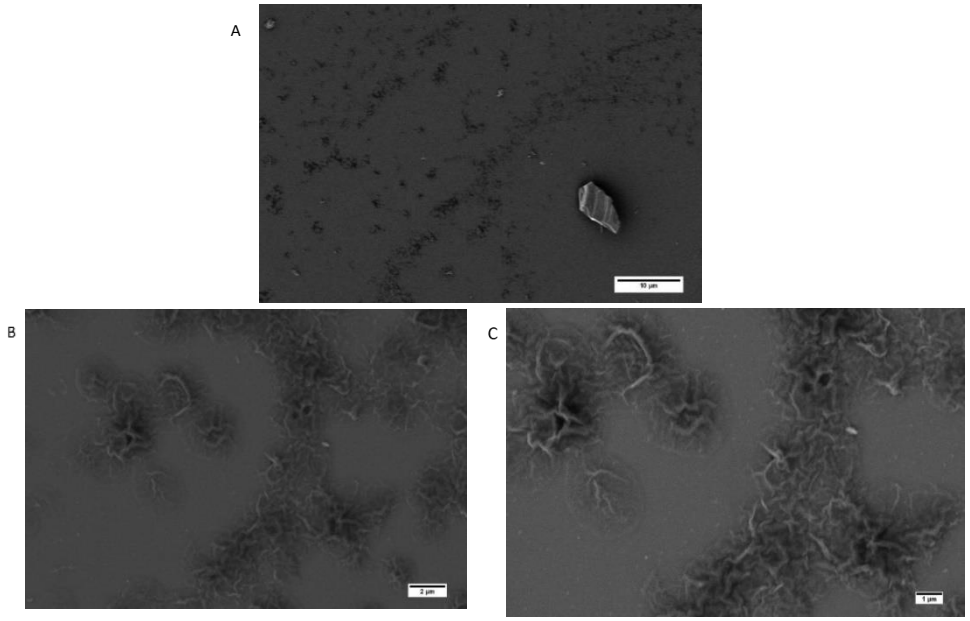

Figure 4.17: *SEM images of* ***55****-Tb-****49*** *when 20 µL of its solution with c = 1 x 10^{-5} M in THF was deposited onto the silica wafer. Scale bar (A) 20 µm (B) 10 µm and (C) 1 µm.*

section around 10 μm and a length of *c.a* 20 μm. The same reaction mixture was subjected to microwave irradiation for 1 h at 100 °C and the sample was dropcasted onto the silica wafer slide to take the SEM images, the and results is reported in **Figure 4.17**. The images demonstrate that **55**-Tb-**49** self-assembled in THF into entangled structures that seem to be fibrous in nature. Comparing the results with the images taken before the microwave irradiation the results show structures with a smaller size. **Figure 4.17** C shows the coil structure with a magnitude of 1μm and the section of potentially fibres with the size measured to around 0.15μm. Further studies will be focused on finding the right condition to make the gel, increasing the concentration of **55** and **Tb-49** in different solvents with the focus into using THF as the solvent, this because **55** is not soluble in THF, but the complex **55-Tb-49** it is, so would be good investigate in that direction

4.4 Conclusions

The focus of the work described in this chapter was the synthesis of a tripodal (BTA based) molecule and the formation of a 1:3 complex using Tb(III) cyclen-based complex. All the luminescence data were fitted using reactlab[163] and from the UV-vis and the fluorescence titration data it was possible to observe only the formation of the 1:2 and the 1:3 complexes, but fitting from the phosphorescence data all 3 complexes. The binding constants have been calculated and the results confirmed that the 1:3 species is the more stable having a higher constant.

The SEM images of the assemblies have been taken for **55**-Tb-**49** (1:3) deposited from both MeOH and THF solutions, before and after the microwave irradiation. The morphology of the dry layer prepared from the solution of Tb-**49** ($c = 1 \times 10^{-5}$ M) in MeOH was investigated and the images did not show any formation of hierarchical supramolecular assemblies on the surface, the molecules arranged themselves in a rod-like structure.

The possible application of the of 55-Tb-49 will be investigate in the future works, in order to prove the ability of the aggregate to incorporate gas.

In the next Chapter, the ability of the lanthanide to be used as probe for cell imaging have been investigated.

Chapter 5

5.0 Introduction

One of the most important imaging techniques to examine internal organs in the human body is the Magnetic Resonance Imaging (MRI) (**Figure 5.0)**. One of the main advantages of this technique is that it is non-invasive and relatively safe. The system works similarly to an NMR, detecting the signals emitted from the protons of water and fatty molecules. Human fatty tissues have H-bonds among the water molecules at 90 M. Healthy tissues have a different rate of re-establishment of equilibrium compared to the diseased tissue. [164] By using a strong magnetic field in a target region it is possible to align an excess of proton spins with the direction of the applied field. Absorption of radio-waves, which are modulated at a certain frequency, cause a spin-flip of the protons that changes the magnetic moment of the protons which then opposes the applied magnetic field. Once the radio waves are stopped, the tissues emitting the absorbed frequencies excite the protons in the higher energy states, relaxing to the lower energy state, therefore aligning their spin again with the magnetic field. The images are obtained by plotting the data relative to the intensity of the signal and are shown on a grey scale (**Figure 5**). As the intensity of the emitted signal is generally weak around the regions of the body that are investigated,

Figure A *MRI image of the organs in human body.*

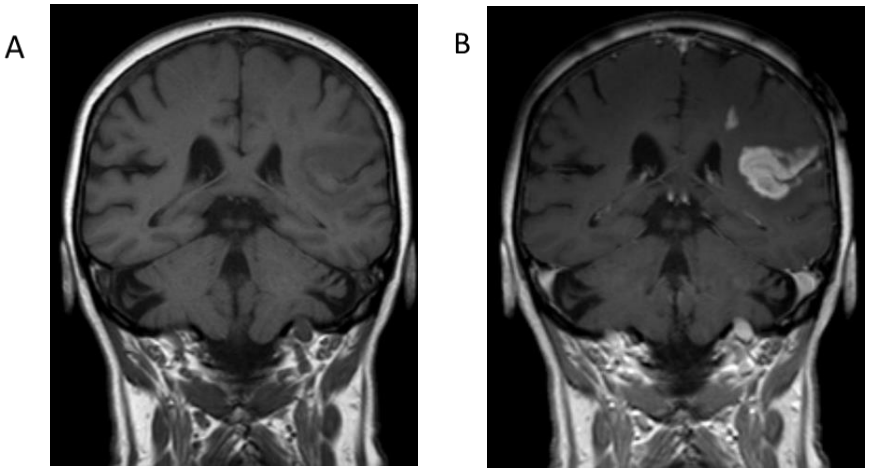

Figure 5.1: *MRI images of the human brain after a stroke (A) without and (B) with the contrast agent.*

received coils are placed. Based on these processes it is possible to diagnostic the human anomaly.[165-169] One of the main advantages of the MRI is that it does not apply strong ionizing radiation to produce images (like the computed tomography and x-ray) so it is relatively safe for the patients. The mains drawbacks are the weak signal intensity and the longer acquisition time for the images so to overcome to these problems a high relaxivity contrast agent is applied.[169, 170]By altering the relaxing time of the water protons, these agents are able to increase the intensity of the signal, resulting in better quality of the images (**Figure 5.1**).

Most of the contrast agents work by causing a shortening of the spin-lattice or longitudinal relaxation time (T_1) that indicates the amount of energy transferred from the nuclei in higher energy spin state to the surrounding lattice. During the relaxation all the nuclei that have their spin aligned against the applied magnetic field which is less stable, return to the original, more stable, lower energy spin state which is aligned with the magnetic field. During this process, the energy is released in the form of heat. The use of the contrast agent also shortens the necessary time to acquire an MRI scan.[53, 164, 171-174]

It is possible to classify two categories of MRI contrast agent for the relaxation process. The T_1 agents that cause an enhancement of the spin-lattice relaxation rates ($1/T_1$) compared to the spin-spin relaxation states ($1/T_2$) of the water protons in the tissues. Using the T_1 contrast agents the water protons appear as bright spots and they are called "positive contrast agents" which are based on gadolinium and manganese chelates. The T_2 agents, which are known as negative contrast agents, have a larger spin-spin relaxation rate and cause a decrease in the intensity of the signal resulting in the production of darker images. By using the T_2 agents the relaxation process occurs through a transfer of energy between the interaction of the excited nuclei and nuclei at lower energy. Siloxane or dextran coated with super paramagnetic iron oxide represent this class of the contrast agents. T_1 agents are preferred to T_2 agents not only because they produce brighter images, but also because they can be easily expelled from the body causing lower toxicity. Gd(III) is the perfect candidate to create a complex that can be used as T_1 contrast agents, it has 7 unpaired electrons in the 4*f* orbitals and has a long electronic relaxation time ($\simeq 1 \times 10^{-9}$) and a large magnetic moment.[175] These unique properties make Gd(III)

able to produce a strong influence on the spin-lattice relaxation time of the water protons.

As mentioned in Chapter 1, Gd(III) is a rare-earth *f*-block lanthanide element which is toxic for the living system so to be used as a contrast agent needs to be complexed with organic ligands. It has been reported that Gd(III) cyclen based complexes show

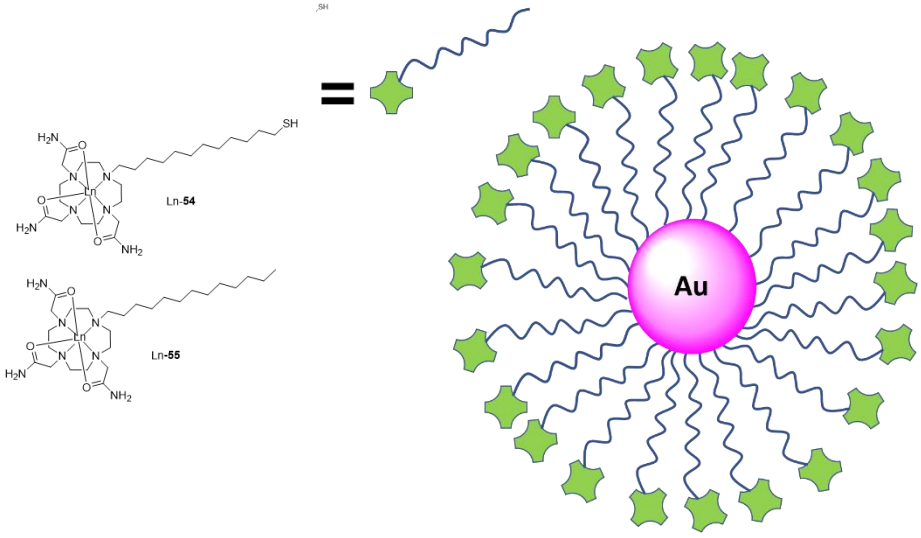

Scheme 5.1: Schematic representation of Ln-Au-probe

greater thermodynamic and kinetic stability. Therefore, cyclen-based contrast agents are safer for clinical use due to their lower toxicity.[176] In this chapter the pursuit to develop a self-assembled MRI contrast agent is described. The following sections will describe the synthesis, characterization and potential of application of a new cyclen based ligand complexed with Tb(III) and Gd(III) that could be applied in several fields with the main focus on Gd-**49** and its potential application as MRI contrast agent in order to minimize the sides effect of the contrast agent.

Compounds Au-**54** and Au-**55** was developed by the Gunnlaugsson group as potential MRI contrast agents and employed in NMRD-measurements. The schematic of the system is illustrated in Scheme 5.1which is based on the functionalization of gold nanoparticles, forming a Ln-AuNP.

NTA and Thenoyltrifluoroacetone **(TTA)** were employed as antennae for compound **54** and compound **55** respectively. The Eu/Tb complexes were implemented in the formation of luminescent self-assembled ternary structures, and we demonstrated that the lanthanide emission for 1.Eu/Tb and 2.Eu/Tb 'switched on' only in the presence of appropriate sensitizing antennae. Compound 55 was

complexed with Gd(III) and formed a self-assembled micelle-type structure. The functionalised gold nanoparticles, Ln-AuNP were also synthesized from 1.Ln. In the free complexes, the Ln-emission was 'switched on' for Eu/Tb-AuNP in the presence of the antennae.

In order to design the luminescent lanthanide probes, the design of the pendant arms is crucial to optimize the cellular intake. The probes need to be able to penetrate the cell wall, without damaging.

5.1 Synthesis of the ligand 57

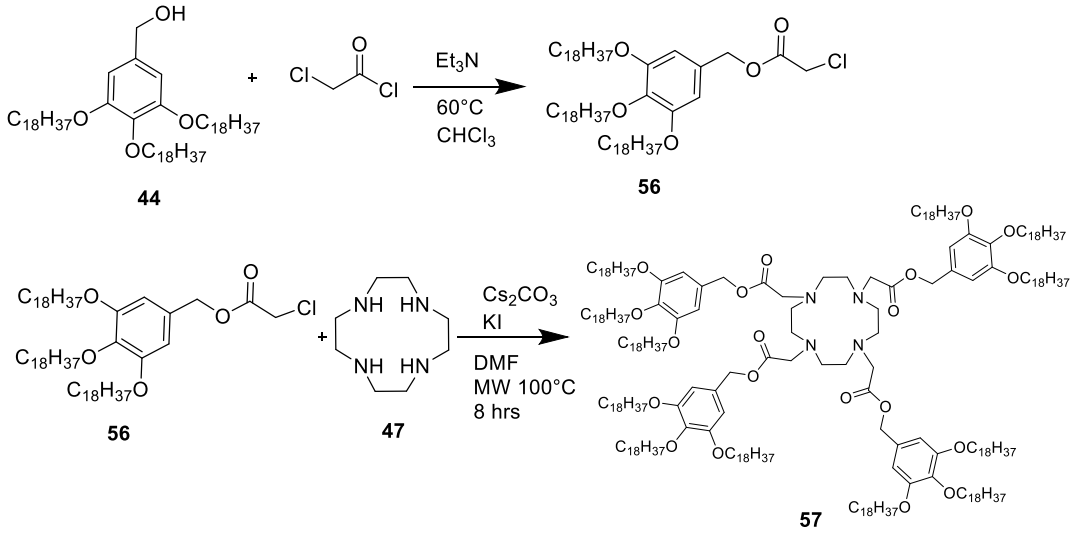

The synthesis of ligand **57** was achieved by dissolving 1 equivalent of compound **44** (synthesis reported in Chapter 2) in chloroform. To this solution 1.2 equivalents of chloroacetyl chloride was added in the presence of 1.2 equivalents of triethylamine and the reaction was refluxed at 60 °C for 5 hrs. After cooling to room temperature, the organic layer containing compound **57** was washed with HCl 0.1

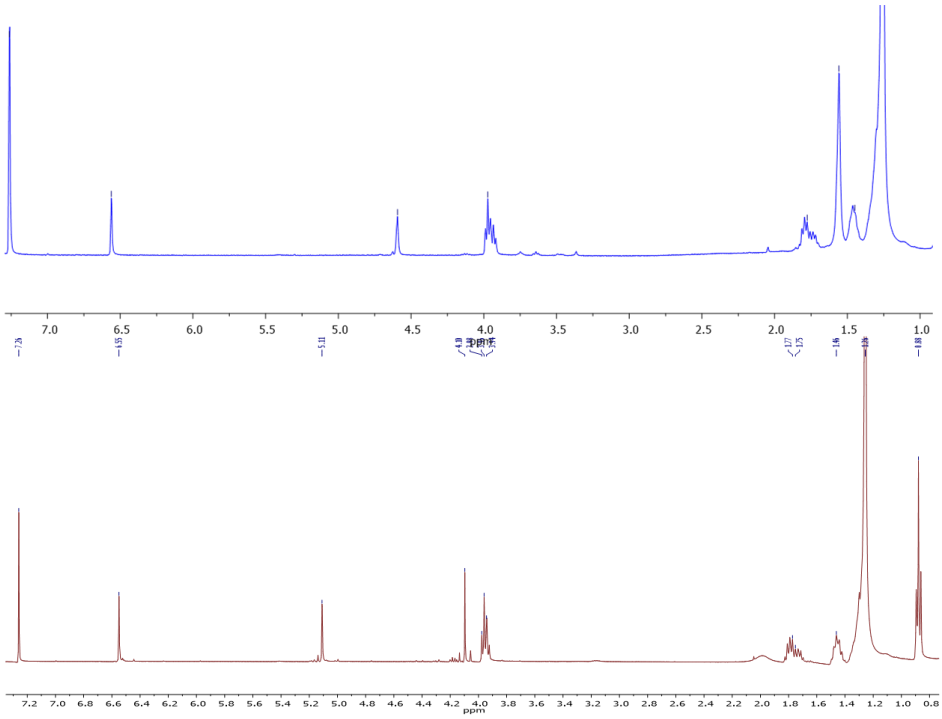

***Figure 5.2**: ^{1}H-NMR (400 MHz, $CDCl_3$) of **44** (blue) and **56** (red).*

M in order to remove the excess of the base. The solvent was then evaporated under vacuum which resulted in the formation of a yellow-brown solid that was obtained in a 65% yield. No further purification was necessary

Figure 5.2 shows the ^{1}H-NMR spectra (400 MHz,$CDCl_3$) of compound **44**. The signal for two protons of the CH_2-OH at 4.59 ppm are shifted to 4.1 ppm in Figure **5.2**. The signal relative for two protons of CH_2-Cl are located at 5.11 ppm. Mass spectra confirmed the formation of compound **56** where the signal at 989.2207 *m/z* was observed corresponding to $[M + Na]^+$. It was then reacted with cyclen **47** using a stoichiometric ratio of 5:1 in microwave for 8 hours at 100 °C in the presence of 5 equivalents of Cs_2CO_3 and 5 equivalents of KI using DMF as solvent. The solvent was then removed under reduced pressure and the resulting reaction mixture was dissolved in $CHCl_3$. The organic layer was washed with 0.1M NaOH to remove remained DMF and the unreacted molecules. Then the resulting organic layer was dried over $MgSO_4$ and the solvent was removed under pressure to obatain a brown

solid in 30% yield. Mass spectra confirmed the formation of compound **58** with the signal showing at 4008.6982 *m/z* corresponding to $[M + Na]^+$. ^1H NMR (400 MHz, $CDCl_3$) of the ligand **56** (Appendix 5.x) shows 9 CH_3 protons terminating the alkyl chains resonating as triplet at 0.90 ppm, while the cyclen 16 CH_2 protons are located as the multiplet between 3.06 ppm and 2.91 ppm.

Complexes Gd-**56** and Tb-**56** were obtained by reacting 1 molar equivalent of the appropriate lanthanide triflate with **56** in freshly distilled acetonitrile (5 mL) for 40 minutes in microwave at 90 °C. Then the solvent of the reaction mixture was removed under reduced pressure, and complexes were isolated by re-dissolving in a minimal amount of methanol and precipitating by adding diethyl ether (200 mL). Due to the paramagnetic properties of these lanthanides complexes, the NMR spectra (Appendix 5.x) shows a broad signal. In addition, Mass spectra and luminescence studies confirmed the formation of the complexes.

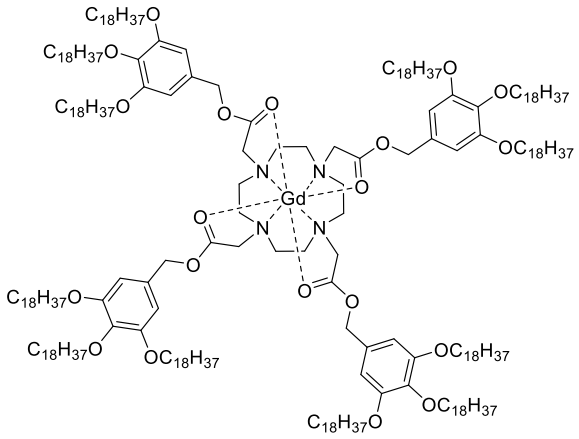

Gd-56

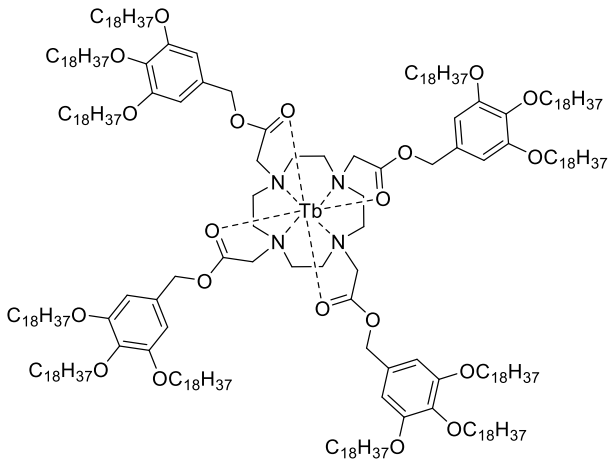

Tb-56

5.2 Photophysical studies

The photophysical evaluation of the **Gd-56** was not conclusive, because Gd(III) have the f→f transition are located at high energy level giving extreme stability to its half-filled f-shell.[15] Usually the lowest energy level for f→f transition becomes visible due to the emission band at 312 nm. And the Gd(III) complexes are often characterized by emissive intra-ligand states at lower energies. Gd(III) is a paramagnetic heavy atom and this induces a strong singlet-triplet mixing in the ligand resulting in an strong quenching of the fluorescence.[16]

Figure 5.3 A shows the UV visible absorption spectra of Tb-**56** in MeOH (conc. = $1x10^{-5}$ M). Unfortunately, it was not possible to observe any relevant band probably because of the low molar extinction coefficient. **Figure 5.3 D** shows the fluorescence spectra under same experimental conditions with the emission band at 350 nm (λ_{ex} = 270) relative to the phenyl ring of the pendent arms. But only a weak phosphorescence signal relative to the Tb(III) metal centre was observed. In contrast, **figure 5.3 B** shows the phosphorescence emission spectra of all the transition of the Tb(III) metal centre. Even without the use of an external antenna, the four aromatic rings of the ligand are able to populate the Tb(III) energy level, resulting in Tb-emission of the relative bands. All the spectra were recorded upon exciting into the phenyl ring at 270 nm.

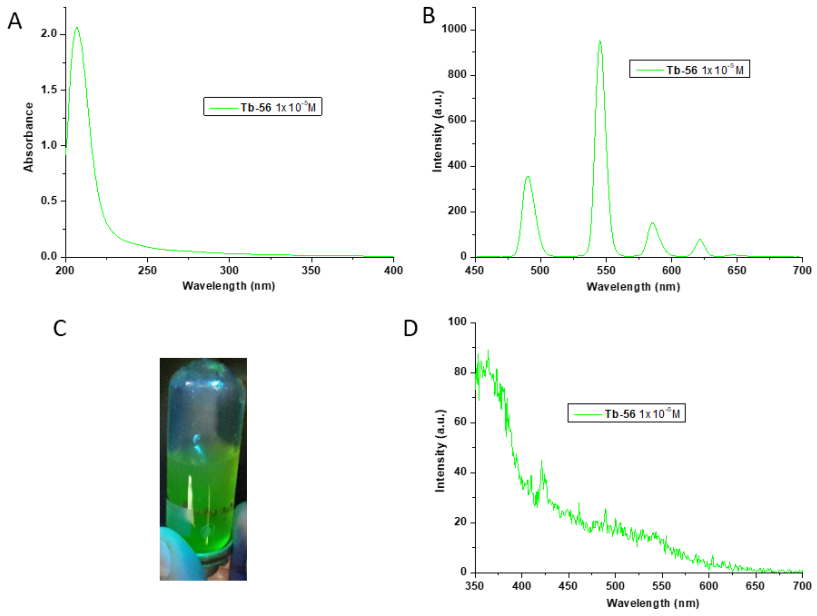

Figure 5.3: (A) *The UV-vis absorption spectra,* ***(B)*** *fluorescence spectra and,* ***(D)*** *fluorescence and of Tb-**56** (λex = 270).*

As previously mentioned, the phosphorescence signal of the Gd(III) is not detectible because of its high energy level state as shown in **Figure 5.4**. The the fluorescence spectra show the luminescence of the ligand at 350 nm. The phosphorescence spectra shows very weak signal at 545 nm, corresponding to some Tb(III) impurity normally present in the Gadolinium triflate.

Once the photophysical studies proved the formation of complex Tb-**56,** we next focused our investigation on the of the morphology. The self-assembly properties of the ternary complex were investigated to study its micro/nano scale properties using SEM microscopy.

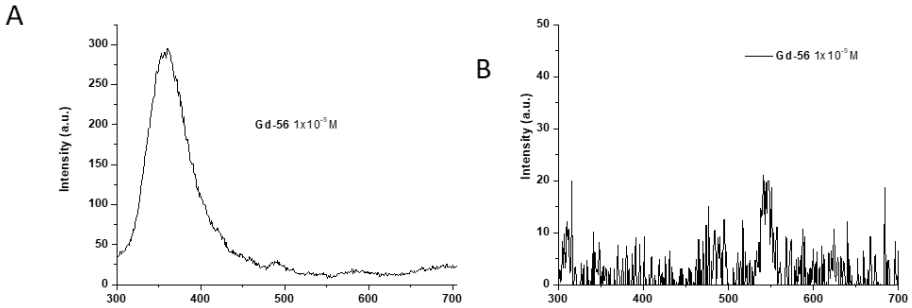

Figure 5.4 A) *The UV-vis absorption spectra,* ***(B)*** *fluorescence spectra of Gd-**56***

5.3 Morphology studies

In order to understand the self-assembly properties of the Tb-complex, the morphology of ligand **56** and Tb-**56** in DMF was investigated by Scanning Electron Microscopy (SEM). The SEM images were recorded by Emanuele Cappello, a PhD student from the Gunnlaugsson group. The reaction mixture containing ligand **56** performed in microwave was investigated, due to its high viscosity (**Figure 5.5** E). A small volume of the reaction mixture was deposited onto a silica wafer and dried in vacuo for 48 hours. The sample was after coated with a thin layer of gold. The images recorded at different magnification are shown in **Figure 5.5.** The reaction mixture presents an intricate network that branches from some centres with a diameter of *c.a* 12 μM. Probably this network was able to restrain the solvent creating a supramolecular gel. Ligand **56** was investigated after the work up, spreading 20 μL of solution $1x10^{-5}$ in MeOH onto the quartz slide and was then left to evaporated for 48 hrs under vacuo. After the coating the samples, the images were taken at different magnification are shown in **Figure 5.7.** The images show that the

network present before the work up was not present anymore, and the structure seems to not present any organization.

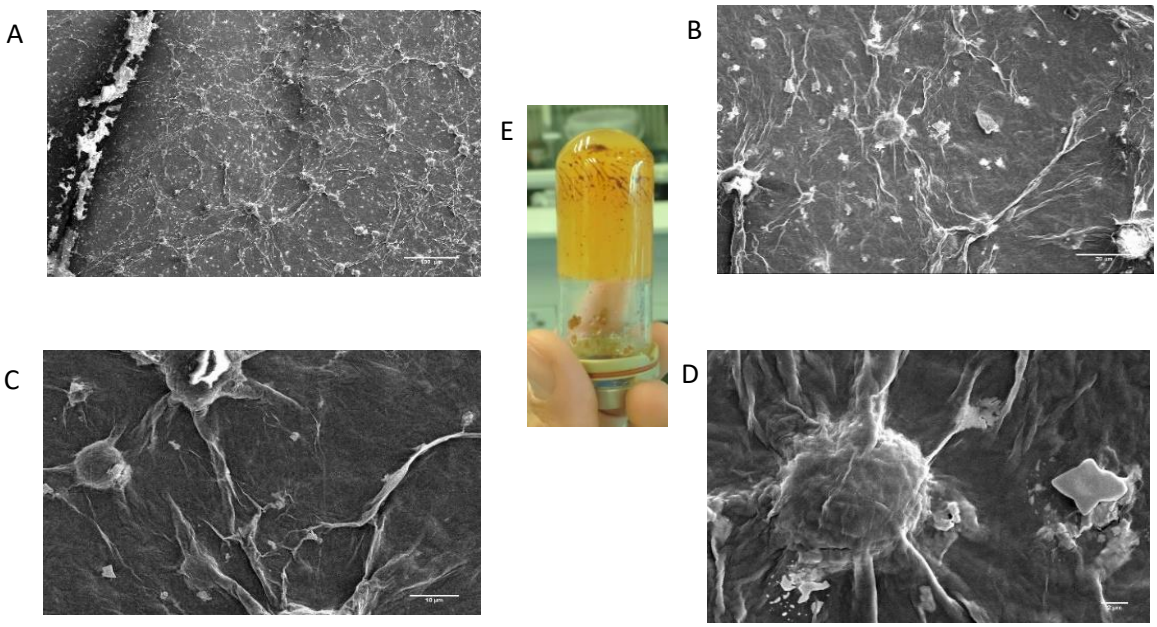

Figure 5.6: *SEM images of* ***56*** *before the work up, when 20 µL of its MeOH solution with c = 1 x 10^{-5}M was deposited onto the silica wafer; scale bar (A) 100 µm and (B) 20 µm.(C) 10 µm.(D) 2 µm.*

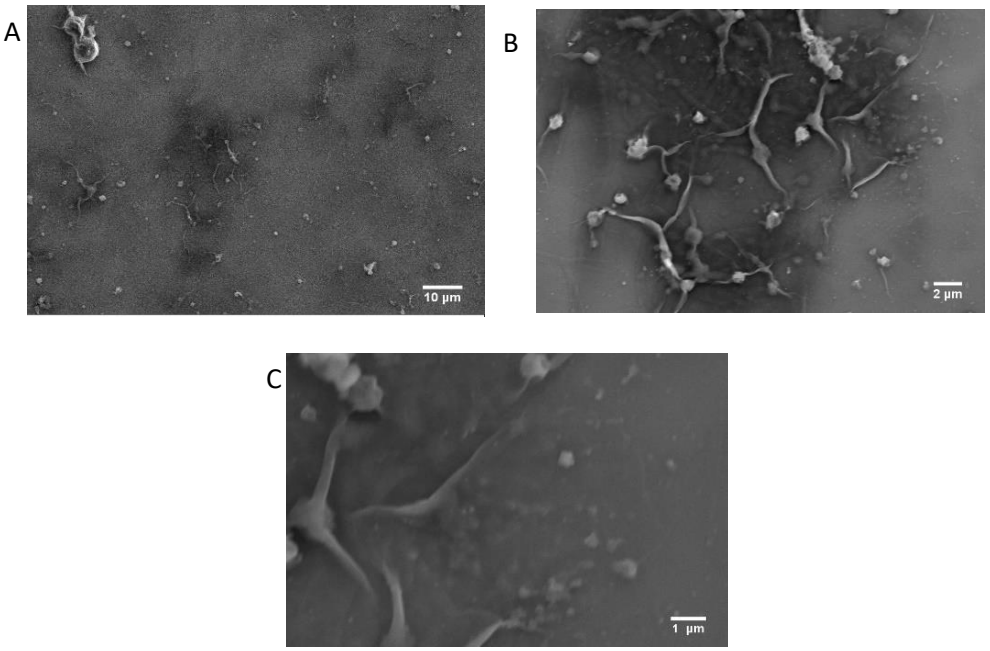

Figure 5.7: *SEM images of* ***56*** *after the work up, when 20 µL of its MeOH solution with c = 1 x 10^{-5}M was deposited onto the silica wafer; scale bar (A) 10 µm and (B) 2 µm.(C) 10 µm.(D) 1 µm.*

Upon the complexation with the Tb(III) the structures was observed by the same imaging are radically changing. As shown in **Figure 5.8** the system seems to start a self-assembly, to "force" this process the same reaction mixture was placed under microwave irradiation for 1 hr at 100 °C, then 20 μL of solution at a concentration of $1x10^{-5}$M was spread onto the quartz slide and this was then left to evaporate for 48 hrs under vacuo. After the coating the images and the results are shown in **Figure 5.9.**

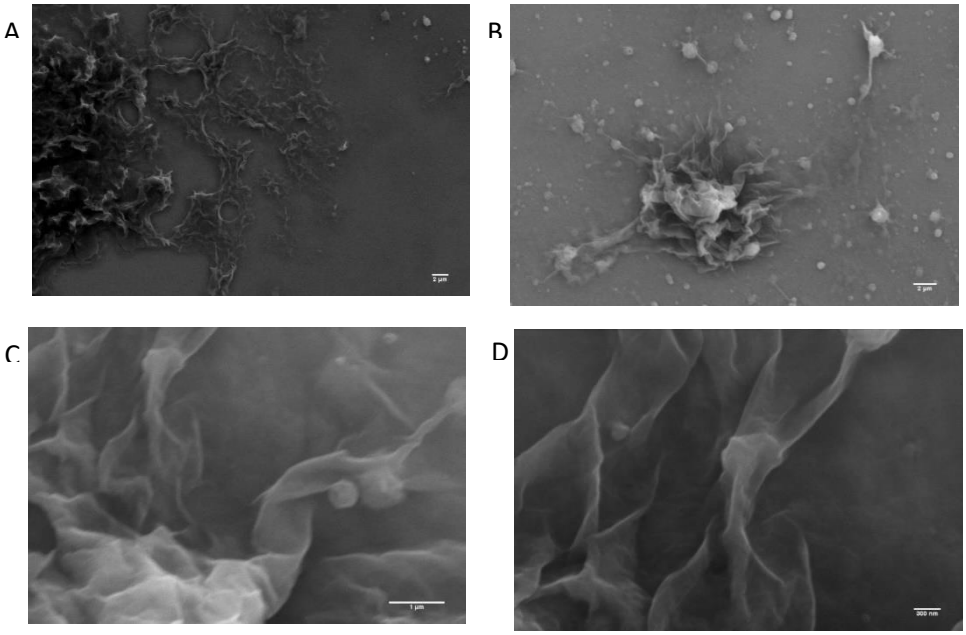

*Figure 5.9: SEM images of Tb-**56** after microwave irradiation, when 20 μL of its MeOH solution with c = 1 x 10^{-5}M was deposited onto the silica wafer; scale bar (A-B) 2 μm and.(C) 1 μm.(D) 200 nm.*

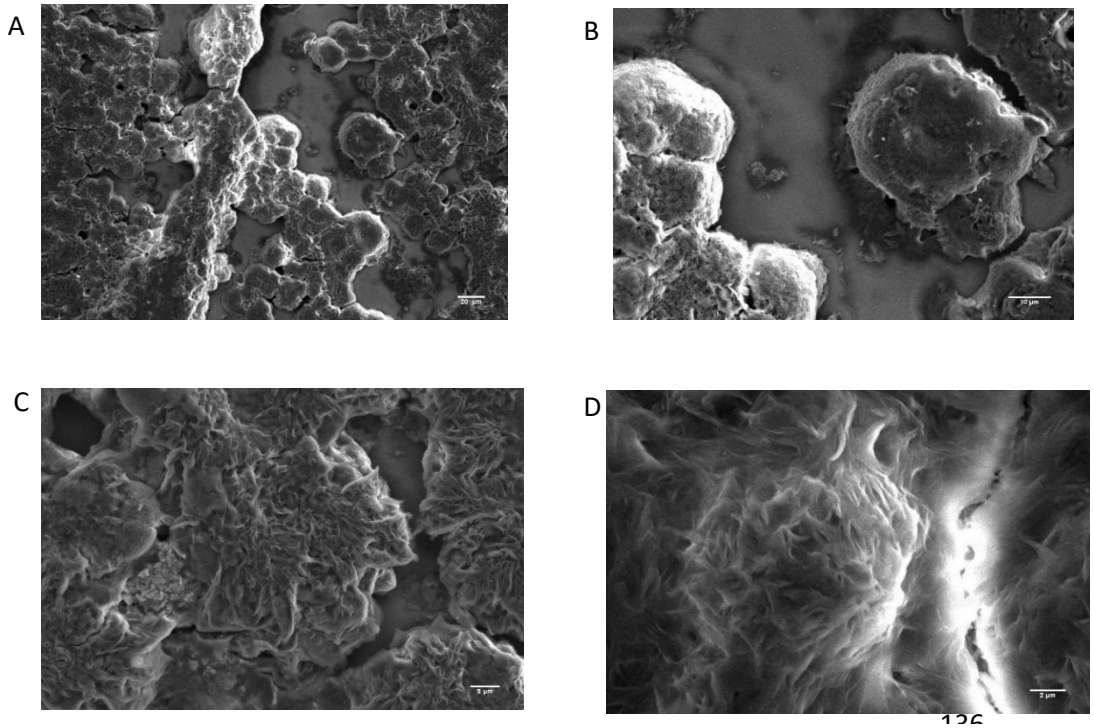

***Figure 5.8**: SEM images of Tb-**56** when 20 μL of its MeOH solution with c = 1 x 10^{-5}M was deposited onto the silica wafer; scale bar (A-B) 20 μm and.(C) 50 μm.(D) 2 μm.*

The images demonstrate that the Tb-**56,** after the microwave irradiation forms coils with a strong entangled structure as showb in **Figure 5.9 D** (taken a high magnification, 200 nm). It is possible to observe structures that could be fibres with a section of 590 nm. These structures are probably able to trap solvent and form gels.

After the morphology properties were investigated, we moved to the next stage, the investigation of the cellular uptake in order to understand the ability of the Tb-**56** to interact with the cell wall.

5.4 Cellular uptake studies

The experiments were carried out by Stefania Magnano, a PhD Student from the Daniela Zisterer's group. The cells used for this evaluation were the SCC4 and SCC9 (**Figure 5.10**), they are both epithelial-like cells isolated from the human tongue of 51 and 25 old males respectively.[177] SCC4 cells were grown in Dulbecco's Modified Eagles (DMEM) GlutaMAXTM supplemented with 10% (v/v) Foetal Bovine Serum (FBS) and 1% (v/v) penicillin-streptomycin. Thus, the cells were seeded at 4000/well in a 96-well plate and cell viability measured after 24 h of treatment using different concentration of Tb-C prepared in water/DMSO (0.1% v/v). The preliminary studies were performed using a multi well fluorimeter with excitation at 270 nm (straight into the Tb(III) metal centre) and the emission was recorded at 545 nm.. All the tests were performed in triplicate and the results reported in **Figure 5.11** are relative to the averages of the data obtained.

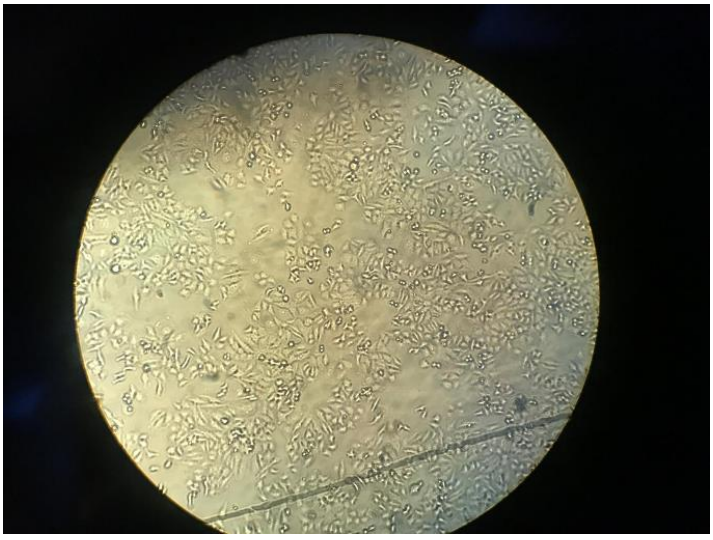

Figure 5.10*: Zooming 10x of the cells attached on the petri dish*

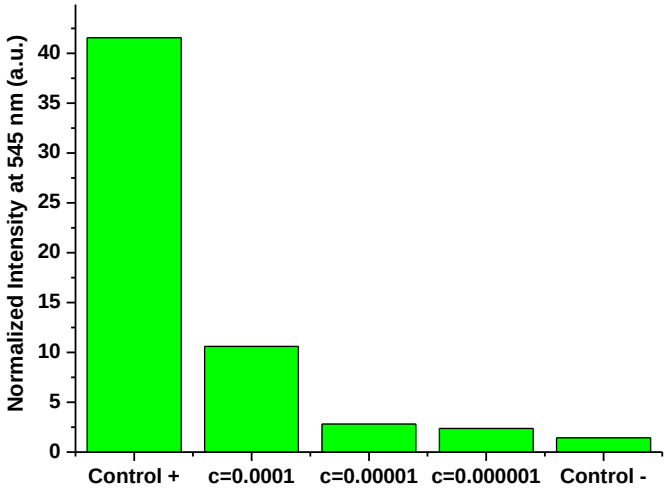

Figure 5.11: *Luminescence spectra of the Tb-49 at 545 nm incorporated from the cells* λ_{ex}*=270 nm*

Figure 5.11 illustrated the observed Tb(III) emission relative to the three different concentrations used ($1x10^{-4}$M, $1x10^{-5}$M, $1x10^{-6}$M) in addition two control experiments which were also performed. All the experiments were carried out in water/DMSO (0.1% v/v).

The positive control (control +) represents the luminescence signal relative to the cell immersed in the media containing compound **Tb-56** with c= 10^{-4} M without washing the plates, this control proves that at this concentration, the fluorimeter it is able to measure the Tb(III) centred emission of compound **Tb-56**. The negative control (control -) represents the luminescent background of the cells and the media. This value was subtracted from the luminescence observed for all other data in order to have a clear measurement of the Tb(III) luminescence. The graph shows that by using concentrations (1 x 10^{-5}M and 1 x 10^{-6} M) of **Tb-56** no significant emission was found, however by increasing the concentration to 1 x 10^{-4}M the Tb(III) centred emission increased by 375 % compared to the emission at 1 x 10^{-5}M. All these experiments were performed by removing the media with the solution containing the **Tb-56**, which proves that the enhancement is due to an interaction between **Tb-56** and the cells; not solely from the Tb(III) complex present in the solution.

The next stage was to investigate the type of interaction established, as the luminescence signal observed here does not prove that **Tb-56** is localised within the cells. Another possibility is that the long alkyl chains interact with the cell wall without being fully internalized, which would enable the use of **Tb-56** as cellular membrane probe.

Figure 5.12: *Two photos support plates for cells*

Normally confocal microscopy would be used to further analyse these samples. Confocal microscopy, a form of fluorescence microscopy that uses particular optical components to generate high-resolution images of material which is stained with the fluorescent probes. Unfortunately, the limit of this technique is the excitation wavelength, it is not possible to use an excitation wavelength below 400nm because the higher excitation energy results in the damage to the biological tissue.[46, 81, 178] As widely explained in Chapter 1, lanthanides have the *f-f* transitions which are Laporte forbidden, so their excited states are normally populated with sensitizing antennae. This often requires a high excitation energy, which is illustrated by the excitation wavelength for **Tb-56** is 270 nm. To overcome this issue Two Photon Microscopy (TPE) can be used. This technique differs from the conventional confocal fluorescence microscopy. The excitation wavelength is shorter than the emission wavelength therefore the wavelengths of the two exciting photons are longer than the wavelength of the resulting emitted light. The use of infrared light reduces the scattering in the tissue and the background signal is strongly suppressed.

The preparation of the samples was slightly different, because the images were taken by placing the sample "upside down." The samples were prepared following the protocol and they were deposited onto the specific support (**Figure 5.12**). Two different samples were imaged, one with the fluorescent stain **DAPI** and one with only the sample. **DAPI** (4′,6-diamidino-2-phenylindole) is a fluorescent stain used in the fluorescence microscopy because it can pass through an intact cell

membrane.[179]**DAPI** has an excitation wavelength of 360 nm, whereas **Tb-56** has an excitation wavelength of 270 nm, but the emission wavelength is 460 nm, which can partially overlap with the Tb(III) centred emission.

The first sample investigated was the one treated with the **DAPI** which is the image shown in **Figure 5.13**

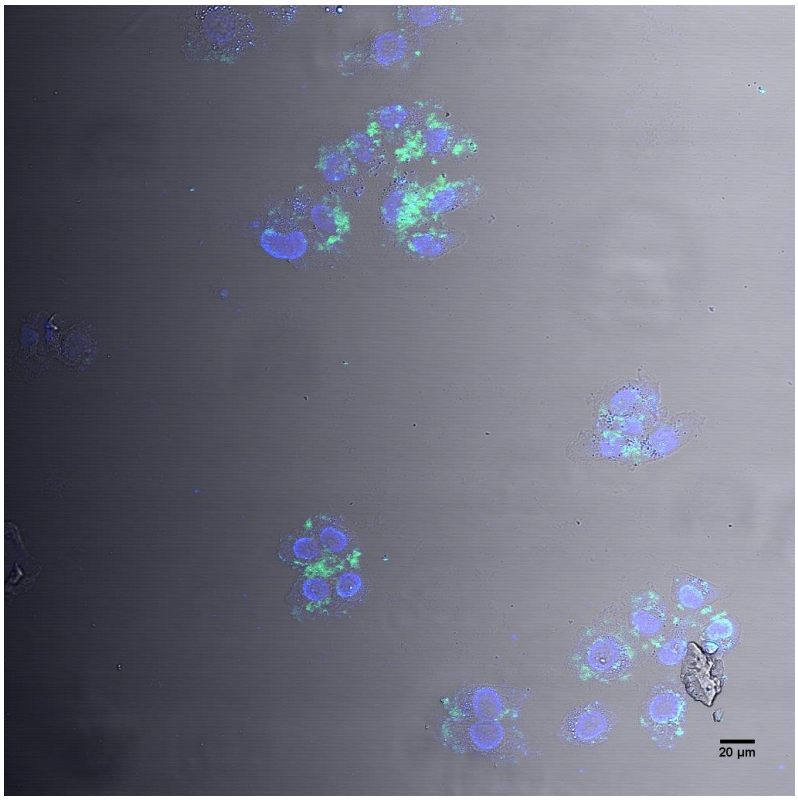

Figure 5.13*: images taken with the two photons microscopy of the cells SCC4 incubate for 24 hours treated with DAPI and Tb-49.*

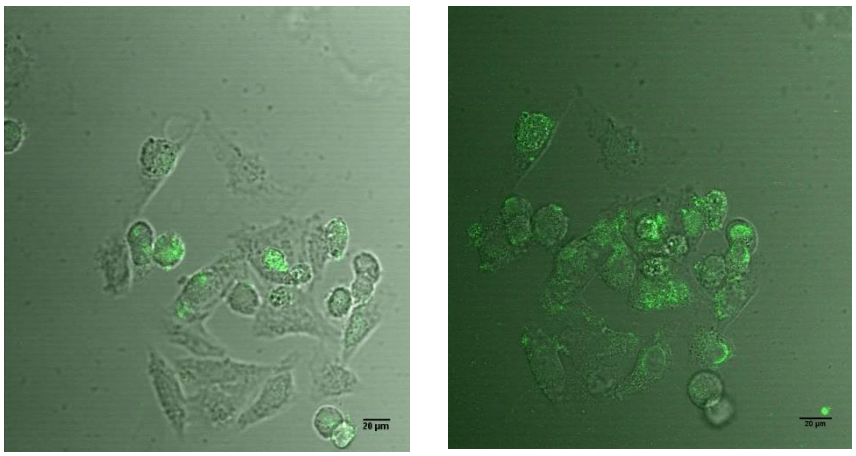

Figure 5.14*: images taken with the two photons microscopy of the cells SCC4 incubate for 24 hours treated without DAPI and Tb-49.*

The cells were treated with **DAPI** and after the **Tb-56** complex at C= 1 x 10^{-4}M (incubated for 24 h) was spread in the culture media for 24 h, after which the cells were washed with water in order to remove the media solution and complexes from the surface.In **Figure 5.13** it is possible to distinguish the two compounds present in the cells, the **DAPI** (blue) and the **Tb-56** (green). The compound is in contact with the cells and was not washed out when the media solution was removed. From this image is not possible to say if there is an external interaction with the cell wall or if the compound is incorporated inside the cytoplasm. Moreover, **DAPI** was added first, so there is the possibility that the Tb(III) complex could not reach the nucleus due to the **DAPI**. For this reason, another batch of cells was investigated these were treated in the same way as the previous sample but without **DAPI**.

The images reported in **Figure 5.14** show that in the absence of **DAPI,** the compounds appear to be fully incorporated in the cytoplasm, indeed it is possible to see the Tb(III) complex located around the nucleus. **Tb-56** proved to be able to interact with the wall cell and the long amphiphilic chains are able to pass through the cell wall thereby "locking" the probe.

5.5 Conclusions

In this chapter, I have described the development of lanthanide cyclen based luminescent complexes with the purpose of creating a probe for cellular imaging. The Tb-cylclen based ligand was successfully synthesised and characterised and the photophysical evaluations of the Tb-complexes was carried out, because of the luminescence properties of the Gd(III), it was not possible carry out the luminescent studies.

The SEM images of the assemblies have been taken for Tb-**56**(1:3) deposited from MeOH solutions, before and after the microwave irradiation.

The ability of Tb-**56** to interact with the cells was next investigated. The cells were treated with different concentrations of the Tb(III) complex and after were washed to remove the media. By using a multi well fluorimeter and an excitation wavelength of 270 nm the emission of the Tb(III) was found at 460 nm.

To understand of the type of interaction that is established between the Tb(III) complex and the cells, two photon microscopy was employed to image the cells treated with Tb-**56**. A comparison with **DAPI**, the fluorescent stain used for probes,

was also performed. The image showed the internalization of the long alkyl chain in the cells therefore proving the ability of the Tb (III) complex to be attributed from the cells.

Future works will be performed to better understand the ability of the ligand to act as a stain in vivo. The characterization of the Gd-56 complex will be performed using different method in order to prove the formation of the stable complex

Experimental Details

General: All chemicals were purchased from Sigma-Aldrich Ireland Ltd., Acros Organics, TCI Ltd., or Chematech, and were used without further purification, unless otherwise stated. Dry solvents were prepared in accordance with standard procedures described by Vogel, with distillation prior to each use. Thin-layer chromatography (TLC) was conducted using Merck Kiesegel 60 F254 silica plates, and the separation was observed by UV light or developed in an iodine chamber. Chromatographic columns were run on a Teldyne Isco Combiflash Rf200 automatic machine using pre-packed silica columns. Melting Points were determined using an Electrothermal IA900 digital melting point apparatus.

Deuterated solvents for NMR analysis were purchased from Apollo Scientific. NMR spectra were recorded using either a Bruker DPX-400 Avance spectrometer, operating at 400.13 MHz for ^{1}H NMR and 100.60 MHz for ^{13}C NMR, or a Bruker AV-600 spectrometer, operating at 600.10 MHz for ^{1}H NMR and 150.90 MHz for ^{13}C NMR. All NMR spectra were measured at 293 K. Tetramethylsilane (TMS) was used as an internal standard and chemical shifts were referenced relative to the internal non-deuterated solvent signal, with chemical shifts being expressed in parts per million (ppm or δ). For ^{1}H NMR spectra, the number of protons, splitting pattern, coupling constant where applicable, and proton assignment are also reported (in that order). Multiplicities are abbreviated as follows; singlet (s), doublet (d), triplet (t), quartet (q), quintet (qu), multiplet (m), and broad (br).

Electrospray mass spectra were recorded on a Bruker microTOF-Q III spectrometer connected to Dionex UltiMate 3000 LC detector using HPLC grade CH_3CN or CH_3OH as carrier solvents. Accurate molecular weights were determined by a peak-matching method, using Agilent Technologies ESI-1 low concentration tuning mix as the internal lock mass. Maldi-Q-Tof mass spectra were carried out on a MALDI-Q-TOF-Premier (Waters Corporation, Micromass MS technologies, Manchester, UK). High-resolution mass spectrometry was performed using leucine enkephaline (H-Tyr-Gly-Gly-Phe-Leu-OH) as the standard reference (m/z = 556.2771); all accurate mass were reported within ± 5 ppm of the expected mass.

Infrared spectra were recorded on a Perkin Elmer Spectrum One FT-IR spectrometer fitted with a universal ATR sampling accessory. Elemental analysis weas performed on an Exeter Analytical C3440 elemental analyser at the Microanalysis Laboratory, School of Chemistry and Chemical Biology, University College Dublin.

Ultraviolet-visible Spectroscopy

The UV-visible absorption spectra were recorded at room temperature using 1.0 cm path length quartz cells in a Varian Cary 50 spectrometer. The solvents utilised were of spectrophotometric grade. The wavelength range was set from 200 to 500 nm with a scan rate of 300 nm/min. The blank used was a sample of the solvent system in which the titration was carried out i.e. CH_3OH. Before the start of the titration a baseline correction was used in all spectra. Stock solutions of ligand with concentrations of either 1×10^{-3} or 2×10^{-3} M for the titration in CH_3OH were prepared and then diluted to the desired concentrations before titrating (*ca*. 1×10^{-5} or 5×10^{-6} M). The $Eu(CF_3SO_3)_3$ stock solution was prepared in CH_3OH (1×10^{-3} M) and diluted to 5×10^{-4} M for the titration. The titrations were repeated 3 to 5 times in order to ensure the reproducibility of the results.

Luminescence measurements

The luminescence measurements were carried out on a Varian Cary Eclipse Fluorimeter using a 1.0 cm path length quartz cell at room temperature. The solvents used were all of spectroscopic grade. Fluorescence data were collected between 320 and 700 nm. The concentrations of the ligands and the complexes were the same as those used for the UV-vis absorption measurements.

Procedure 1: Selective monoalkylation of cyclen[3]

The relevant alkyl halide (1 equiv.) was added to a freshly distilled $CHCl_3$ solution of cyclen (4 or 8 equiv.) and freshly distilled NEt_3 (1.2 or 2.4 equiv.). The resulting solution was refluxed at 65 ^oC for 16 hours under an inert atmosphere. After cooling to room temperature, the organic solution was washed three times with 20 mL of a 1 M NaOH solution to remove the excess cyclen and then three times with 10 mL of water, followed by drying over $MgSO_4$, filtering and removing the solvent under reduced pressure.

Procedure 2: Synthesis of lanthanide complexes using $Ln(CF_3SO_3)_3$

All lanthanide complexes were prepared using microwave irradiation. To a microwave vial was added the relevant ligand with 1 molar equivalent of the appropriate lanthanide triflate in freshly distilled methanol (5 mL), before heating at 60^oC for 40 minutes. After removal of solvent under reduced pressure, the

complexes were isolated by dissolving them in a minimal amount of methanol and precipitating from swirling diethyl ether (200 mL). ^{1}H NMR spectra of the lanthanide complexes consisted of very broad signals and therefore were not fully characterised, *i.e.* integration of the signals was not possible. The paramagnetic properties of lanthanides prevented ^{13}C NMR spectra from being obtained.

Experimental part for Chapters 1, 2 and 3

Methyl 3,4,5-tris(octadecyloxy)benzoate (43)

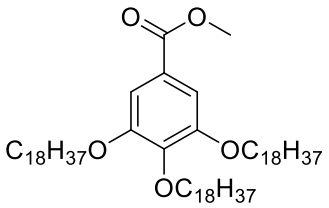

1-Bromooctadecane (3.61 g, 1.08×10^{-2} mol, 4.0 equiv.) was added to a solution of methyl gallate (0.500 g, 2.71×10^{-3} mol, 1.0 equiv.), KI (2.70 g, 1.63×10^{-2} mol, 6.0 equiv.) and K_2CO_3 (2.25 g,1.63×10^{-2} mol, 6.0 equiv.) in 100 mL of freshly distilled THF and 25 mL of dry DMF. The reaction was refluxed for 48 hours at 90 °C. The amount of THF was reduced and 50 mL of chloroform was added. This mixture was washed with 3 × 50 ml portions of 0.1 M HCl to remove the salts and then was washed with 6 × 30 ml portions of water to remove the remaining DMF. The organic layer was separated and dried over $MgSO_4$. The mixture was filtered, and the solvent removed under reduced pressure to give a brown mixture. The mixture was diluted with 25 mL of heptane and a brown solid appeared. This brown solid was purified by recrystallization from hexane. After the filtration, a white solid was obtained in 77% yield (1.89 g, 2.01×10^{-3} M). Mp 60.2-61.6 °C. HRMS (*m/z*) (ESI^{+}) Calculated for $C_{62}H_{116}O_5$ *m/z* = 940.8802 $[M+H]^{+}$. Found *m/z* = 940.8823; ^{1}H NMR (400 MHz, $CDCl_3$) δ_H: 7.23 (s, 2H, ArH), 3.99 (m, 6H, 3 × OCH_2), 3.87 (s, 3H, $COOCH_3$), 1.8 (q, *J* = 6.0 Hz, 4H, 2 × OCH_2CH_2) 1.76 (q, *J* = 6.0 Hz, 2H, OCH_2CH_2), 1,45 (m, 6H OCH_2CH_2), 1.24 (m. 84 H, CH_2), 0. 86 (t, *J* = 8.0 Hz, 9H, 3 × CH_3); ^{13}C NMR (100 MHz, $CDCl_3$), δ_C: 166.89, 152.76, 142.31, 124.59, 107.93, 77.16, 73.44, 69.12, 520.5, 31.89, 30.29, 38.67, 29.63, 29.60, 29.53, 29.35, 29.32, 29.26, 26.04, 22.65. IR (ATR) ν_{max} (cm^{-1}); 2915, 2847, 1717, 1589, 1506, 1.438, 1429, 1468, 1.38, 1337, 1257, 1244, 1220, 1151, 1124, 1019, 980, 860, 807, 769, 720.

[3,4,5-Tris(octadecyloxy)phenylmethanol (44)

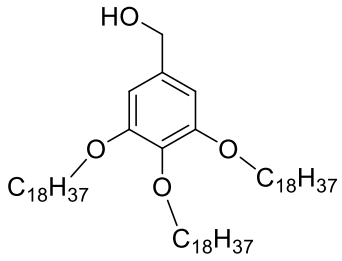

A mixture of KBH_4 (1.29 g, 2.39×10^{-2} mol, 50 equiv.) and LiCl (1.01 g, 2.39×10^{-2} mol, 50 equiv.) was refluxed in dry THF (50 mL) for 2 hours. Methyl-3,4,5-tris(octadecyloxy)benzoate (**43**) (0.468 g, 4.97×10^{-4} mol, 1.0 equiv.) in THF (10 mL) was added dropwise to the solution and refluxed at 70 ºC for 24 hours. The solvent was removed and 0.1 M HCl (50 mL) was added to the resulting compound. This solution was then extracted with CH_2Cl_2 (3 × 50 mL). The combined organic extracts were dried over $MgSO_4$ and the solvent removed under reduced pressure to give a white solid (1.21 g, 1.32 mmol, 90% yield). HRMS (*m/z* ES^+) Calculated for $C_{61}H_{116}O_4$ *m/z* = 912.8874 $[M + H]^+$. Found *m/z* = 912.8885; ^1H NMR (400 MHz, $CDCl_3$) δ_H ppm: 6.58 (2H, s, Ar-H), 4.61 (2H, m, CH_2OH), 3.98 (6H, m, 3 × CH_2O), 1.80 (6H, m, 3 × CH_2CH_2O), 1.48 (6H, m, 3 × $CH_2CH_2CH_2O$), 1.28 (84H, m, 42 × CH_2), 0.90 (9H, m, 3 × CH_3); ^{13}C NMR (100 MHz, $CDCl_3$) δ_C ppm: 153.26, 137.62, 135.97, 105.35, 73.39, 69.09, 65.65, 31.89, 30.30, 29.68, 29.62, 29.59, 29.39, 29.33, 26.11, 26.07, 22.65, 14.07; IR (ATR) υ_{max} (cm^{-1}): 3500, 2916, 2848, 1593, 1463, 1223, 1118, 719.

5-(Bromomethyl)-1,2,3-tris(octadecyloxy) benzene (45)

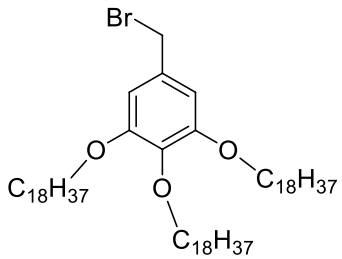

Compound **44** (0.200 g, 0.220 mmol, 3 equiv.) was dissolved in dry toluene (40 mL) and cooled to 0 ºC in an ice bath. Tribromophosphine (0.19 g, 0.73 mmol, 1 eq) was added dropwise. The solution was stirred at room temperature for 3 hours. The solvent was reduced and 0.1 M HCl (50 mL) was added and the solution extracted with CH_2Cl_2 (3 × 50 mL). The combined organic extracts were dried over $MgSO_4$ and the solvent removed under reduced pressure to give a white solid in 87% yield (0.187 g, 0.191 mmol). HRMS (*m/z*) (ES^+) Calculated for $C_{61}H_{115}O_3Br$ *m/z* = 974.8030 $[M^{\cdot}]^+$. Found *m/z* = 974.8061; ^1H NMR (400 MHz, $CDCl_3$) δ_H: 6.59 (2H, s, Ar-H), 4.46 (2H, s, CH_2Br), 3.98 (6H, m, 3 × CH_2O), 1.78 (6H, m, 3 × CH_2CH_2O), 1.48 (6H, m, 3 × $CH_2CH_2CH_2O$), 1.28 (84H, m, 42 × CH_2), 0.90 (9H, m, 3 × CH_3); ^{13}C NMR (100 MHz, $CDCl_3$) δ_C: 153.13, 132.46, 107.51, 73.42, 69.11, 34.58, 31.89, 30.29, 29.68, 29.63, 29.61, 29.57, 29.37, 29.33, 26.07, 26.05, 22.65, 14.07; IR υ_{max} (cm^{-1}): 2916, 2848, 1590, 1466, 1440, 1245, 1128, 1113, 720.

1-[3,4,5-Tris(octadecyloxy)benzyl]-1,4,7,10-tetraazacyclododecane (46)

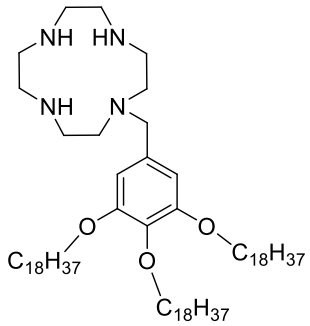

Compound **46** was synthesised according to **Procedure 1** using **45** (0.180 g, 0.190 mmol, 1.0 equiv.), cyclen (**47**) (0.130 g, 0.760 mmol, 4.0 equiv.) and triethylamine (0.03 mL, 0.230 mmol, 1.2 equiv.). A white waxy solid was obtained in 81% yield (0.160 g, 0.150 mmol). HRMS (*m/z*) (MALDI) Calculated for $C_{69}H_{135}N_4O_3$ $[M+H]^+$ *m/z* = 1068.0505. Found *m/z* = 1068.0534; ^{1}H NMR (400 MHz, $CDCl_3$) δ_H: 6.53 (2H, s, Ar-H) 3.96 (6H, m, 3 × CH_2O), 3.53 (2H, s, CH_2), 3.986 (6H, m, 3 × CH_2O), 2.84-2.60 (16H, m, cyclen CH_2), 1.79 (6H, m, 3 × CH_2CH_2O), 1.45 (6H, m, 3 × CH_2CH_2CH_2O), 1.30 (84H, m, 42 × CH_2), 0.90 (9H, m, 3 × CH_3); ^{13}C NMR (100 MHz, $CDCl_3$) δ_C: 152.99, 134.16, 107.18, 73.42, 69.06, 51.22, 47.35, 46.56, 45.31, 31.94, 30.37, 29.74, 29.68, 29.50, 29.38, 26.18, 22.70, 14.13. IR υ_{max} (cm^{-1}): 3450, 2916, 2849, 1584, 1466, 1331, 1232, 1116, 720.

2,2',2''-{10-[3,4,5-Tris(octadecyloxy)benzyl]-1,4,7,10-tetraazacyclododecane-1,4,7-triyl}tris(*N*,*N*-dimethylacetamide) (49)

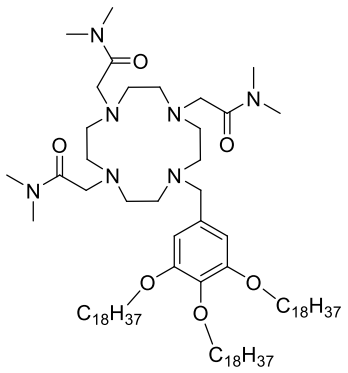

Compound **48** (0.360 g, 0.340 mmol, 1.0 equiv.), 2-chloro-*N*,*N*-dimethylacetamide (0.120 g, 1.05 mmol, 3.1 eq), KI (0.190 g, 1.19 mmol, 3.5 eq) and K_2CO_3 (0.160 g, 1.19 mmol, 3.5 eq) were dissolved in acetonitrile (40 mL). The solution was refluxed for 5 days. The solution was then filtered, and the solvent was removed under reduced pressure. The resulting product was redissolved in $CHCl_3$, filtered and the solvent removed once more under reduced pressure. Purification was achieved by alumina column chromatography using a solvent gradient of 100 CH_2Cl_2 to 80:20 CH_2Cl_2:CH_3OH. The desired product was obtained as a brown oil in 49% yield (0.230 g, 0.170 mmol). Calculated

for $C_{81}H_{155}N_7O_6.3CHCl_3.2H_2O$: C, 58.74; H, 9.51; N, 5.71. Found C, 58.69; H, 9.60; N, 5.90; HRMS (*m/z*) (MALDI) Calculated for $C_{81}H_{155}N_7O_6Na$ *m/z* = 470.3813 [M + Na^+]. Found *m/z* = 470.3818; ^{1}H NMR (400 MHz, $CDCl_3$) δ_H: 6.68 (2H, s, Ar-H), 4.02-3.77 (8H, m, 3 × CH_2O, CH_2), 3.06-2.91 (34H, m, cyclen 8 × CH_2, 9 × CH_2), 1.80 (12H, m, 6 × CH_2), 1.48 (6H, m, 2 × CH_2), 1.27 (84H, m, 6 × CH_3, 33 × CH_2), 0.90 (9H, t, *J* = 7.0 Hz, 3 × CH_3); ^{13}C NMR (100 MHz, $CDCl_3$) δ_C: 190.89, 171.04, 170.51, 170.28, 170.03, 169.12, 168.09, 165.34, 163.38, 162.93, 153.02, 152.72, 152.58, 152.39, 137.71, 136.92, 135.96, 133.15, 131.73, 108.80, 108.58, 107.60, 72.94, 72.85, 72.59, 69.08, 68.86, 68.73, 68.53, 68.19, 61.48, 60.83, 59.33, 59.17, 55.60, 55.31, 55.25, 54.61, 52.41, 51.54, 51.13, 49.57, 48.84, 36.82, 36.43, 36.33, 31.46, 29.26, 29.22, 29.21, 29.06, 28.90, 22.22; IR υ_{max} (cm^{-1}): 3546, 2916, 2849, 1667, 1502, 1466, 1099, 719.

Eu-**49**

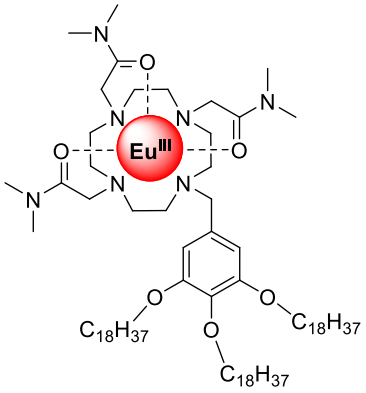

Complex Eu-**49** was synthesised according to **Procedure 2** using ligand **49** (0.050 g, 0.030 mmol, 1.0 equiv.) and $Eu(CF_3SO_3)_3$ (0.020 g, 0.03 mmol, 1.0 eq). A brown solid was obtained in 69% yield (0.050 g, 0.020 mmol). m.p. decomposed above 250°C; Calculated for $C_{105}H_{164}N_{10}O_6Eu.3CF_3SO_3.3Et_2O$: C, 58.00; H, 7.86; N, 5.63. Found C, 58.32; H, 8.21; N, 5.65; ^{1}H NMR (400 MHz, CD_3CN) δH: 8.00, 7.54, 6.45, 6.25, 3.90, 3.50, 3.49, 2.71, 1.73, 1.45, 1.27, 0.90, 0.09; IR υmax (cm^{-1}): 3503, 2917, 2849, 1646, 1502, 1437, 1331, 1234, 1099, 720.

Tb-49

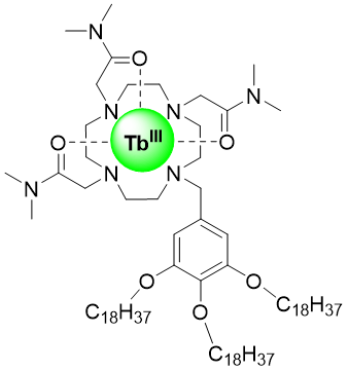

Complex Tb·**49** was synthesised according to **Procedure 2** using ligand **96** (0.050 g, 0.040 mmol, 1.0 equiv.) and $Tb(CF_3SO_3)_3$ (0.030 g, 0.040 mmol, 1.0 equiv.). A white solid was obtained in 76% yield (0.070 g, 0.030 mmol). m.p. decomposed above 250°C; Calculated for $C_{81}H_{155}N_7O_6Tb.3CF_3SO_3$: C, 52.29; H, 8.09; N, 5.08. Found C, 52.72; H, 7.85; N, 4.59; HRMS (m/z) (MALDI) Calculated for $C_{82}H_{154}N_7O_9F_3STb$ m/z = 1629.0734 [M-]. Found m/z = 1629.0778; ^{1}H NMR (400 MHz, CD_3CN) δH: 9.70, 7.28, 6.46, 5.10, 3.91, 3.66, 3.34, 2.98, 2.85, 1.72, 1.45, 1.27, 1.02, 0.90, 0.09, -0.81, -2.50,

Experimental part for Chapter 4

The synthesis was performed by Emanuele Cappello who was a co-worker on this project. He provided all the steps reaction details for compound **55**

Synthesis of Tris-Methylbenzoate-benzene-1,3,5-tricarboxamide

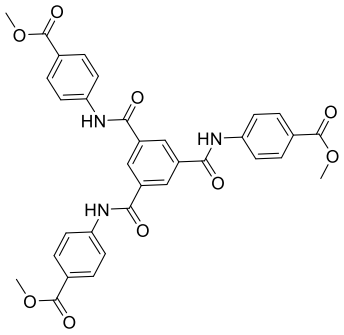

A solution of methyl 4-aminobenzoate (3.5 equiv.), 1,3,5-benzenetricarboxylic acid chloride (1.0 equiv.), and K_2CO_3 (3.5 equiv.) in acetone was stirred for 12 h at 80 °C. The resulting solid was filtered, then washed with CH_3OH and water and then air-dried to obtain a white solid in a 87% yield. HRMS (m/z) (ESI MS+) calculated for $C_{33}H_{28}N_3O_9$ m/z = 610.1820 [M+H], found m/z = 610.1805. ^{1}H NMR (400 MHz, DMSO-d_6) δ 10.90 (3H, s, N-H), 8.73 (9H, s, Ar-H), 8.00 (12H, dd, Ar-H), 3.83 (9H, s, OCH_3). ^{13}C NMR (400 MHz, DMSO-d_6) δ 166.25, 165.26, 143.77, 135.62, 130,75, 130.68, 125.15, 120.17, 55.42.

Synthesis of Tris-(L-Alanine)-benzene-1,3,5-tricarboxamide (55)

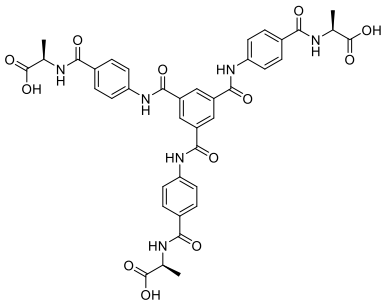

. 0.200 g of Tris-Benzoic acid-benzene-1,3,5-tricarboxamide (0.211 mmol, 1 equiv.) were dissolved in 20 ml of anhydrous DCM and reacted with 3 ml of TFA (excess). After removal of DCM and precipitation in water, the compound was retrieved as a white powder (0.150 g, 91% yield). **HRMS** (m/z) (ESI MS-) calculated for $C_{39}H_{34}N_6O_{12}$ m/z = 389.112284 [M -2H], found m/z = 389.113096. **^{1}H NMR** (400 MHz, DMSO-d_6) δ 10.77 (3H, s, N-H), 8.72 (3H, s, Ar-H), 8.55 (3H, d, N-H), 7.90 (12H, s, Ar-H), 4.38 (3H, q, C-H), 1.3 (9H, d, C-H3). **^{13}C NMR** (400 MHz, DMSO-d_6) δ 174.73, 166.00, 165.12, 142.07, 135.72, 130.55, 129.60, 128.74, 119.92, 49.04, 17.39.

1. J.-M. Lehn, *Angewandte Chemie International Edition in English*, 1988, **27**, 89-112.
2. G. M. Whitesides and B. Grzybowski, *Science*, 2002, **295**, 2418-2421.
3. V. Alexander, *Chemical reviews*, 1995, **95**, 273-342.
4. B. Dietrich, J. Lehn and J. Sauvage, *Tetrahedron Letters*, 1969, **10**, 2889-2892.
5. C. J. Pedersen, *Journal of the American Chemical Society*, 1967, **89**, 7017-7036.
6. P. L. Anelli, P. R. Ashton, R. Ballardini, V. Balzani, M. Delgado, M. T. Gandolfi, T. T. Goodnow, A. E. Kaifer and D. Philp, *Journal of the American Chemical Society*, 1992, **114**, 193-218.
7. G. Gokel, *J. Am. Chem. Soc*, 1983, **105**, 586-593.
8. L. Baldini, A. Casnati, F. Sansone and R. Ungaro, *Chemical Society Reviews*, 2007, **36**, 254-266.
9. S. M. Goldup, D. A. Leigh, P. J. Lusby, R. T. McBurney and A. M. Slawin, *Angewandte Chemie*, 2008, **120**, 7107-7111.
10. A. I. Prikhod'ko, F. Durola and J.-P. Sauvage, *Journal of the American Chemical Society*, 2008, **130**, 448-449.
11. T. Gunnlaugsson and J. P. Leonard, *Chemical Communications*, 2005, 3114-3131.
12. D. Parker, R. S. Dickins, H. Puschmann, C. Crossland and J. A. Howard, *Chemical Reviews*, 2002, **102**, 1977-2010.
13. A. P. de Silva, I. M. Dixon, H. N. Gunaratne, T. Gunnlaugsson, P. R. Maxwell and T. E. Rice, *Journal of the American Chemical Society*, 1999, **121**, 1393-1394.
14. L. A. Moran, H. R. Horton, K. G. Scrimgeour and M. D. Perry, *Principles of biochemistry*, Pearson Boston, 2012.
15. K. Binnemans, *Chemical reviews*, 2009, **109**, 4283-4374.
16. M. A. Katkova and M. N. Bochkarev, *Dalton Transactions*, 2010, **39**, 6599-6612.
17. S. Faulkner, L. S. Natrajan, W. S. Perry and D. Sykes, *Dalton Transactions*, 2009, 3890-3899.
18. E. Toth, L. Burai and A. E. Merbach, *Coordination Chemistry Reviews*, 2001, **216**, 363-382.
19. J.-C. G. Bünzli, *Accounts of chemical research*, 2006, **39**, 53-61.
20. S. Faulkner and B. P. Burton-Pye, *Chemical Communications*, 2005, 259-261.
21. I. Lukeš, J. Kotek, P. Vojtíšek and P. Hermann, *Coordination Chemistry Reviews*, 2001, **216**, 287-312.
22. M. R. Spirlet, J. Rebizant, J. F. Desreux and M. F. Loncin, *Inorganic chemistry*, 1984, **23**, 359-363.
23. A. R. Pease, J. O. Jeppesen, J. F. Stoddart, Y. Luo, C. P. Collier and J. R. Heath, *Accounts of chemical research*, 2001, **34**, 433-444.
24. K. Rurack and U. Resch-Genger, *Chemical Society Reviews*, 2002, **31**, 116-127.
25. M. Rosser, D. Parker, G. Ferguson, J. F. Gallagher, J. A. K. Howard and D. S. Yufit, *Journal of the Chemical Society, Chemical Communications*, 1993, DOI: 10.1039/C39930001267, 1267-1269.
26. O. Kotova, S. Comby and T. Gunnlaugsson, *Chemical Communications*, 2011, **47**, 6810-6812.
27. M. Fujiwara, S. Tsukahara and H. Watarai, *Physical Chemistry Chemical Physics*, 1999, **1**, 2949-2951.

28. E. P. Achterberg, T. W. Holland, A. R. Bowie, R. F. C. Mantoura and P. J. Worsfold, *Analytica Chimica Acta*, 2001, **442**, 1-14.
29. A. Thibon and V. C. Pierre, *Analytical and bioanalytical chemistry*, 2009, **394**, 107-120.
30. D. M. Dias, J. M. Teixeira, I. Kuprov, E. J. New, D. Parker and C. F. Geraldes, *Organic & biomolecular chemistry*, 2011, **9**, 5047-5050.
31. G. Yu, X. Yan, C. Han and F. Huang, *Chemical Society Reviews*, 2013, **42**, 6697-6722.
32. S. Y.-L. Leung, S. Evariste, C. Lescop, M. Hissler and V. W.-W. Yam, *Chemical Science*, 2017, **8**, 4264-4273.
33. J. R. Moffat, G. J. Seeley, J. T. Carter, A. Burgess and D. K. Smith, *Chemical Communications*, 2008, DOI: 10.1039/B809077G, 4601-4603.
34. S. E. Braslavsky, *Pure and Applied Chemistry*, 2007, **79**, 293-465.
35. B. Valeur and M. N. Berberan-Santos, *Molecular fluorescence: principles and applications*, John Wiley & Sons, 2012.
36. A. de Silva, *Journal*, 2013.
37. J. Andréasson and U. Pischel, *Chemical Society Reviews*, 2010, **39**, 174-188.
38. A. P. de Silva and S. A. de Silva, *Journal of the Chemical Society, Chemical Communications*, 1986, 1709-1710.
39. F. A. Abebe, C. S. Eribal, G. Ramakrishna and E. Sinn, *Tetrahedron leters*, 2011, **52**, 5554-5558.
40. B. Turfan and E. U. Akkaya, *Organic letters*, 2002, **4**, 2857-2859.
41. N. Jiang, J. Fan, F. Xu, X. Peng, H. Mu, J. Wang and X. Xiong, *Angewandte Chemie*, 2015, **127**, 2540-2544.
42. Y. Shirota, Y. Kuwabara, D. Okuda, R. Okuda, H. Ogawa, H. Inada, T. Wakimoto, H. Nakada, Y. Yonemoto and S. Kawami, *Journal of Luminescence*, 1997, **72**, 985-991.
43. R. G. Pearson, *Journal of Chemical Education*, 1968, **45**, 643.
44. R. Chang, *Physical chemistry for the biosciences*, University Science Books, 2005.
45. J.-C. G. Bünzli and C. Piguet, *Chemical Society Reviews*, 2005, **34**, 1048-1077.
46. M. C. Heffern, L. M. Matosziuk and T. J. Meade, *Chemical Reviews*, 2014, **114**, 4496-4539.
47. J.-C. G. Bünzli, *Chemistry letters*, 2008, **38**, 104-109.
48. D. E. Barry, D. F. Caffrey and T. Gunnlaugsson, *Chemical Society Reviews*, 2016, **45**, 3244-3274.
49. S. V. Eliseeva and J.-C. G. Bünzli, *Chemical Society Reviews*, 2010, **39**, 189-227.
50. J.-C. G. Bünzli, S. Comby, A.-S. Chauvin and C. D. Vandevyver, *Journal of rare earths*, 2007, **25**, 257-274.
51. C. M. dos Santos, A. J. Harte, S. J. Quinn and T. Gunnlaugsson, *Coordination Chemistry Reviews*, 2008, **252**, 2512-2527.
52. A. Beeby, I. Clarkson, R. Dickins, S. Faulkner, D. Parker and L. Royle, *J. Chem. Soc., Perkin Trans*, 1999, **2**, 493.
53. P. Caravan, J. J. Ellison, T. J. McMurry and R. B. Lauffer, *Chemical reviews*, 1999, **99**, 2293-2352.
54. S. J. Franklin, *Current opinion in chemical biology*, 2001, **5**, 201-208.
55. A. Pol, T. R. Barends, A. Dietl, A. F. Khadem, J. Eygensteyn, M. S. Jetten and H. J. Op den Camp, *Environmental microbiology*, 2014, **16**, 255-264.
56. S. E. Plush, N. A. Clear, J. P. Leonard, A.-M. Fanning and T. Gunnlaugsson, *Dalton Transactions*, 2010, **39**, 3644-3652.
57. A. Beeby, S. Faulkner, D. Parker and J. G. Williams, *Journal of the Chemical Society, Perkin Transactions 2*, 2001, 1268-1273.

58. A. Beeby, I. M. Clarkson, R. S. Dickins, S. Faulkner, D. Parker, L. Royle, A. S. De Sousa, J. G. Williams and M. Woods, *Journal of the Chemical Society, Perkin Transactions 2*, 1999, 493-504.
59. J. P. Leonard, C. B. Nolan, F. Stomeo and T. Gunnlaugsson, in *Photochemistry and Photophysics of Coordination Compounds II*, Springer, 2007, pp. 1-43.
60. J. Georges, *Analyst*, 1993, **118**, 1481-1486.
61. S. J. Butler, *Chemical Communications*, 2015, **51**, 10879-10882.
62. S. J. Pope and R. H. Laye, *Dalton Transactions*, 2006, 3108-3113.
63. C. M. dos Santos, P. B. Fernández, S. E. Plush, J. P. Leonard and T. Gunnlaugsson, *Chemical Communications*, 2007, 3389-3391.
64. M. Andrews, J. E. Jones, L. P. Harding and S. J. Pope, *Chemical Communications*, 2011, **47**, 206-208.
65. T. Gunnlaugsson, A. J. Harte, J. P. Leonard and M. Nieuwenhuyzen, *Supramolecular Chemistry*, 2003, **15**, 505-519.
66. R. A. Poole, G. Bobba, M. J. Cann, J.-C. Frias, D. Parker and R. D. Peacock, *Organic & Biomolecular chemistry*, 2005, **3**, 1013-1024.
67. M. Mayer and B. Meyer, *Journal of the American Chemical Society*, 2001, **123**, 6108-6117.
68. L. C. Costello and R. B. Franklin, *Molecular cancer*, 2006, **5**, 1.
69. R. Pal, A. Beeby and D. Parker, *Journal of pharmaceutical and biomedical analysis*, 2011, **56**, 352-358.
70. R. Pal, D. Parker and L. C. Costello, *Organic & biomolecular chemistry*, 2009, **7**, 1525-1528.
71. D. G. Smith, G.-l. Law, B. S. Murray, R. Pal, D. Parker and K.-L. Wong, *Chemical Communications*, 2011, **47**, 7347-7349.
72. D. F. Caffrey and T. Gunnlaugsson, *Dalton Transactions*, 2014, **43**, 17964-17970.
73. H. M. Burke, T. Gunnlaugsson and E. M. Scanlan, *Organic & biomolecular chemistry*, 2016, **14**, 9133-9145.
74. R. Apweiler, H. Hermjakob and N. Sharon, *Biochimica et Biophysica Acta (BBA)-General Subjects*, 1999, **1473**, 4-8.
75. E. M. Surender, S. Comby, B. L. Cavanagh, O. Brennan, T. C. Lee and T. Gunnlaugsson, *Chem*, 2016, **1**, 438-455.
76. T. C. Lee, S. Mohsin, D. Taylor, R. Parkesh, T. Gunnlaugsson, F. J. O'Brien, M. Giehl and W. Gowin, *Journal of Anatomy*, 2003, **203**, 161-172.
77. B. McMahon, P. Mauer, C. P. McCoy, T. C. Lee and T. Gunnlaugsson, *Journal of the American Chemical Society*, 2009, **131**, 17542-17543.
78. R. Parkesh, T. C. Lee and T. Gunnlaugsson, *Tetrahedron Letters*, 2009, **50**, 4114-4116.
79. O. S. Wolfbeis, *Chemical Society Reviews*, 2015, **44**, 4743-4768.
80. M. Eichelbaum and K. Rademann, *Advanced Functional Materials*, 2009, **19**, 2045-2052.
81. C. Andraud and O. Maury, *European Journal of Inorganic Chemistry*, 2009, **2009**, 4357-4371.
82. A. T. Bui, M. Beyler, Y.-Y. Liao, A. Grichine, A. Duperray, J.-C. Mulatier, B. L. Guennic, C. Andraud, O. Maury and R. Tripier, *Inorganic chemistry*, 2016, **55**, 7020-7025.
83. L. K. Truman, S. J. Bradberry, S. Comby, O. Kotova and T. Gunnlaugsson, *ChemPhysChem*, 2017, **18**, 1746-1751.
84. S. Erbas-Cakmak, S. Kolemen, A. C. Sedgwick, T. Gunnlaugsson, T. D. James, J. Yoon and E. U. Akkaya, *Chemical Society Reviews*, 2018, **47**, 2228-2248.
85. I. Langmuir, *Journal of the American chemical society*, 1916, **38**, 2221-2295.

86. K. B. Blodgett, *Journal of the American Chemical Society*, 1934, **56**, 495-495.
87. K. B. Blodgett and I. Langmuir, *Physical Review*, 1937, **51**, 964.
88. K. B. Blodgett, *Journal of the American Chemical Society*, 1935, **57**, 1007-1022.
89. M. C. Petty, *Langmuir-Blodgett films: an introduction*, Cambridge University Press, 1996.
90. A. Ulman, *An Introduction to Ultrathin Organic Films: From Langmuir--Blodgett to Self--Assembly*, Academic press, 2013.
91. D. J. Wales and J. A. Kitchen, *Chemistry Central Journal*, 2016, **10**, 72.
92. A. Gole, N. R. Jana, S. T. Selvan and J. Y. Ying, *Langmuir*, 2008, **24**, 8181-8186.
93. E. Oh, M.-Y. Hong, D. Lee, S.-H. Nam, H. C. Yoon and H.-S. Kim, *Journal of the American Chemical Society*, 2005, **127**, 3270-3271.
94. P. J. Dutton and L. Conte, *Langmuir*, 1999, **15**, 613-617.
95. D.-J. Qian, H. Nakahara, K. Fukuda and K.-Z. Yang, *Langmuir*, 1995, **11**, 4491-4494.
96. D.-J. Qian, K.-Z. Yang, H. Nakahara and K. Fukuda, *Langmuir*, 1997, **13**, 5925-5932.
97. R.-J. Zhang, H.-G. Liu, K.-Z. Yang, Z.-K. Si, G.-Y. Zhu and H.-W. Zhang, *Thin Solid Films*, 1997, **295**, 228-233.
98. R.-J. Zhang, K.-Z. Yang, A.-C. Yu and X.-S. Zhao, *Thin Solid Films*, 2000, **363**, 275-278.
99. L. Gomes, K. de Oliveira and C. Neri, *J. Lumin*, 2008, **128**, 1339-1347.
100. F. Sousa, A. Ferreira, R. S. Ferreira, A. Cavaleiro, L. Carlos, H. Nogueira and T. Trindade, *Journal of alloys and compounds*, 2004, **374**, 371-376.
101. T. Ito, H. Yashiro and T. Yamase, *Journal of Cluster Science*, 2006, **17**, 375-387.
102. H. Lemmetyinen, E. Vuorimaa, A. Jutila, V. M. Mukkala, H. Takalo and J. Kankare, *Luminescence: The journal of biological and chemical luminescence*, 2000, **15**, 341-350.
103. D. Zhou, C. Huang, K. Wang, G. Xu, X. Zhao, X. Xie, L. Xu and T. Li, *Langmuir*, 1994, **10**, 1910-1912.
104. M. Rodriguez-Mendez, Y. Gorbunova and J. De Saja, *Langmuir*, 2002, **18**, 9560-9565.
105. J. Souto, L. Tomilova, R. Aroca and J. DeSaja, *Langmuir*, 1992, **8**, 942-946.
106. R. D. Adati, F. J. Pavinatto, J. H. Monteiro, M. R. Davolos, M. Jafelicci and O. N. Oliveira, *New Journal of Chemistry*, 2012, **36**, 1978-1984.
107. C. Lincheneau, C. Destribats, D. E. Barry, J. A. Kitchen, R. D. Peacock and T. Gunnlaugsson, *Dalton Transactions*, 2011, **40**, 12056-12059.
108. Y. Lvov, H. Haas, G. Decher, H. Moehwald, A. Mikhailov, B. Mtchedlishvily, E. Morgunova and B. Vainshtein, *Langmuir*, 1994, **10**, 4232-4236.
109. A. A. Mamedov, N. A. Kotov, M. Prato, D. M. Guldi, J. P. Wicksted and A. Hirsch, *Nature materials*, 2002, **1**, 190.
110. C. Jiang, H. Ko and V. V. Tsukruk, *Advanced Materials*, 2005, **17**, 2127-2131.
111. S. W. Keller, H.-N. Kim and T. E. Mallouk, *Journal of the American Chemical Society*, 1994, **116**, 8817-8818.
112. E. R. Kleinfeld and G. S. Ferguson, *Science*, 1994, **265**, 370-373.
113. K. Arora, S. Chand and B. Malhotra, *Analytica Chimica Acta*, 2006, **568**, 259-274.
114. Y. Lvov and H. Möhwald, *Protein architecture: interfacing molecular assemblies and immobilization biotechnology*, Marcel Dekker New York, 2000.
115. M. Campàs and C. O'Sullivan, *Analytical letters*, 2003, **36**, 2551-2569.
116. Z. Tang, Y. Wang, P. Podsiadlo and N. A. Kotov, *Advanced materials*, 2006, **18**, 3203-3224.

117. L.-N. Sun, J.-B. Yu, H.-J. Zhang, Q.-G. Meng, E. Ma, C.-Y. Peng and K.-Y. Yang, *Microporous and mesoporous materials*, 2007, **98**, 156-165.
118. K. Lunstroot, K. Driesen, P. Nockemann, C. Görller-Walrand, K. Binnemans, S. Bellayer, J. Le Bideau and A. Vioux, *Chemistry of materials*, 2006, **18**, 5711-5715.
119. K. Binnemans, *Coordination Chemistry Reviews*, 2015, **295**, 1-45.
120. .
121. C. B. Murphy, Y. Zhang, T. Troxler, V. Ferry, J. J. Martin and W. E. Jones, *The Journal of Physical Chemistry B*, 2004, **108**, 1537-1543.
122. C. Gandolfi, N. Miyashita, D. G. Kurth, P. N. Martinho, G. G. Morgan and M. Albrecht, *Dalton Transactions*, 2010, **39**, 4508-4516.
123. J. Mei, N. L. Leung, R. T. Kwok, J. W. Lam and B. Z. Tang, *Chemical reviews*, 2015, **115**, 11718-11940.
124. A. Gorlyak, I. Khramtsovsky and V. Solonukha, 2001.
125. H. Tompkins and E. A. Irene, *Handbook of ellipsometry*, William Andrew, 2005.
126. D. Brewster, *Philos. Trans. R. Soc. London*, 1815, **105**, 125-130.
127. L. A. Frohman, *Hospital Practice*, 1975, **10**, 54-67.
128. S. Udenfriend and J. B. Wyngaarden, *Biochimica et biophysica acta*, 1956, **20**, 48-52.
129. H. Akiba, J. Sumaoka and M. Komiyama, *ChemBioChem*, 2009, **10**, 1773-1776.
130. L. R. Hill, T. J. Sørensen, O. A. Blackburn, A. Brown, P. D. Beer and S. Faulkner, *Dalton Transactions*, 2013, **42**, 67-70.
131. A. Grote, A. Chang, C. Söhngen, C. Munaretto, I. Schomburg, M. Lang, M. Scheer, M. Rother, M. Stelzer, S. Placzek, S. Ulas and D. Schomburg, *Nucleic Acids Research*, 2012, **41**, D764-D772.
132. C. B. Anfinsen, *Science*, 1973, **181**, 223-230.
133. X. S. Puente, L. M. Sánchez, C. M. Overall and C. López-Otín, *Nature Reviews Genetics*, 2003, **4**, 544.
134. L. M. Coussens, B. Fingleton and L. M. Matrisian, *Science*, 2002, **295**, 2387-2392.
135. W. P. Esler and M. S. Wolfe, *Science*, 2001, **293**, 1449-1454.
136. M. G. Acker and D. S. Auld, *Perspectives in Science*, 2014, **1**, 56-73.
137. V. Škedelj, T. Tomašić, L. P. Mašič and A. Zega, *Journal of medicinal chemistry*, 2011, **54**, 915-929.
138. G. Manning, D. B. Whyte, R. Martinez, T. Hunter and S. Sudarsanam, *Science*, 2002, **298**, 1912-1934.
139. D. Hanahan and R. A. Weinberg, *cell*, 2011, **144**, 646-674.
140. N. E. Hynes and G. MacDonald, *Current opinion in cell biology*, 2009, **21**, 177-184.
141. P. A. Jänne, J. A. Engelman and B. E. Johnson, *Journal of clinical oncology*, 2005, **23**, 3227-3234.
142. E. Pazos and M. E. Vázquez, *Biotechnology journal*, 2014, **9**, 241-252.
143. H. A. Dewia, B. S. Fangben Mengb, C. Guoa, B. Norlingc, X. Chenb and S. Lima.
144. E. M. Surender, S. J. Bradberry, S. A. Bright, C. P. McCoy, D. C. Williams and T. Gunnlaugsson, *Journal of the American Chemical Society*, 2017, **139**, 381-388.
145. H.-P. Kleber, *Journal of Basic Microbiology*, 1990, **30**, 384-384.
146. W. W. Cleland, *Biochemistry*, 1964, **3**, 480-482.
147. O. Shaul, *Biometals*, 2002, **15**, 307-321.
148. A. M. Romani and M. E. Maguire, *Biometals*, 2002, **15**, 271-283.
149. A. Pilotelle-Bunner, F. Cornelius, P. Sebban, P. W. Kuchel and R. J. Clarke, *Biophysical journal*, 2009, **96**, 3753-3761.
150. K. Mena-Ulecia, A. Vergara-Jaque, H. Poblete, W. Tiznado and J. Caballero, *PloS one*, 2014, **9**, e109639.

151. C. C. Minghui Sun, Lihua Chen, Baolian Su, *Front. Chem. Sci. Eng.*, 2016, **10**, 301-347.
152. Z. Zhang and M. J. Zaworotko, *Chemical Society Reviews*, 2014, **43**, 5444-5455.
153. L. E. Kreno, K. Leong, O. K. Farha, M. Allendorf, R. P. Van Duyne and J. T. Hupp, *Chemical Reviews*, 2012, **112**, 1105-1125.
154. J.-C. G. Bünzli, *Chemical Reviews*, 2010, **110**, 2729-2755.
155. S. J. Bradberry, G. Dee, O. Kotova, C. P. McCoy and T. Gunnlaugsson, *Chemical Communications*, 2019, **55**, 1754-1757.
156. G. Tobin, S. Comby, N. Zhu, R. Clérac, T. Gunnlaugsson and W. Schmitt, *Chemical Communications*, 2015, **51**, 13313-13316.
157. E. Pershagen and K. E. Borbas, *Angewandte Chemie International Edition*, 2015, **54**, 1787-1790.
158. R. Daly, O. Kotova, M. Boese, T. Gunnlaugsson and J. J. Boland, *ACS Nano*, 2013, **7**, 4838-4845.
159. P. Terech and R. G. Weiss, *Chemical reviews*, 1997, **97**, 3133-3160.
160. J. A. Foster, D. W. Johnson, M.-O. M. Pipenbrock and J. W. Steed, *New Journal of Chemistry*, 2014, **38**, 927-932.
161. J. P. Leonard, C. M. G. dos Santos, S. E. Plush, T. McCabe and T. Gunnlaugsson, *Chemical Communications*, 2007, DOI: 10.1039/B611487C, 129-131.
162. P. Vojtíšek, P. Cígler, J. Kotek, J. Rudovský, P. Hermann and I. Lukeš, *Inorganic Chemistry*, 2005, **44**, 5591-5599.
163. R. Equilibria, *Fremantle, Australia*, 2018.
164. P. Caravan, *Chemical Society Reviews*, 2006, **35**, 512-523.
165. R. B. Lauffer, *Chemical reviews*, 1987, **87**, 901-927.
166. R. A. Novelline and L. F. Squire, *Squire's fundamentals of radiology*, La Editorial, UPR, 2004.
167. D. L. Pavia, G. M. Lampman, G. S. Kriz and J. R. Vyvyan, *Introduction to Spectroscopy*, 2009, 587.
168. H. U. Rashid, K. Yu and J. Zhou, *Journal of Structural Chemistry*, 2013, **54**, 223-249.
169. A. Berger, *BMJ: British Medical Journal*, 2002, **324**, 35.
170. E. Kluza, D. W. Van Der Schaft, P. A. Hautvast, W. J. Mulder, K. H. Mayo, A. W. Griffioen, G. J. Strijkers and K. Nicolay, *Nano letters*, 2009, **10**, 52-58.
171. D. L. Pavia, G. M. Lampman, G. S. Kriz and J. R. Vyvyan, *Introduction to Spectroscopy*, 2009, 177.
172. H. U. Rashid, M. A. U. Martines, J. Jorge, P. M. de Moraes, M. N. Umar, K. Khan and H. U. Rehman, *Bioorganic & medicinal chemistry*, 2016, **24**, 5663-5684.
173. A. Gupta, S. A. Willis, T. Stait-Gardner, M. J. Moghaddam and W. S. Price, *Magnetic Resonance in Chemistry*, 2016, **54**, 58-61.
174. S. S. Silva, C. Lopes, A. L. Teixeira, M. J. C. D. Sousa and R. Medeiros, *Forensic Science International: Genetics*, 2015, **14**, 1-10.
175. S. Y. Dan'Kov, A. Tishin, V. Pecharsky and K. Gschneidner, *Physical Review B*, 1998, **57**, 3478.
176. G. Hervé, H. Bernard, N. L. Bris, M. L. Baccon, J. J. Yaouanc and H. Handel, *Tetrahedron Letters*, 1999, **40**, 2517-2520.
177. J. G. Rheinwald and M. A. Beckett, *Cancer research*, 1981, **41**, 1657-1663.
178. A. J. Amoroso and S. J. A. Pope, *Chemical Society Reviews*, 2015, **44**, 4723-4742.
179. J. Kapuscinski, *Biotechnic & Histochemistry*, 1995, **70**, 220-233.

Appendix Chapter 2

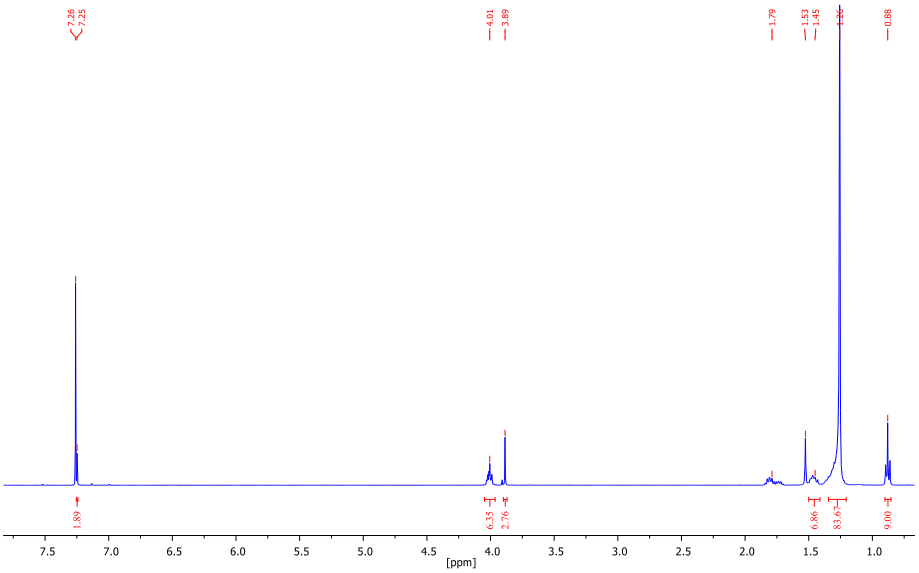

Figure A2.0 The *^{1}H NMR spectrum (400 MHz, CD_3Cl) of* ***43****.*

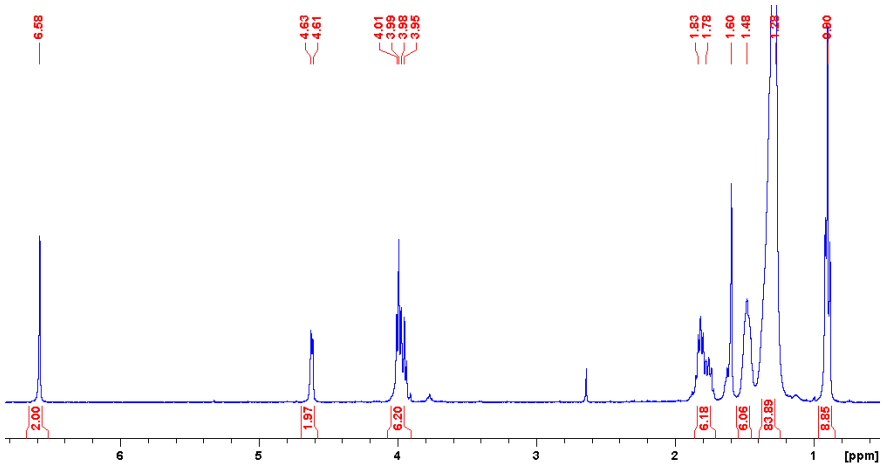

Figure A2.1*: The ^{1}H NMR spectrum (400 MHz, CD_3Cl) of* ***44****.*

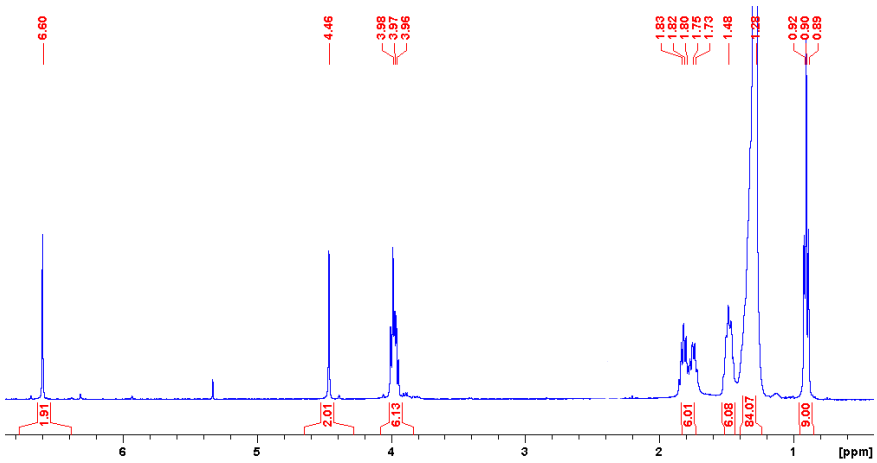

***Figure A2.2**: The ^{1}H NMR spectrum (400 MHz, CD_3Cl) of **45**.*

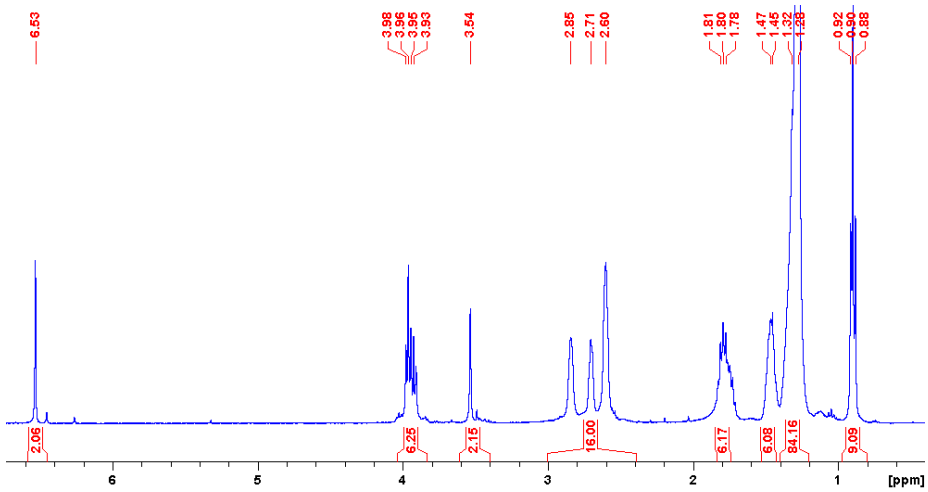

***Figure A2.3**: The ^{1}H NMR spectrum (400 MHz, CD_3Cl) of **46**.*

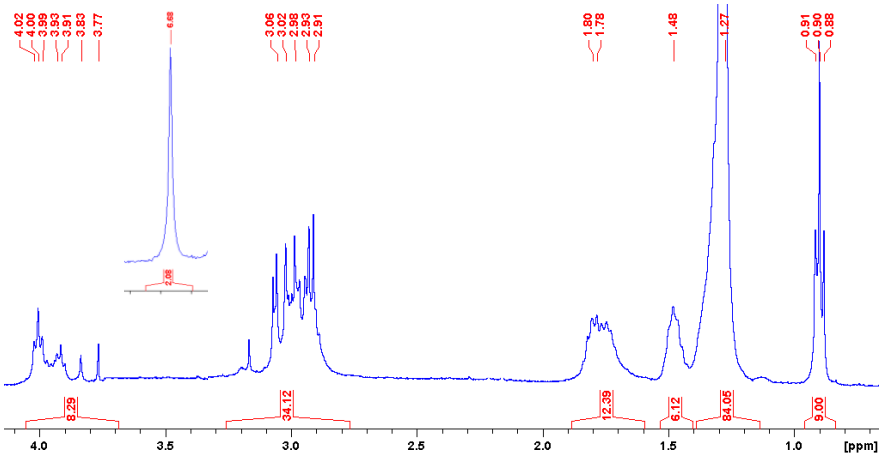

***Figure A2.4**: The ^{1}H NMR spectrum (400 MHz, CD_3Cl) of **49**.*

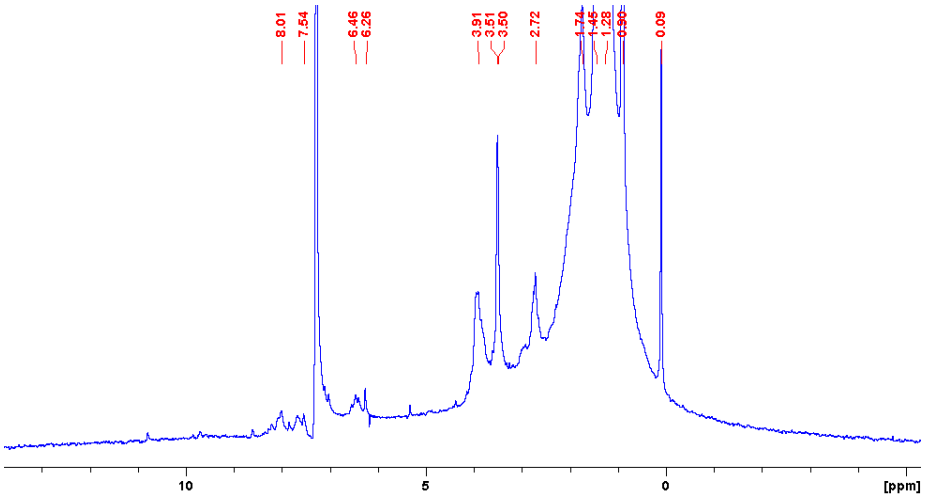

***Figure A2.5**: The ^{1}H NMR spectrum (400 MHz, CD_3CN) of complex Eu-49.*

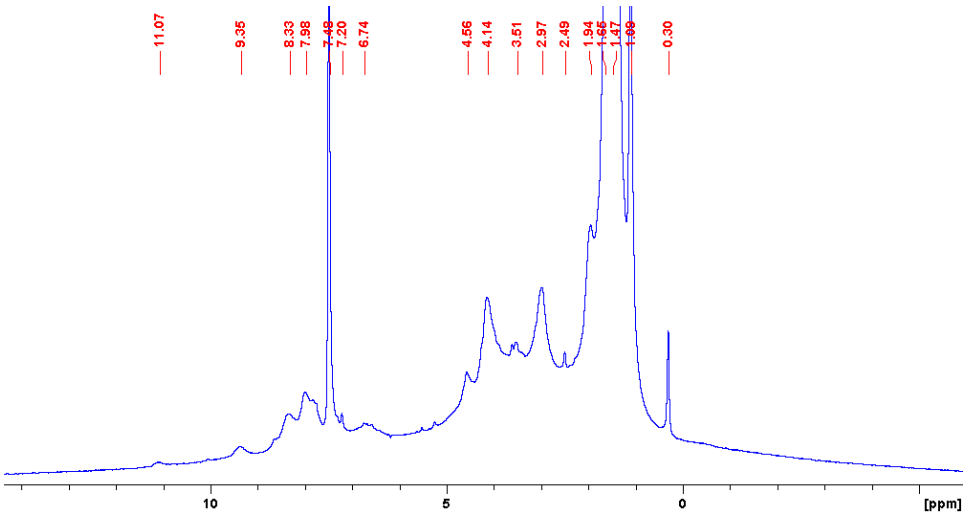

***Figure A2.6**: The ^{1}H NMR spectrum (400 MHz, CD_3CN) of complex Tb-**49**.*

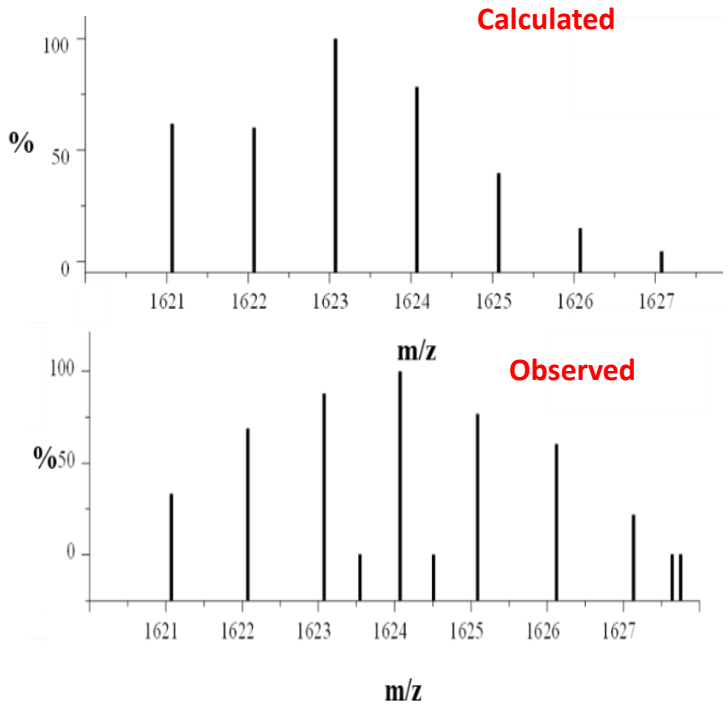

*F**igure A2.7**: The MALDI mass spectrum of Eu-49 displaying the expected Eu(III) isotopic distribution pattern for the $[Eu\text{-}49 + CF_3SO_3]^{2+}$ species.*

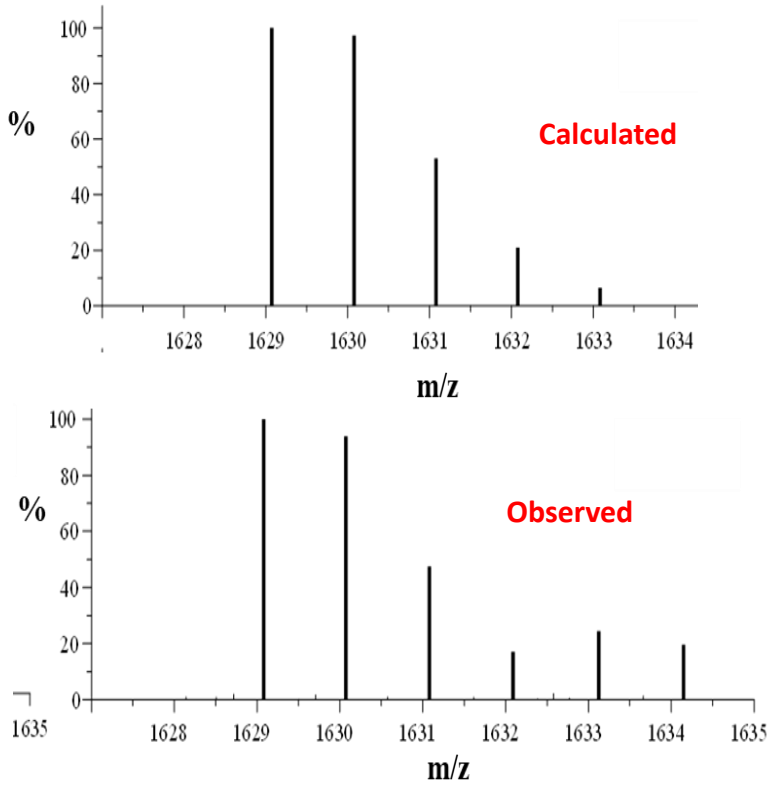

***Figure A2.8**: The MALDI mass spectrum of Tb-49 displaying the expected Tb(III) isotopic distribution pattern for the [Tb-49 + CF_3SO_3]$^{2+}$ species.*

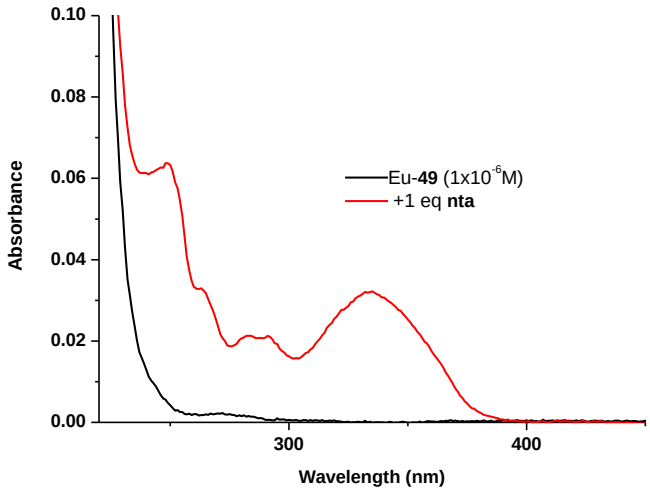

***Figure A2.9:** The UV-vis absorption spectra of **Eu-49** in the absence (-) and presence (-) of one equivalent of the antenna **nta** in MeOH solution (1× 10^{-6} M).*

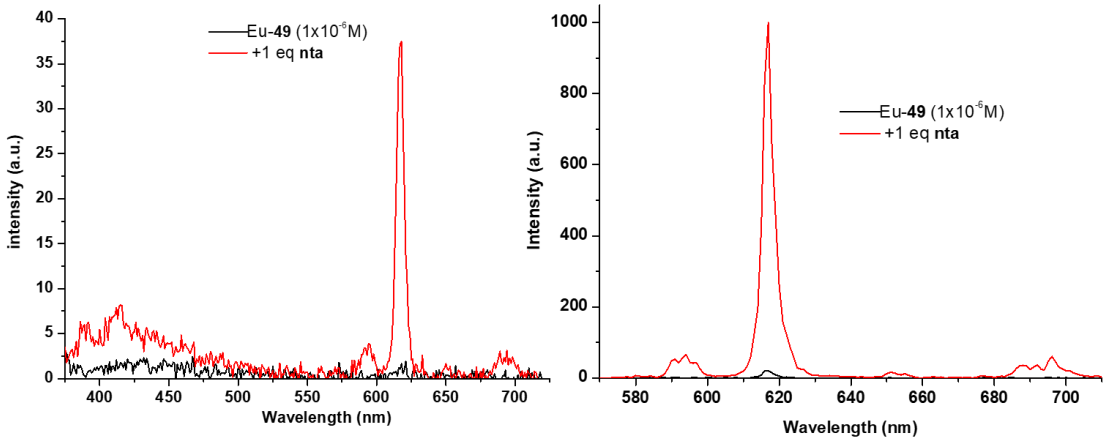

Figure A2.10: *(left) The fluorescence and (right) phosphorescence spectra of* ***Eu-49*** *in the absence (-) and presence (-) of one equivalent of the antenna* ***nta*** *in MeOH solution (λ_{ex} = 330 nm, 1 x 10^{-6} M).*

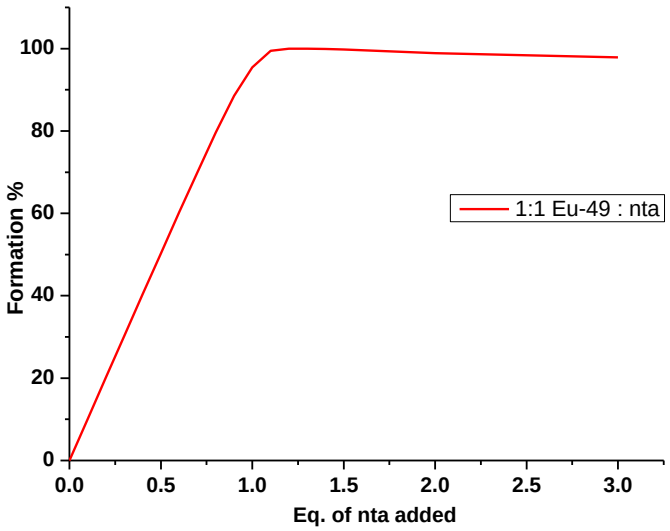

Figure 2.11: *Speciation distribution diagram obtained from non-linear regression analysis of the phosphorescence titration data of* ***Eu-49*** *with* ***nta*** *in MeOH.*

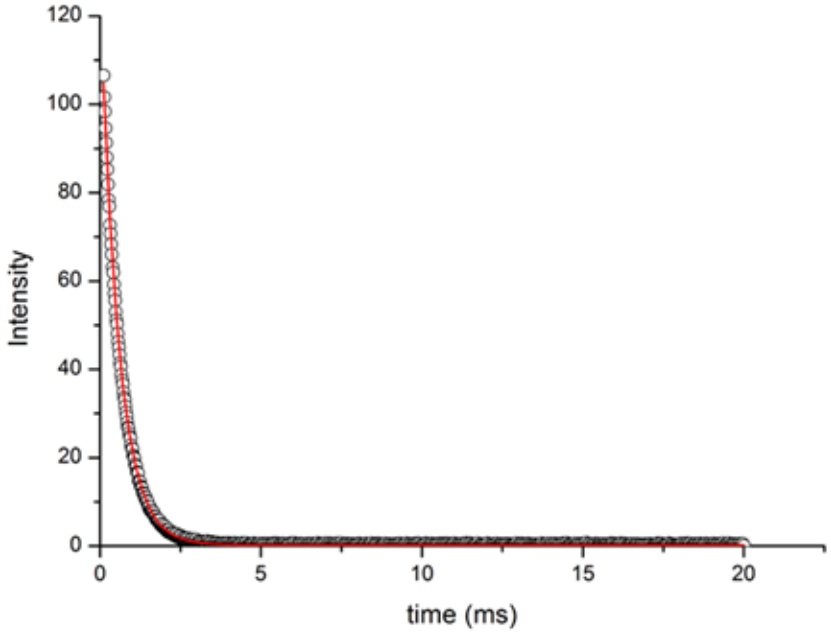

Figure 2.10: *The luminescence decay of the complex* ***Eu-49*** *and its fit to a monoexponential decay in MeOH.*

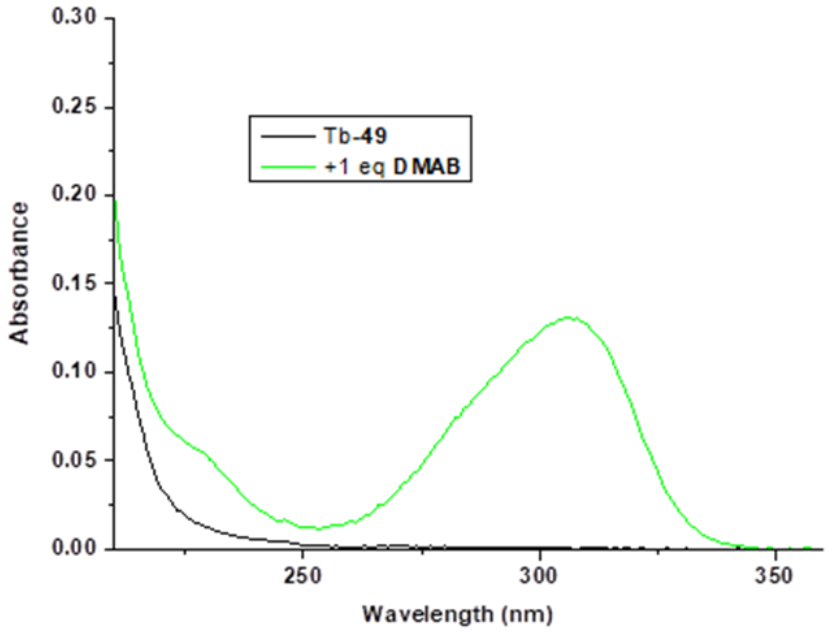

Figure A2.12: *The UV-vis absorption spectra of Tb-****49*** *in the absence (-) and presence (-) of one equivalent of the antenna* ***DMAB*** *in MeOH solution (1× 10^{-6} M).*

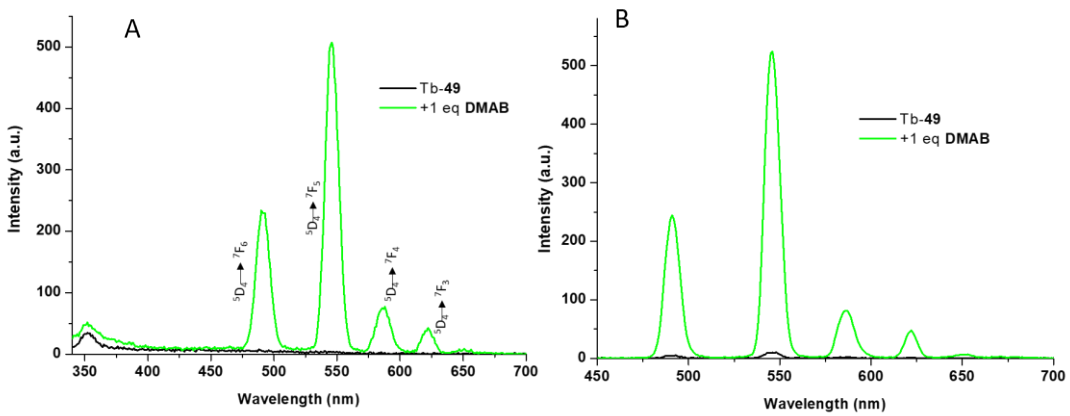

Figure A2.13: *(A) The fluorescence and (B) phosphorescence spectra of* ***Tb-49*** *in the absence (-) and presence (-) of one equivalent of the antenna* ***DMAB*** *in MeOH solution (1 x 10^{-6} M) at λ_{ex} = 300 nm.*

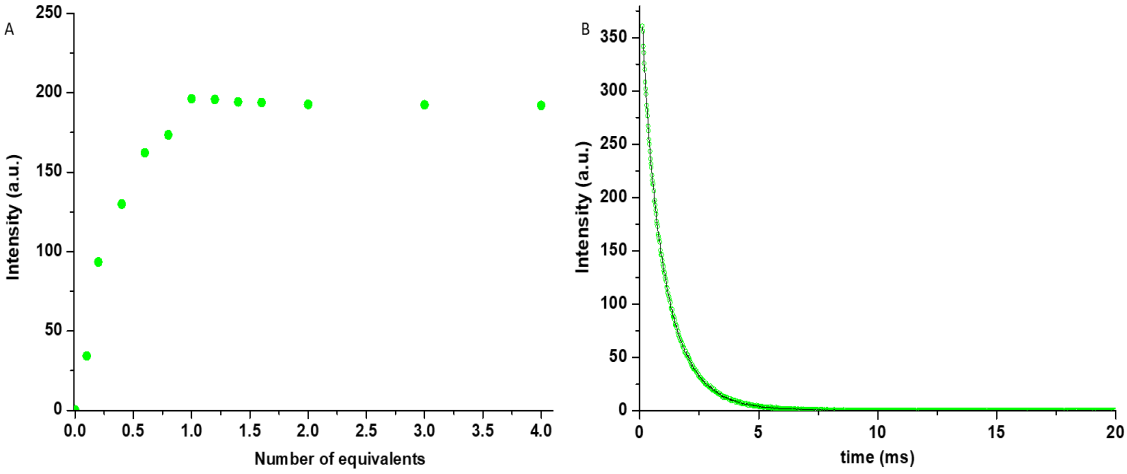

Figure 2.14*: (A) The changes in the Tb(III)-centred emission of* ***Tb-49*** *complex (1 x 10^{-6}M) in MeOH at 545 nm as a function of number of equivalents of* ***DMAB*** *added, (B) Luminescence decay of the complex* ***Tb-49*** *and its fit to a monoexponential decay and recorded in MeOH.*

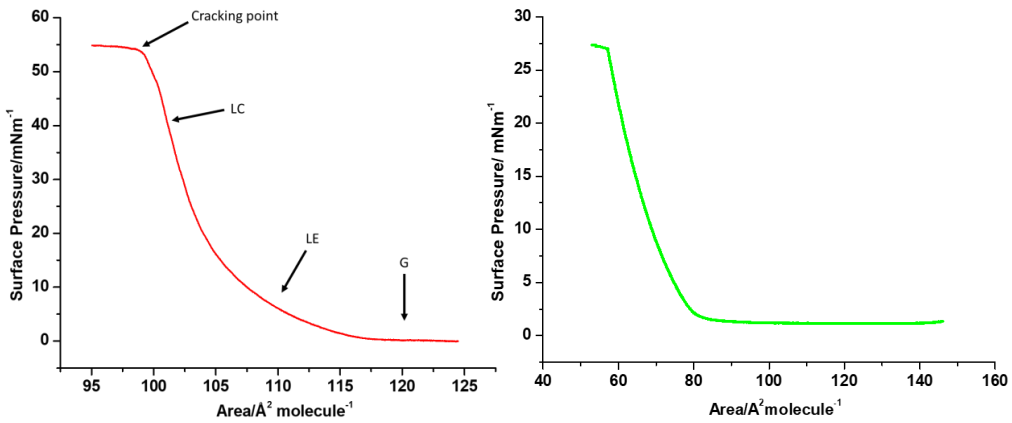

Figure A2.15*: Surface pressure-area isotherm of (left) Eu-**49** and (right) Tb-**49**indicating phase transitions and a cracking point.*

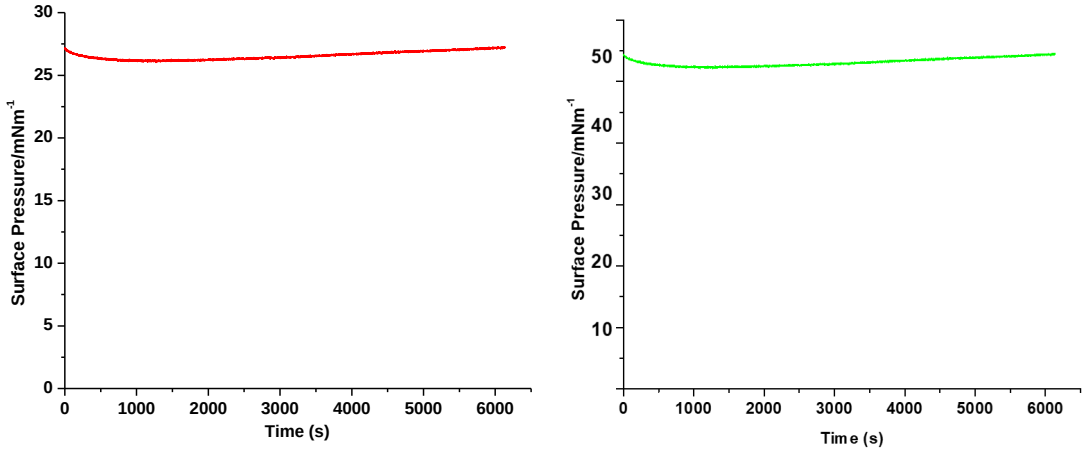

Figure A2.16: *Stability plots for (A)* ***Eu-49*** *and (B)* ***Tb-49.***

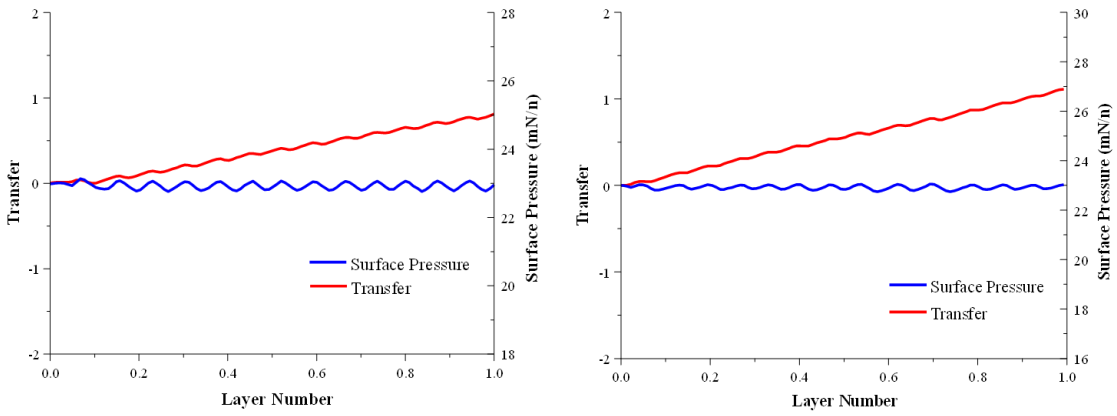

Figure A2.17*: Langmuir monolayer deposition graph of (left) Eu-49-nta and (right) Tb-49-DMAB.*

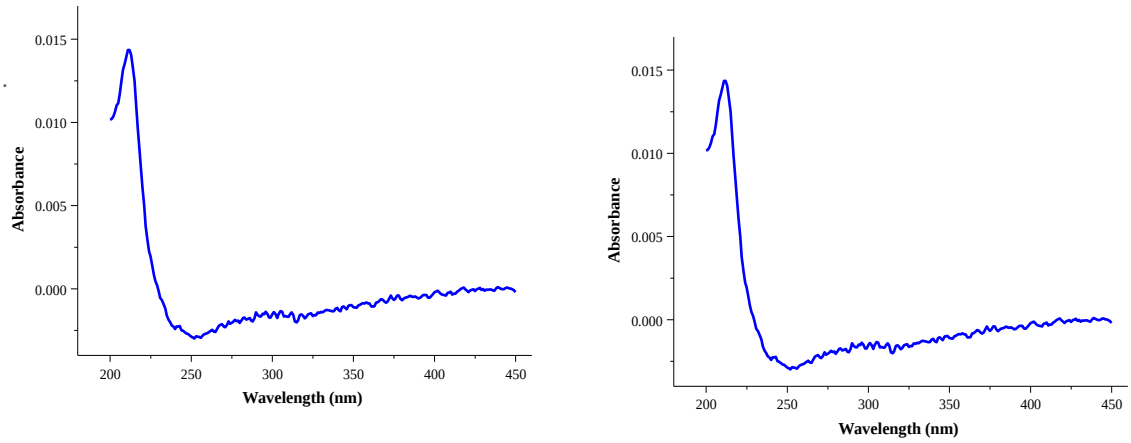

***Figure A2.18**: The UV-vis absorption spectra of the LB film of (left) Eu-49-nta and (right) Tb-49-DMAB on quartz slides*

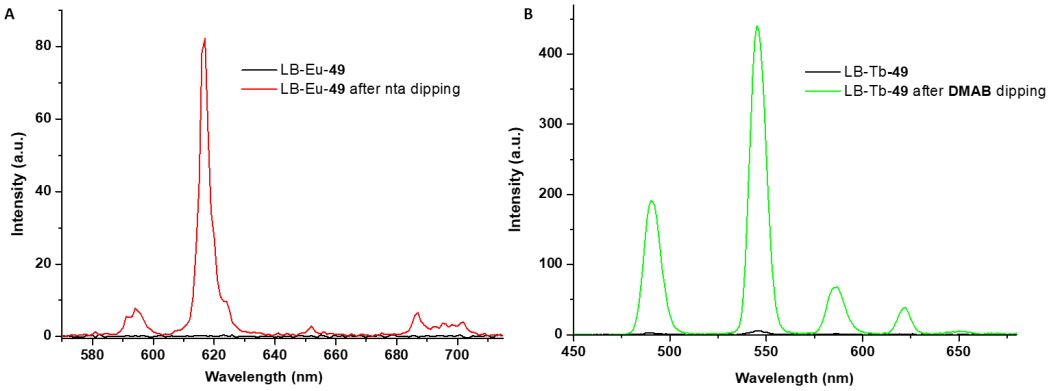

***Figure A2.19:** (A) Eu(III)-centred emission from the monolayer LB-**Eu-49** before (black) and after (red) the dipping into an aqueous solution of **nta** 1 x 10^{-4}M, λ_{ex} = 330 nm and (B) (A Tb(III)-centred emission from the monolayer LB-**Tb-49** before (black) and after (green) the dipping into an aqueous solution of **DMAB** 1x10^{-4}M, λ_{ex} = 306 nm.*

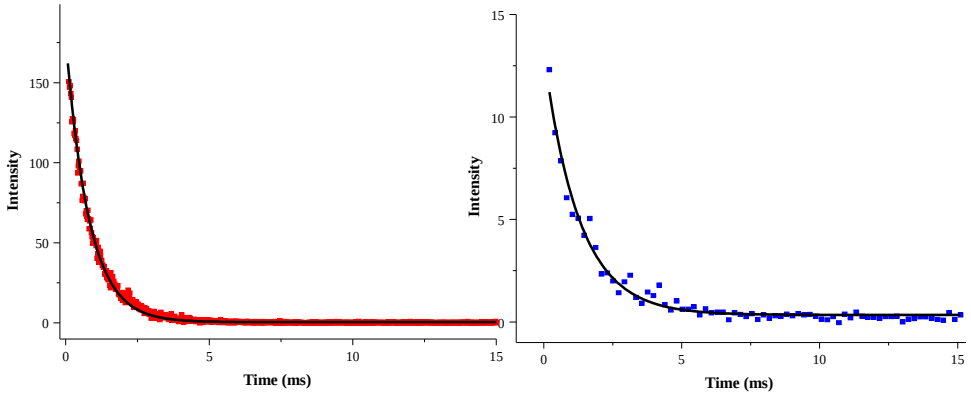

Figure A2.19*: Luminescence decay fit to monoexponential of LB films on quartz slides of (left) Eu-**49**-nta (λ_{ex} = 330 nm, λ_{em} = 615 nm) and (right) Tb496-DMAB (λ_{ex} = 220 nm, λ_{em} = 545 nm).*

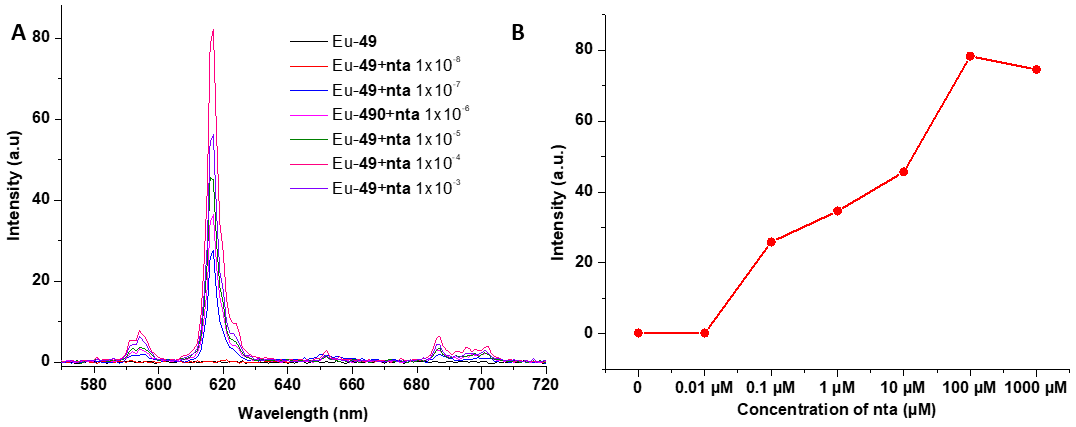

Figure A2.20: *LOD studies of LB-**Eu-49** monolayers upon dipping into **nta** aqueous solution at different concentrations from 1 x 10^{-8} M to 1 x 10^{-3} M (λ_{ex} = 330 nm) showing (left) Eu(III)-centred emission spectra and (right) increase of emission at 616 nm vs concentration.* —

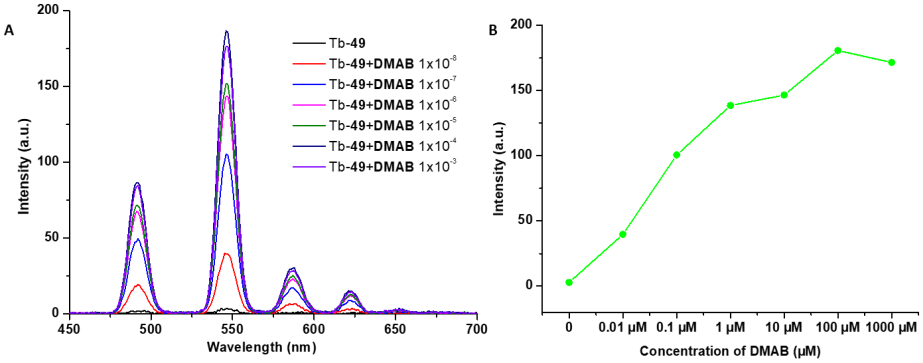

Figure A2.21: *LOD studies of LB-**Tb-49** upon dipping into **DMAB** aqueous solution at different concentration from 1 x 10^{-8} M to 1 x 10^{-3} M (λ_{ex} = 306 nm) where () shows the changes in Tb(III)-centred emission spectra and (B) increase of the emission at 545 nm vs concentration recorded in phosphorescence mode.*

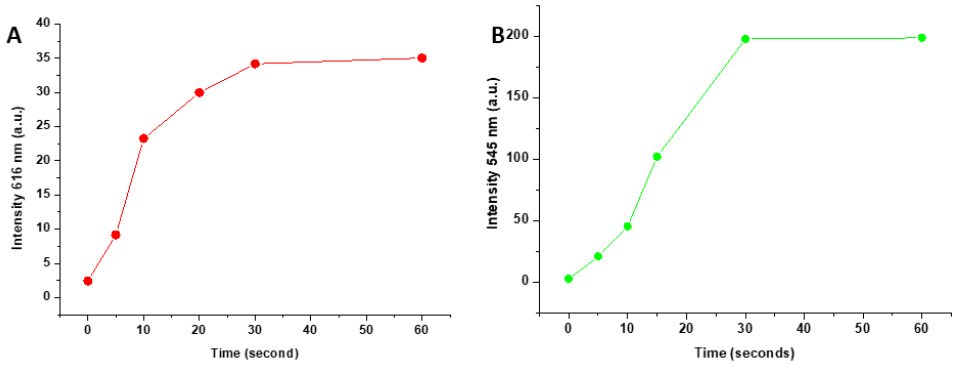

Figure A2.22: *Kinetic studies where (A) LB-**Eu·49** was immersed into an aqueous solution of **nta** at 1 x 10^{-4}M for different times (0-60 sec), λ_{ex} 330 nm and (B) LB-**Tb·49** was immersed into an aqueous solution of **DMAB** at 1 x 10^{-4} M for different times (0-60 sec), λ_{ex} 306 nm*

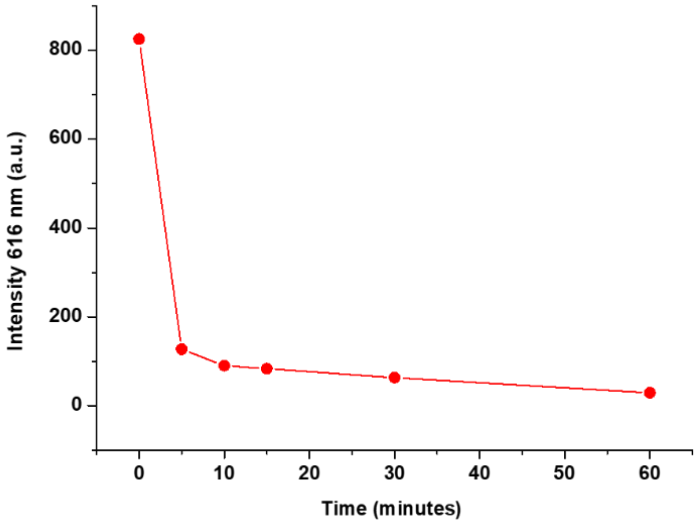

Figure A2.23: *Representation of flow cell setup with quartz slide inside the beaker under constant water flow (left). The changes in the LB-**Eu-49** emission at 616 nm for 60 minutes (λ_{ex} = 330 nm) under the water flow.*

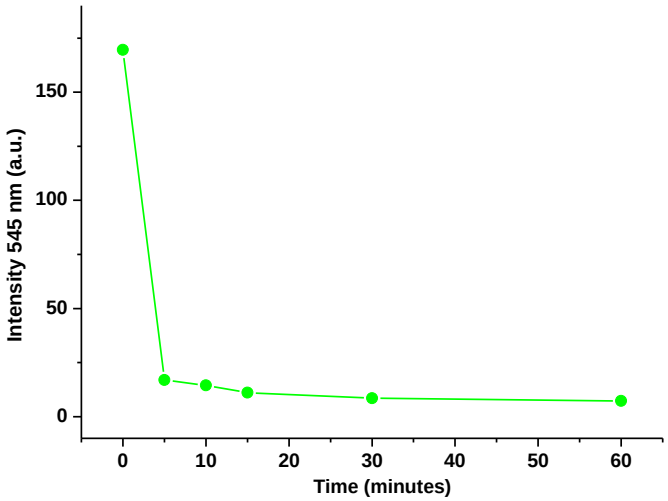

Figure A2.24: *The changes in the Tb(III)-centred emission of LB-**Tb-49** over a period of 60 minutes under the water flow (λ_{ex} = 306 nm).*

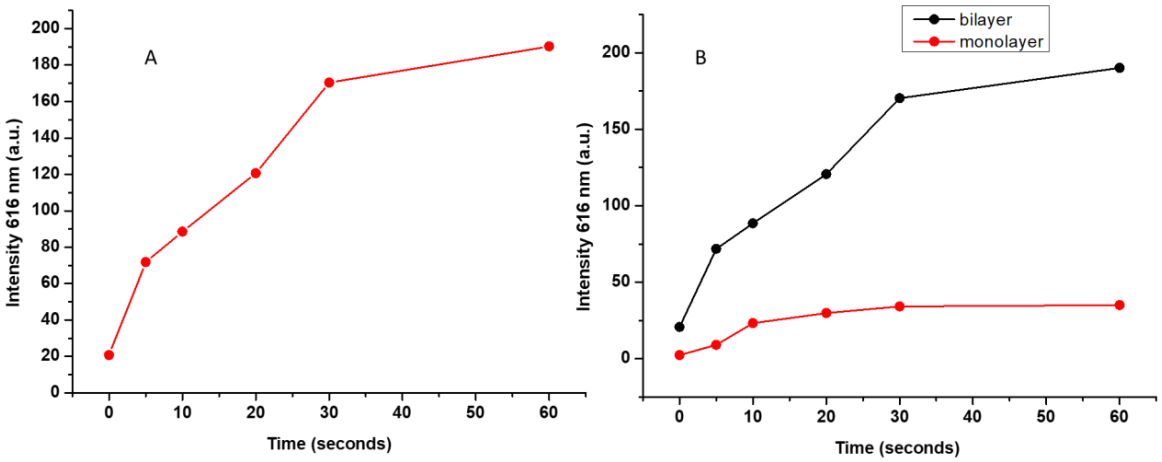

Figure A2.25: *(A) The changes of the Eu(III)-centred emission of LB-**Eu-49** bilayer upon dipping the slide into the **nta** 1 x 10^{-4} M aqueous solution (λ_{ex} = 330 nm) for different amount of time (0 – 60 seconds); (B) the comparison of the Eu(III)-centred emission intensity between the LB-**Eu-49** monolayer (red) and bilayer (black) using the same instrumental parameters.*

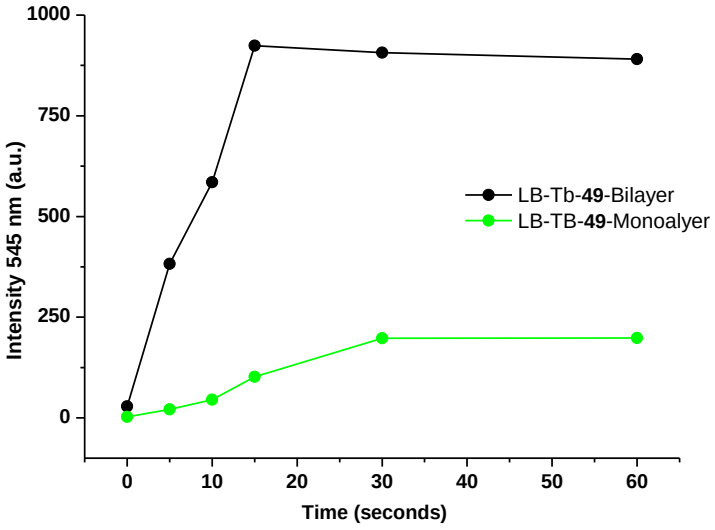

Figure A2.26: *The comparison of the Tb(III)-centred emission intensity of the LB-**Tb-49** monolayer (green) and the bilayer (black) when dipped in aqueous solution of **DMAB** 1 x 10^{-4}M (λ_{ex} = 306 nm).*

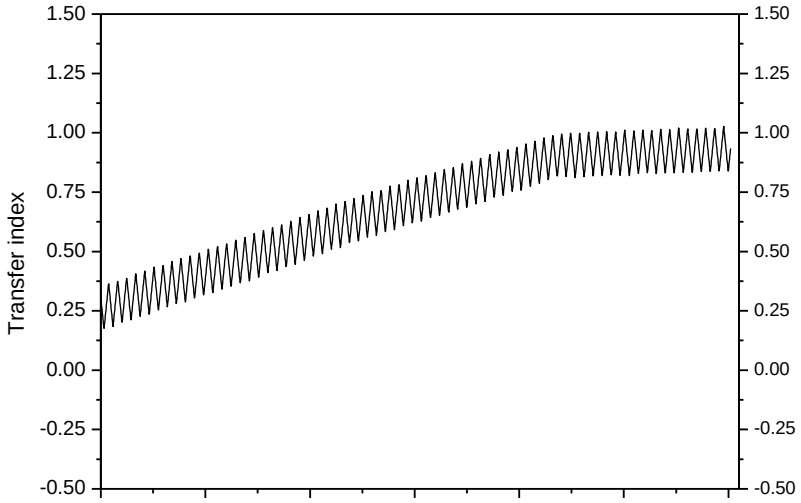

***Figure A2.27**: Langmuir monolayer deposition graph **Tb-49 -Eu-49** bilayer*

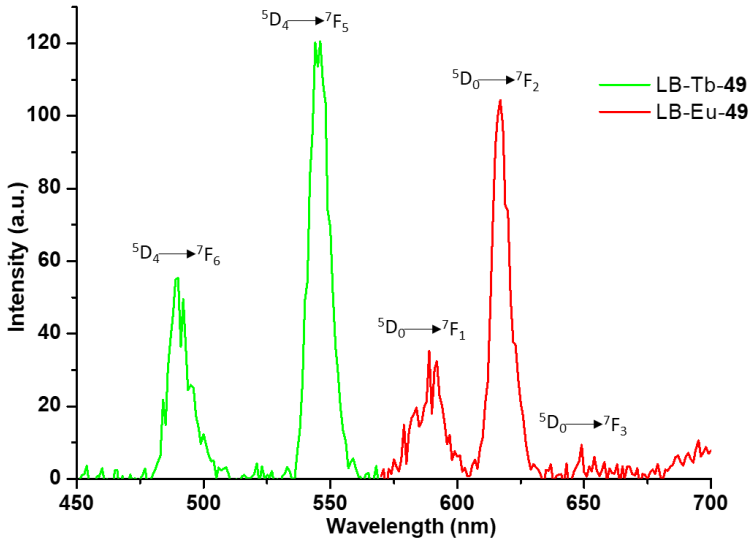

***Figure A2.28**: Luminescence spectra of LB-**Tb-49 -Eu-49** showing the characteristic Tb(III) $^5D_4 \rightarrow {}^7F_J$ (J = 6, 5) and Eu(III) $^5D_0 \rightarrow {}^7F_J$ (J = 1–3) transitions (λ_{ex} = 300 nm). (B):*

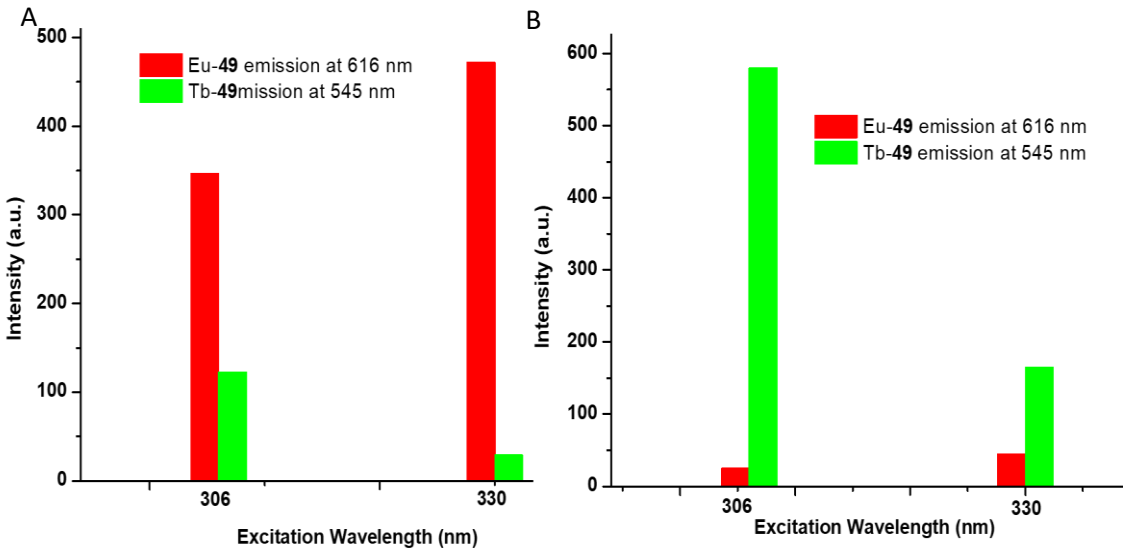

***Figure A2.29**: Eu(III)- or Tb(III)-centred emission at 545 nm and 616 nm of LB-**Eu-49/Tb-49** bilayer after dipping into (A) the aqueous solution of **nta** 1 x 10^{4} M and the following dipping of the same layer (B) into the aqueous solution of **DMAB** 11 x 10^{-4} M.*

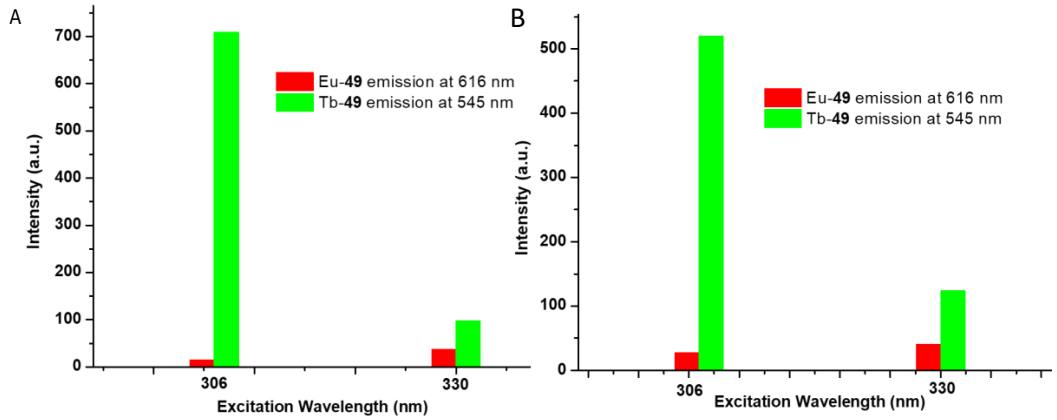

***Figure A2.30**: Eu(III)- or Tb(III)-centred emission of LB-**Eu-49/Tb-49** bilayer at 616 nm and 545 nm after dipping into (A) the **DMAB** aqueous solution 1 x 10^{-4} M and the following dipping of the same layer into (B) aqueous solution of **nta** 1 x 10^{-4} M.*

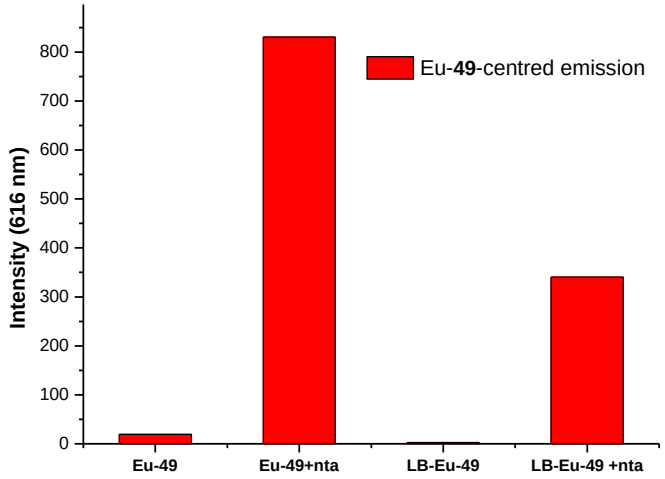

***Figure A2.31**: Comparison of Eu(III)-centred emission at 616 nm for **Eu-49** in the solution of MeOH at 1 x 10^{-5} M and upon addition of 1 equivalent of **nta** with the same system deposited onto the surface of the quartz slide LB-**Eu-49** and upon its dipping into the aqueous solution of **nta** 1 x 10^{-4} M.*

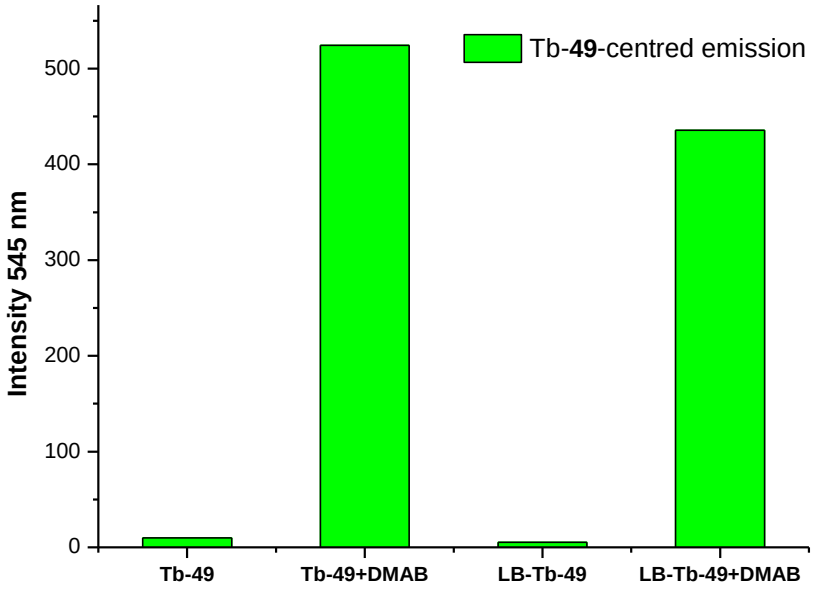

***Figure A2.32**: Comparison of Tb(III)-centred emission at 545 nm for **Tb-49** in the solution of MeOH at 1 x 10^{-5} M and upon addition of 1 equivalent of **DMAB** with the same system deposited onto the surface of the quartz slide LB-**Tb-49** and upon its dipping into the aqueous solution of **DMAB** 1 x 10^{-4} M.*

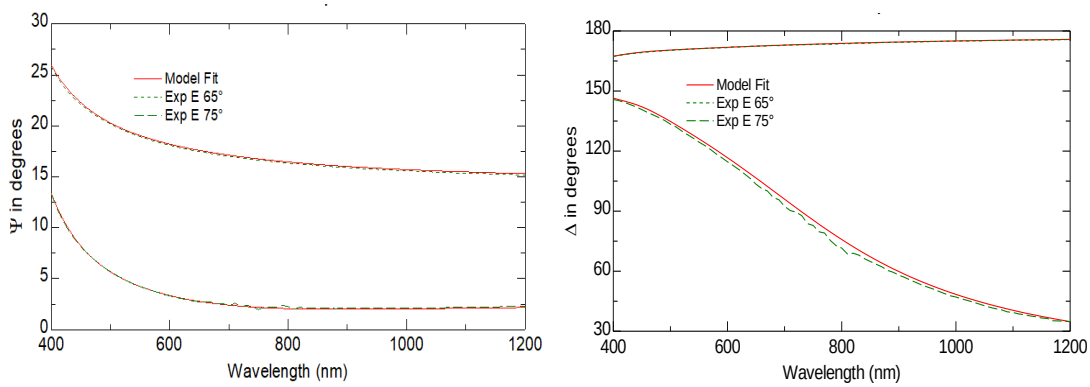

Figure A2.33: *(left) Variation of the amplitude and (right) of the phase as function of wavelength for LB-**Eu-49.***

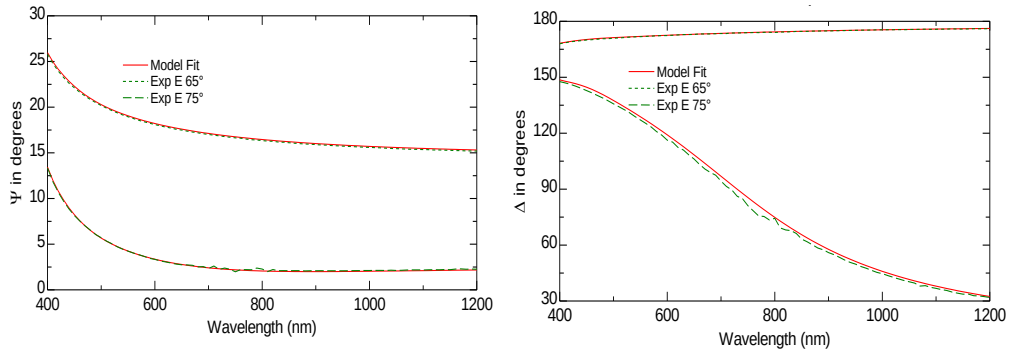

Figure A 2.34: *Variation of (left) the amplitude and (right) the phase as function of wavelength for LB-**Tb-49.***

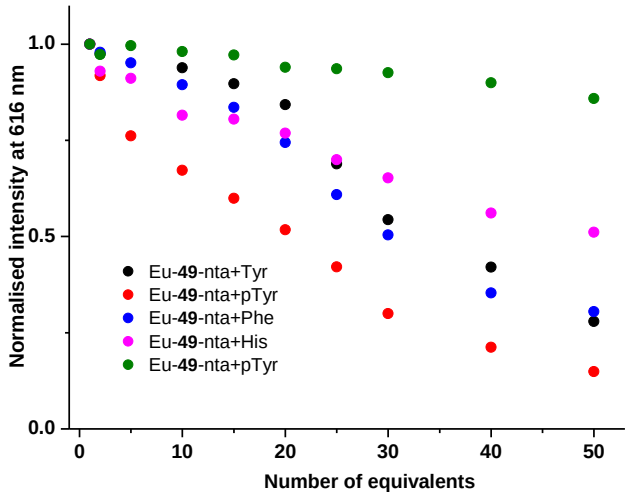

Figure A2.35*: Normalised Eu(III) emission at 616 nm (λ_{ex} = 330 nm) of **Eu·49nta** ($c = 1 \times 10^{-6}$ M) in MeOH upon the addition of 50 equivalents of various amino acids,*

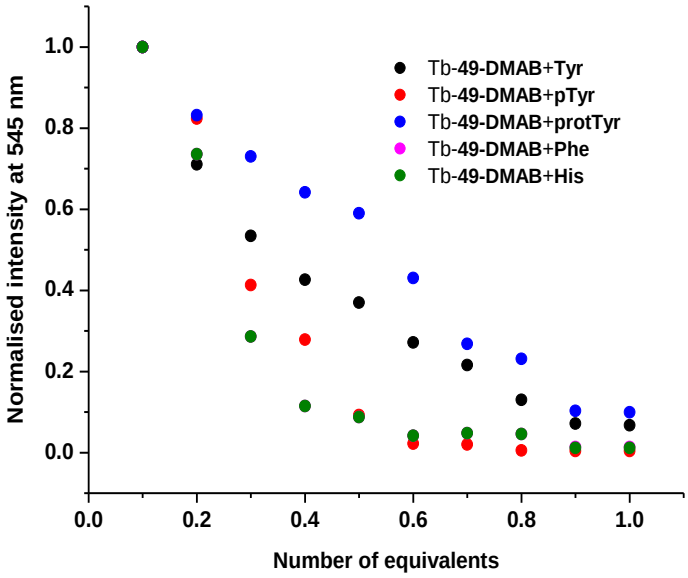

***Figure A2.36**: Normalised Tb(III) emission at 545 nm (λ_{ex} = 306 nm) of **Tb-49-DMAB** ($c = 1 \times 10^{-6}$ M) in MeOH upon the addition of 1 equivalent of amino acid.*

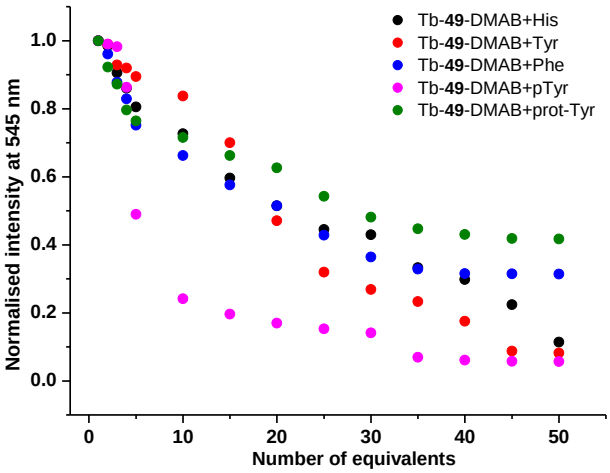

***Figure A2.37:** Normalised Tb(III)-centred emission at 545 nm (λ_{ex} = 306 nm) of **Tb-49-DMAB** ($c = 1 \times 10^{-6}$ M) in HEPES pH 7.2 upon the addition of 50 equivalents of different amino acids*

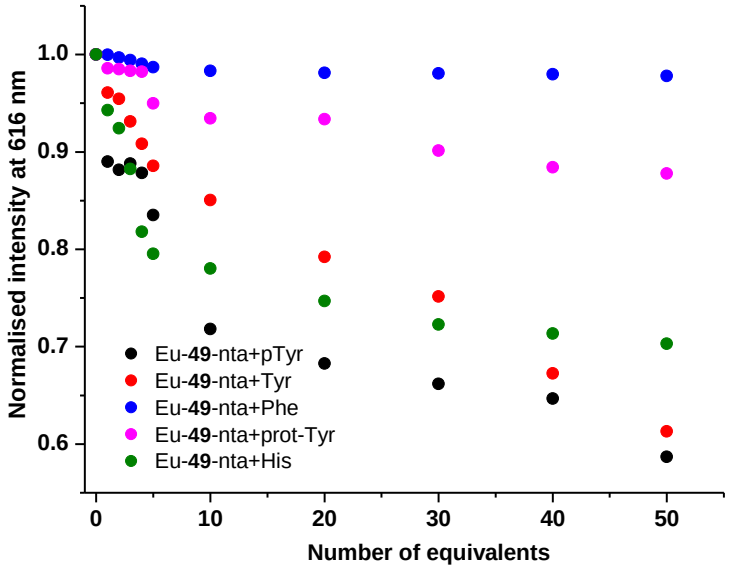

***Figure A2.38**: Normalised Eu(III)-centred emission at 616 nm (λ_{ex} = 330 nm) of **Eu-49-nta** ($c = 1 \times 10^{-6}$ M) in Tris buffer pH 7.2 upon the addition of 50 equivalents of different amino acid*

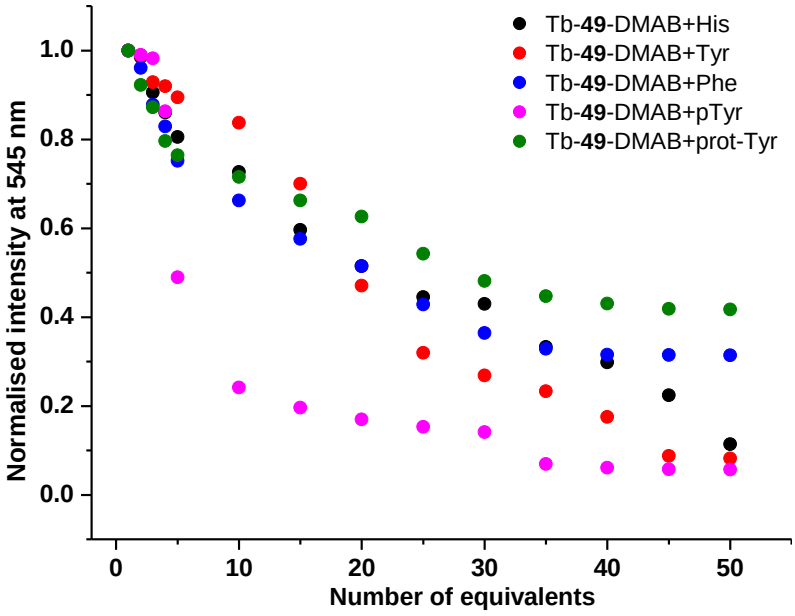

***Figure A2.39**: Normalised Tb(III)-centred emission at 545 nm (λ_{ex} = 306 nm) of **Tb-49-DMAB** ($c = 1 \times 10^{-6}$ M) in Tris buffer pH 7.2 upon the addition of 50 equivalents of different amino acid.*

Appendix Chapter 3

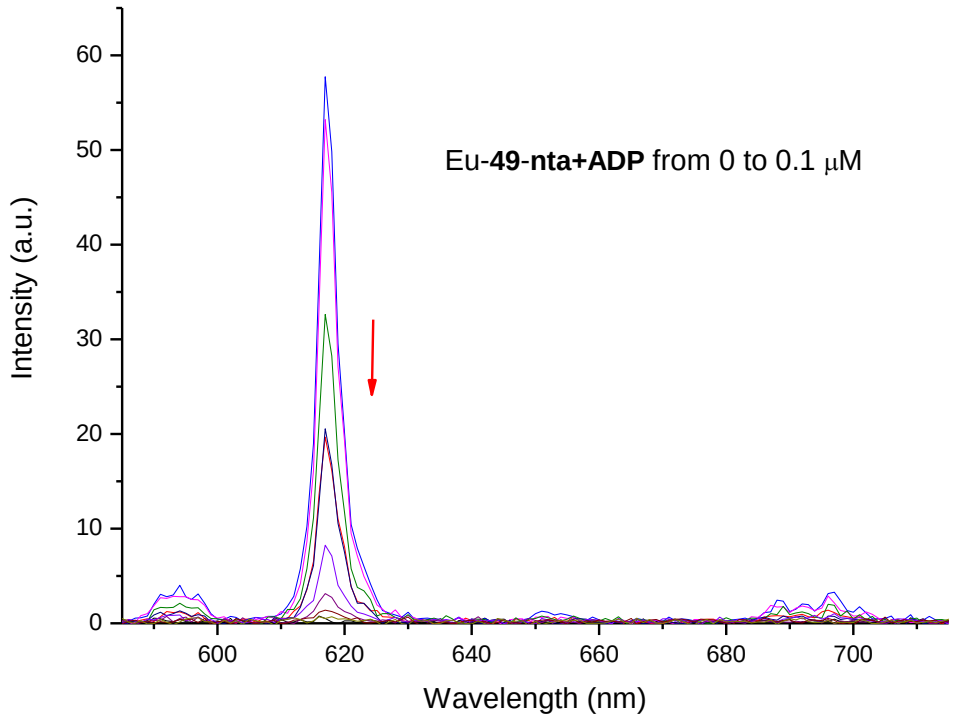

Figure A3.1**: Changes in the Eu(III)-centred emission at 616 nm (λ_{ex} = 330 nm) of **Eu-49-nta** ($c = 8 \times 10^{-3}$ M) in HEPES buffer pH 7.2 upon the addition of several equivalents of **ATP

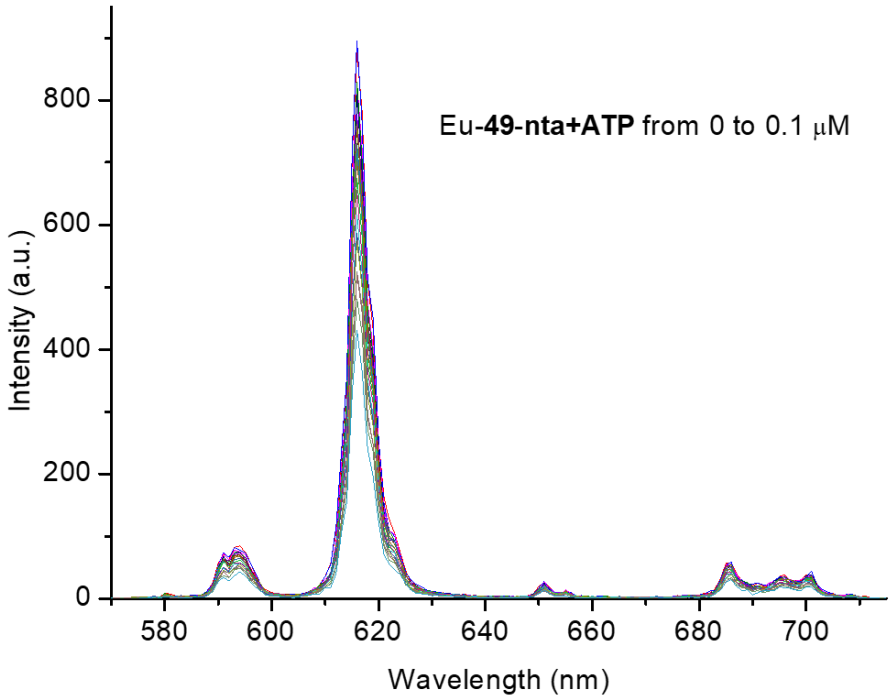

Figure A3.2**: Changes in the Eu(III)-centred emission at 616 nm (λ_{ex} = 330 nm) of **Eu-49-nta** ($c = 8 \times 10^{-3}$ M) in HEPES buffer pH 7.2 upon the addition of several equivalents of **ADP

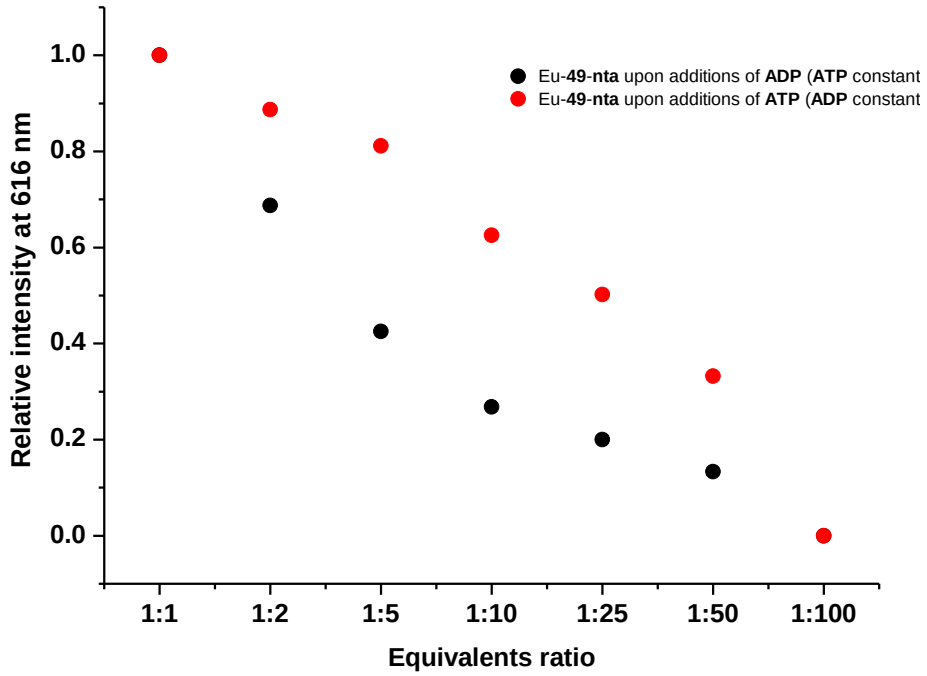

***Figure A3.3**: Changes in the Eu(III)-centred emission of **Eu-49-nta** ($c = 8 \times 10^{-3}$M) at 616 nm (λ_{ex} = 330 nm) in HEPES buffer pH 7.2 upon the addition of 0→100 equivalents of **ATP** (**ADP** constant, $c = 8 \times 10^{-3}$ M) and **ADP** (**ATP** constant $c = 8 \times 10^{-3}$ M).*

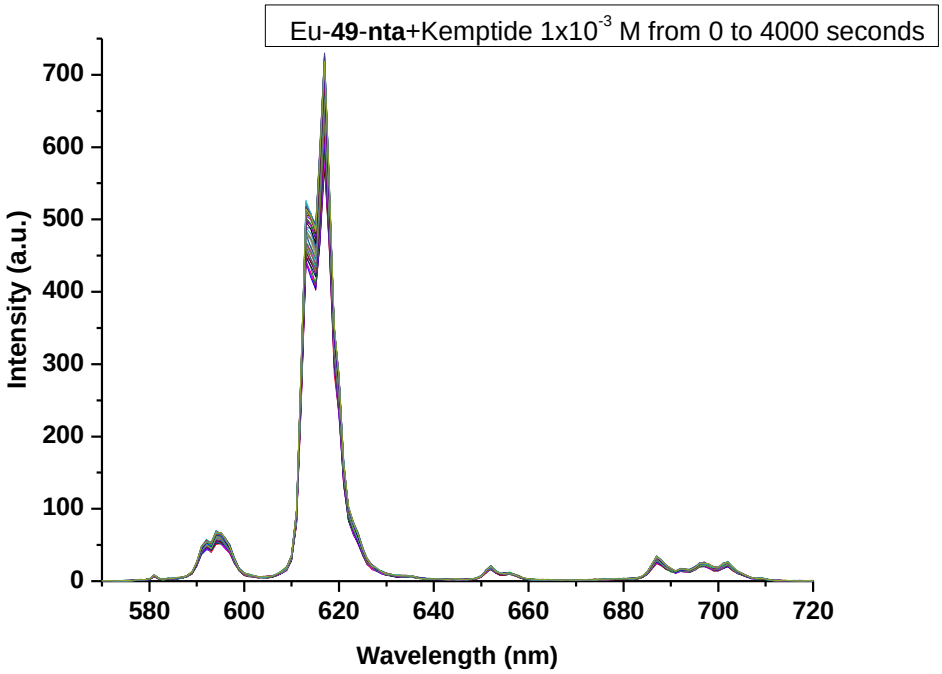

***Figure A3.4:** Change in the Eu(III)-centred emission of **Eu-49-nta** at 616 nm ($c = 8 \times 10^{-3}$ M) (λ_{ex} = 330 nm) in HEPES buffer pH 7.2 upon the addition of kemptide ($c = 1 \times 10^{-3}$ M) versus the time (0→4000 seconds).*

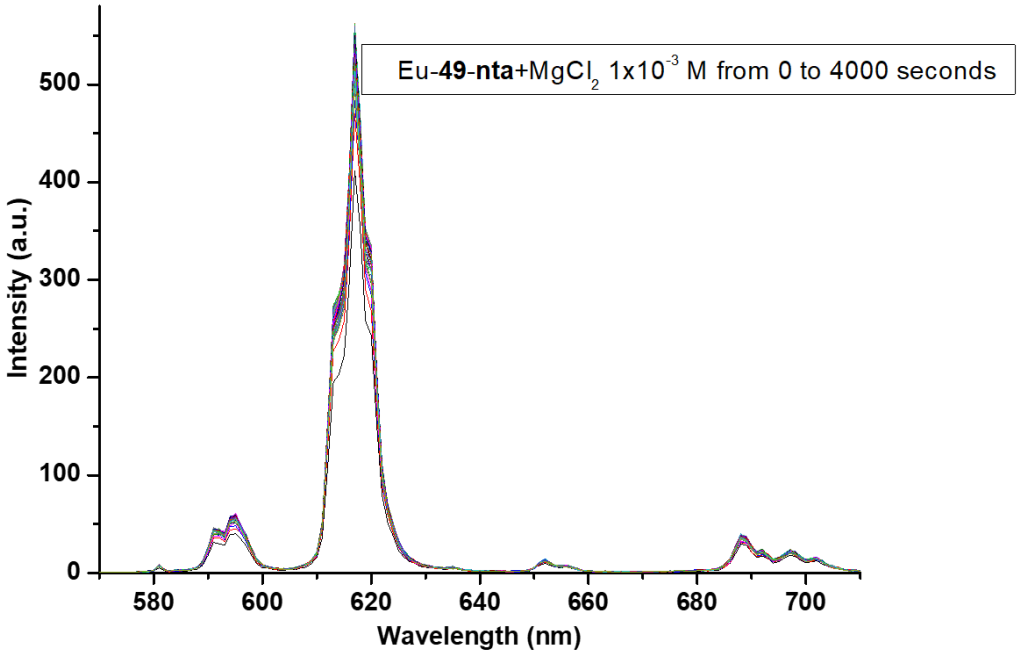

*Figure A3.5: Change in the Eu(III)-centred emission of Eu-**49-nta** at 616 nm (c = 8 x 10^{-3} M) (λ_{ex} = 330 nm) in HEPES buffer pH 7.2 upon the addition of $MgCl_2$ (c = 1 x 10^{-3} M) versus the time (0→4000 seconds*

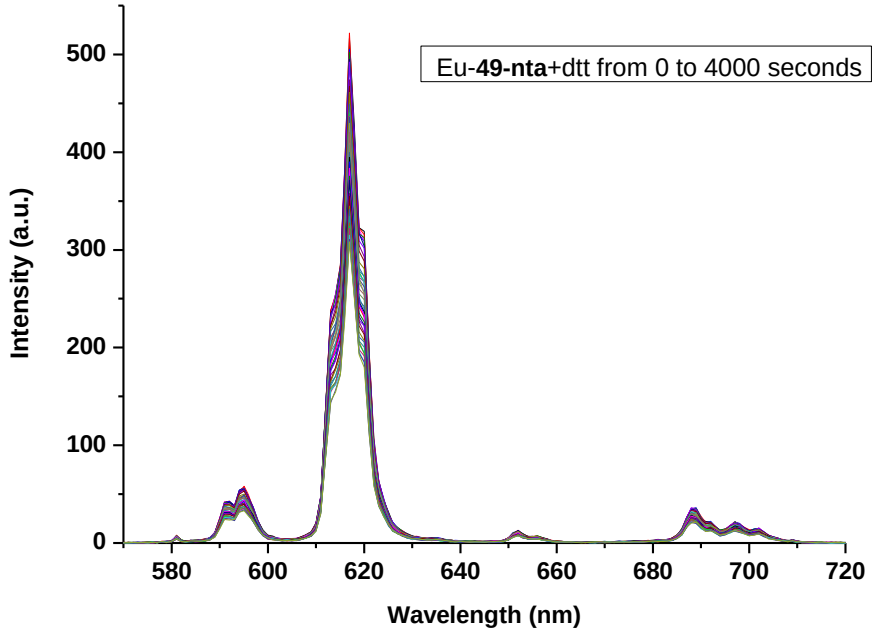

***Figure A3.6:** Change in the Eu(III)-centred emission of **Eu-49-nta** at 616 nm (c = 8 x 10^{-3} M) (λ_{ex} = 330 nm) in HEPES buffer pH 7.2 upon the addition of DTT (c = 2.5 x 10^{-3} M) versus the time (0→4000 seconds).*

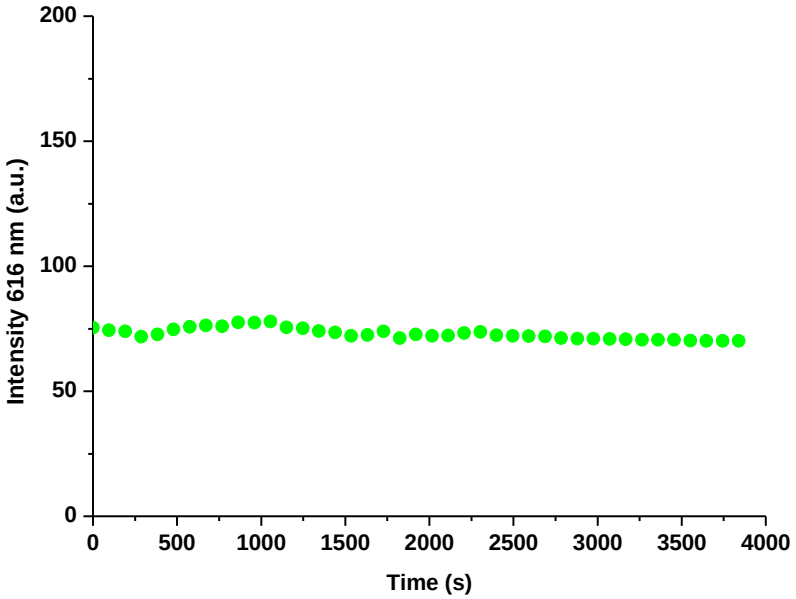

***Figure A3.7**: Change in the Eu(III)-centred emission of **Eu-49-nta** at 616 nm (c = 8 x 10^{-3} M) (λ_{ex} = 330 nm) in HEPES buffer pH 7.2 upon the addition of PKAC (c = 3 x 10^{-5} M) versus the time (0→4000 seconds).*

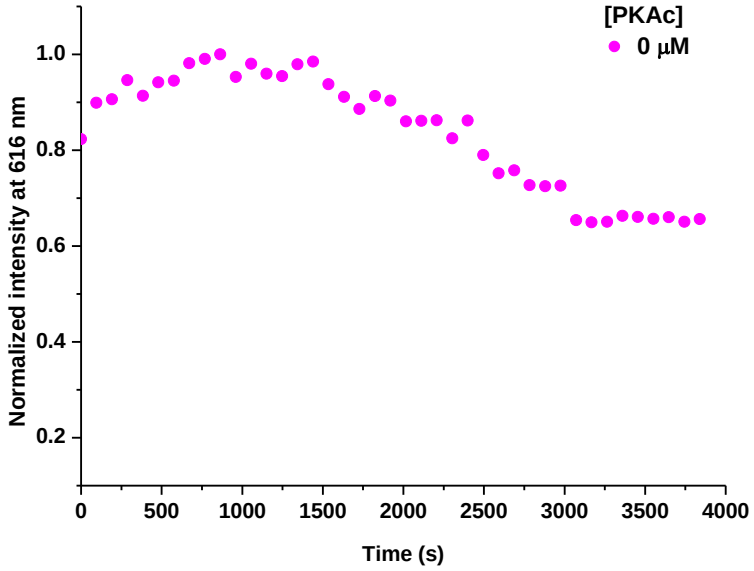

***Figure A3.8:** Change in the Eu(III)-centred emission of **Eu-49-nta** (c = 8x10^{-3} M) at 616 nm (λ_{ex} = 330 nm) in HEPES buffer pH 7.2 upon the addition of kemptide (c = 1 x 10^{-3} M), DTT (c = 2.5 x 10^{-3} M), $MgCl_2$ (c = 3 x 10^{-3} M) and **ATP** (c = 1 x 10^{-3} M) simultaneously.*

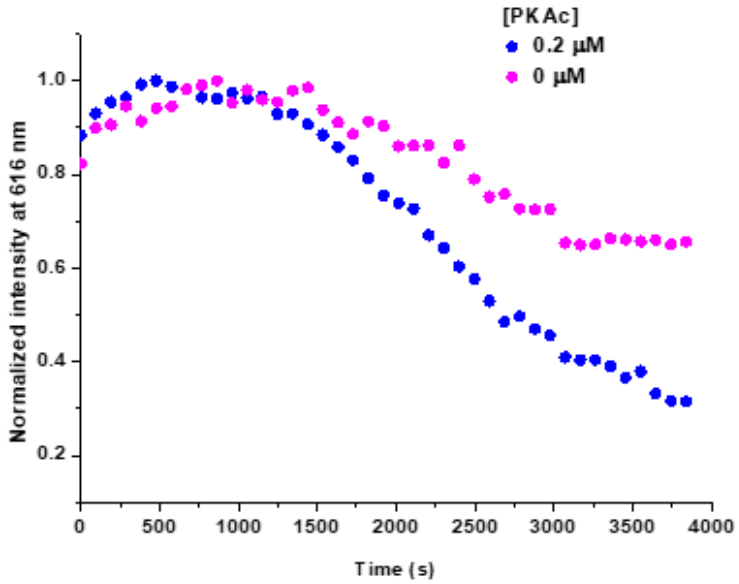

Figure A3.9: *Change in the Eu(III)-centred emission of* ***Eu-49-nta*** *(c = 8 x 10^{-3} M) at 616 nm (λ_{ex} = 330 nm) in HEPES buffer pH 7.2 upon the addition of kemptide (c = 1 x 10^{-3} M), DTT (c = 2.5 x 10^{-3} M), $MgCl_2$ (c = 3x10^{-3} M) and* ***ATP*** *(c = 1 x 10^{-3} M) and PKAc (c = 0.2 x 10^{-3} M) added simultaneously.*

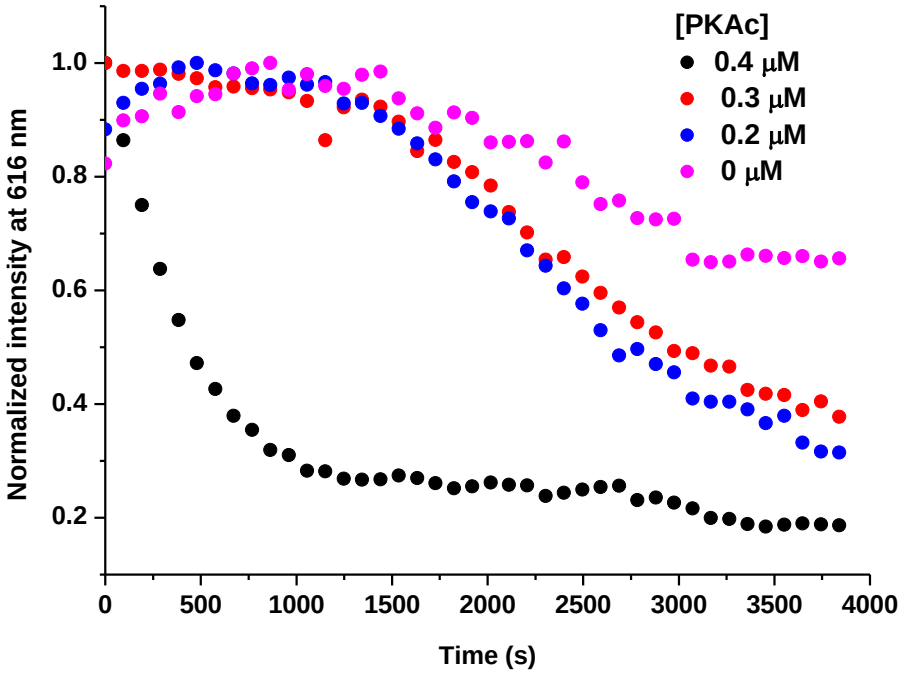

Figure A3.10*: Change in the Eu(III)-centred emission of* ***Eu-49-nta*** *(c = 8 x 10^{-3} M) at 616 nm (λ_{ex} = 330 nm) in HEPES buffer pH 7.2 upon the addition of kemptide (c = 1 x 10^{-3} M), DTT (c = 2.5 x 10^{-3} M), $MgCl_2$ (c = 3 x 10^{-3} M) and* ***ATP*** *(c = 1 x 10^{-3} M) and PKAc (c = 0.4 x 10^{-3} M) added simultaneously.*

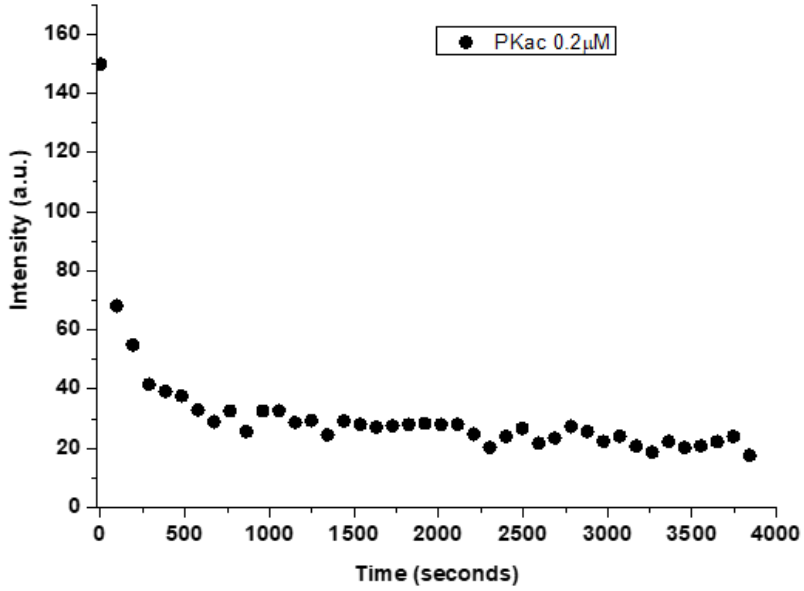

Figure A3.11: *Change in the Eu(III)-centred emission of LB-**Eu-49-nta** monolayer at 616 nm (λ_{ex} = 330 nm) upon the dipping in a solution of Kemptide (c = 1 x 10^{-3} M), DTT (c = 2.5 x 10^{-3} M), $MgCl_2$ (c = 3 x 10^{-3} M) and **ATP** (c = 1 x 10^{-3} M) and PKAc (c = 0.2 x 10^{-3} M) in HEPES buffer pH 7.2.*

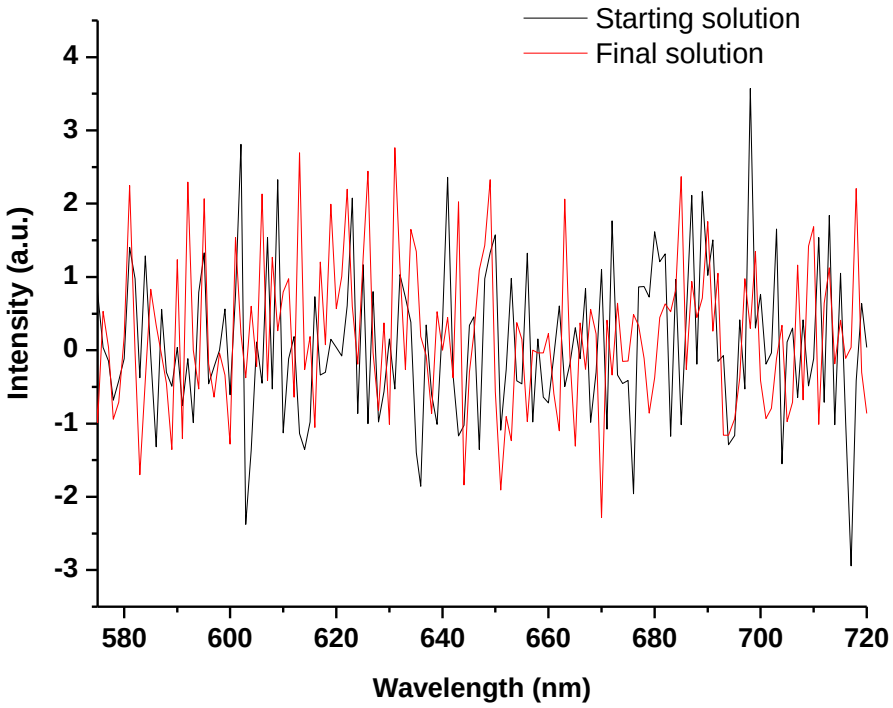

Figure A3.12: *Eu(III)-centred emission at 616 nm (λ_{ex} = 330 nm) of a solution containing kemptide (c = 1 x 10^{-3} M), DTT (c = 2.5 x 10^{-3} M), $MgCl_2$ (c = 3 x 10^{-3} M) and **ATP** (c = 1 x 10^{-3} M) and PKAc (c = 0.2 x 10^{-3} M) before (black) and after (red) the dipping of the LB-**Eu-49** monolayer in HEPES buffer pH 7.2.*

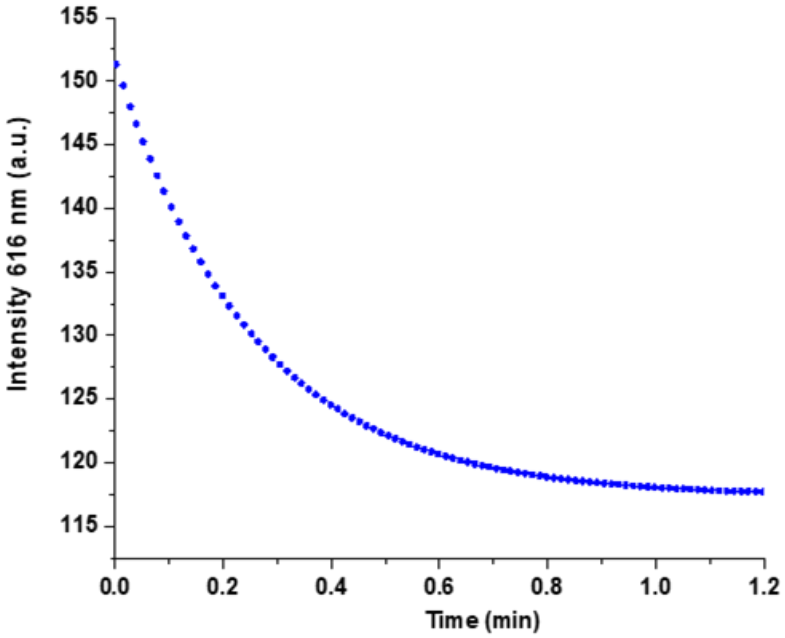

Figure A3.13: *Change in the Eu(III)-centred emission of LB-**Eu-49-nta** at 616 nm (λ_{ex} = 330 nm) upon dipping in a solution of kemptide (c = 1 x 10^{-3} M), DTT (c = 2.5 x 10^{-3} M), $MgCl_2$ (c = 3 x 10^{-3} M) and **ATP** (c = 1 x 10^{-3} M) and PKAc (c = 0.3 x 10^{-3} M) in HEPES buffer pH 7.2*

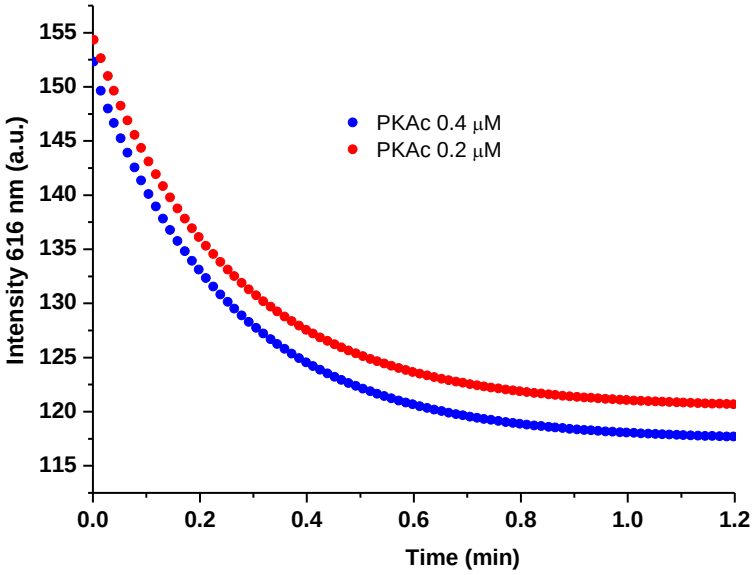

Figure A3.14: *Comparison of the change in the Eu(III)-centred emission at 616 nm (λ_{ex} = 330 nm) of LB-Eu-**30-nta** upon the dipping in a solution of Kemptide (c =1 x 10^{-3} M), DTT (c = 2.5 x 10^{-3} M), $MgCl_2$ (c = 3 x 10^{-3} M) and **ATP** (c = 1 x 10^{-3} M) and PKAc (c = 0.2 x 10^{-3} M, red) and (c = 0.4 x 10^{-3} M blue).*

Appendix for Chapter 4

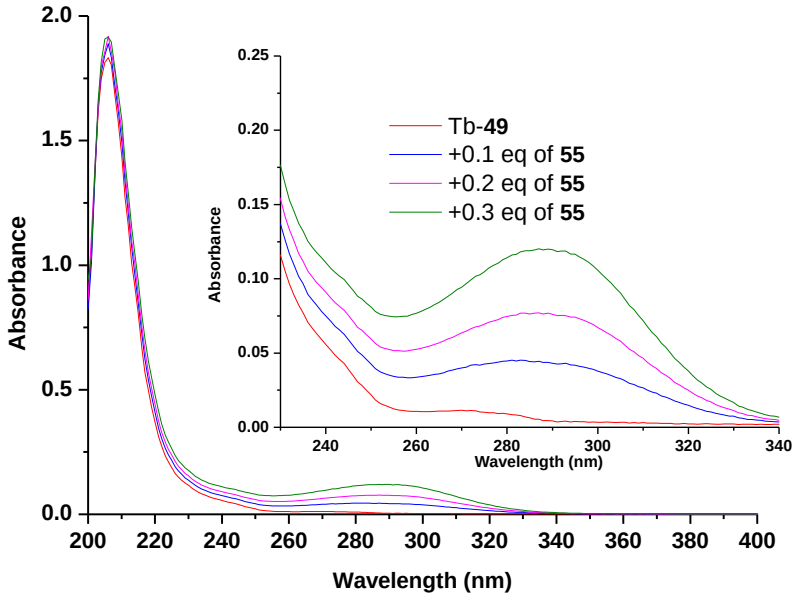

***Figure A4.1**: UV-Vis absorption spectra of Tb-**49** (c = 1 x 10^{-5} M) upon the addition of 0.3 equivalents of **55** in MeOH.*

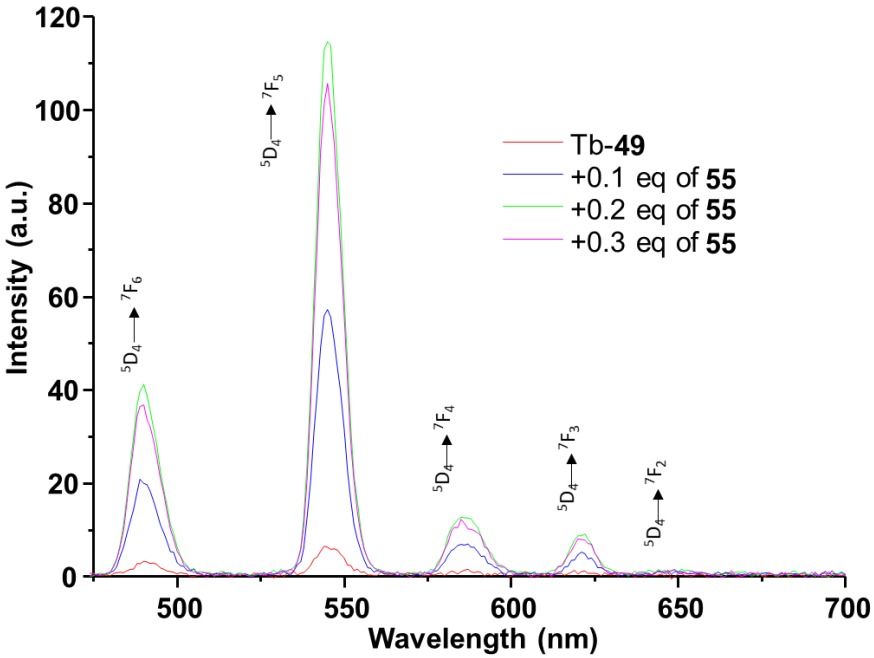

***Figure A4.2**: The enhancement of Tb(III)-centred emission for Tb-49 (c = 1 x 10^{-5} M in MeOH, λ_{ex} = 288 nm) upon the addition of antenna 0 to 0.3 equivalents of 55.*

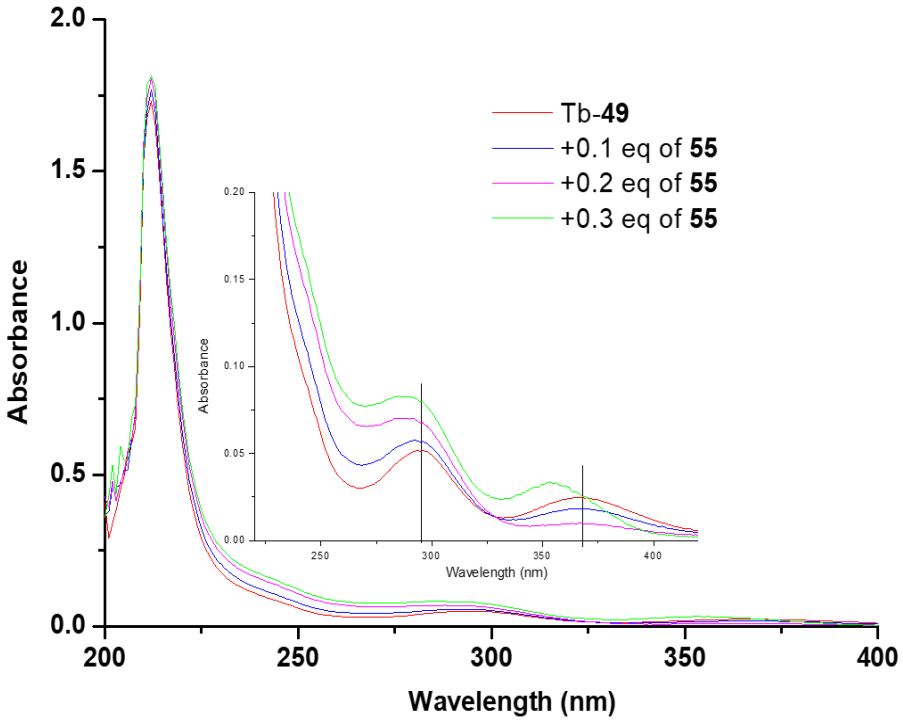

***Figure A 4.5**: UV-Vis absorption spectra of Tb-**49** (c = 1 x 10^{-5} M) upon the addition of 0.3 equivalents of **55** in THF.*

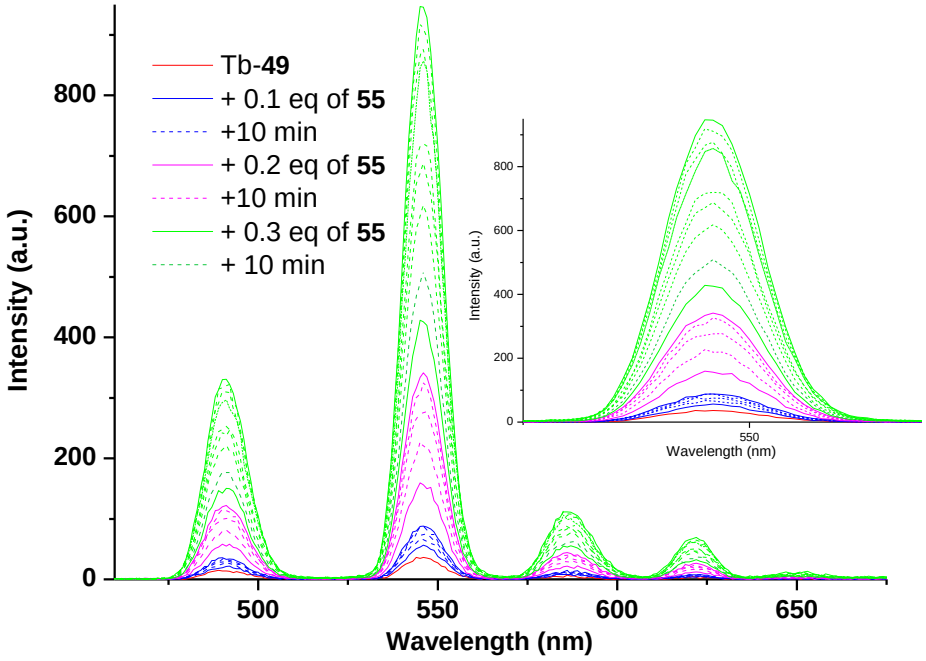

***Figure A4.6**: Change in the Tb(III)-centred emission of Tb-**49** (c = 1x10^{-5} M in THF, λ_{ex}= 288 nm) upon the addition of antenna 0 to 0. 3 equivalents of **55**.*

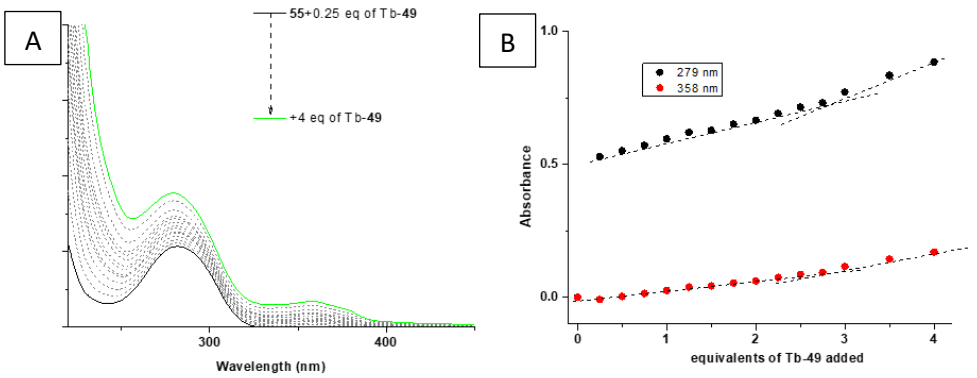

Figure A4.7: *(A) Changes in the absorption spectra of* ***55*** *(c = 1 x 10^{-5} M) upon titrating with Tb-****49*** *(0 to 4 equivalents) in MeOH. (B) Binding isotherms recorded at 279 and 358 nm.*

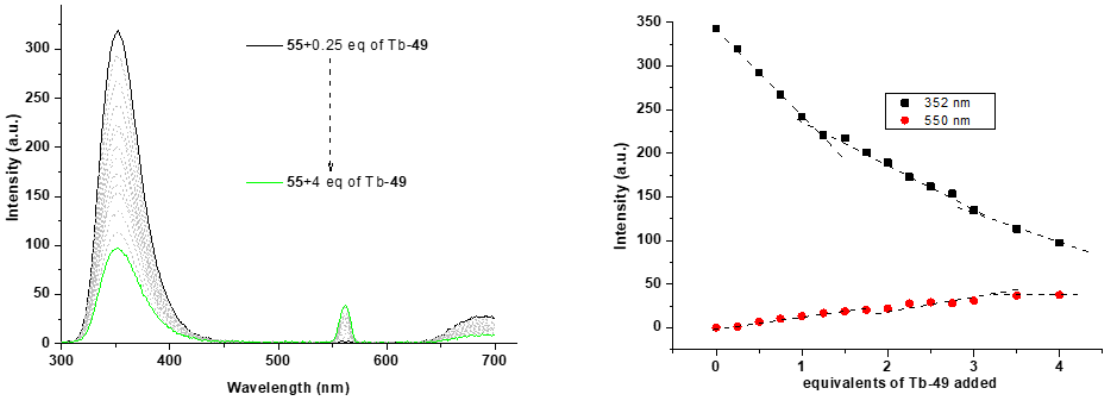

Figure A4.8: *(A)Fluorescence spectra of* ***55*** *(c = 1 x 10^{-5}M in MeOH, λ_{ex} = 288 nm) upon titrating with Tb-****49*** *(0 to 4 equivalents) in MeOH. (B) binding isotherms recorded at 352 and 550 nm*

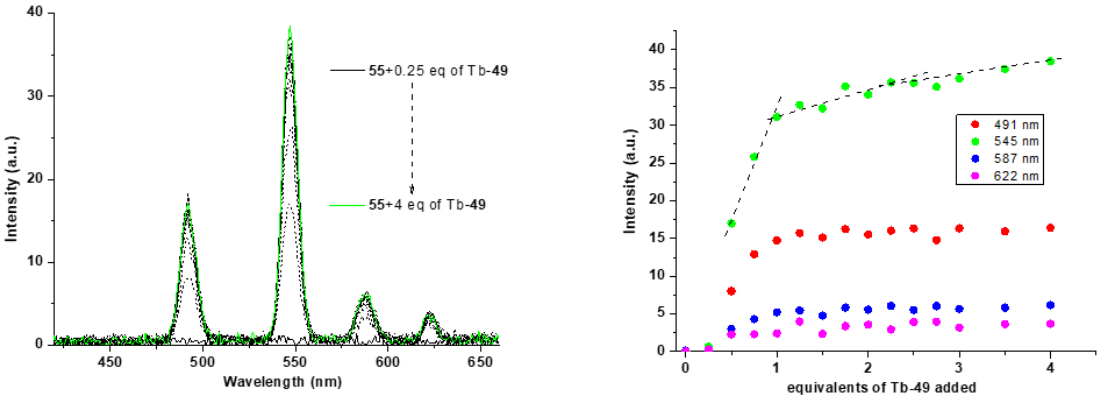

Figure A4.9: *(A) Phosphorescence spectra of* ***55*** *(c = 1 x 10^{-5} M in MeOH, λ_{ex} = 288 nm) upon titrating with Tb-****49*** *(0 to 4 equivalents) in MeOH. (B) Binding isotherms recorded at 491, 545,587 and 622 nm.*

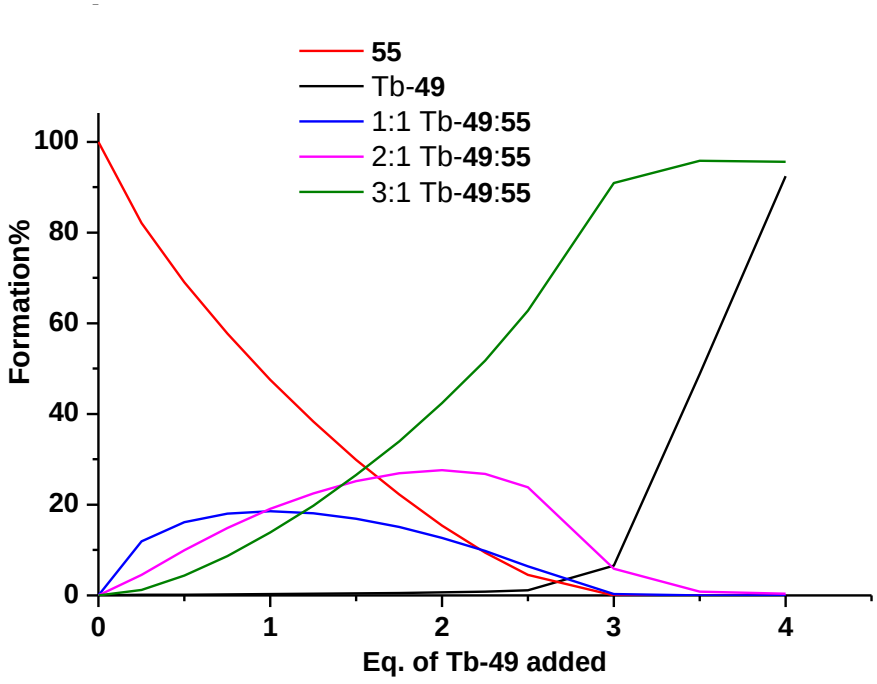

Figure A4.10: *Speciation distribution diagram obtained from the fitting of the phosphorescence titration of* ***55*** *with Tb-****49*** *in MeOH.*

Appendix Chapter 5

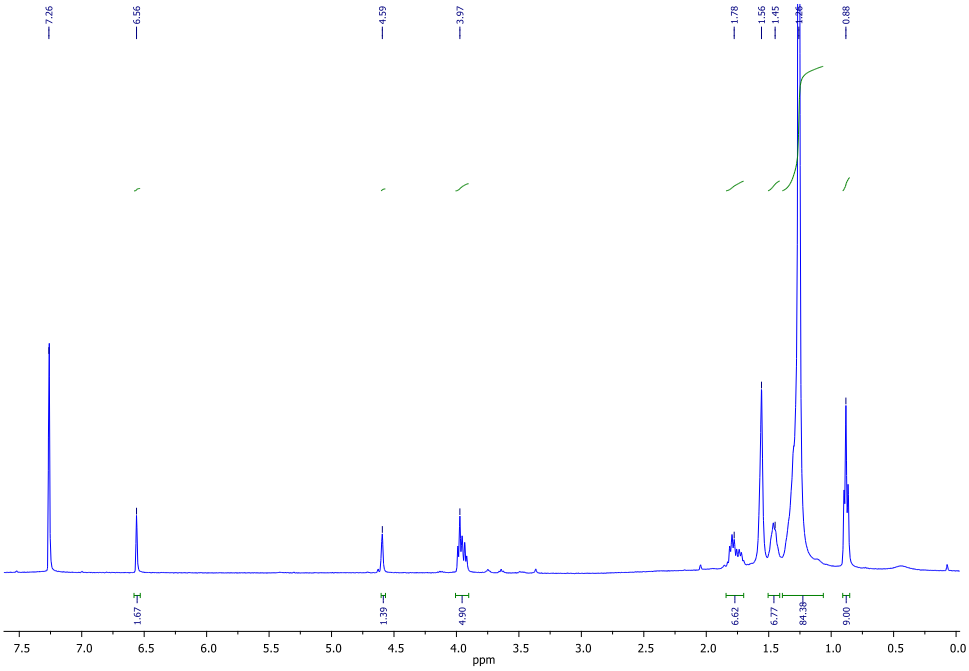

Figure A5.0**: [1]H-NMR (400 MHz, $CDCl_3$) of **44

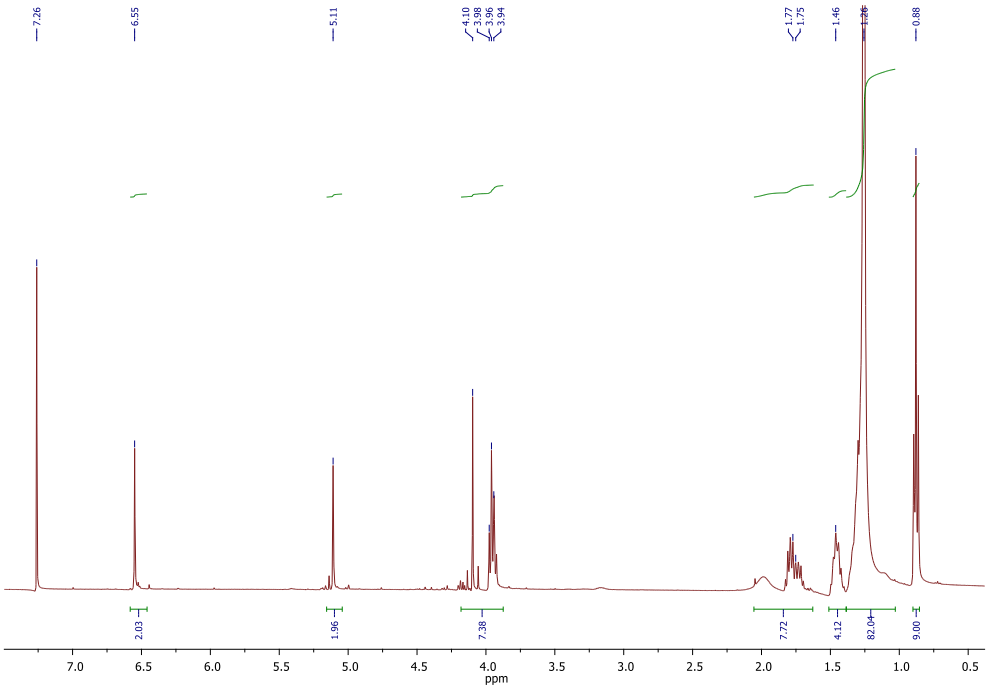

Figure A5.1**: [1]H-NMR (400 MHz, $CDCl_3$) of **56

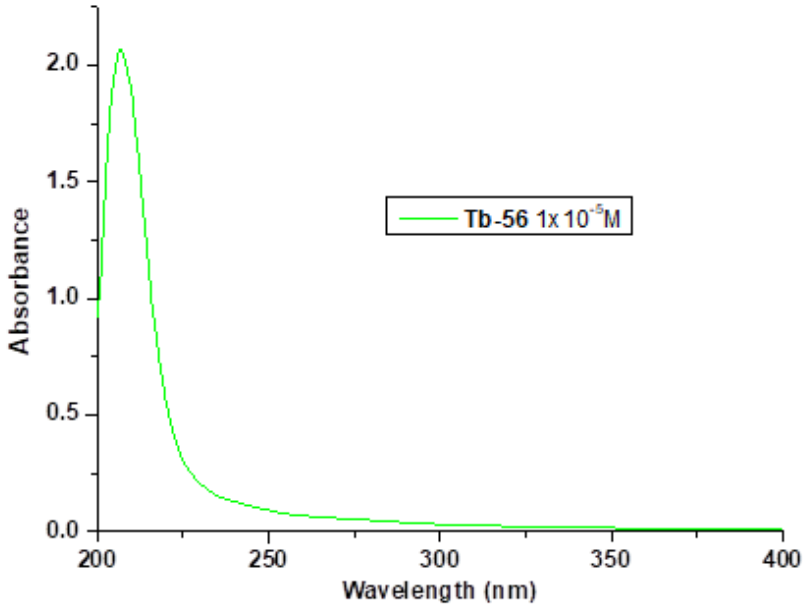

Figure A5.2*The UV-vis absorption spectra of Tb-**56***

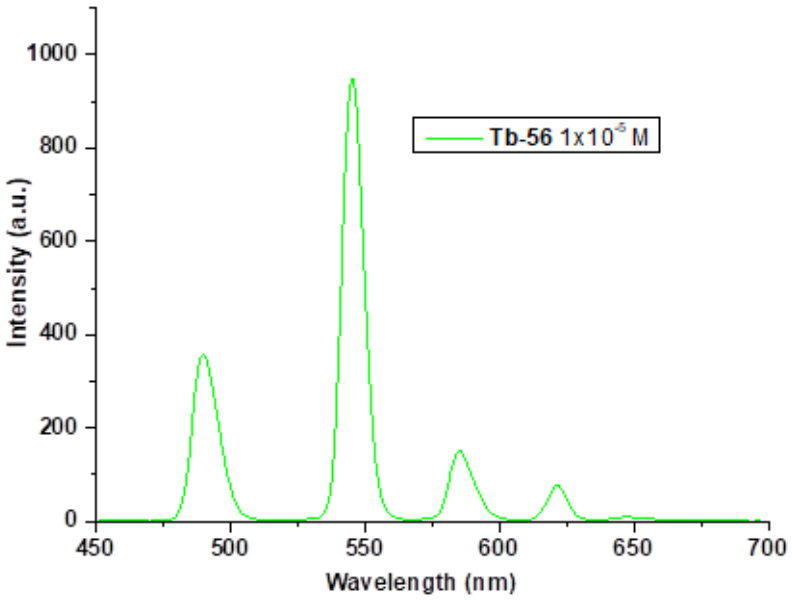

Figure A5.3: *The fluorescence spectra of Tb-**56***

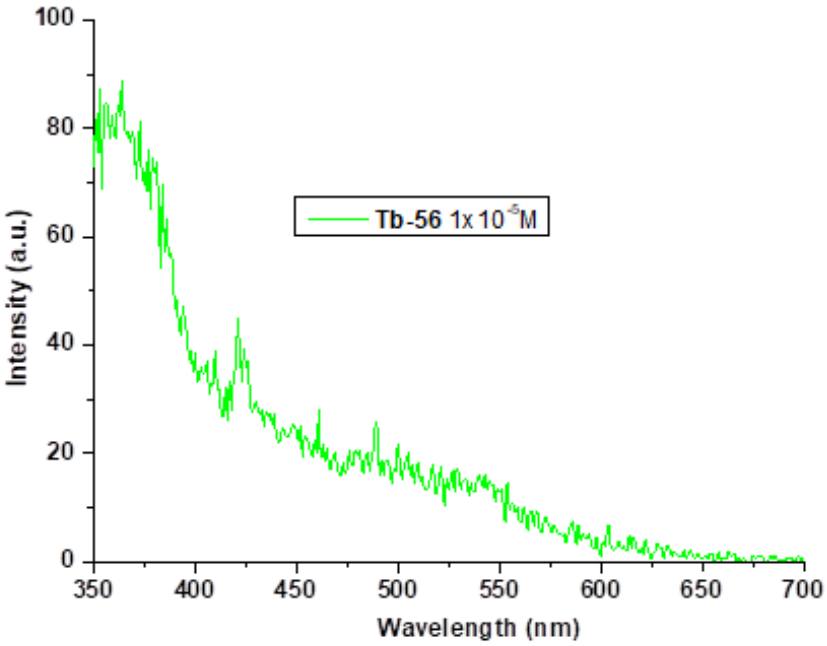

Figure 5.3: (A) *The phosphorescence spectra of Tb-**56***

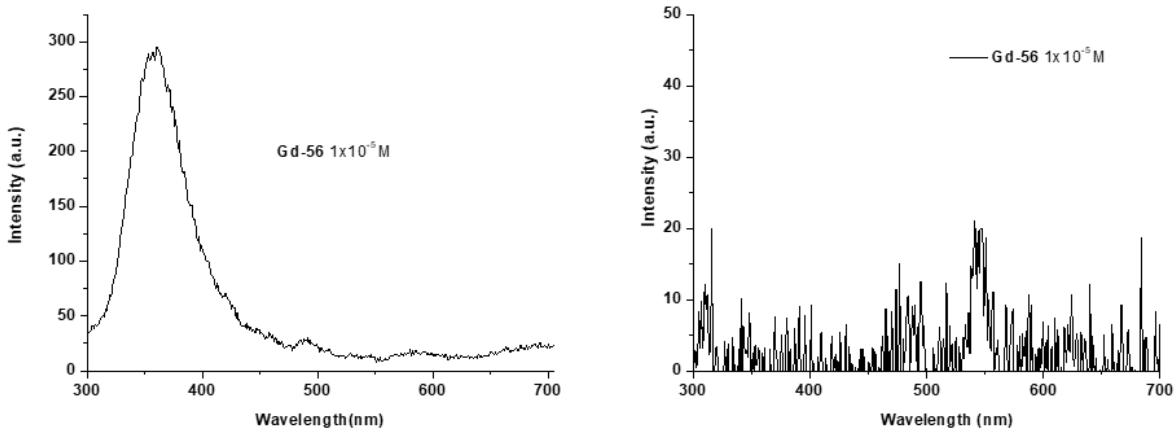

Figure 5.4 A) *The UV-vis absorption spectra, **(B)** fluorescence spectra of Gd-**56***